Mechanistic Insights into Dynamic Predictions of Pathogens in Engineered Systems

by

Ashley Heida

A Dissertation Presented in Partial Fulfillment
of the Requirements for the Degree
Doctor of Philosophy

Approved March 2023 by the
Graduate Supervisory Committee:

Kerry Hamilton, Chair
Margaret Garcia
Rebecca Muenich
Amanda Wilson

ARIZONA STATE UNIVERSITY

May 2023

ABSTRACT

Pathogens can proliferate in the built environment and can cause disease outbreaks if water and wastewater are not properly managed. Understanding pathogens that grow in engineered systems is crucial to protecting public health and preventing disease. Using dynamic computational models can reveal mechanistic insights into these systems to aid in understanding risk drivers and determining risk management strategies.

The first research chapter of this thesis investigates tradeoffs for reducing the cost associated with Legionnaire's Disease, hot water scalding, and energy use using a computational framework for evaluating an optimal water heater temperature set point. The model demonstrated that the optimal temperature set point was highly dependent on assumptions made regarding the dose response parameter for a common configuration of an electric water heater in a hospital setting. The optimal temperature was 55°C or 48°C for subclinical vs. clinical severity dose response, respectively, compared with current recommendations of 60°C to kill bacteria and 49°C to prevent scalding and conserve energy.

The second research chapter models the population dynamics of antibiotic-susceptible *Escherichia coli* (*E. coli*) and antibiotic-resistant *E. coli* with a population ecology-exposure assessment model in surface water to quantify the risk of urinary tract infection from recreational swimming activities. Horizontal gene transfer (HGT) was modeled in the environment and the human gastrointestinal tract for several scenarios.

HGT was generally not a dominant driver of exposure estimates compared to other factors such as growth and dilution, however, the rank order of factors was scenario-dependent.

The final research chapter models pathogen transport from wastewater treatment plant (WWTP) exposures and assesses the risk to workers based on several exposure scenarios. Case studies were performed to investigate infection risk drivers across different scenarios, including adjustments for the timing of exposure and personal protective equipment. A web application was developed for use by WWTP risk managers to be used with site-specific data.

The proposed modeling frameworks identified risk drivers across several microbial risk scenarios and provide flexible tools for risk managers to use when making water treatment and use decisions for water management plans used for premise plumbing as well as for wastewater treatment practices.

ACKNOWLEDGMENTS

I would like to thank my PI, Dr. Kerry Hamilton, for all the time she invested in my work and for helping me grow as a scientist through countless discussions, written revisions, and opportunities to work with our collaborators. I would also like to thank my committee members, Drs. Margaret Garcia, Rebecca Muenich, and Amanda Wilson for taking the time to serve on my committee and offer thoughtful recommendations to strengthen my work. A special thanks to Dr. Amanda Wilson for her comments on this dissertation and for working with Dr. Hamilton and I to expand chapter 4 into a useful tool.

I would also like to thank my family for their support over the years. My parents have always supported me to follow my dreams and for that, I am incredibly thankful. I would also like to my Mom and Bill for their feedback on the graphical abstracts and other figures in this dissertation.

Lastly, to my friends who have been by my side since the beginning, I am so thankful for you and I can't wait to see where life takes us next.

TABLE OF CONTENTS

Page

LIST OF TABLES vii

LIST OF FIGURES viii

CHAPTER

1 INTRODUCTION 1

1.1 Importance of Research 1

1.2 Goals and Objectives of the Research 7

2 COMPUTATIONAL FRAMEWORK FOR EVALUATING RISK TRADE-OFFS IN COSTS ASSOCIATED WITH LEGIONNAIRES' DISEASE RISK, ENERGY, AND SCALDING RISK FOR HOSPITAL HOT WATER SYSTEMS 10

2.1 Abstract 10

2.2 Introduction 11

2.3 Methods 18

2.4 Results 38

2.5 Discussion 50

2.6 Conclusion 62

CHAPTER Page

2.7 References....64

3 DEVELOPMENT AND SENSITIVITY ANALYSIS OF A POPULATION ECOLOGY- EXPOSURE ASSESSMENT MODEL FOR ANTIBIOTIC-SUSCEPTIBLE AND ANTIBIOTIC-RESISTANT *E. COLI* HEALTH RISK IN RECREATIONAL WATER 77

3.1 Abstract....77

3.2 Introduction....79

3.3 Methods 85

3.4 Results....99

3.5 Discussion....104

3.6 Additional Proposed Work....115

3.7 Acknowledgements 116

4 QUANTITATIVE MICROBIAL RISK ASSESSMENT (QMRA) TOOL FOR MODELING SARS-COV-2 AND OTHER INFECTION RISKS FOR WASTEWATER TREATMENT PLANT WORKERS 117

4.1 Abstract....117

4.2 Introduction....119

CHAPTER Page

4.3 Methods 125

4.4 Results 141

4.5 Discussion 155

4.6 Conclusion 163

5 CONCLUSION 165

REFERENCES 174

APPENDIX

A SUPPLEMENTAL INFORMATION FOR CHAPTER 2 215

B SUPPLEMENTAL INFORMATION FOR CHAPTER 3 266

C SUPPLEMENTAL INFORMATION FOR CHAPTER 4 282

D PUBLISHED WORKS AND PRESENTATIONS 290

E PERMISSION TO USE PUBLISHED WORKS 295

LIST OF TABLES

Table Page

1. Case Conditions Tested on this Model 42

2. Risk Model Parameters 97

3. Summary of Model Simplifying Assumptions 109

4. Exposure Settings and Associated Partitioning Coefficients with Exposure Times for Aerosol Inhalation, and Accidentally Ingested Volume from Droplet or Hand-to-Mouth Exposures 130

5. Health Endpoint Associated with each Pathogen and Available Dose Response Parameters 134

6. Risk Calculator Tool Inputs 137

7. Parameters, Distributions, and their Sources 138

8. Summary of risk results for scenario analysis 145

LIST OF FIGURES

Figure Page

1. Graphical Abstract of a Computational Framework to Evaluate Trade-offs in Energy, Scalding, and Legionnaires' Disease Illness Risk Costs 11

2. Conceptual Flow Chart of Model Sections with Select Inputs and Outputs.....19

3. Schematic of Selected Simplified, Exemplary Premise Plumbing Hospital System Model 20

4. Water Heater Schematic Divided into Nodes for Temperature Calculations Following Methods used in Kleinbach et al. (1993). 22

5. Median of 10,000 Monte Carlo Iterations for Temperature, Free Chlorine Concentration, and *L. pneumophila* Concentration in Bulk Water for Case 0 for 49°C and 60°C.....39

6. Comparison of Select Scenarios and Effect on Total Cost and Corresponding Optimum Water Heater Set Point.....45

7. Spearman Rank Correlation Coefficient Heatmap for Subclinical and Clinical Dose Response, and Sobol Global Sensitivity Analysis for Case 0 47

8. The Modeled Transformations of both Susceptible and ESBL *E. coli* Populations 78

9. Conceptual Model for Exposure to Antibiotic Susceptible *E. coli* and ESBL *E. coli* During Recreational Swimming.....86

Figure Page

10. Modeling Scenarios for Antibiotic Susceptible *E. coli* and ESBL *E. coli*.....87

11. Species Count in the Environment with Different Initial Antibiotic Susceptible and ESBL *E. coli* Starting Concentrations.....99

12. Species Count in the Body with and without Background Populations in the Gut 101

13. Dose With and Without Background *E. coli* in the Gut 102

14. Sensitivity Analysis using Spearman's Correlation Coefficients for Antibiotic Susceptible and ESBL *E. coli* final dose.....104

15. Calculator Page with Individual Pathogen Risks and Total Risks for Ingestion and Inhalation.....142

16. Calculator Page with Pathogen Specific Parameters for *C. hominis* 143

17. Ingestion and Inhalation Risk Graphs for all Pathogens Modeled for a "High Contact" Exposure Setting during Peak Hours 145

18. Infection Risk from *C. hominis* for Different Exposure Settings with Late Morning Exposure and No PPE 147

19. Infection Risk from *L. pneumophila* for Different Exposure Settings with Late Morning Exposure and No PPE 148

Figure Page

20. Ingestion Risks for Available Pathogens during Peak Hours and Non-peak Hours for “High Contact” without PPE 150

21. Inhalation Risks for Available Pathogens during Peak Hours and Non-peak Hours for “High Contact” without PPE 151

22. Inhalation Risks during Peak Hours with and without Face Covering 152

23. Respiratory Infection Risks used in the Sensitivity Analysis for a High Contact Exposure Scenario during Peak Hours with an N95 Respirator 153

24. Sensitivity Analysis with Spearman’s Correlation Coefficients for Monte Carlo Variables.....154

CHAPTER 1

INTRODUCTION

1.1 Importance of research

Understanding pathogens that grow in water and wastewater systems is crucial to protecting public health and reducing the risk of disease. Regulatory entities such as the United States Environmental Protection Agency (USEPA) provide guidance on the level of treatment for water and wastewater, typically in terms of acceptable levels of contaminants or as treatment requirements (e.g. log removals) according to a particular purpose. For example, for direct potable (wastewater) reuse, the California Department of Public Health has implemented the "12-10-10 rule" requiring a 12-log removal of viruses, and a 10-log removal of *Cryptosporidium* and *Giardia* (California Department of Public Health, 2011). The USEPA has legally enforceable maximum contaminant levels (MCL) that are contaminant-specific for drinking water (US EPA, 2015). The maximum contaminant levels goals (MCLG) for all pathogens are zero, although there have been efforts to derive risk-based targets (e.g. for *Legionella pneumophila* (Hamilton et al., 2019)). However, currently, all MCLG requirements for pathogens are treatment technology-based.

Despite advances in water and wastewater treatment and regulations, some pathogens remain a threat due to insufficient barriers. In a drinking water setting, insufficient barriers, such as long residence times or lack of necessary disinfectants, could lead to an increase in microbial growth. In a wastewater setting, a lack of personal protective equipment or

extended exposure to wastewater aerosols could lead to an increased risk of infection from wastewater pathogens. Due to treatment performance and other water quality assurance lapses (potentially from engineering malfunctions or human error), it is essential to investigate health risks and take preventative action if needed. Modern water and wastewater treatment have significantly decreased the waterborne disease burden in the US and globally (CDC, 1999). However, some situations continue to remain a challenge today for pathogen management including (1) pathogens that can (re)grow in drinking water (premise plumbing) systems (CDC et al., 2015); (2) the contribution of water and wastewater to the antimicrobial resistance (AMR) crisis (CDC, 2019; Murray et al., 2022; O'Neill, 2016); and (3) multi-route and multi-pathogen exposures, especially for wastewater exposures (Amoah et al., 2022; Xu et al., 2020). Exposures to pathogens during wastewater treatment are a concern and will serve as an exemplar of the need for holistic pathogen management.

(1) Pathogens that can regrow in drinking water (premise plumbing) systems: One example of a situation where insufficient barriers to human exposure are present is in drinking water carried by premise plumbing in the built environment. Water systems in buildings can harbor opportunistic pathogens in biofilms on the inner surfaces of water pipes which can contribute to pathogen persistence or growth if not properly managed, such as with *Legionella pneumophila (L. pneumophila)* (CDC, 2015; NASEM, 2006). *L. pneumophila* is a species of bacteria that can cause the pulmonary disease known as Legionnaires' Disease (LD) or the febrile illness Pontiac Fever. LD can be contracted when a person is exposed to bacteria-laden bioaerosols (Beer, 2015). *L. pneumophila* serogroup 1 is the most frequently responsible for LD and grows at elevated temperatures between

25°C-45°C (Paranjape et al., 2020). For this reason, a water heater can act as a source or amplifier of *L. pneumophila* in indoor environments. Existing management guidance, including that of the World Health Organization (WHO), and the National Academies of Sciences, Engineering, and Medicine (NASEM), recommend flushing water or elevating water heater temperatures (the water heater "set point") to 60°C to kill *L. pneumophila* bacteria (NASEM, 2019; WHO, 2007). However, scalding is a concern at these temperatures (Lévesque et al., 2004). Additionally, concerns for increasing sustainability would dictate that the energy cost associated with high water heater temperatures should be minimized. The Consumer Product Safety Commission (CPSC) and the US Department of Energy (DOE) recommend setting water heater temperatures to 49°C to prevent scalding in addition to minimizing energy costs (DOE, 2016; Shields et al., 2013). There is a lack of federal laws and regulations around balancing the risk of scalding with the risk of LD. The current work focuses on hospital premise plumbing systems, with the intention of applying the modeling framework beyond hospital systems with modified input parameters. To evaluate trade-offs in microbial quality (specifically *L. pneumophila* growth and subsequent risks), energy cost, and scalding risks, I developed a computational framework for evaluating an optimal water heater temperature set point to minimize risks and cost. The overall risk management goals are to reduce the burdens of illness, injury, and death associated with building water supplies while maintaining an economically viable approach that conserves energy.

(2) The contribution of water and wastewater to the antimicrobial resistance (AMR) crisis: Water and wastewater environments have the potential to result in pathogen exposures or serve as a "hot spot" for the development of antibiotic resistance (Hong et al.,

2018). Antimicrobial resistance (AMR) can develop when microorganisms acquire antibiotic resistance genes (ARG) that enable them to survive exposure to antibiotics (World Health Organization et al., 2016). As new ARGs develop to overcome existing antibiotics, simple antibiotic treatments for a disease may no longer be effective. Thus, antibiotic resistance and the transfer of ARGs are critical issues in public health. Extended-Spectrum Beta-Lactamase (ESBL)-producing *Escherichia coli* (ESBL *E. coli*) are labeled by the Centers for Disease Control and Prevention (CDC) as a "Serious Threat" (CDC, 2019) that are commonly found in wastewater and recreational waters (Blaak et al., 2014, 2015). ESBL *E. coli* is a leading cause of UTIs, which affect up to 150 million people every year worldwide (Picozzi et al., 2014). Recreational water has been highlighted as a potential area for the spread and/or dissemination of AMR (Nappier et al., 2020; Tyagi & Kumar, 2020). Several epidemiological studies have also implicated recreational water via surfing (Leonard et al., 2018), swimming in the ocean (Jorgensen et al., 2017; Søraas et al., 2013; van den Bunt, 2019), or exposure to spa pools (Begier et al., 2004), with a focus on *E. coli* and ESBL *E. coli*. This model will therefore serve as a framework to address these gaps by (1) integrating a population ecology model accounting for changes in bacterial populations due to HGT of ARG into the exposure assessment aspect of a quantitative microbial risk assessment (QMRA) framework; (2) using literature-based estimates of HGT rates for ESBL *E. coli* in the environment and higher growth conditions meant to mimic the type of conditions found within the human body; (3) quantifying the final dose of antibiotic susceptible *E. coli* and resistant ESBL *E. coli* populations during recreational exposure to wastewater-impacted surface waters; and (4) evaluating potential exposure scenarios and prioritizing their driving factors. Combining population ecology and QMRA

approaches will provide insight into risk drivers for environmentally mediated AMR, with a focus on the impact of HGT in the spread of ARG to guide public health protection actions.

(3) Multi-route and multi-pathogen exposures: Wastewater treatment plants (WWTP) provide an essential public service by treating wastewater to remove contaminants so that the treated water can be discharged back into the environment (Rice et al., 2013). The treatment process involves multiple steps that involve the mechanical movement or aeration of wastewater (Dada & Gyawali, 2021; Korzeniewska & Harnisz, 2013). These processes produce bioaerosols that contain pathogens. It is known that bioaerosol exposure increases risks to human health (Lu et al., 2020). Consequently, WWTP working environments pose potential hazards and risks to workers (Malakahmad et al., 2012). WWTP workers are known to have a greater prevalence of self-reported illness and report a variety of symptoms including respiratory, flu-like, and skin ailments (Kallawicha et al., 2016; Khuder et al., 1998; Smit et al., 2005). As a result, this work aims to (1) aggregate information related to multi-pathogen and multi-pathway risk assessment for wastewater workers; (2) develop a QMRA model for multi-pathogen and multi-pathway risks; and (3) create a web-based application to perform and communicate risk calculations for wastewater workers.

Identifying exposure routes for WWTP workers can be difficult, as the tasks that workers are asked to perform can vary greatly from cleaning tasks to office work (Maal-Bared, 2023; Medema et al., 2004). Two exposure routes were identified: (1) accidental ingestion (including hand-to-mouth ingestion for certain exposure scenarios and ingestion

of non-respirable aerosols, and (2) aerosol inhalation (<5 μm) (Randall et al., 2021). These two exposure routes were evaluated over seven different worker tasks: an office setting, walking the WWTP, minor contact, moderate contact, high contact, direct splash, and wastewater lagoon sampling. Eight different pathogens were evaluated: *Cryptosporidium hominis*, *Escherichia coli*, *Giardia duodenalis*, *Legionella pneumophila*, norovirus, rotavirus, and SARS-CoV-2 delta and omicron variants. PPE was also considered including cloth masks, surgical masks, and N95 respirators. A QMRA was preformed using values from the literature and the final risks for each pathogen evaluated. The results were compiled into a web-based application that can be used by WWTP managers to better understand the driving factors of occupational risk.

Using computational tools such as quantitative microbial risk assessment (QMRA) can help evaluate the health risks of these situations and intervention strategies can be modeled to determine the effect these strategies may have on mitigating health risks for the population of interest (Haas et al., 1999). QMRA is a computational method for assessing the risk associated with different conditions of exposure to infectious microorganisms (Haas et al., 1999). The approach is divided into four steps: identifying an environmental microbial hazard (hazard identification), assessing the degree of exposure to the hazard from an activity (exposure assessment), relating a dose to a probability of an adverse outcome (dose response assessment), and characterizing the risk either through point estimates or stochastic analysis (risk characterization) (Gerba, 2015; Haas et al., 2014).

Risk assessment allows for quantitative comparison of the probability of adverse effects for different health endpoints (e.g., infection, illness, or death) based on variable

inputs. Modifying these variables allows for the testing of strategies used to mitigate risk to evaluate and rank relative risk reduction benefits. Sensitivity and scenario analysis can offer mechanistic insights into the most influential variables in a model. Sensitivity analysis can be used to identify the variables that have the most influence on the final result. These variables can be ranked in order of importance (typically influenced by the magnitude of their monotonic relationship with estimated infection risk) and can then be identified as driving factors of risks to inform resource allocation for additional data collection or intervention strategies. Additionally, multivariate indices, such as Sobol' indices, can be used to evaluate variable interactions within a model. This allows for potentially uncovering unexpected variable interactions that could lead to more powerful intervention strategies than single variables alone. Scenario analysis allows for the exploration of model limitations to provide insight into how the final results are impacted by changes in assumptions and/or inputs.

1.2 Goals and objectives of the research

The overall purpose of this work is to model the fate and transport of pathogens and their risk to human health through different exposure routes. The objectives of this research are to (1) identify key uncertainties in each model and (2) incorporate key mechanistic insights to develop a customizable model framework that can be taken and used by decision-makers for their specific settings to better inform the decision-making process. The three research chapters explore these types of models in three different settings: a premise plumbing system representative of a section of a hospital plumbing system

(Chapter 2), a recreational swimming area downstream of treated wastewater effluent discharge (Chapter 3), and multiple occupational exposures at a wastewater treatment plant facility (Chapter 4). A final chapter highlights conclusions and future work (Chapter 5).

Chapter 2 has been published as a journal article titled "Computational framework for evaluating risk trade-offs in costs associated with legionnaires' disease risk, energy, and scalding risk for hospital hot water systems", in *Environmental Science: Water Research & Technology*. This work evaluated the trade-offs between the risk of infection from *Legionella pneumophila*, the risk of scalding, and the cost of energy in heating water to find an optimal water heater temperature setting, or "set point", for a premise plumbing system that is representative of a section of hospital plumbing including a water heater, hot water line and recirculating line with a shower head. Influential variables and data gaps were identified to make recommendations for optimal water heater set points that balance public health and energy sustainability.

Chapter 3 is in preparation for journal submission. This chapter describes the development of a framework to model the population dynamics of *E. coli* susceptible to developing antibiotic resistance (antibiotic susceptible *E. coli*) and ESBL *E. coli* in recreational surface water that contains treated wastewater effluent and in the gastrointestinal tract for the case of non-dietary ingestion of recreational water for an adult during a swimming event. To prevent the spread of antibiotic resistant infections, it is essential to understand the primary drivers of environmental exposures. QMRA is used to quantify the risk due to susceptible *E. coli* and ESBL *E. coli*, with a scenario analysis for different conditions given some uncertainties. A sensitivity analysis will be conducted to

identify the most influential variables in the model and strategic risk management interventions.

Chapter 4 considers multiple pathogens and exposure pathways to risks of occupational exposures within a WWTP and informs management of strategies to reduce overall infection risks for ingestion and inhalation pathways. The objectives of this chapter are to (1) aggregate information related to multi-pathogen and multi-pathway risk assessment for wastewater workers; (2) develop a QMRA model for multi-pathogen and multi-pathway risks; and (3) create a web-based application to perform and communicate risk calculations for wastewater workers. Eight pathogens were evaluated for exposure risks from seven different working tasks. Ingestion infection risks with a health endpoint of gastrointestinal infection and inhalation risks with a health endpoint of respiratory infections were calculated for each pathogen and task where appropriate, and total risks for each health endpoint were also calculated. The web-based application is available to the public for use and displayed as a risk calculator. It is a generalized model that contains options for user input to make the risk calculations site-specific.

Chapter 5 contains concluding remarks from this work and future work to be conducted from these chapters.

CHAPTER 2

COMPUTATIONAL FRAMEWORK FOR EVALUATING RISK TRADE-OFFS IN COSTS ASSOCIATED WITH LEGIONNAIRES' DISEASE RISK, ENERGY, AND SCALDING RISK FOR HOT WATER SYSTEMS

This chapter was published as a journal article: Heida, A., Mraz, A., Hamilton, M.T., Weir, M., Hamilton, K.A., 2022. *Computational framework for evaluating risk trade-offs in costs associated with legionnaires' disease risk, energy, and scalding risk for hospital hot water systems*. Environmental Science: Water Research & Technology 8 (1), 76-97.

2.1 Abstract

Legionella pneumophila are bacteria that when inhaled cause Legionnaires' disease (LD) and febrile illness Pontiac fever. As of 2014, LD is the most frequent cause of waterborne disease outbreaks due to drinking water exposure in the United States. The optimal temperature for the bacteria's growth is between 25–45 °C, and water heaters that are set within this range can become an environment for *L. pneumophila* to grow. The recommended water heater temperature varies across organizations, from 60 °C to kill *L. pneumophila* bacteria to 49 °C to prevent scalding and minimize energy costs. To evaluate these trade-offs, we have developed a computational framework for evaluating an optimal water heater temperature set point for reducing cost and health risks. This framework uses a quantitative microbial risk assessment (QMRA) to assess the risk of infection from a single shower aerosol exposure in terms of disability-adjusted life years (DALY) and costs.

The model demonstrated that the optimal water heater temperature set point for reducing cost and health risks was 55 °C or 48 °C for a common configuration of an electric water heater used in a hospital setting, using a subclinical infection or clinical severity infection dose response model, respectively. Based on these preliminary results, we expect this modeling framework will be able to provide useful insight into the optimal water heater temperature set point for hospitals based on their specific premise plumbing system configurations and constraints and can inform computational tools used to make site-specific decisions.

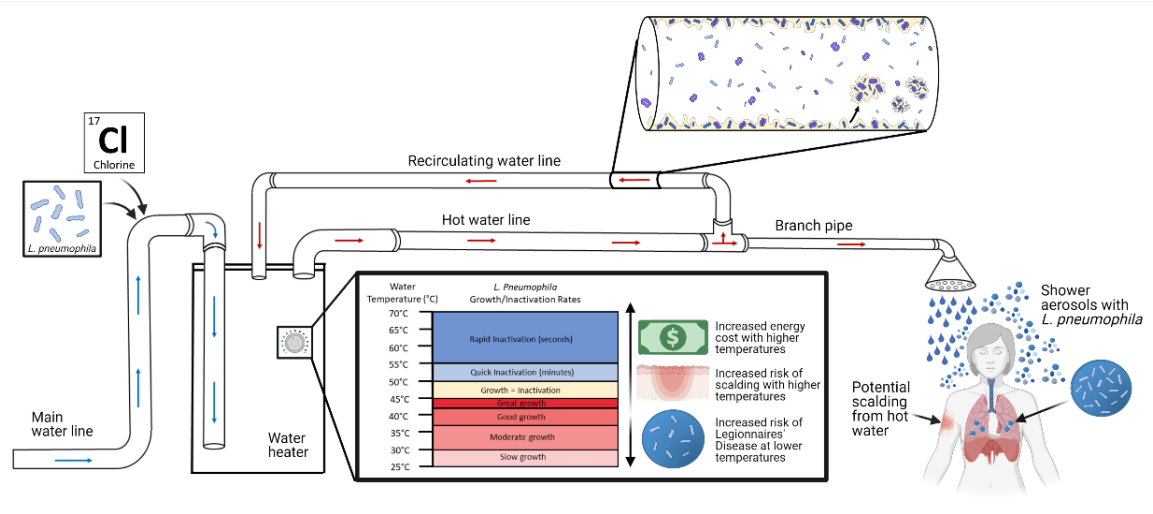

Figure 1. Graphical abstract of a computational framework to evaluate trade-offs in energy, scalding, and Legionnaires' Disease illness risk costs.

2.2 Introduction

Legionella pneumophila (*L. pneumophila*) is a species of bacteria that can cause the pulmonary disease known as Legionnaires' Disease (LD) or the febrile illness, Pontiac

Fever. LD can be contracted when a person is exposed to bacteria-laden bioaerosols (Beer, 2015), most commonly generated by devices such as water fixtures, cooling towers, spa pools, or other sources (Hamilton et al., 2018; van Heijnsbergen et al., 2015). In 2017, there were 7,400 reported cases in the United States, which corresponded to 2.29 cases/ 100,000 persons (CDC, 2018; NASEM, 2019). LD is the most frequently identified cause of waterborne disease outbreaks involving drinking water in the United States and is known to be found in building plumbing systems where they can be aerosolized by numerous water fixtures to cause disease (CDC, 2015; NASEM, 2006). Outbreaks can also result from non-potable exposures to contaminated aerosols originating from other sources (Hamilton et al., 2018). Together, biofilm-associated waterborne pathogens nontuberculous mycobacteria, *Pseudomonas*, and *Legionella* cost the US $2.39 billion annually in hospitalizations and deaths (Collier et al., 2021).

Over 60 different species of *Legionella* spp. have been described (Gomez-Valero & Buchrieser, 2019), with the most commonly implicated species being *L. pneumophila* serogroup 1, which grows at elevated temperatures between 25°C-45°C (Paranjape et al., 2020). For this reason, a water heater can act as a source or amplifier of *L. pneumophila* in indoor environments. Existing management guidance, including that of the World Health Organization (WHO), and the National Academies of Sciences, Engineering and Medicine (NASEM) recommend setting water heater temperatures (the water heater "set point") at 60°C to kill *L. pneumophila* bacteria (NASEM, 2019; WHO, 2007). However, scalding is a concern at these temperatures (Lévesque et al., 2004). Additionally, concerns for increasing sustainability would dictate that the energy cost associated with high water heater temperatures should be minimized. The Consumer Product Safety Commission

(CPSC) and the US Department of Energy (DOE) recommend setting water heater temperatures to 49°C to prevent scalding in addition to minimizing energy costs (DOE, 2016; Shields et al., 2013). A review by Singh et al. (2020) highlighted values from several national and international guidance documents which covered multiple set point recommendations in this range (Singh et al., 2020). Subsequently, a debate continues over what the recommended set point temperature(s) is to prevent *L. pneumophila* growth, reduce scalding risks, and increase energy savings. A quantitative and systematic framework is needed for evaluating these tradeoffs for different plumbing systems and scenarios to support guidance efforts.

Due to its public health importance, regulatory and guidance efforts have focused on LD prevention (ASHRAE, 2018; CDC, 2017; Parr et al., 2015), with a focus on healthcare premise plumbing environments (CMS, 2018) as they are the setting for transmission of a large portion of LD cases (Hamilton et al., 2018). Hospital and residential premise plumbing systems can differ substantially in design, with hospital systems having larger, more complex water systems that can promote *Legionella* spp. growth if not maintained properly, and also serve susceptible populations who are more likely to contract LD due to underlying health conditions (CDC, 2021). The focus of this work will be primarily on a simplified hospital water system.

The financial burden associated with LD has many contributing factors that can vary greatly between cases. In addition to the loss of life experienced from LD, the infection has a significant cost associated with medical treatment, outbreak investigation, and business closures. It is estimated that $434 million is paid by insurers for medical treatment of LD

each year (Collier et al., 2012), with individual costs varying greatly (Lock et al., 2008). In addition to the costs of medical treatment, the cost of investigating a suspected outbreak must be considered as it often requires a great deal of effort to locate and confirm the source of an outbreak (Lock et al., 2008). The economic cost from lost productivity due to business closures at suspected outbreak locations also contributes to the total cost associated with LD, although specific estimates of the dollar value of this cost are not available (Collier et al., 2012; Lock et al., 2008).

Tap water scalds are a potential public health concern and have been well documented in residential settings (Hockey, 2002; Katcher, 1981; Lowell et al., 2008; Potter et al., 2017). Approximately 1500 hospital admissions and 50 deaths from scalding due to excessively hot tap water are reported annually in the United States (Peck et al., 2010). The majority of these cases affect children under 5, disabled persons, and people over age 65. Handicapped patients and geriatric patients are often unable to remove themselves from excessively hot water, and when grouped with young children account for 85% of hot tap water burns (Graitcer & Sniezek, 1988). Scalds can be particularly concerning when elderly populations are exposed to showers and bathtubs where prolonged exposure to elevated temperatures can cause significant damage but go unnoticed initially due to their decreased sensitivity to high temperatures (Graitcer & Sniezek, 1988; NASEM, 2019). Specific cases of this have been documented and can result in extended hospitalization or death (Katcher, 1981). It is acknowledged that the exact circumstances and causes of a scald injury cannot be fully ascertained based on the available scalding data due to factors such as the abuse of children. However, in a study where families were questioned about the nature of a child's burn, 15 out of 17 cases were assumed to be accidental and not child

abuse (Katcher, 1981).This aligns with a 2005 study from the UK that found approximately 90% of pediatric burn cases were accidental (Chester et al., 2005). Public health initiatives have been implemented over the years to reduce preset water heater temperatures in residential settings to lower the risk associated with tap water scalding but were deemed unsuccessful (Katcher, 1981) or had a statistically significant but small (4%) change in risk reduction while increasing the risk of *L. pneumophila* (Barnsley & Barnsley, 2007). Passing legislation to reduce water heater temperatures upon installation in residential settings has been shown to decrease average water heater temperature in some settings (Erdmann et al., 1991), decreasing water scalds. A study of hot water scalds after a change in Ontario, Canada building codes to require residential water heaters in new or renovated buildings to be set at 49°C resulted in a significant decrease in the age-standardized monthly ambulatory scald cases per 100,000 population of 0.01055 and long-term decrease of 0.19 per 100,000, but the number of hospitalized cases did not significantly change (Clouatre et al., 2013). These residential cases emphasize the importance of considering scalding risk while determining optimal water heater temperature set points to reduce *L. pneumophila* in both residential and hospital or healthcare settings.

There is a lack of federal laws and regulations around balancing the risk of scalding with the risk of LD. This is described in the NASEM (2019) report highlighting some ambiguity regarding water temperature control guidance (NASEM, 2019). The Center for Medicare & Medicaid Services (CMS), which has regulatory authority over hospitals, states that patients should not be in "immediate jeopardy" concerning hot water scalds, which is defined as "access to hot water of sufficient temperature to cause tissue injury" (CMS, 2000). This is interpreted by individual states to correspond to a variety of

temperatures. However, this varied interpretation is not inconsistent with true variation in the range of temperatures that can cause tissue damage. Experimental studies on skin burns are understandably rare; using skin from pigs, second-degree burns can be achieved in temperatures as low as 44°C if the skin is exposed for extended periods (Moritz & Henriques, 1947).

Globally, various approaches have been taken regarding scalding and *Legionella* spp. tradeoffs. The Canadian government recommends that residential water heater temperatures be reduced to 49ºC to reduce the risk of scalding and lower energy costs (Government of Canada, 2011). Singh et al. (2020) summarizes findings from 15 guidance documents and interviews of 22 premise plumbing subject matter experts, including nine documents (from the World Health Organization [WHO], US CDC, USEPA, NASEM, Department of Veterans Affairs, European Guidelines, and International Plumbing Code) with all recommendations for hot water temperatures >50°C and most hot water heater temperature recommendations greater than 60°C for *Legionella* spp. control (Singh et al., 2020).

In addition to direct health risks like LD and scalding, sustainability has risen as a priority for the built environment. Consequently, there are national efforts to increase water and energy efficiency that can have unintended consequences for public health. As the popularity of green buildings increases, green certification programs such as Leadership in Energy and Environmental Design (LEED) encourage the minimization of water usage. Decreasing water usage is commonly implemented by installing low-flow fixtures or eliminating the use of potable water for landscaping purposes. While decreasing the use of

potable water is generally encouraged, it can increase the residence time of the water in the premise plumbing system. These increases in water age have been found to have consequences for the water chemistry, temperature, and microbial growth which leaves these new energy-efficient buildings more susceptible to *L. pneumophila* contamination (Rhoads et al., 2016; Rhoads et al., 2015). One factor contributing to increased microbial concentrations is the rapid loss of disinfectant residual in green buildings. For example, it has been found that 60-91% of the chloramine residual is lost after a stagnation time of only six hours in copper pipes (Nguyen et al., 2012; Zhang & Edwards, 2009).

Due to competing objectives for managing water in buildings, trade-offs can exist. The current work focuses on hospital premise plumbing systems, with the intention of applying the modeling framework beyond hospital systems with modified input parameters. To evaluate trade-offs in microbial quality (specifically *L. pneumophila* growth and subsequent risks), energy cost, and scalding risks, we have developed a computational framework for evaluating an optimal water heater temperature set point. The overall risk management goals are to reduce the burdens of illness, injury, and death associated with building water supplies while maintaining an economically viable approach that conserves energy. Weighing these objectives is not always straightforward and a model is designed to provide a framework for judgment by building designers and analysts. The model is not designed to be used as a direct risk communication tool but rather an *in silico* testbed for evaluating tradeoffs. The goal is for this model is therefore to be able to provide useful insight into the optimal water heater temperature set point for hospitals based on their specific premise plumbing system configurations and constraints. As a result, our objectives are: (1) to develop a conceptual model which incorporates the risk of *Legionella*

infection, the risk of scalding, and the cost of energy associated with a specific water heater set point; (2) to demonstrate the utility of applying such a model using a test case of a premise plumbing system from a design that would be representative of a section of the type of system seen in a hospital; and (3) to identify influential factors and data gaps for making recommendations for optimal water heater set points that balance public health and energy sustainability.

2.3 Methods

2.3.1 Modeling Framework

As a starting point, a use-case was developed for a hypothetical hospital room located in the United States that would serve a susceptible hospitalized population, however the generalized model proposed here is not currently regionally- or geographically-specific (although a site- or region-specific model could be adapted from this framework). Our computational framework is composed of three sub-models that are expressed in final terms of daily cost (2020 US dollars per day): (1) *L. pneumophila* bacteria growth, decay, health risk, and subsequent cost of infection and disease; (2) scalding risk and subsequent cost of burn injuries; and (3) energy cost. All models are normalized to "per day" costs. All models rely upon water temperature calculations throughout a premise plumbing system. The water temperature and concentration of *L. pneumophila* being dispensed at the showerhead are calculated for various water heater set points scenarios, from 48°C to 63 °C at intervals of 1°C. This range was chosen to include a setting lower than the recommended temperature from the DOE and the CPSC, to the highest temperature that *Legionella* spp. has been isolated from water (Borella et al., 2004). However, the water

heater used as an exemplar in this model is advertised to deliver a temperature range from 43.3°C to 76.7°C (Westinghouse, 2020). A conceptual flow chart of the described methods is shown in **Figure 2** to help guide the reader through the model.

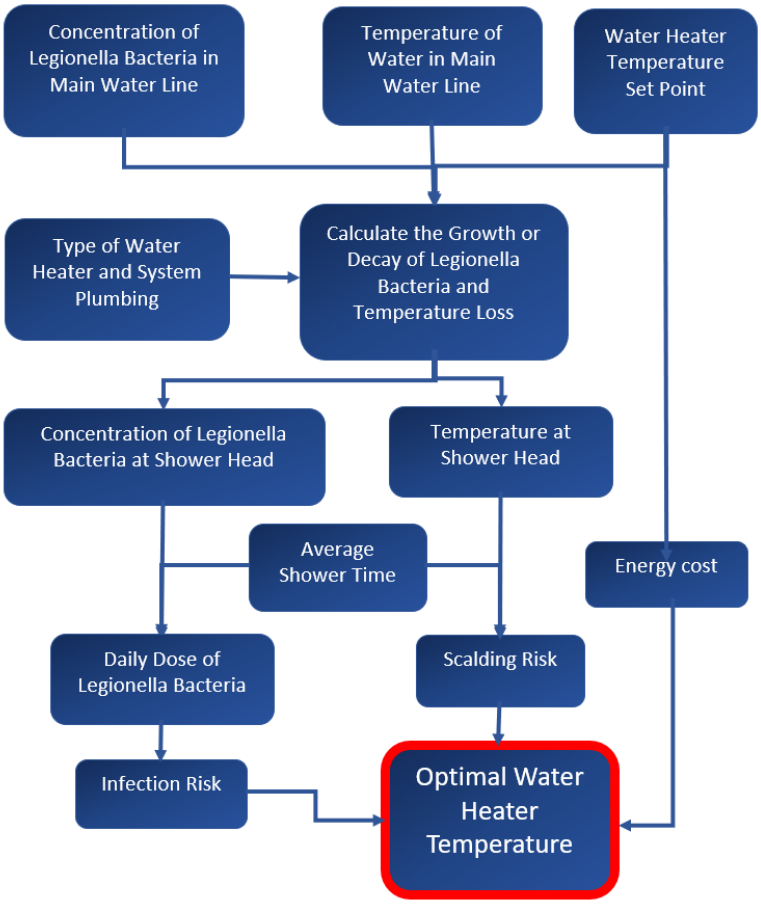

Figure 2. Conceptual flow chart of model sections with select inputs and outputs.

2.3.2 Simplified hot water plumbing system chosen for analysis

Building plumbing systems are extremely heterogeneous, therefore it is not possible to designate a single system that is representative of every situation in this analysis. The example chosen premise plumbing system represents a simplified section of what might

exist in the patient rooms of a hospital that will provide patients with hot water for bathing and showering (Reiling et al., 2008). It is common in the healthcare setting to have at least two large water heaters to meet the building's peak demand. This model is comprised of a single 316L water heater with a 295L storage rating (Westinghouse, 2020) and a hot water outlet pipe ¾" in diameter. Subsequent branches that lead to the outlet at the showerhead are ½" diameter (IAPMO, 2016; Westinghouse, 2020). Only one branching pipe leading to a showerhead is considered in this model, any other branching pipes are ignored. A full recirculating line ¾" in diameter is assumed at the junction of the ½" branching pipe to continually carry water back to the water heater. A cold-water line leading to a mixing valve before the showerhead would also be expected but is excluded for this model. A schematic of the selected system layout can be seen in **Figure 3**.

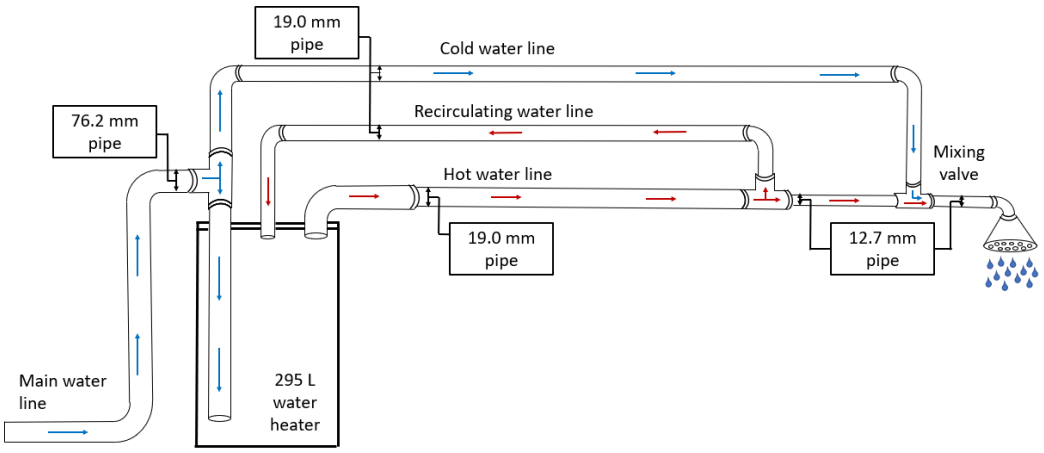

Figure 3. Schematic of selected simplified, exemplary premise plumbing hospital system model.

Large hospitals might choose a steam system instead of water heaters (Watts et al., 2018). The size of the water heaters and the quantity needed to meet peak demand varies for each building and is calculated on a case by case basis (Scruggs, 2020). A water heater of the size chosen (295L) would serve approximately five showers of 59L each to meet peak demand. This would not be considering other fixtures on the floor such as sinks or dishwashers. Two of these water heaters would be optimal for a small hospital floor. Water heaters of this size commonly have ¾" diameter pipe outlets to disperse the hot water throughout the building, so that is why this diameter was chosen (Westinghouse, 2020).This water heater and pipe system is large enough to meet peak demand for a floor with 5-10 showers. The sections below describe heat loss throughout the premise plumbing system and water heater, with an assumption made that heat is not lost through the walls of the water heater.

2.3.3 Water temperature in the water heater

A one-dimensional, multi-node model was selected to approximate the temperature change throughout different sections of the premise plumbing system (Kleinbach et al., 1993). This method divides the water heater into twelve equal nodes (i = 1-12) stacked on top of each other vertically (**Figure 4**). This aligns with standing water heater models (a common configuration in the US) and the stratification experienced will be replicated by the nodes that are assumed to be completely mixed at each timestep (Brazeau & Edwards, 2013). This model for the water heater is similar to a one-dimensional plug flow model with the exception that there is an assumed percentage of mixing between nodes and intermittent flow is ignored. In this water heater, water enters the system from the mainline

at the lowest node, and water exits to the hot water line from the highest node. **Equation 1** represents the temperature of each node based on the flow of water at each timestep. These equations were modified from their original form in Kleinbach et al. (1993) (Kleinbach et al., 1993) as discussed in **Appendix A, Section 1** to allow for implementation in Python.

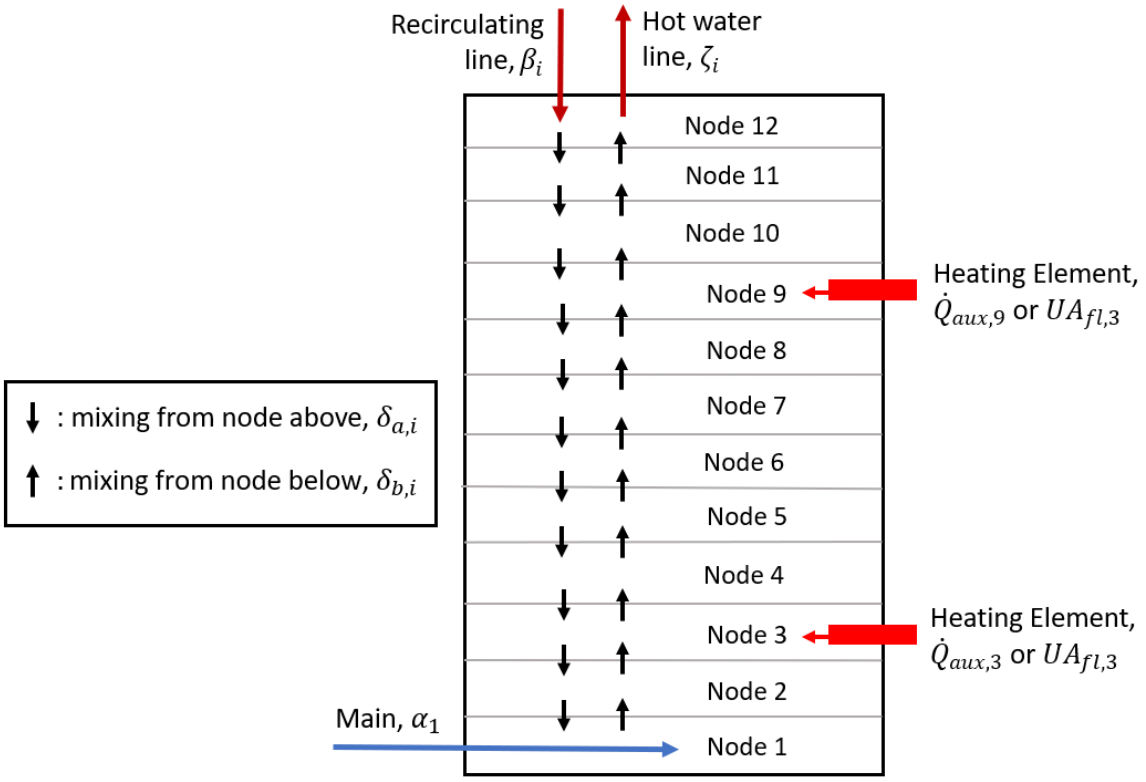

Figure 4. Water heater schematic divided into nodes for temperature calculations following methods used in Kleinbach et al. (1993).

$$T_i(t) = \frac{1}{V_i}\alpha_i v_{main} T_{main} + \beta_i v_{rec} T_{rec}(t-1) + \delta_{a,i} v_{mix} T_{i+1}(t-1) + \delta_{b,i}(v_{mix}+v_{main}) T_{i-1}(t-1) + V_{new} T_i(t-1) \quad (1)$$

V_i is the volume in each node [L], α_i is an indicator variable equal to one at the location of the main line and zero elsewhere, and v_{main} is the flow rate of water entering the water

heater from the main line [L/s]. β_i is an indicator variable equal to one at the location of the recirculating line and zero elsewhere, and v_{rec} is the flow rate of water entering the uppermost node from the recirculating water line [L/s]. $\delta_{a,i}$ is equal to one when a node exists above the node of interest, $\delta_{b,i}$ is equal to one when a node exists below the node of interest, and v_{mix} is the flow rate of fluid mixing between the nodes [L/s]. T_{main} is the temperature of the municipal water from the main line [℃]. Here, T_{main} is assumed to be a concatenated uniform distribution ranging from 16.5°C to 21.5°C in the winter and 17°C to 24°C in the summer (Blokker & Pieterse-Quirijns, 2013), which aligns with the highest main line water temperature (25°C) observed in a study in Poland (Chmielewska, 2018). T_{rec} is the temperature of the water entering the water heater from the recirculating line [ºC], T_i is the temperature of each node [ºC], and V_{new} is the remaining original volume of the node [L].

Once the temperature in each node has been calculated, the average temperature in the tank is measured to determine whether the heating element is on at each timestep. This water heater has two heating elements of equal power placed at the third and ninth nodes. Both are either fully on or fully off. When the heating elements are on, they add 5,500 J of heat to the node at each timestep. This energy input is represented by Q_i in **equation 2** and is equivalent to a 0.05ºC rise in temperature for a 26.33 L node. This is equivalent to 5,500 W at that node (Westinghouse, 2020). When the heating elements are off, it is assumed that a small amount of heat is lost through the elements (Kleinbach et al., 1993). UA_i is the heat lost equal to a 0.005℃ drop in temperature, or 550 W (**Appendix A, Section 1**). The change in the node temperature described by **equation 2** is accounted for at each timestep

after the initial temperature calculation. It is assumed that no heat is lost through the walls of the water heater.

$$T_{i=3,9}(t) = \begin{cases} T_{i=3,9} + Q_{i=3,9}\, t & if\ on \\ T_{i=3,9} - UA_{i=3,9}\, t & if\ off \end{cases} \quad (2)$$

2.3.4 Water temperature in the premise plumbing pipes

Heat loss as water flows through the pipes is modeled using one-dimensional plug flow where heat loss occurs radially. Each pipe was divided into 1 m sections for calculations at each time step and complete mixing within each section of the pipe is assumed. The pipes will experience turbulent flow when water is not stagnant due to their Reynolds number being greater than 4000. Water exiting the water heater is distributed to the pipe system and flows at a constant velocity of 3.04 m/s (**Appendix A, Section 2**). The hot water line ¾" in diameter is assumed to have rubber pipe insulation with a thickness of ½". The branching pipe will have rubber pipe insulation with a thickness of ½" for cases where branching pipe insulation is present as specified in **Table 1**. The ½" rubber insulation has a thermal conductivity of 0.16 W/ mK (Incropera et al., 2007). Insulation thickness on the recirculating pipe is sufficient enough that the temperature loss is not greater than 3.3°C for a pipe length of 24 m (ASHRAE, 2019; Guyer, 2016). The water velocity and insulation are changed during the scenario analysis described in section 4.4.

As the water moves through the pipes, heat is lost through radial convection. The new temperature is calculated using Newton's law of cooling (**equation 3**) and the formula

for heat capacity (**equation 4**), as discussed in **Appendix A, Section 3**. Q is the heat transfer [W], U is the heat transfer coefficient for a multi-layer pipe [W/m^{2}K] (**Appendix A, Section 4**), $T(x)$ is the temperature of the section being analyzed [°C], and T_{env} is the air temperature inside the building of interest surrounding the premise plumbing system, assumed to be uniform distribution ranging from 20°C to 27°C (ASHRAE, 2010; EPA, 2009). c_p is the specific heat of water [J/ kg K] and m is the mass of water inside the pipe section [kg].

$$\frac{dQ}{dt} = U(T(x) - T_{env})dA \tag{3}$$

$$\frac{dQ}{dt} = -c_p \frac{dm}{dt} dT \tag{4}$$

Solving for the temperature in pipe section n ($T_{pipe,n}$) results in **equation 5**. ρ is the density of water [kg/ m^3], v is water velocity [m/ s], and D is the diameter of the pipe [m]. The values for these parameters are summarized in **Table A2**.

$$T_{pipe,n}(t) = (T_{pipe,n-1}(t-1) - T_{env})e^{-\frac{4U}{c_p \rho v D}} + T_{env} \tag{5}$$

2.3.5 Free chlorine residual concentrations throughout the system

The free chlorine concentration is first calculated in the nodes of the water heater based on the fluid dynamics of the system and water temperature. The concentration is calculated at each timestep using **equation 6**.

$$Chl_i(t) = \frac{1}{V_i}\alpha_i v_{main} Chl_{main} + \beta_i v_{rec} Chl_{rec}(t-1) + \delta_{a,i} v_{mix} Chl_{i+1}(t-1) + \delta_{b,i}(v_{mix} + v_{main}) Chl_{i-1}(t-1) + V_{new} Chl_i(t-1) \tag{6}$$

Chl_i is the free chlorine concentration in each node (i = nodes 1-12*)* [mg/ L], and Chl_{rec} is the free chlorine concentration of the water in the recirculating line [mg/ L]. Chl_{main} is the free chlorine concentration in the water entering the system from the main line ranging from 0.01 to 4 mg/ L of chlorine (AWWA, 2018).

Assuming first-order kinetics, the chlorine concentration throughout the plumbing system (Chl) will decay due to temperature and is calculated at each point using **equation 7.** The decay rate of chlorine due to temperature (k_{chl}) is calculated using the Arrhenius equation, which considers total organic carbon concentrations in the system that were estimated to be between 1 and 3 mg/ L (**Appendix A, Section 5)**. Chl_0 is the initial chlorine concentration [mg/ L].

$$Chl(t) = Chl_0\, e^{-k_{chl}t} \tag{7}$$

2.3.6 *Legionella pneumophila* concentration throughout the system

L. pneumophila concentrations are modeled as a function of fluid flow, chlorine concentration, temperature, and time throughout the system (**Appendix A, Section 6)**. The *L. pneumophila* concentration is first calculated in the nodes of the water heater based on the fluid flow of the system at each timestep using **equation 8**.

$$L_i(t) = \frac{1}{V_i}\alpha_i v_{main} L_{main} + \beta_i v_{rec} L_{rec}(t-1) + \delta_{a,i} v_{mix} L_{i+1}(t-1) + \delta_{b,i}(v_{mix}+v_{main}) L_{i-1}(t-1) + V_{new} L_i(t-1) \tag{8}$$

L_i is the *L. pneumophila* concentration in each node (i =1-12*)* [CFU/ L], and L_{rec} is the *L. pneumophila* concentration in the water in the recirculating line [CFU/ L]. L_{main} is the *L.*

pneumophila concentration in the water in the main line [CFU/ L] which is estimated as a lognormal distribution [untransformed mean of 1,012 CFU/L and a standard deviation of 958 CFU/L] (Borella et al., 2004). The growth of the planktonic *L. pneumophila* was limited by an upper bound concentration of $10^{4.17}$ CFU / L, the maximum culturable concentration observed in an experiment where *L. pneumophila* was allowed to remain in stagnant water for 21 days, to avoid a scenario of unrealistic unconstrained growth (Yee & Wadowsky, 1982). This information was combined with kinetic constants (**Appendix A, Section 7**) as a function of chlorine residual, time, and temperature in **equation 9.** C_p is the concentration of planktonic *L. pneumophila* [CFU/ L], k_{temp} is the rate of growth or inactivation due to water temperature for both planktonic and sloughed *L. pneumophila* [s^{-1}], and $k_{p,chl}$ is the rate of inactivation for planktonic *L. pneumophila* due to the chlorine concentration [s^{-1}]. $C_{p,0}$ is the initial concentration of planktonic *L. pneumophila* [CFU/ L].

$$C_p(t) = C_{p,0} e^{(k_{temp} + k_{p,chl})t} \tag{9}$$

2.3.7 Modeling the biofilm sloughing throughout the system

The amount of *L. pneumophila* in the system due to biofilm sloughing at the time that the shower is turned on (t_s) is calculated by **equations 10-11**.

$$C_{s,0} = \frac{A\, C_b\, S_b(t_s)}{D_b V} \tag{10}$$

$$C_s(t) = C_{s,0}\, e^{(k_s + k_{b,chl} Chl + k_{temp}) t_s} \tag{11}$$

The concentration of *L. pneumophila* sloughed from the biofilm, $C_{s,0}$, is calculated using the inner surface area of the pipes, A [cm^2], the quantity of *L. pneumophila* in the

biofilm, C_b [CFU/ cm^2] (Thomas, 2012), the biofilm density D_b [g/ cm^3] (Garny et al., 2009), the mean volume of biofilm per unit area of pipe V [cm^3/ cm^2] (Garny et al., 2009) and the biofilm sloughing rate, $S_b(t_s)$ [g/ cm^2 s] (Garny et al., 2009). The rate of biofilm sloughing will decrease over time with the decay rate k_s if the shower remains on and is assumed to be zero if the shower is off. It is acknowledged that some migration of *L. pneumophila* may occur from the biofilm under stagnant conditions but are considered negligible in comparison to flow events in the absence of data regarding the dynamics of biofilm behavior under prolonged stagnation (Rhoads & Hammes, 2021). There is not currently a consensus about whether the *L. pneumophila* will migrate from the biofilm to the bulk water under stagnant conditions, or whether the rate of migration will change with the plumbing parameters (Rhoads & Hammes, 2021). The change in biofilm sloughing rate, k_s, is modeled using two first order rates that are dependent on how long the shower has been on (Huang et al., 2020). The concentration of *L. pneumophila* sloughed from the biofilm will become inactivated due to chlorine in the system and the water temperature. The inactivation rate due to temperature, $k_{b,chl}$, is given in units of (mg/ L min)$^{-1}$ and is multiplied by the residual chlorine concentration, Chl, so that $k_{b,chl}Chl$ is in units of s^{-1} as seen in **equation 11** (Huang et al., 2020). Biofilm kinetic parameters for *L. pneumophila* in the biofilm are shown in **Table A9** and discussed in **Appendix A, Section 7**.

These equations collectively allowed for computation of the temperature, chlorine residual concentration, decay rate of chlorine due to temperature, decay rate of *L. pneumophila* due to temperature and chlorine, and final *L. pneumophila* concentration from planktonic and sloughed biofilm to be simulated at all points throughout the system at each

timestep (1 s). The temperature, chlorine concentration, planktonic *L. pneumophila*, and biofilm *L. pneumophila* were initialized for a 24-hour period prior to the Monte Carlo for cost analysis (**Appendix A, Section 8**).

2.3.8 QMRA model

The temperature and *L. pneumophila* concentration at the showerhead is used in a quantitative microbial risk assessment (QMRA). QMRA is a computational method for assessing the risk associated with different conditions of exposure to infectious microorganisms (Haas et al., 1999). The QMRA model used here assesses the daily risk of infection from shower aerosol exposure in terms of monetary cost, as determined in the case of health risks through a relationship to disability-adjusted life years (DALYs). This is then combined with models to assess the cost associated with water heater energy consumption and the cost associated with different outcomes related to scalding risk.

A previously derived QMRA model for *L. pneumophila* was used from Hamilton et al. (2018) (Hamilton et al., 2019). The $dose$ is calculated using the concentration of *L. pneumophila* at the showerhead and the shower time (**equation 12-14**).

$$L_{air}(t_s) = C_{Leg}\,(t_s) \sum C_{aero}\, V_{aero} \sum F\, D \tag{12}$$

$$L_{acc}(t_s) = L_{air}(t_s - 1)e^{-d_i t_s} + L_{air}(t_s) \tag{13}$$

$$dose = \sum L_{acc}\, B\, t_s \tag{14}$$

The total *L. pneumophila* concentration at the fixture, C_{Leg}, is the sum of the planktonic *L. pneumophila* C_p and the sloughed *L. pneumophila* C_s over the duration of the

shower. The dose is calculated using equations by multiplying the *L. pneumophila* concentration C_{Leg} [CFUs / L s], the concentration of aerosols C_{areo} [# aerosols / m^2] (*i.e.* the number of water droplets of diameter i in each respirable size bin 1-10 μm, with the majority of respirable droplets falling in the 1-5 μm range), the volume of aerosols V_{areo} [L / # aerosols], the fraction of *L. pneumophila* that partition to each of the aerosol diameters, F, the alveolar deposition efficiency, D, the rate of inhalation, B [m^3/min], the aerosol removal rate, d_i (Huang et al., 2020), and the duration of the shower (**Appendix A, Section 9**), t_s [s] (Hamilton et al., 2018). The *L. pneumophila* concentration released into the air, $L_{air}(t_s)$, is used to calculate an air concentration assuming accumulation of aerosols, $L_{acc}(t_s)$, and removal due to ventilation at a rate of d_i which was found using a weighted average of aerosol size (Hamilton et al., 2018) and aerosol decay rate (Huang et al., 2020). The accumulated concentration of aerosols is used with the average breathing rate to determine the accumulating dose, $dose$, that is inhaled at each timestep.

Two dose response models have been previously used to describe *L. pneumophila* subclinical infection or clinical severity infection, where a subclinical infection would be a case not requiring seeking of medical attention or potentially Pontiac fever, and a clinical severity infection would be a case requiring seeking of healthcare resources (Armstrong & Haas, 2007, 2008). The dose response parameter for subclinical infection (r_s) and clinical severity infection (r_c) were used and were modeled as lognormal distributions. For subclinical infection, the risk of infection ($Risk_{inf}$) can be calculated with **equation 15**. The risk of illness from subclinical infection can be calculated from the risk of infection modified to be the risk of illness using the morbidity ratio for elderly individuals (MR_e) in

equation 16 (Weir et al., 2019). For the clinical dose response, the risk of illness can be calculated directly from the dose response parameter for clinical severity infection (r_c) and the dose of *L. pneumophila* with **equation 17**. The use of the clinical severity endpoint as representative of illness is supported by an analysis that used a dose response model with the same order of magnitude median effective dose (N_{50}) used to reproduce epidemic curves that aligned with well-documented LD outbreaks (Prasad et al., 2017).

$$Risk_{\text{inf}} = 1 - e^{-r_s\, dose} \tag{15}$$

$$Risk_{ill} = Risk_{inf}\, MR_e \tag{16}$$

$$Risk_{ill} = 1 - e^{-r_c\, dose} \tag{17}$$

The cost associated with the risk of illness for each daily showering event, $C_{illness}$, was calculated in **equations 18-19**. An approach to monetizing a DALY was taken as described in Robinson and Hammitt (2019) (Robinson et al., 2019), making use of the value of a statistical life year (VSLY). A VSLY is derived from the value of a statistical life (VSL), which is not the value that is placed on saving an identified life with certainty but rather is indicative of an individuals' willingness to exchange money for a small change in their own risk (Robinson et al., 2019). A recent (2020) estimate for the United States VSL corrected for inflation and changes in real income with a low, central, and high estimate of 5.3M, 11.4M, and 17.4M USD, respectively was used (US Department of Health and Human Services, 2021). In order to calculate a VSLY from a VSL, the VSL must be divided by an estimate of the remaining life years (remaining life expectancy) used to estimate the underlying VSL estimate, not the remaining years applicable to the impact

of the policy since the idea is to convert a VSL to an equivalent VSLY. A simplifying assumption was made that a constant VSLY was applicable and therefore that the value of mortality risk reduction increases with life expectancy i.e. decreases with age, averaging health status over future life years; the limitations of this assumption are discussed further elsewhere (Robinson et al., 2019; Viscusi, 2005; Viscusi, 2008). The estimates for VSL derived by the US Department of Health and Human Services (US Department of Health and Human Services, 2021) were derived from a meta-analysis of VSL values published in the literature (Robinson & Hammitt, 2016), and therefore, it was not possible to ascertain a single life expectancy value. To compute a remaining life expectancy, the difference was taken between the US average life expectancy in the year the meta-analysis was performed (2013) with a point estimate of 78.8 years (Arias et al., 2017) and a normal distribution computed for the age of the living adult (>18 years) population in December 2013 with a mean of 36.0 years and standard deviation of 18.7 years (US Census Bureau, n.d.). The disability adjusted life year for LD ($DALY$) of 0.97 years was used from a study of a Netherlands population and assumed to be representative of a US population (Hamilton et al., 2019). QMRA parameters are summarized in **Table A10.**

$$C_{illness} = Risk_{ill} * DALY * VSLY \tag{18}$$

Where:

$$VSLY = \frac{VSL}{Life\ expectancy\ of\ adult\ used\ to\ compute\ VSL} \tag{19}$$

2.3.9 Scalding model

A set of simple linear regressions for scalding risk as a function of water temperature and shower time were developed based on data from Moritz and Henriques (1947) (**Appendix A, Section 10**). Burns from Moritz and Henriques (1947) were categorized by epidermal injury and epidermal necrosis for humans and pigs. Human data were used, and the regressions were employed to define temperature-time combinations that resulted in each injury type (no injury, injury, or necrosis). Based on the temperature computed at the point of use (at the showerhead) and the shower duration, an injury category was assigned along with a corresponding cost. The range of temperatures considered in this model ranged from 48°C to 63°C. The shower times were modeled as a truncated normal distribution with a mean of 7.8 minutes and a standard deviation of 1.2 minutes (DeOreo et al., 2016). The reaction time, *i.e.* the time an elderly person would be exposed to scalding hot water before moving away from the water, was modeled as a uniform distribution from one to five seconds.

The daily scalding costs ($C_{scalding}$) were approximated as uniform distributions in 2020 US dollars (USD) that ranged from 142-222 USD for a clinical visit for an injury, and from 629-863 USD for an emergency room visit (necrosis injury category) (Blue Cross Blue Shield, 2009). There is uncertainty associated with these values as they can vary based on insurance types, geographic region, individual susceptibilities, and the care provider.

2.3.10 Energy cost model

The daily energy cost (C_{energy}) used in this model was calculated in USD/ day for a storage tank water heater using the Department of Energy's (DOE) method for estimating costs and efficiency of water heaters (DOE, n.d.). This was done by first calculating the amount of water used and multiplying by the difference in water temperature from the desired set point (Q_{degree}) as shown in **equation 20** [(L/ day) K]. The average water use per capita was estimated as the national average of 291.47 L (77 gallons) per day (Dieter et al., 2018). However, this includes both cold and hot water. The U.S. Geological Survey estimates that the low end of shower water usage to be two gallons of water per minute (USGS, 2021). Assuming an average shower time of 7.8 minutes, the average hot water usage for showering (Q_{in}) is approximately 59 L/ day. Therefore, an additional 59 L/ day will need to enter the water heater from the main line to replenish the water used for the shower. This quantity is multiplied by the difference between the temperature set point ($Setpt$) and the main line temperature (T_{main}). The cost to heat the water that has cooled in the recirculating line was also considered. The volume of water that needed to be reheated was calculated from the flow rate in the recirculating line over 24 hours (Q_{rec}). The difference in temperature that the water needed to be reheated was calculated from the difference between the set point and the water temperature at the end of the recirculating line (T_{end}).

The cost to heat a liter of water by one degree ($c_{degree\ liter}$) is calculated in **equation 21**. The price per kWh (P_{kWh}) varies by region across the US for residential energy usage with the average from the US Energy Information Administration (EIA) being 13.04 cents

per kWh in 2019 (U.S. Energy Information Administration, n.d.). The Energy Factor (*EF*) is a standardized metric used for the energy efficiency of different appliances. It is calculated as a ratio of the theoretical energy use required during a 24-hour period over the actual energy use of the appliance. For water heater tanks vary between 0.904 and 0.95, with some manufacturers of electric heaters claiming higher values (ENERGY STAR, 2008). A higher EF corresponds to a more efficient water heater. For this model, the *EF* was modeled as a uniform distribution ranging from 0.904 to 0.95. c_p is the specific heat of water in J/ kg K and is multiplied by the conversion factor from Joules to kilowatt-hours [2.77×10^{-7} kWh/ J] to reach c_p units of kWh/ kg K.

The daily energy cost (C_{energy}) is calculated in **equation 22** with the cost to heat a liter of water by one degree ($c_{degree\ liter}$) multiplied by the amount of water used with temperature difference (Q_{degree}).This temperature will vary based on the geographical region the premise plumbing system is in, thus, the energy cost will change greatly based on the difference between the main water line and the water heater set point. Energy parameters are summarized in **Table A12**.

$$Q_{degree} = Q_{in}\,(Setpt - T_{main}) + Q_{rec}\,(Setpt - T_{end}) \tag{20}$$

$$c_{degree\ liter} = \frac{P_{kWh}\,c_p\,(2.77e{-}7)}{EF} \tag{21}$$

$$C_{energy} = c_{degree\ liter}\,Q_{degree} \tag{22}$$

2.3.11 Integration of infection risk, scalding risk, and energy cost models

The total cost for each water heater setpoint was calculated with **equation 23**. Once the total cost for each set point was calculated, the minimum cost was selected from the array.

$$C_{total} = C_{infection} + C_{scalding} + C_{energy} \quad (23)$$

2.3.12 Scenario analysis and sensitivity analysis

To investigate various scenarios for varying the branching pipe insulation, pipe length, water velocity, and dose response parameter, 15 additional test cases were considered (**Table 1**). A sensitivity analyses was conducted to examine the impact of individual variables (input-output correlations using Spearman rank correlation coefficients) for all cases. Additionally, for Case 0 (insulation of the branch pipe, 26 m long recirculating line, 3.04 m/s velocity of water, and subclinical dose response parameter), interactions between variables and their impact on the model output was analyzed using a global Sobol sensitivity analysis. The Spearman rank correlation coefficient was calculated using the Spearmanr function from the stats package in Python. A Spearman rank correlation coefficient ranges from -1 to 1, indicating that parameters closer to these limits have a strongly negative or positive correlation in ranks whereas a value of zero would indicate no meaningful relationship. Parameters with *p* values less than 0.05 were determined to be statistically significant. The Sobol global sensitivity analysis was performed with the SALib package in Python (Herman et al., 2017). For each variable that was represented as a distribution on the model, the total, first-order, and second-order indices were calculated. Total-order indices (ST) account for the influence of a single variable as well as higher-

order effects over the entire parameter space. First-order indices (S1) measures the influence of a single variable on the output and are displayed by the filled circles near each variable name. Second-order indices (S2) measures the contribution of interactions to the output as displayed by the thickness of the gray connecting line between two variables. Higher values of sensitivity indices represent a greater influence of the parameter(s) on the model output. Variables below the threshold value of 0.005 in the SALib package were considered non-influential and were not displayed.

2.3.13 Computational specifications

All simulations were conducted in Python v 3.6.8. Monte Carlo simulations were conducted with 10,000 iterations (Burmaster & Anderson, 1994), a 24-hour model initialization period, and using random sampling. Several Python libraries were used including torch, torch.nn, torchdiffeq (odeint), matplotlib,pyplot, matplotlib.patches (Patch, math), torch.distributions, time, typing, pickle, numpy, pandas, seaborn, os, scipy, SALib.sample (saltelli), SALib.analyze (sobol), SALib.tesst_functions (Ishigami), itertools, math (pi), and matplotlib.legend_handler (HandlerPatch) (see supplemental code files).

Differential equations were solved using the 5^{th} order Dormand-Prince method, an adaptive step ODE solver with a relative tolerance limit of .0001 and absolute tolerance limit 0.01 (Dormand & Prince, 1980). We implement ODE equations using PyTorch and solve these equations using the "torchdiffeq" package (Paszke et al., 2019). This architecture allows for parallel processing of thousands of simulations at once, GPU acceleration, and end-to-end differentiability. In particular, our system's differentiability

allows users to tune simulation parameters to real-world data using gradient descent. This enables integration and joint optimizations with other machine learning systems and neural differential equations (Chen et al., 2018).

2.4 Results

2.4.1 Simulation of conditions throughout the premise plumbing system

The temperature, chlorine, planktonic *L. pneumophila* concentration, sloughed (biofilm-associated) *L. pneumophila* concentration, and remaining *L. pneumophila* in the biofilm were calculated throughout the system for all simulated time points for a base case (Case 0) as well as different combinations of system parameters (Case 1-15) (**Appendix A, Section 13**). The values for the temperature, chlorine, and planktonic *L. pneumophila* concentration were displayed over time in the heatmaps in **Figure 5** for Case 0 for select water heater set points to demonstrate trends. As the water heater temperature set point was increased, the temperatures throughout the system increase. Despite the variation in set point from 48°C to 63°C, free chlorine residual concentrations throughout the system were all at low concentrations until chlorinated water from the main line entered as the shower turned on (t_s = 1). The manufacturer-reported lower limit of the analytical range for some commonly used spectrophotometric methods for free and/or total chlorine in practice is approximately 0.02 mg/ L (low range kits) to 0.2 mg/L (high range kits), with measurements below this range having a greater associated error and therefore indicating some potential challenges with measuring very low chlorine concentrations in practice (Hach, 2018). The concentration of *L. pneumophila* in both the planktonic form and within the biofilm decreased as the water heater set point was increased over the range of set

points. The planktonic *L. pneumophila* concentrations remain relatively constant at a set point between 48°C and 54°C, but will decrease rapidly in the heated regions ≥60°C. Similarly, the concentration in the biofilm also rapidly decreases with an increase in temperature. The majority of the *L. pneumophila* in the system is originating from the biofilm rather than the planktonic state (the ratio of planktonic to biofilm ranges from ~1.6% to 2.4% in the current model), consistent with estimates of about only 5% of microbial cells thought to exist in the planktonic state in a pipe (Flemming et al., 2002). The branching pipe will be stagnant until the shower is turned on and consequently, the temperature in the branch is more isolated and consequently less impacted by the set point temperature until the shower is turned on. The biofilm residing on the inner surfaces of the water heater was not considered due to a high degree of heterogeneity and complexity related to biofilms within the water heater.

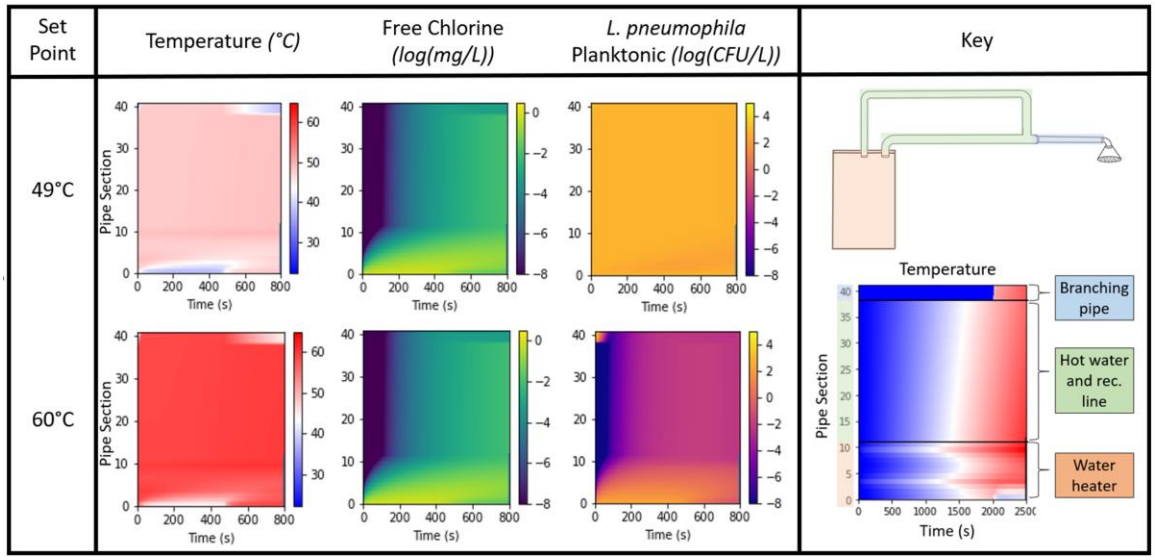

Figure 5. Median of 10,000 Monte Carlo iterations for temperature, free chlorine concentration, and *L. pneumophila* concentration in bulk water for Case 0 for 49°C and

60°C. Case 0 includes insulation of the branch pipe, 26 m long recirculating line, and velocity of the water is 3.04 m/s.

2.4.2 Identification of optimal water heater set point

The parameters of the plumbing system calculated throughout the model were used to calculate the costs of infection, energy usage, and scalding per showering event as shown in **Figure 6** for an elderly hospital room occupant for each scenario. The total cost was calculated from the sum of these values for subclinical and clinical dose response parameter scenarios. The optimal water heater set point corresponds to the minimum total cost for each set of conditions. Considerations regarding the magnitude of each cost are included in the discussion. The optimal water heater temperature set point based on the minimum total cost for each case is shown in **Table 1**. Optimum set points ranged from 48°C to 59°C for all cases.

A large difference in optimal set point was observed depending on the choice of dose response model (subclinical or clinical severity infection) (**Figure 6**). The use of a subclinical infection dose response model generally resulted in higher optimal setpoints (55-59°C) due to a more conservative treatment of the health endpoint (any infection vs. an infection requiring clinical attention) and therefore in the cost calculations will result in a prioritization of infection risks compared to the other considerations. Therefore, for the case of subclinical dose response, the infection cost is the driver of the total cost, whereas the energy cost is the driver of total cost in the scenario where the clinical dose response parameter is used. For the base case scenario (Case 0), optimum set points were determined to be 56°C if using a subclinical dose response model and 48°C if using a clinical severity

dose response model (Case 8). These had median cost values of 88.31 USD and 3.47 USD respectively. The costs for the subclinical dose response parameter ranged from 86.25-2,902 USD while the costs for clinical dose response ranged from 3.47-11.73 USD. This is expected due to the more conservative treatment costs associated with subclinical infection and emphasizes the importance of the choice of dose response parameter for the scenario of interest.

Table 1. Case conditions tested on this model. Variations included insulation on the branching pipe, pipe length, water velocity and dose response parameter. Additionally, results for optimal set point for tested case conditions and median costs associated with optimal set point are also displayed.

Scenarios					Decision analysis result	Results at optimum set point					
Case Number	Branch Insulation	Pipe Length	Water Velocity	Dose Response Parameter	Optimal Temperature Set Point	Energy cost (USD-5th, 50th, 95th)	Microbial risk cost (USD- 5th, 50th, 95th)	Median scald cost (USD-5th, 50th, 95th)	Total cost (USD-5th, 50th, 95th)	Median microbial risk (5th, 50th, 95th)	Scald risk (no injury, injury, necrosis)*
Case 0	Yes	26 m	3.04 m/s	Subclinical	56°C	2.50 3.82 5.83	3.69 84.43 7356.96	0.00 0.00 0.00	7.54 88.31 7360.23	1.58E-05 2.82E-04 3.64E-03	1.00 0.00 0.00
Case 1	Yes	52 m	3.04 m/s	Subclinical	56°C	4.76 7.26 11.08	3.70 82.89 6912.72	0.00 0.00 0.00	11.19 90.13 6917.08	1.61E-05 2.78E-04 3.80E-03	1.00 0.00 0.00
Case 2	Yes	26 m	1.52 m/s	Subclinical	55°C	2.43 3.66 5.68	7.78 185.37 18060.44	0.00 0.00 0.00	11.76 188.62 18063.78	3.46E-05 6.30E-04 9.06E-03	1.00 0.00 0.00
Case 3	Yes	26 m	1.90 m/s	Subclinical	56°C	2.50 3.81 5.82	5.97 141.37 10694.75	0.00 0.00 0.00	9.80 145.33 10698.88	2.64E-05 4.69E-04 6.35E-03	1.00 0.00 0.00
Case 4	Yes	52 m	0.30 m/s	Subclinical	55°C	4.30 6.49 10.08	118.85 2903.31 210791.99	0.00 0.00 0.00	126.03 2911.33 210798.13	5.15E-04 9.95E-03 1.24E-01	1.00 0.00 0.00

Case 5	Yes	52 m	1.52 m/s	Subclinical	55°C	4.59 6.92 10.76	8.08 185.23 18313.66	0.00 0.00 0.00	15.35 192.59 18327.57	3.45E-05 6.31E-04 8.95E-03	1.00 0.00 0.00
Case 6	Yes	26 m	0.30 m/s	Subclinical	56°C	2.42 3.69 5.63	125.61 2897.83 195685.96	0.00 0.00 0.00	129.21 2902.13 195690.37	5.26E-04 9.83E-03 1.18E-01	1.00 0.00 0.00
Case 7	No	26 m	3.04 m/s	Subclinical	59°C	2.72 4.17 6.39	3.62 82.05 8068.23	0.00 0.00 0.00	7.83 86.25 8071.15	1.55E-05 2.83E-04 3.69E-03	1.00 0.00 0.00
Case 8	Yes	26 m	3.04 m/s	Clinical	48°C	1.88 2.87 4.42	0.02 0.31 13.52	0.00 0.00 0.00	2.14 3.46 16.65	8.17E-08 8.02E-07 7.78E-06	1.00 0.00 0.00
Case 9	Yes	52 m	3.04 m/s	Clinical	48°C	3.56 5.44 8.40	0.03 0.35 13.92	0.00 0.00 0.00	3.93 6.21 19.53	9.63E-08 9.38E-07 8.03E-06	1.00 0.00 0.00
Case 10	Yes	26 m	1.52 m/s	Clinical	48°C	1.87 2.86 4.40	0.04 0.64 27.50	0.00 0.00 0.00	2.25 3.84 30.18	1.38E-07 1.67E-06 1.70E-05	1.00 0.00 0.00
Case 11	Yes	26 m	1.90 m/s	Clinical	48°C	1.87 2.86 4.41	0.04 0.49 23.18	0.00 0.00 0.00	2.21 3.68 26.43	1.14E-07 1.28E-06 1.37E-05	1.00 0.00 0.00
Case 12	Yes	52 m	0.30 m/s	Clinical	55°C	4.21 6.49 9.97	0.20 4.66 229.80	0.00 0.00 0.00	5.71 11.78 238.22	6.32E-07 1.18E-05 1.34E-04	1.00 0.00 0.00
Case 13	Yes	52 m	1.52 m/s	Clinical	48°C	3.53 5.40 8.33	0.05 0.68 31.33	0.00 0.00 0.00	4.08 6.65 36.82	1.59E-07 1.81E-06 1.82E-05	1.00 0.00 0.00
Case 14	Yes	26 m	0.30 m/s	Clinical	56°C	2.42 3.69 5.62	0.21 4.55 299.61	0.00 0.00 0.00	3.51 8.51 302.36	6.63E-07 1.17E-05 1.34E-04	1.00 0.00 0.00
Case 15	No	26 m	3.04 m/s	Clinical	48°C	1.88 2.87 4.42	0.02 0.31 13.75	0.00 0.00 0.00	2.14 3.45 16.98	8.23E-08 8.01E-07 7.91E-06	1.00 0.00 0.00

*proportion of scald model iterations that fall within the injury category

Subclinical dose response model		Clinical severity infection dose response	
(A) Effect of branch insulation			
Case 0 – with insulation	Case 7- without insulation	Case 8 - with insulation	Case 15 - without insulation
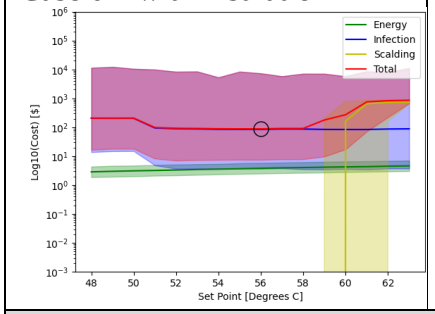	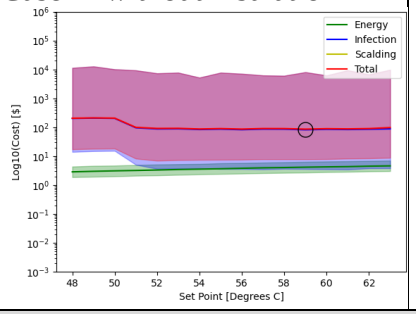	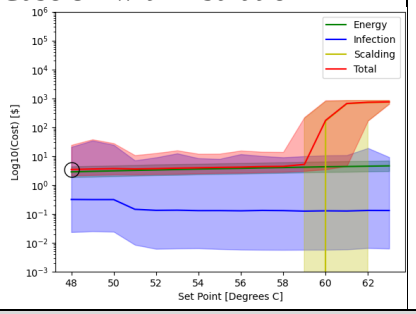	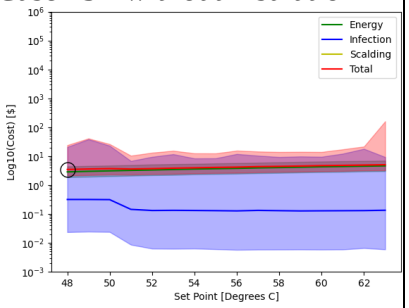
(B) Effect of length of hot water line and recirculation line at a faster velocity			
Case 0- short line, fast velocity	Case 1- long line, fast velocity	Case 8 - short line, fast velocity	Case 9 - long line, fast velocity
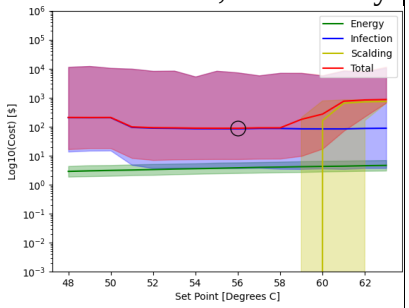	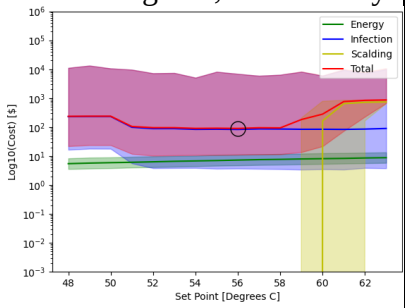	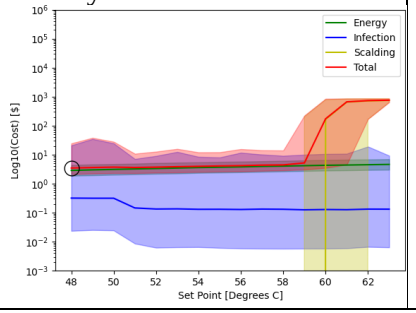	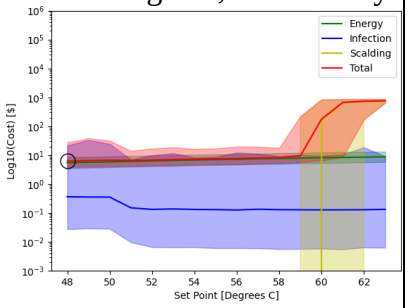

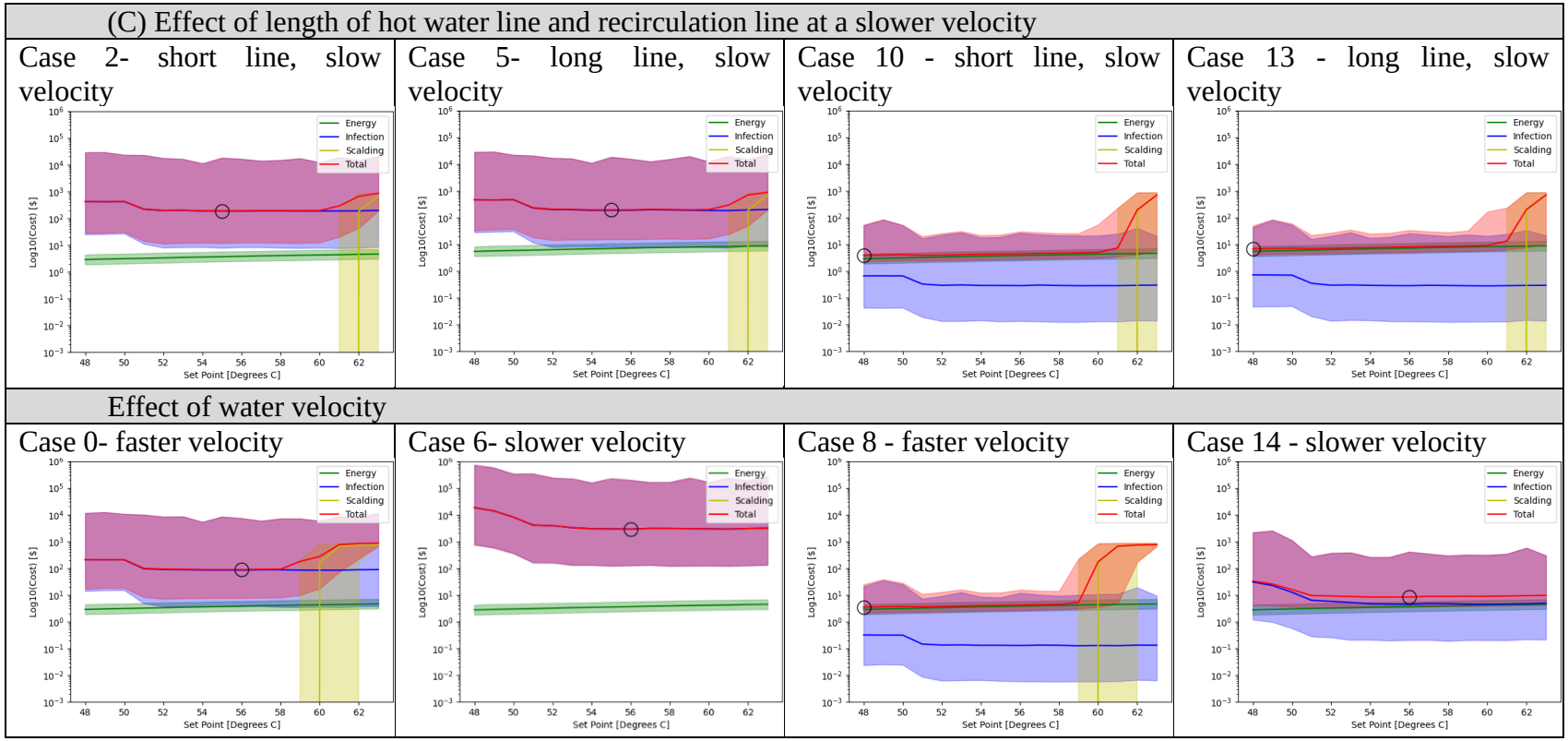

Figure 6. Comparison of select scenarios and effect on total cost and corresponding optimum water heater set point. The dark lines of each color are the median for that cost with the shaded regions being the 5th and 95th percentiles. The optimal water heater temperature to minimize costs has been circled on each graph.

2.4.3 Scenario analysis for multiple cases and sensitivity analysis for Case 0

2.4.3.1 Spearman rank correlation for all cases

The associated Spearman rank coefficient for correlations between input distributions and the total cost for all cases is shown in **Figure 7 (left panel)**. For subclinical cases (0-7), there was a strong negative correlation with the shower duration, biofilm density, and VSLY (i.e., Monte Carlo variable for remaining life expectancy). There was a strong positive correlation with the initial CFU in the biofilm. Using a clinical dose response model (cases 8-15), the response time ("jump time"), the price per watt, and the initial CFU in the biofilm show the largest positive correlation coefficients and are statistically significant ($p < 0.05$), indicating that these parameters are the most influential parameters for the clinical dose response. The shower duration, biofilm density, and VSLY show a negative correlation.

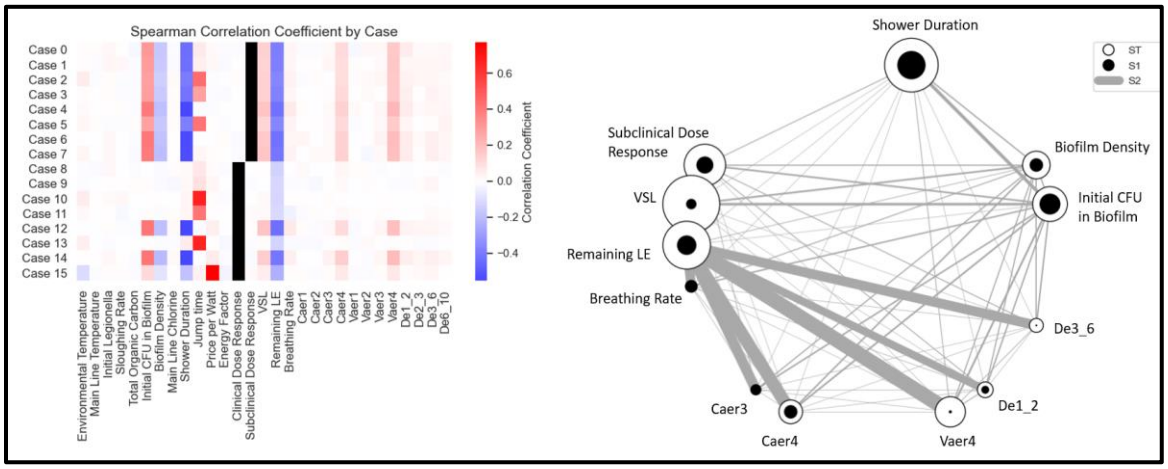

Figure 7. Left: Spearman rank correlation coefficient heatmap for subclinical and clinical dose response. Parameters shown in black do not apply to the indicated scenario. Right:

Sobol Global Sensitivity Analysis for Case 0. The total-order indices (ST) are shown by hollow circles. First-order indices (S1) measures the influence of a single variable on the output. Second-order indices (S2) measures the contribution of interactions to the output.

2.4.3.2 Sobol global sensitivity analysis for Case 0

The Sobol global sensitivity analysis for Case 0 is shown in **Figure 7 (right panel)**. The variables with significant indices were the shower duration, dose response, VSLY (remaining life expectancy and VSL Monte Carlo parameters), select aerosolization values, initial CFU in the biofilm, biofilm density, and breathing rate. The values of the indices are represented by the size of the circles. The variables with the largest total and first-order indices were shower duration, initial CFU in the biofilm, subclinical dose response, and VSLY (remaining life expectancy). These four parameters were influential independently as well as with other parameters. The most notable second-order index as displayed by the thickness of the gray connecting lines is between the remaining life expectancy to the breathing rate and select aerosolization values, which have non negligible correlation coefficients on the final costs. These variables together have a notable influence on the model, also confirmed by the Spearman correlation coefficients for Case 0 (**Figure 7**). The strong interactions between these variables occur in the intermediate calculations for the cost of infections.

2.4.4 Scenario analysis

The scenario analysis varied several parameters determined to be uncertain (**Table 1**) including the branch insulation (insulated vs. not insulated), length of the recirculating line (26 or 52 m), the velocity of water in the pipes (0.30 to 3.04 m/s), and dose response model (subclinical or clinical severity infection). A comparison of select scenarios is shown in **Figure 6** for effects of changing the branch pipe insulation (5A), varying the length of the hot water line and recirculating line (5B-C), and varying the water velocity (5D).

Insulation on the branching pipe leading to the shower has the greatest effect on the scalding cost. Removing the insulation from the branch will drastically decrease the scalding risk for the proposed model (**Figure 6A**). The length of the pipe and the recirculating line will also influence the energy cost. As the water in the pipe has increasing time to cool down, the water heater must use more energy to heat the recirculated water back to the set point temperature (**Figure 6B**). At slower water velocities, the infection cost increases in addition to the energy cost for longer pipes (**Figure 6C**). Slower water velocity increases the time water spends in the pipe and recirculating line and the water can reach lower temperatures that are better for *L. pneumophila* growth. The increased *L. pneumophila* growth increases the infection cost (**Figure 6D**). As noted in Section 4.2, the dose response parameter chosen will have the greatest impact on determining which variable has the greatest influence over the optimal set point. The selection of a subclinical dose response parameter increases the cost of infection, which will be greater than the energy cost and unaffected by the risk of scalding until temperatures of 59°C. Using the

clinical dose response parameter lowers the cost of infection to be at the same order of magnitude or lower than the energy cost, making energy cost the most influential variable. As a result, it is recommended that the dose response chosen should be carefully considered prior to conducting a decision analysis. The importance of considering multiple dose response models has previously been emphasized for QMRA of other pathogens (Van Abel et al., 2017).

2.5 Discussion

The physical system modeled was a simplified model of what might be found in a hospital plumbing system leading to a patient room. A water heater, hot water line, recirculating line, and branching pipe were included for analysis. The cold water line and any mixing valves were excluded from this model as a simplifying assumption but will be necessary for a full consideration of risk; incorporating mixing would also presumably lower the scalding risk even at higher temperatures but could present opportunities for growth on the surfaces of valve components or the introduction of zones of stagnation into the system that will vary depending on the placement of the valve (Brûlet et al., 2008; Hugo Johansson et al., 2006; Rasheduzzaman et al., 2020). The branching pipe from the hot water line to the shower was the only branching pipe considered, although many other lines leading to other showers, sinks, and equipment would also be present in a real building. The water heater chosen is large and could be used in a hospital setting, although many buildings will have more than one large water heater in service to meet peak demand. Additionally, some hospitals may use point-of-use heating devices or thermostatic devices

that limit temperature ranges to below scalding temperatures. The impact of different water heater types, valves, and pipe materials was not considered. However, with additional information, this model can presumably be scaled up and applied to a more complete hospital premise plumbing configuration but requires validation in order to do so. Demand information from a residential setting was used for describing individual patient water demand in this model and may not fully describe hospital water demand; water demand can be modified if specific information is available for a particular hospital or other setting.

Sufficient information is not yet available to quantitatively predict concentrations of *L. pneumophila* as a combination of water quality factors. It is presumed that different water qualities such as soft vs. hard water, warm vs. cold water, or surface water vs. groundwater sources would impact quality and therefore the propensity for *Legionella* growth. In areas where hard water is an issue, water softeners may also be employed which will affect water chemistry as well. Investigation of the effects of softeners was beyond the scope of the current modeling effort, but recent data from an Arizona study of a commercial building indicated potential removal of free chlorine residual by a water softener system, which could impact *Legionella* spp. growth (Richard et al., 2020). Water quality factors such as high organic carbon (e.g. total organic carbon [TOC] or assimilable organic carbon [AOC]) may also lead to the growth of opportunistic pathogens (LeChevallier et al., 1993, 1996; van der Kooij, 1990; Volk et al., 2000). The relative composition of AOC and TOC may play a role in *Legionella* spp. growth and differ between hot and cold water (van der Kooij et al., 2017). TOC was addressed in the *L. pneumophila* kinetic parameters based on

available experimental data (AWWA, 2018), however more detailed analysis of the relationship between the type of organic carbon present and *L. pneumophila* could be accounted for in a more detailed model.

Hard water caused by the presence of multivalent cations can cause scaling (Van der Bruggen et al., 2009). Scaling in the plumbing system was not considered for this model despite its potential to influence the lifetime of the water heater, add regular maintenance costs, and increase energy cost because buildup on the heating elements will decrease heat transfer efficiency (Hofman et al., 2007). Different methods for scaling prediction have been proposed, but the complexity of scaling leads to many limitations that are acknowledged (Brink et al., 2004; International Desalination Association, 2006). New methods have recently been developed to calculate the calcium carbonate saturation in drinking water that can be explored in future iterations of this model if a chemical assessment of the water entering the premise plumbing system is conducted (de Moel et al., 2013).

The scalding model used in this decision analysis evaluated the endpoints of epidermal injury or epidermal necrosis defined in Moritz and Henriques (1947) to be a 1^{st} degree reaction with hyperemia without loss of the epidermis or a 2^{nd} or 3^{rd} degree reaction with complete epidermal necrosis. Using regression equations fit to data from Moritz and Henriques (1947), we used three injury categories for scalding (no injury, injury, or necrosis). However, different assumptions regarding how scalding data are pooled can result in slightly different values for optimum set point (**Appendix A, Section 10**). The

scalding severity was determined by using data from human and pig skin experimentation from Moritz and Henriquez (Moritz & Henriques, 1947), which was performed using a running stream of hot water brought into direct contact with the skin using a metal cup covered with a pad of closed-cell sponge rubber to insure a watertight contact. This situation produced time-temperature-injury curves but may be slightly conservative due to the stringent contact conditions. A reaction time of five seconds was assumed the maximum time the model for removing a hot stimulus, and this may be overly optimistic given that some elderly populations in hospital care may have reduced reaction times to injuries or other conditions. Scalding and infection injuries were considered only from showers; however, sinks and toilets may also be a source of LD or Pontiac Fever infections (Hamilton et al., 2019), and scalding could reasonably occur at sinks or bathtubs as well. Bathtubs were not considered in the current model.

For the purposes of this model, a clinical visit cost was assumed if the time of exposure and water temperature was above the epidermal injury threshold but below the epidermal necrosis threshold. An emergency room visit cost was assumed if the time of exposure and water temperature was above the epidermal necrosis threshold. This may be a conservative estimate due to 1st degree or epidermal burns being categorized as burns with minimal damage, whereas 2nd degree or dermal burns extend past the epidermal layer causing damage in the dermal layer, and 3rd degree or subdermal burns are complete destruction of the dermis (Martin & Falder, 2017). However, a great number of factors can affect the severity of a burn. Location of the burn on the body is expected to vary in severity due to

the variation of skin thickness throughout the body. Skin thickness is also impacted by age and underlying disease. After burn care can also greatly affect the severity of a burn. All these variables should be considered on an individual basis, making a generalizable burn model very difficult to achieve (Martin & Falder, 2017).

Numerous challenges exist for verification and/or validation of this model and similar premise plumbing models. Validation of health risk predictions would involve comparison with disease outcome statistics which in most cases would not be possible at the desired level of granularity and therefore our focus here will be on verification. Calibrating the concentration portion of this model will involve operating premise plumbing systems at multiple scales with well-developed, representative biofilms and conducting frequent sampling of *L. pneumophila*, free chlorine, temperature, and other meta-data. A variety of disparate laboratory scale experimental models exist for monitoring *L. pneumophila* growth within various plumbing system schematics that are challenging to integrate with a full-scale, decision-relevant mechanistic model as has been done here. While several bench- and pilot scale laboratory studies (Proctor, 2014; Rhoads et al., 2015, 2017) and some studies at the building-scale (Ley et al., 2020; Salehi et al., 2018) have informed the knowledge base for *Legionella* spp. growth, these concepts have not yet been linked in a quantitative way to predict the "trouble spots" in real buildings for informing interventions before an outbreak arises and significant barriers exist to integrating this information across multiple scales. Full-scale plumbing systems that include both the water heater and the pipes have been analyzed (Rhoads et al., 2016), along with the effects of the pipe

orientation within the premise plumbing system (Rhoads et al., 2015). A variety of simulated water heaters scaled to a benchtop size have also been investigated (Proctor et al., 2017; Shaheen et al., 2019). The simulated water heater allows for controlled environments where microbial growth can be closely monitored in response to changing water temperatures, pipe material, and initial water chemistry. Models using software packages such as EPANET or others have been proposed for modeling lead in premise plumbing (Burkhardt et al., 2020) or temperature (Hillebrand & Blokker, 2021) for various aspects of hot and cold water systems but have not integrated these approaches for modeling *Legionella* spp. specifically. Stone et al. (2019) addressed *Legionella* growth and infection risks in a horizontal water heater using the advanced computational fluid dynamics (CFD) software ANSYS (Stone et al., 2019). However, these models exclude the pipes leading to the shower and the recirculating lines in their computational analysis, and do not consider health risks.

A quantitative relationship for *L. pneumophila* growth in operational premise plumbing systems has not yet been proposed, and few computational models have assessed *L. pneumophila* growth in plumbing systems. The goal is to use this model is therefore to use it as a basis for proposing additional work and identifying the drivers of the model so that information collection can be more judiciously targeted toward high-impact parameters during a calibration effort. The generalized framework presented here could also be easily adapted for a variety of building situations and configurations. This approach also allows for a greater degree of complexity to be added if such information were available for a

particular building. Therefore, prior to application of this model in practice, verification is needed (1) at the pilot scale; and (2) at the full building-scale for a variety of pipe materials and configurations, operational strategies, and exposure scenarios. Ideally, information on pathogens in both biofilm and bulk water could be collected along with a rich set of meta-data to support such an effort. In contrast, Saetta et al. (2021) (Saetta et al., 2021) used a data-driven approach to chlorine residuals without accounting for mechanistic aspects of the system using gradient-boosting machine models, indicating that in the future either mechanistic models with learned parameters or purely data-driven models could provide improved predictive power for *L. pneumophila*.

The quantity of *L. pneumophila* in the biofilm and in sloughing events will vary greatly due to the fluid dynamics within the pipes, stagnation, chlorine residual, and the available nutrients in the local water among other things. All the parameters used to calculate the biofilm contributions to this model were taken from scenario-specific cases at the bench scale, and more information would be needed to be integrated to reflect the type of heterogeneity expected in a full-scale system. A simple modified plug-flow approach with axial dispersion in the water heater only was taken for modeling flow dynamics in the system due to simplicity in this framework. However, with additional system-specific information, a more complex approach such as CFD or similar methods could be used for a more nuanced consideration of flow within the system. In the current work, a planktonic concentration upper-bound limit of $10^{4.17}$ CFU/L after 21 days of incubation at 37°C in tap water was used for constraining the simulated 24-h stagnation period prior to a shower

event, as this was the highest concentration observed in a study of *L. pneumophila* stagnation (Yee & Wadowsky, 1982), however the authors noted that the plate count may be an underestimation of viable *L. pneumophila* present due to differences between laboratory stock strains and those adapted to growing in water. Additionally, uncertainty regarding the net impacts of stagnation and other water quality factors on *L. pneumophila* concentrations remains uncertain (Rhoads & Hammes, 2021), and additional sensitivity analysis on the impact of this constraining variable is warranted.

The model made use of a large literature of disparate kinetic information for *L. pneumophila* behavior in the planktonic and biofilm-associated forms in the presence of free chlorine disinfectant as well as different temperatures. Many of these experiments were performed at the bench scale under various conditions for solute concentrations and reactor setup, indicating the need for more information to reliably fill out this parameter space. To calculate kinetic constants beyond the observed ranges of information for chlorine inactivation at various temperatures, the Arrhenius equation was used. However, the authors cautioned against extrapolating their results beyond 25°C, which in this case was required due to a lack of additional experimental information for all required temperatures needed for the model. Chlorine demand due to other water quality aspects aside from TOC were not considered, resulting in conservative estimates for the concentration of chlorine in the modeled system. Recent studies have added to the literature on kinetic information (Papagianeli et al., 2021), and additional kinetic information would improve the robustness of this model. It is also noted that the water heater set point may

not always be fully accurate or fully encompass temperature variations. Consideration of temperature and disinfection kinetics in the context of stagnation time, nutrient availability, and other considerations is also needed. A disinfectant dose-dependent variability in disinfection efficacy for *L. pneumophila* was not considered and a more rigorous meta-analysis of disinfection models for *L. pneumophila* is recommended as an outcome of this work.

Several uncertainties to address involve the selection of dose response models and morbidity ratios for LD infection. Two dose response parameters were used in the case studies to calculate the risk of infection which influences the optimal water heater temperature set point, with terminologies of "subclinical" vs. "clinical severity infection" used from prior QMRA work (Armstrong & Haas, 2007, 2008). A morbidity ratio specific to elderly populations (Weir et al., 2019) was used in addition to DALYs, VSL, and life expectancy to calculate the cost of infection. A DALY estimate from the Netherlands was used that did not differentiate between clinical and subclinical cases. Overall, there is a lack of information on DALY estimates from the US for LD or Pontiac fever, and US-based estimates would be needed to update this estimate in the model. The same morbidity ratio, DALYs, VSL, and life expectancy was applied for both dose response scenario and the VSL was not corrected for age. Therefore, the health-associated parameters would not apply to all populations as the focus here was on an elderly hospital vulnerable population. However, these data could be included if other populations were to be considered. Future efforts for dose response model validation could be made to examine the implications of

subclinical infections and account for these costs more explicitly in the calculation for a DALY.

Perhaps counterintuitively, the clinical severity dose response results in a lower cost of infection despite having a greater severity due to the fact that the dose response relationship results in a lower likelihood of illness using the clinical severity dose response relationship compared to multiplying the probability of infection generated with the subclinical infection dose response model by a morbidity ratio. While the clinical severity infection relationship aligns with efforts to use QMRA to re-produce epidemic curves (Prasad et al., 2017), additional validation of dose response and morbidity ratio relationships would be useful for identifying specific modulating factors in susceptibility and modifying the currently developed model to other scenarios and populations of interest. Further validation efforts for dose response datasets would be useful for clarifying the interpretation of the outcomes of subclinical infection and clinical severity infection as distinct independent versus conditional outcomes.

The type of susceptible subpopulation considered could also impact the exposure factors chosen; in this case, a 1.0 to 5.0-second reaction time was conservatively chosen for an elderly person removing themselves from a water temperature that could pose a danger of scalding. Reaction times to a stimuli can be shorter than 1s (Brenner & Smeets, 2019). However, while contact heat pain thresholds may not differ between the elderly and other populations (El Tumi et al., 2017), actual duration of contact with the hot water of up to 5 seconds is assumed to be reasonable as elderly individuals can have co-occurring

conditions and decreased mobility compared to younger, healthy individuals (Durand et al., 2012; Hewitt et al., 2007; Huyer & Corkum, 1997; Stone et al., 2000).

Cost assumptions were made for the risk of infection, risk of scalding, and energy cost. The predicted costs will vary regionally according to local energy costs, medical costs, as well as costs of illness and can be discounted or have uncertainty accounted for accordingly in a more detailed consideration of situation-specific costs. This model was limited to only a small section of a clinical plumbing system, the average daily water use per capita was estimated to be the use for a single patient. The average was used to calculate the approximate energy cost to heat the used and recirculating water. This value inherently has a lot of uncertainty, as a patient might need a lot more or a lot less water depending on the reason for hospitalization. For example, patients with scalding might require that they have baths multiple times a day, whereas other patients might not require a bath for 24 hours. The cost of heating the water will also depend on the location of the patient room relative to the water heater. The further the room, the more the water will cool down and the more energy will be required to heat it again. The model did not account for variations beyond a single day of operation and exposure, and therefore future models could account for the dynamics of the costs over a more comprehensive timeframe, including construction and operation, health risks, and scalding risks during a longer time-frame, accounting for discounting or weighting preferences for these attributes.

Choosing appropriate time horizons will be needed for applying discount rates and estimating the effects of decision-making over a more realistic operational timeline. To this

end, it would be complex to consider the dynamics of pathogen growth over a longer time range without additional kinetic information and quantitative relationships between performance, stagnation, and occurrence of *L. pneumophila* in the biofilms and bulk water. Presumably if an issue such as an outbreak or scalding episode were to occur, changes would be made to water operation that would impact the putative risks. More mechanistic understanding of these relationships would allow for implementation of such a model. Importantly, the costs associated with remediating a system after a *L. pneumophila* contamination event and the role an initial colonization an event can play in re-seeding the system were not considered but presumably would further elevate the importance of infection risk as a driving factor in the model. The current model is initialized over a 24-h period but could be modified to allow for different stagnation periods. While systematic studies of the costs of remediation are not currently available, follow-up studies of *Legionella* spp. after colonization events indicate that long-term measures such as building-level disinfection may be necessary to control colonization and would incur additional costs (Coniglio et al., 2018), in addition to sampling costs, maintenance, legal, and personnel costs. Recolonization after disinfection, heat treatment, or UV treatment may occur on a timeframe of weeks to months in water distribution systems and/or premise plumbing (Lin et al., 1998; Liu et al., 1995, 1998; Rhoads et al., 2016). Only direct costs were considered for infection and scalding and did not account for example, for lost wages due to missed work or other costs such as lawsuits resulting from a case of illness or injury, pain and suffering, or long-term impacts and associated future costs from infection and/or

scalding. Additional cost evaluation methodology such as cost-benefit or cost-effectiveness approaches could also be used.

2.6 Conclusion

A computational framework is presented for evaluating an optimal water heater temperature set point for reducing energy costs and health risks for a single showering exposure event. This framework uses a quantitative microbial risk assessment (QMRA) model to assess the risk of infection from shower aerosol exposure in terms of DALYs and daily costs. The cost associated with the risk of scalding was evaluated, along with the cost of energy used to heat the water for a variety of uncertain assumptions related to the system design, operation, and risk assumptions. As a starting point, a use-case was developed for a hypothetical hospital room located in the United States that would serve a susceptible hospitalized population.

The model provides a valuable means of exploring the impact of interactions between the assumptions and evaluated tradeoffs between infection risk for LD, scalding risk, and energy costs. Overall, the model was most sensitive to assumptions regarding the system configuration and dose response model chosen for analysis. In all cases, the scalding risk was not a driver of total cost until the higher set points, assuming no thermostatic mixing valve in use (≥59°C). The use of a subclinical infection vs. a clinical severity infection dose response model dictated the rank order of infection and energy costs, with the more conservative (subclinical) model resulting in a prioritization of infection considerations

over the other (energy cost or scalding) considerations. The sensitivity analyses indicated that biofilm dynamics drove risk estimates, as well as assumptions regarding energy price. Limitations and additional considerations for the model were discussed.

The approach proposed in this work should be a companion tool to other simple, direct evidence-based approaches and a complex model may not be warranted in every situation. The uncertainties identified in this work could also be reduced with the use of site-specific information regarding building design and operation. With further validation, this model could be used by building owners and architects to assess the cost associated with the risk of infection or scalding, as well as the energy cost to heat different plumbing configurations in different climates. Ideally, architects will be able to use this tool to minimize total costs for different scenarios by evaluating pipe materials, pipe lengths, pipe sizes, stagnant dead ends, or insulation prior to the construction phase. Building owners can use this tool for existing plumbing systems to make operational improvements by determining the optimal water heater temperature set point, adding or removing insulation, or taking regular preventative measures to mitigate *L. pneumophila* growth. This model contributes to the mechanistic understanding of system dynamics within premise plumbing systems and serves as a good base for the addition of other pathogens like mycobacteria, disinfection byproducts, or the cost of emissions for fossil fuel usage. As such, the current analysis could constitute a piece in a larger consideration of more holistic building design and operational decision support tools.

2.7 References

Arias, E., Heron, M., & Xu, J. (2017). United States Life Tables, 2013. *NVSS*, *66*(3), 64.

Armstrong, T. W., & Haas, C. N. (2007). A Quantitative Microbial Risk Assessment Model for Legionnaires' Disease: Animal Model Selection and Dose-Response Modeling: A Quantitative Microbial Risk Assessment Model for Legionnaires' Disease. *Risk Analysis*, *27*(6), 1581–1596. https://doi.org/10.1111/j.1539-6924.2007.00990.x

Armstrong, T. W., & Haas, C. N. (2008). Legionnaires' disease: Evaluation of a quantitative microbial risk assessment model. *Journal of Water and Health*, *6*(2), 149–166. https://doi.org/10.2166/wh.2008.026

ASHRAE. (2018). *ANSI/ASHRAE Standard 188: Legionellosis: Risk Management for Building Water Systems*. https://ashrae.iwrapper.com/ViewOnline/Standard_188-2018

ASHRAE. (2019). *ANSI/ASHRAE/IES Standard 90.1-2019—Energy Standard for Buildings Except Low-Rise Residential Buildings* (D-86270, 86270; p. 424). https://www.ashrae.org/technical-resources/bookstore/standard-90-1

ASHRAE, Brian M., Lynch, B. M., & Arens, E. A. (2010). ANSI/ASHRAE Standard 55: Thermal Environmental Conditions for Human Occupancy. *ASHRAE*. http://arco-hvac.ir/wp-content/uploads/2015/11/ASHRAE-55-2010.pdf

AWWA. (2018). *2017 Water Utility Disinfection Survey Report*. American Water Works Association. https://www.awwa.org/Portals/0/AWWA/ETS/Resources/2017DisinfectionSurveyReport.pdf?ver=2018-12-21-163548-830

Barnsley, G. P., & Barnsley, S. E. (2007). *Rate of pediatric tap water scald injuries in eastern Ontario*. *15*(1), 5.

Beer, K. D., Gargano, J. W., Roberts, V. A., Hill, V. R., Garrison, L. E., Kutty, P. K., Hilborn, E. D., Wade, T. J., Fullerton, K. E., & Yoder, J. S. (2015). Surveillance for Waterborne Disease Outbreaks Associated with Drinking Water—United States, 2011-2012. *MMWR. Morbidity and Mortality Weekly Report*, *64*(31), 842–848. https://doi.org/10.15585/mmwr.mm6431a1

Blokker, E. J. M., & Pieterse-Quirijns, E. J. (2013). Modeling temperature in the drinking water distribution system. *Journal - American Water Works Association*, *105*(1), E19–E28. https://doi.org/10.5942/jawwa.2013.105.0011

Blue Cross Blue Shield. (2009). *Typical Costs for Common Medical Services*. Blue Cross and Blue Shield of Massachusetts.

Borella, P., Montagna, M. T., Romano-Spica, V., Stampi, S., Stancanelli, G., Triassi, M., Neglia, R., Marchesi, I., Fantuzzi, G., Tatò, D., Napoli, C., Quaranta, G., Laurenti, P., Leoni, E., De Luca, G., Ossi, C., Moro, M., & D'Alcalà, G. R. (2004). *Legionella* Infection Risk from Domestic Hot Water. *Emerging Infectious Diseases*, *10*(3), 457–464. https://doi.org/10.3201/eid1003.020707

Brazeau, R. H., & Edwards, M. A. (2013). Role of Hot Water System Design on Factors Influential to Pathogen Regrowth: Temperature, Chlorine Residual, Hydrogen Evolution, and Sediment. *Environmental Engineering Science*, *30*(10), 617–627. https://doi.org/10.1089/ees.2012.0514

Brenner, E., & Smeets, J. B. J. (2019). How Can You Best Measure Reaction Times? *Journal of Motor Behavior*, *51*(5), 486–495. https://doi.org/10.1080/00222895.2018.1518311

Brink, H., Slaats, P. G. G., & van Eekeren, M. W. M. (2004). Scaling in domestic heating equipment: Getting to know a complex phenomenon. *Water Science and Technology*, *49*(2), 129–136. https://doi.org/10.2166/wst.2004.0106

Brûlet, A., Nicolle, M.-C., Giard, M., Nicolini, F.-E., Michallet, M., Jarraud, S., Etienne, J., & Vanhems, P. (2008). Fatal Nosocomial *Legionella pneumophila* Infection Due to Exposure to Contaminated Water From a Washbasin in a Hematology Unit. *Infection Control & Hospital Epidemiology*, *29*(11), 1091–1093. https://doi.org/10.1086/591739

Burkhardt, J. B., Woo, H., Mason, J., Shang, F., Triantafyllidou, S., Schock, M. R., Lytle, D., & Murray, R. (2020). Framework for Modeling Lead in Premise Plumbing Systems Using EPANET. *Journal of Water Resources Planning and Management*, *146*(12), 04020094. https://doi.org/10.1061/(ASCE)WR.1943-5452.0001304

CDC. (2017). *Developing a Water Management Program to Reduce Legionella Growth & Spread in Buildings*. https://www.cdc.gov/legionella/downloads/toolkit.pdf

CDC. (2018). *Legionella (Legionnaires' Disease and Pontiac Fever)*. CDC. https://www.cdc.gov/legionella/about/history.html

CDC. (2021). *Legionella: Healthcare Water Management Program FAQs*. https://www.cdc.gov/legionella/wmp/healthcare-facilities/healthcare-wmp-faq.html

CDC, Barskey, A., Binder, A., Edens, C., Lee, S., Smith, J., Schrag, S., Whitney, C., & Cooley, L. (2015). *Legionnaires' Disease Surveillance Summary Report, United States- 2014 and 2015*. Center for Disease Control and Prevention. https://www.cdc.gov/legionella/health-depts/surv-reporting/2014-15-surv-report-508.pdf

Chen, T. Q., Rubanova, Y., Bettencourt, J., & Duvenaud, D. K. (2018). *Neural Ordinary Differential Equations*. 12.

Chester, D. L., Jose, R. M., Aldlyami, E., King, H., & Moiemen, N. S. (2005). Non-accidental burns in children—Are we neglecting neglect? *Burns*, *32*(2), 222–228. https://doi.org/10.1016/j.burns.2005.08.018

Chmielewska, A. (2018). Fluctuating temperature of the mains water throughout the year and its influence on the consumption of energy for the purposes of DHW preparation. *E3S Web of Conferences*, *44*, 00017. https://doi.org/10.1051/e3sconf/20184400017

Clouatre, E., Pinto, R., Banfield, J., & Jeschke, M. G. (2013). Incidence of Hot Tap Water Scalds After the Introduction of Regulations in Ontario: *Journal of Burn Care & Research*, *34*(2), 243–248. https://doi.org/10.1097/BCR.0b013e3182789057

CMS. (2000). *State operations manual Appendix Q. Guidelines for determining immediate jeopardy. Rev. 102*. file:///C:/Users/ashle/Dropbox/Ashley%20Heida/Water%20heater%20project/Water%20Heater%20Papers/CMS_2014.pdf

CMS. (2018). *Centers for Medicare and Medicaid Services. SUBJ: Requirement to Reduce Legionella Risk in Healthcare Facility Water Systems to Prevent Cases and Outbreaks of Legionnaires' Disease (LD). *Revised to Clarify Expectations for Providers, Accrediting Organizations, and Surveyors**. Memorandum. https://www.cms.gov/Medicare/Provider-Enrollment-and-Certification/SurveyCertificationGenInfo/Downloads/QSO17-30-HospitalCAH-NH-REVISED-.pdf

Collier, S. A., Deng, L., Adam, E. A., Benedict, K. M., Beshearse, E. M., Blackstock, A. J., Bruce, B. B., Derado, G., Edens, C., Fullerton, K. E., Gargano, J. W., Geissler, A. L., Hall, A. J., Havelaar, A. H., Hill, V. R., Hoekstra, R. M., Reddy, S. C., Scallan, E., Stokes, E. K., … Beach, M. J. (2021). *Estimate of Burden and Direct Healthcare Cost of Infectious Waterborne Disease in the United States—Volume 27, Number 1—January 2021—Emerging Infectious Diseases journal—CDC*. https://doi.org/10.3201/eid2701.190676

Collier, S. A., Stockman, L. J., Hicks, L. A., Garrison, L. E., Zhou, F. J., & Beach, M. J. (2012). Direct healthcare costs of selected diseases primarily or partially transmitted by water. *Epidemiology and Infection*, *140*(11), 2003–2013. https://doi.org/10.1017/S0950268811002858

Coniglio, M. A., Ferrante, M., & Yassin, M. H. (2018). Preventing Healthcare-Associated Legionellosis: Results after 3 Years of Continuous Disinfection of Hot Water with Monochloramine and an Effective Water Safety Plan. *International Journal of Environmental Research and Public Health*, *15*(8), Article 8. https://doi.org/10.3390/ijerph15081594

de Moel, P. J., van der Helm, A. W. C., van Rijn, M., van Dijk, J. C., & van der Meer, W. G. J. (2013). Assessment of calculation methods for calcium carbonate saturation in drinking water for DIN 38404-10 compliance. *Drinking Water Engineering and Science*, *6*(2), 115–124. https://doi.org/10.5194/dwes-6-115-2013

DeOreo, W. B., Mayer, P. W., Dziegielewski, B., Kiefer, J., Dziegielewski, B., & Dziegielewski, B. (2016). Residential End Uses of Water, version 2. *Water Research Foundation*, 18.

Dieter, C. A., Maupin, M. A., Caldwell, R. R., Harris, M. A., Ivahnenko, T. I., Lovelace, J. K., Barber, N. L., & Linsey, K. S. (2018). *Estimated Use of Water in the United States in 2015: U.S. Geological Survey Circular 1441*. U.S. Geological Survey.

DOE. (n.d.). *Estimating Costs and Efficiency of Storage, Demand, and Heat Pump Water Heaters*. DOE. Retrieved February 7, 2020, from https://www.energy.gov/energysaver/estimating-costs-and-efficiency-storage-demand-and-heat-pump-water-heaters

DOE. (2016). *Savings Project: Lower Water Heating Temperature*. DOE. https://www.energy.gov/energysaver/services/do-it-yourself-energy-savings-projects/savings-project-lower-water-heating

Dormand, J. R., & Prince, P. J. (1980). A family of embedded Runge-Kutta formulae. *Journal of Computational and Applied Mathematics*, *6*(1), 19–26. https://doi.org/10.1016/0771-050X(80)90013-3

Durand, M. A., Green, J., Edwards, P., Milton, S., & Lutchmun, S. (2012). Perceptions of tap water temperatures, scald risk and prevention among parents and older people in social housing: A qualitative study. *Burns*, *38*(4), 585–590. https://doi.org/10.1016/j.burns.2011.10.009

El Tumi, H., Johnson, M. I., Dantas, P. B. F., Maynard, M. J., & Tashani, O. A. (2017). Age-related changes in pain sensitivity in healthy humans: A systematic review

with meta-analysis. *European Journal of Pain*, *21*(6), 955–964. https://doi.org/10.1002/ejp.1011

ENERGY STAR. (2008). *ENERGY STAR Residential Water Heaters: Final Criteria Analysis*. ENERGY STAR. https://www.energystar.gov/ia/partners/prod_development/new_specs/downloads/water_heaters/waterheateranalysis_final.pdf

EPA. (2009). *Indoor Air Quality Tools for Schools Reference Guide*. EPA. https://www.epa.gov/sites/production/files/2014-08/documents/reference_guide.pdf

Erdmann, T. C., Feldman, K. W., & Rivara, P. (1991). *Tap Water Burn Prevention: The Effect of Legislation*. 8.

Flemming, H.-C., Percival, S. L., & Walker, J. T. (2002). Contamination potential of biofilms in water distribution systems. *Water Supply*, *2*(1), 271–280. https://doi.org/10.2166/ws.2002.0032

Garny, K., Neu, T. R., & Horn, H. (2009). Sloughing and limited substrate conditions trigger filamentous growth in heterotrophic biofilms—Measurements in flow-through tube reactor. *Chemical Engineering Science*, *64*(11), 2723–2732. https://doi.org/10.1016/j.ces.2009.03.009

Gomez-Valero, L., & Buchrieser, C. (2019). Intracellular parasitism, the driving force of evolution of Legionella pneumophila and the genus Legionella. *Microbes and Infection*, *21*(5–6), 230–236. https://doi.org/10.1016/j.micinf.2019.06.012

Government of Canada. (2011). *Water Temperature and Burns/Scalds*. https://www.canada.ca/en/public-health/services/water-temperature-burns-scalds.html

Graitcer, P. L., & Sniezek, J. E. (1988). HOSPITALIZATIONS DUE TO TAP WATER SCALDS, 1978-1985. *Public Health Surveillance of 1990 Injury Control Objectives for the Nation*, *37*, 4.

Guyer, J. P. (2016). *An Introduction to Hospital Domestic Water Systems*. 36.

Haas, C. N., Rose, J. B., & Gerba, C. P. (1999). *Quantitative Microbial Risk Assessment*. John Wiley & Sons, Inc.

Hach. (2018). *Chlorine, Free and Total, Low Range: USEPA DPD Method 8021 (Free) 8167 (Total) DOC316.53.01450*. https://www.hach.com/asset-get.download-en.jsa?code=163953

Hamilton, K. A., Prussin, A. J., Ahmed, W., & Haas, C. N. (2018). Outbreaks of Legionnaires' Disease and Pontiac Fever 2006–2017. *Current Environmental Health Reports*, *5*(2), 263–271. https://doi.org/10.1007/s40572-018-0201-4

Hamilton, K., Hamilton, M. T., Johnson, W., Jjemba, P., Bukhari, Z., LeChevallier, M., & Haas, C. N. (2018). Health risks from exposure to Legionella in reclaimed water aerosols: Toilet flushing, spray irrigation, and cooling towers. *Water Research*, *134*, 261–279. https://doi.org/10.1016/j.watres.2017.12.022

Hamilton, K., Hamilton, M. T., Johnson, W., Jjemba, P., Bukhari, Z., LeChevallier, M., Haas, C. N., & Gurian, P. L. (2019). Risk-Based Critical Concentrations of *Legionella pneumophila* for Indoor Residential Water Uses. *Environmental Science & Technology*, *53*(8), 4528–4541. https://doi.org/10.1021/acs.est.8b03000

Herman, J., Usher, W., Mutel, C., Trindade, B., Hadka, D., Woodruff, M., Rios, F., Hyams, D., & Xantares. (2017). *SALib*. MIT. https://salib.readthedocs.io/en/latest/license.html

Hewitt, A., Macarthur, C., & Raina, P. (2007). The Role of Evidence in Public Health Policy: An Example of Linkage and Exchange in the Prevention of Scald Burns. *Healthcare Policy | Politiques de Santé*, *3*(2), 59–66. https://doi.org/10.12927/hcpol.2007.19392

Hillebrand, B., & Blokker, E. J. M. (2021). *Modeling the Influence of District Heating Systems on Drinking Water Temperatures in Domestic Drinking Water Systems within Domestic Properties*. 961–968. https://doi.org/10.1061/9780784483466.088

Hockey, R. (2002). Safe hot tap water and the risk of scalds and legionella infection. *Injury Prevention*, *8*(2), 170–170. https://doi.org/10.1136/ip.8.2.170

Hofman, J., Hoek, J. P. V. D., Nederlof, M., & Groenendijk, M. (2007). *Twenty years of experience with centralised softening in the Netherlands: Water quality, environmental benefits, and costs*. https://researchportal.bath.ac.uk/en/publications/twenty-years-of-experience-with-centralised-softening-in-the-neth

Huang, C., Shen, Y., Smith, R. L., Dong, S., & Nguyen, T. H. (2020). Effect of disinfectant residuals on infection risks from Legionella pneumophila released by biofilms grown under simulated premise plumbing conditions. *Environment International*, *137*, 105561. https://doi.org/10.1016/j.envint.2020.105561

Hugo Johansson, P. J., Andersson, K., Wiebe, T., Schalén, C., & Bernander, S. (2006). Nosocomial transmission of Legionella pneumophila to a child from a hospital's

cold-water supply. *Scandinavian Journal of Infectious Diseases*, *38*(11–12), 1023–1027. https://doi.org/10.1080/00365540600827558

Huyer, D. W., & Corkum, S. H. (1997). Reducing the incidence of tap-water scalds: Strategies for physicians. *CAN MED ASSOC J*, *156*(6), 841–844.

IAPMO. (2016). *2015 Minnesota Plumbing Code Water Pipe Sizing Workshop*. IAPMO.

Incropera, F. P., Dewitt, D. P., Bergman, T. L., & Lavine, A. S. (Eds.). (2007). *Fundamentals of heat and mass transfer* (6th ed). John Wiley.

International Desalination Association (Ed.). (2006). *Innovation and integration - impact on desalination and water reuse costs: IDA International Water Forum, Dubai, UAE, March 5 - 6, 2006*. IDA. https://www.researchgate.net/profile/Hamza-Elfil/publication/323615931_A_New_Index_for_Scaling_Assessment/links/5aa02af60f7e9badd9a0ba07/A-New-Index-for-Scaling-Assessment.pdf

Katcher, M. L. (1981). *Scald Burns From Hot Tap Water*. *245*(11), 1219–1222.

Kleinbach, E. M., Beckman, W. A., & Klein, S. A. (1993). Performance study of one-dimensional models for stratified thermal storage tanks. *Solar Energy*, *50*(2), 155–166. https://doi.org/10.1016/0038-092X(93)90087-5

LeChevallier, M. W., Shaw, N. E., Kaplan, L. A., & Bott, T. L. (1993). Development of a Rapid Assimilable Organic Carbon Method for Water. *Applied and Environmental Microbiology*, *59*(5), 1526–1531. https://doi.org/10.1128/AEM.59.5.1526-1531.1993

LeChevallier, M. W., Welch, N. J., & Smith, D. B. (1996). Full-scale studies of factors related to coliform regrowth in drinking water. *Applied and Environmental Microbiology*, *62*(7), 2201–2211. https://doi.org/10.1128/AEM.62.7.2201-2211.1996

Lévesque, B., Lavoie, M., & Joly, J. (2004). Residential Water Heater Temperature: 49 or 60 Degrees Celsius? *Canadian Journal of Infectious Diseases*, *15*(1), 11–12. https://doi.org/10.1155/2004/109051

Ley, C. J., Proctor, C. R., Jordan, K., Ra, K., Noh, Y., Odimayomi, T., Julien, R., Kropp, I., Mitchell, J., Nejadhashemi, A. P., Whelton, A. J., & Aw, T. G. (2020). Impacts of Municipal Water–Rainwater Source Transitions on Microbial and Chemical Water Quality Dynamics at the Tap. *Environmental Science & Technology*, *54*(18), 11453–11463. https://doi.org/10.1021/acs.est.0c03641

Lin, Y. E., Vidic, R. D., Stout, J. E., & Yu, V. L. (1998). Legionella in water distribution systems. *Journal AWWA*, *90*(9), 112–122. https://doi.org/10.1002/j.1551-8833.1998.tb08503.x

Liu, Z., Stout, J. E., Boldin, M., Rugh, J., Diven, W. F., & Yu, V. L. (1998). Intermittent Use of Copper-Silver Ionization for Legionella Control in Water Distribution Systems: A Potential Option in Buildings Housing Individuals at Low Risk of Infection. *Clinical Infectious Diseases*, *26*(1), 138–140. https://doi.org/10.1086/516283

Liu, Z., Stout, J., Tedesco, L., Boldin, M., Hwang, C., & Lu, V. (1995). Efficacy of ultraviolet light in preventing Legionella colonization of a hospital water distribution system. *Water Research*, *29*(10), 2275–2280. https://doi.org/10.1016/0043-1354(95)00048-P

Lock, K., Millett, C., Heathcock, R., Joseph, C. A., Harrison, T. G., Lee, J. V., Rao, G., Surman-Lee, S., & on behalf of the Outbreak Control Team. (2008). Public health and economic costs of investigating a suspected outbreak of Legionnaires' disease. *Epidemiology and Infection*, *136*(10), 1306–1314. https://doi.org/10.1017/S0950268807000076

Lowell, G., Quinlan, K., & Gottlieb, L. J. (2008). Preventing Unintentional Scald Burns: Moving Beyond Tap Water. *PEDIATRICS*, *122*(4), 799–804. https://doi.org/10.1542/peds.2007-2979

Martin, N. A., & Falder, S. (2017). A review of the evidence for threshold of burn injury. *Burns*, *43*(8), 1624–1639. https://doi.org/10.1016/j.burns.2017.04.003

Moritz, A. R., & Henriques, F. C. (1947). Studies of Thermal Injury: II. The Relative Importance of Time and Surface Temperature in the Causation of Cutaneous Burns. *The American Journal of Pathology*, *23*(5), 695–720.

NASEM. (2006). *Drinking Water Distribution Systems: Assessing and Reducing Risks*. National Academies Press. https://doi.org/10.17226/11728

NASEM, Water Science and Technology Board, Board on Life Sciences, Board on Population Health and Public Health Practice, Division on Earth and Life Studies, Health and Medicine Division, & National Academies of Sciences, Engineering, and Medicine. (2019). *Management of Legionella in Water Systems*. National Academies Press. https://doi.org/10.17226/25474

Nguyen, C., Elfland, C., & Edwards, M. (2012). Impact of advanced water conservation features and new copper pipe on rapid chloramine decay and microbial regrowth. *Water Research*, *46*(3), 611–621. https://doi.org/10.1016/j.watres.2011.11.006

Papagianeli, S. D., Aspridou, Z., Didos, S., Chochlakis, D., Psaroulaki, A., & Koutsoumanis, K. (2021). Dynamic modelling of Legionella pneumophila thermal inactivation in water. *Water Research, 190*, 116743. https://doi.org/10.1016/j.watres.2020.116743

Paranjape, K., Bédard, É., Whyte, L. G., Ronholm, J., Prévost, M., & Faucher, S. P. (2020). Presence of Legionella spp. in cooling towers: The role of microbial diversity, Pseudomonas, and continuous chlorine application. *Water Research, 169*, 115252. https://doi.org/10.1016/j.watres.2019.115252

Parr, A., Whitney, E. A., & Berkelman, R. L. (2015). Legionellosis on the Rise: A Review of Guidelines for Prevention in the United States. *Journal of Public Health Management and Practice*, *21*(5), E17–E26. https://doi.org/10.1097/PHH.0000000000000123

Paszke, A., Gross, S., Massa, F., Lerer, A., Bradbury, J., Chanan, G., Killeen, T., Lin, Z., Gimelshein, N., Antiga, L., Desmaison, A., Kopf, A., Yang, E., DeVito, Z., Raison, M., Tejani, A., Chilamkurthy, S., Steiner, B., Fang, L., … Chintala, S. (2019). *PyTorch: An Imperative Style, High-Performance Deep Learning Library*. 12.

Peck, M., Chang Brewer, A., Pressman, M., Blank, E., & Mickalide, A. (2010). Hot Tap Water Legislation in the United States: *Journal of Burn Care & Research, 31*(6), 918–925. https://doi.org/10.1097/BCR.0b013e3181f93723

Potter, M. D. E., Maitz, P. K. M., Kennedy, P. J., & Goltsman, D. (2017). Perineal tap water burns in the elderly: At what cost?: Perineal tapster burns in the elderly. *ANZ Journal of Surgery*, *87*(11), E188–E192. https://doi.org/10.1111/ans.13439

Prasad, B., Hamilton, K. A., & Haas, C. N. (2017). Incorporating Time-Dose-Response into Legionella Outbreak Models. *Risk Analysis*, *37*(2), 291–304. https://doi.org/10.1111/risa.12630

Proctor, C. R. (2014). *Effect of Various Water Chemistry Factors on Legionella Proliferation and the Premise Plumbing Microbiome Composition*. Virginia Tech.

Proctor, C. R., Dai, D., Edwards, M. A., & Pruden, A. (2017). Interactive effects of temperature, organic carbon, and pipe material on microbiota composition and Legionella pneumophila in hot water plumbing systems. *Microbiome*, *5*(1), 130. https://doi.org/10.1186/s40168-017-0348-5

Rasheduzzaman, M., Singh, R., Haas, C. N., & Gurian, P. L. (2020). Required water temperature in hotel plumbing to control Legionella growth. *Water Research, 182*, 115943. https://doi.org/10.1016/j.watres.2020.115943

Reiling, J., Hughes, R. G., & Murphy, M. R. (2008). Chapter 28. The Impact of Facility Design on Patient Safety. *Patient Safety*, *2*, 26.

Rhoads, W. J., & Hammes, F. (2021). Growth of *Legionella* during COVID-19 lockdown stagnation. *Environmental Science: Water Research & Technology*, *7*(1), 10–15. https://doi.org/10.1039/D0EW00819B

Rhoads, W. J., Ji, P., Pruden, A., & Edwards, M. A. (2015). Water heater temperature set point and water use patterns influence Legionella pneumophila and associated microorganisms at the tap. *Microbiome*, *3*(1). https://doi.org/10.1186/s40168-015-0134-1

Rhoads, W. J., Pruden, A., & Edwards, M. K. (2017). Interactive Effects of Corrosion, Copper, and Chloramines on Legionella and Mycobacteria in Hot Water Plumbing. *Environmental Science & Technology*, *51*(12), 7065–7075. https://doi.org/10.1021/acs.est.6b05616

Rhoads, W., Pruden, A., & Edwards, M. (2016). Convective Mixing in Distal Pipes Exacerbates Legionella pneumophila Growth in Hot Water Plumbing. *Pathogens*, *5*(1), 29. https://doi.org/10.3390/pathogens5010029

Richard, R., Hamilton, K. A., Westerhoff, P., & Boyer, T. H. (2020). Tracking copper, chlorine, and occupancy in a new, multi-story, institutional green building. *Environmental Science: Water Research & Technology*, *6*(6), 1672–1680. https://doi.org/10.1039/D0EW00105H

Robinson, L. A., & Hammitt, J. K. (2016). Valuing Reductions in Fatal Illness Risks: Implications of Recent Research: Valuing Reductions in Fatal Illness Risks. *Health Economics*, *25*(8), 1039–1052. https://doi.org/10.1002/hec.3214

Robinson, L. A., Hammitt, J. K., Cecchini, M., Chalkidou, K., Claxton, K., Eozenou, P. H.-V., de Ferranti, D., Deolalikar, A. B., Guanais, F., Jamison, D. T., Kwon, S., Lauer, J. A., O'Keeffe, L., Walker, D., Wilkinson, T., Wilson, D., & Wong, B. (2019). *Reference Case Guidelines for Benefit-Cost Analysis in Global Health and Development* (p. 126). Bill & Melinda Gates Foundation.

Saetta, D., Richard, R., Leyva, C., Westerhoff, P., & Boyer, T. H. (2021). Data-mining methods predict chlorine residuals in premise plumbing using low-cost sensors. *AWWA Water Science*, *3*(1), e1214. https://doi.org/10.1002/aws2.1214

Salehi, M., Abouali, M., Wang, M., Zhou, Z., Nejadhashemi, A. P., Mitchell, J., Caskey, S., & Whelton, A. J. (2018). Case study: Fixture water use and drinking water quality in a new residential green building. *Chemosphere*, *195*, 80–89. https://doi.org/10.1016/j.chemosphere.2017.11.070

Scruggs, M. (2020). *How to select a commercial water heater*. Consulting - Specifying Engineer. https://www.csemag.com/articles/how-to-select-a-commercial-water-heater/

Shaheen, M., Scott, C., & Ashbolt, N. J. (2019). Long-term persistence of infectious Legionella with free-living amoebae in drinking water biofilms. *International Journal of Hygiene and Environmental Health*, *222*(4), 678–686. https://doi.org/10.1016/j.ijheh.2019.04.007

Shields, W. C., McDonald, E., Frattaroli, S., Perry, E. C., Zhu, J., & Gielen, A. C. (2013). Still Too Hot: Examination of Water Temperature and Water Heater Characteristics 24 Years After Manufacturers Adopt Voluntary Temperature Setting. *Journal of Burn Care & Research*, *34*(2), 281–287. https://doi.org/10.1097/BCR.0b013e31827e645f

Singh, R., Hamilton, K. A., Rasheduzzaman, M., Yang, Z., Kar, S., Fasnacht, A., Masters, S. V., & Gurian, P. L. (2020). Managing Water Quality in Premise Plumbing: Subject Matter Experts' Perspectives and a Systematic Review of Guidance Documents. *Water*, *12*(2), 347. https://doi.org/10.3390/w12020347

Stone, M., Ahmed, J., & Evans, J. (2000). The continuing risk of domestic hot water scalds to the elderly. *Burns*, *26*(4), 347–350. https://doi.org/10.1016/S0305-4179(99)00144-8

Stone, W., Louw, T. M., Gakingo, G. K., Nieuwoudt, M. J., & Booysen, M. J. (2019). A potential source of undiagnosed Legionellosis: Legionella growth in domestic water heating systems in South Africa. *Energy for Sustainable Development*, *48*, 130–138. https://doi.org/10.1016/j.esd.2018.12.001

Thomas, J. M. (2012). *The Risk to Human Health from Free-Living Amoebae Interaction with Legionella in Drinking and Recycled Water Systems*. University of New South Wales.

US Census Bureau. (n.d.). *National Population by Characteristics: 2010-2019*. The United States Census Bureau. Retrieved September 24, 2021, from https://www.census.gov/data/tables/time-series/demo/popest/2010s-national-detail.html

US Department of Health and Human Services. (2021). *Guidelines for Regulatory Impact Analysis Appendix D: Updating Value per Statistical Life (VSL) Estimates for Inflation and Changes in Real Income*. ASPE. https://aspe.hhs.gov/reports/updating-vsl-estimates

U.S. Energy Information Administration. (n.d.). *Electric Power Monthly*. U.S. Energy Information Administration. https://www.eia.gov/electricity/monthly/epm_table_grapher.php?t=epmt_5_6_a

USGS. (2021). *Per capita water use: How much water do you use at home?* [USGS Water Science School]. https://water.usgs.gov/edu/activity-percapita.php

Van Abel, N., Schoen, M. E., Kissel, J. C., & Meschke, J. S. (2017). Comparison of Risk Predicted by Multiple Norovirus Dose-Response Models and Implications for Quantitative Microbial Risk Assessment: Comparison of Risk Predicted by Multiple Norovirus Dose-Response Models. *Risk Analysis*, *37*(2), 245–264. https://doi.org/10.1111/risa.12616

Van der Bruggen, B., Goossens, H., Everard, P. A., Stemgée, K., & Rogge, W. (2009). Cost-benefit analysis of central softening for production of drinking water. *Journal of Environmental Management*, *91*(2), 541–549. https://doi.org/10.1016/j.jenvman.2009.09.024

van der Kooij, D. (1990). Assimilable Organic Carbon (AOC) in Drinking Water. In G. A. McFeters (Ed.), *Drinking Water Microbiology* (pp. 57–87). Springer New York. https://doi.org/10.1007/978-1-4612-4464-6_3

van der Kooij, D., Veenendaal, H. R., van der Mark, E. J., & Dignum, M. (2017). Assessment of the microbial growth potential of slow sand filtrate with the biomass production potential test in comparison with the assimilable organic carbon method. *Water Research*, *125*, 270–279. https://doi.org/10.1016/j.watres.2017.06.086

van Heijnsbergen, E., Schalk, J. A. C., Euser, S. M., Brandsema, P. S., den Boer, J. W., & de Roda Husman, A. M. (2015). Confirmed and Potential Sources of *Legionella* Reviewed. *Environmental Science & Technology*, *49*(8), 4797–4815. https://doi.org/10.1021/acs.est.5b00142

Viscusi, W. (2005). *The value of life* (Discussion paper No. 517; The Harvard John M. Olin Discussion Paper Series). Harvard Law School.

Viscusi, W. K. (2008). How to value a life. *Journal of Economics and Finance*, *32*(4), 311–323. https://doi.org/10.1007/s12197-008-9030-x

Volk, C., Bell, K., Ibrahim, E., Verges, D., Amy, G., & LeChevallier, M. (2000). Impact of enhanced and optimized coagulation on removal of organic matter and its biodegradable fraction in drinking water. *Water Research*, *34*(12), 3247–3257. https://doi.org/10.1016/S0043-1354(00)00033-6

Watts, Aerco, PVI, & Powers. (2018). *Healthcare Solutions F-WWT-Healthcare 1826, MF10448*. http://media.wattswater.com/f-wwt-healthcare.pdf

Weir, M. H., Mraz, A. L., & Mitchell, J. (2019). An Advanced Risk Modeling Method to Estimate Legionellosis Risks Within a Diverse Population. *Water*, *12*(1), 43. https://doi.org/10.3390/w12010043

Westinghouse. (2020). *Westinghouse Grid-Enabled Electric Water Heaters*. 2.

WHO. (2007). *Legionella and the prevention of legionellosis* (J. Bartram, Ed.). World Health Organization.

Yee, R. B., & Wadowsky, R. M. (1982). Multiplication of Legionella pneumophila in Unsterilized Tap Water. *APPL. ENVIRON. MICROBIOL.*, *43*, 5.

Zhang, Y., & Edwards, M. (2009). Accelerated chloramine decay and microbial growth by nitrification in premise plumbing. *Journal - American Water Works Association*, *101*(11), 51–62. https://doi.org/10.1002/j.1551-8833.2009.tb09990.

CHAPTER 3

DEVELOPMENT AND SENSITIVITY ANALYSIS OF A POPULATION ECOLOGY-EXPOSURE ASSESSMENT MODEL FOR ANTIBIOTIC-SUSCEPTIBLE AND ANTIBIOTIC-RESISTANT *E. COLI* HEALTH RISK IN RECREATIONAL WATER

In preparation for a June 2023 journal submission.

This chapter will be prepared as a manuscript for journal submission. The list of current authors is as follows: Ashley Heida, Mark T. Hamilton, Julia Gambino, Kaylee Sanderson, Mary E. Schoen, Michael A. Jahne, Jay Garland, Lucia Ramirez, Allison J. Lopatkin, Kerry A. Hamilton.

3.1 Abstract

Understanding and predicting the role of waterborne environments in transmitting antimicrobial-resistant (AMR) infections is critical for public health. Urinary tract infections (UTI) caused by the waterborne bacteria *Escherichia coli* (*E. coli*) and antibiotic-resistant extended-spectrum beta-lactamase-producing (ESBL) *E. coli* are important causes of disease globally with limited information available regarding the progression from intestinal or extra-intestinal colonization to disease. A population ecology model with an exposure assessment designed to inform quantitative microbial risk assessment (QMRA) is proposed to incorporate mechanistic information on UTI infection development. Parameters describing one horizontal gene transfer (HGT) mechanism, conjugation, were incorporated into the population ecology model to examine the impacts over time on the

potential dose of ingested antibiotic susceptible *E. coli* and ESBL *E. coli*. HGT was prominent in the environment for cases with large starting concentrations of *E. coli*, while bacterial growth was dominant in the body. Conjugation was a significant factor in cases where background *E. coli* in the human gut was considered. A sensitivity analysis demonstrated that the growth rate, conjugation rate, and estimated volume of background *E. coli* in the human gut were influential in predicting the final dose. Key uncertainties were identified for additional data collection to be able to use existing dose response parameters with population ecology models that account for bacterial processes (growth, conjugation, and inactivation) inside the human gut. The model is recommended as a tool to begin the expansion of the QMRA paradigm to explore the impacts of evolutionary changes in AMR risk assessment.

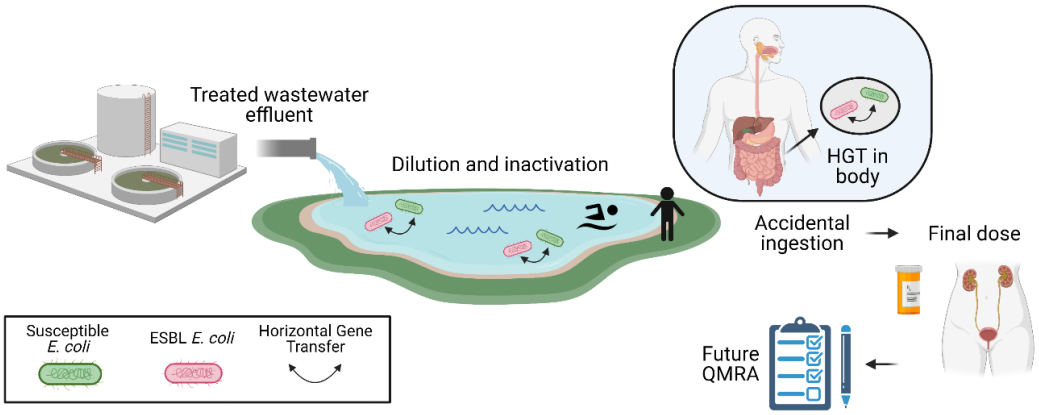

Figure 8: The modeled transformations of both susceptible and ESBL *E. coli* populations are described below from the environment to entry in the human body, colonization at the target organ (gut), and subsequent pathogenesis.

3.2 Introduction

Antimicrobial resistance (AMR) can develop when microorganisms acquire antibiotic resistance genes (ARG) that enable them to survive exposure to antibiotics. As new ARGs develop to overcome existing antibiotics, simple treatments for a disease may no longer be effective. Thus, antibiotic resistance and the transfer of ARGs are critical issues in public health. In the United States alone, more than 2.8 million infections caused by antibiotic resistant bacteria (ARB) occur each year, resulting in 35,000 deaths (CDC, 2019). Globally, the estimated deaths due to ARGs were 4.95 million in 2019 (Murray et al., 2022). Antibiotic resistant infections continue to rise in importance, with the deaths from infection expected to surpass the number of deaths from cancer before the year 2050 (O'Neill, 2016).

Environmental settings such as wastewater may be a "hot spot" where ARB, ARGs, and stressors can co-occur, resulting in the proliferation of antibiotic resistance (Petersen & Hubbart, 2020; Vikesland et al., 2017). While it may not be conducive to population growth, HGT can still occur in the environment and result in a susceptible population having increased access to ARGs. To prevent the spread of antibiotic resistance, it is

essential to understand the primary drivers of human exposures in environmental settings. Healthcare-associated transmissions have historically been the focus of study compared to environmentally-transmitted infections, and the role of the environment as a transmission route for the genetic determinants of AMR is not fully described. While wastewater treatment plants (WWTPs) reduce pathogens in the wastewater before releasing the effluent into surface waters, including recreational water bodies, these treatments can be ineffective in eliminating genetic signals, resulting in discharge of ARGs and subsequent opportunities for HGT and human exposure (Garner et al., 2018, 2021). ARBs can survive the WWTP process and have been found in higher percentages of the total bacterial load after the WWTP process has occurred (Brechet et al., 2014).

Extended-Spectrum Beta-Lactamase (ESBL)-producing *Escherichia coli* (ESBL *E. coli*) are labeled by the Centers for Disease Control and Prevention (CDC) as a "Serious Threat" (CDC, 2019) that are commonly found in wastewater and recreational waters (Blaak et al., 2014, 2015). They have been identified as a priority for focus in environmental matrices (Berendonk et al., 2015), along with their genetic determinants (e.g. antibiotic resistance genes [ARG] $bla_{\text{CTX-M}}$ and bla_{TEM}). The $bla_{\text{CTX-M}}$ gene is a dominant ESBL gene (Bonnet, 2004; Borgogna et al., 2016; D'Andrea et al., 2013). ESBL equips its host to be able to hydrolyze extended-spectrum cephalosporins and other beta-lactam antibiotics, making infections from the bacteria much more difficult to treat (Ghafourian et al., 2015). Nonresistant *E. coli*, referred to throughout as antibiotic susceptible *E. coli*, can acquire a gene encoded for the ESBL enzyme through conjugation

from adjacent ESBL *E. coli* bacteria and will then become an ESBL *E. coli* bacteria (Lopatkin et al., 2017).

ESBL *E. coli* is a leading cause of urinary tract infections (UTIs), which affect up to 150 million people every year worldwide (Picozzi et al., 2014). In 2017, there were approximately 197,400 hospitalized cases and an estimated 9,100 deaths in the United States attributed to ESBL bacteria (CDC, 2019). *E. coli* generally causes enteric UTIs, or sepsis/meningitis infections and is classified into pathotypes or pathovars based on criteria including the site of infection (e.g. intestinal pathogenic *E. coli* [IPEC] and extraintestinal pathogenic *E. coli* [ExPEC]) (Foster-Nyarko & Pallen, 2022; Graham et al., 2021). The causative agent of UTI, uropathogenic *E. coli* (UPEC), is a subset of the ExPEC category (Graham et al., 2021). UPEC (not all UPECs are antibiotic resistant) causes 80-90% of UTI infections (Flores-Mireles et al., 2015; Foxman, 2014). The health burden from environmental exposures remains poorly characterized. Potential environmental exposures to ESBL *E. coli* include non-dietary ingestion of the bacteria during recreational swimming downstream of WWTPs , inhalation of wastewater aerosols (Chen et al., 2021), dermal exposures (Pitol et al., 2020; Yau et al., 2009), or food (including crops irrigated with treated or untreated wastewater) (Collineau et al., 2019; Collineau et al., 2018; Njage & Buys, 2015, 2017). While ingestion of water containing *E. coli* may be linked to UTI, understanding of the impact of oral exposure and colonization of the gut microbiome on development of UTI due to UPEC is incomplete (Graham et al., 2021). The gastrointestinal tract is generally accepted as a reservoir for UPEC strains (Katouli, 2010). Infections are

more common among women due to shorter urethra distance compared to men (Harrington & Hooton, 2000; Medina & Castillo-Pino, 2019). Several authors have highlighted recreational water as a potential area for the spread and/or dissemination of AMR , and several outbreaks due to *Salmonella* spp., *Enterococcus* spp., *E. coli*, and *Vibrio cholerae* have also been attributed to sewage-impacted water (Chatterjee et al., 2018; Food Safety News, 2022). Epidemiological studies have also implicated recreational water via surfing (Leonard et al., 2018), swimming in the ocean (Jorgensen et al., 2017; Søraas et al., 2013; van den Bunt, 2019), or exposure to spa pools (Begier et al., 2004), as areas for dissemination of AMR to people with a focus on *E. coli* and ESBL *E. coli*.

Typically, quantitative estimates of microbial risk rely on the use of quantitative microbial risk assessment (QMRA), an approach for identifying an environmental microbial hazard, assessing the degree of exposure to the hazard from an activity (such as swimming), relating a dose to a probability of an adverse outcome, and characterizing the risk either through point estimates or stochastic analysis (Haas et al., 2014). However, current QMRA approaches have generally not yet accounted for complexities related to the evolution of AMR due to lack of quantitative data on evolutionary kinetics or process rates, and uncertainties regarding the impact of factors such as microbial community and environmental matrix on these processes. Acquisition of AMR occurs due to genetic mutations and/or recombination, selection and clonal expansion, or horizontal gene transfer (HGT) (Banerji et al., 2019; Boolchandani et al., 2019). HGT is thought to be a dominant process in the development of AMR and encompasses mechanisms of conjugation,

transduction, and transformation which results in a gene being transferred from one organism to another (Burmeister, 2015; Emamalipour et al., 2020; Ochman et al., 2000; Sun et al., 2019; Thomas & Nielsen, 2005). Conjugation can happen in a given matrix (e.g. WWTPs, the environment, or the human microbiome) throughout the bacterial cell cycle (Wang & Levin, 2009) and can be efficient in transferring ARG, especially in environments with close cell-to-cell contact (Stalder & Top, 2016). The relative importance of conjugation is emphasized for environmental matrices and is a function of multiple factors including host, recipient, and plasmid identities, media type, and environmental conditions (Pruden et al., 2018; Tamanai-Shacoori et al., 1995).

Existing approaches for assessing the risk of ESBL *E. coli* using quantitative models have focused primarily on environmental exposures without incorporating the impact of HGT on resultant risks, highlighting a gap in understanding the linkage between ARB and ARG in the natural environment with the risk to humans (Leonard et al., 2015; Leonard, Yin, et al., 2018; Leonard, Zhang, et al., 2018, 2018; Njage & Buys, 2017; O'Flaherty, Cummins, et al., 2019; O'Flaherty, Solimini, et al., 2019; Rousham Emily K. et al., n.d.; Schijven et al., 2015). Quantitatively accounting for HGT in the continuum of events leading to the development of antibiotic resistant infections has been identified as a critical gap for developing such models (Hamilton et al., 2022; Moralez et al., 2021). A single resistant *E. coli* risk model has considered ARG exposure through swimming events in recreational water to quantify maximum allowable concentrations of antibiotic susceptible and ESBL *E. coli*. A recent model developed to estimate Methicillin-resistant

Staphylococcus aureus (MRSA) risk from wastewater reuse accounted for HGT among susceptible and resistant *Staphylococcus aureus* (SA) populations but did not consider this as a dynamic process (Schoen et al., 2021). The field of population ecology provides a framework for integrating HGT into models of ARB occurrence and therefore risk as a function of the donor, recipient, and transconjugant cells per time (Lopatkin et al., 2017; Lopatkin, Huang, et al., 2016; Lopatkin, Sysoeva, et al., 2016), but to date has not been combined with approaches for assessing risk.

The proposed model will therefore serve as a framework to address these gaps by (1) integrating a population ecology model accounting for changes in bacterial populations due to HGT of ARG into a quantitative microbial risk assessment (QMRA) framework; (2) using literature-based estimates of HGT rates for ESBL *E. coli* in the environment and higher growth conditions meant to mimic the type of conditions found within the human body; (3) quantifying the risk of exposure for antibiotic susceptible *E. coli* and resistant ESBL *E. coli* populations during recreational exposure to wastewater-impacted surface waters; and (4) evaluating potential risk scenarios and prioritizing their risk drivers. Combining population ecology and QMRA approaches will provide insight into risk drivers for environmentally mediated AMR, with a focus on the impact of HGT in the spread of ARG to guide public health protection actions.

3.3 Methods

3.3.1 Conceptual model

A conceptual model was developed for unifying elements of a QMRA approach with a population ecology model to evaluate antibiotic susceptible *E. coli* and ESBL *E. coli* exposure via non-dietary oral ingestion during recreational swimming in wastewater-impacted surface waters (**Figure 9**). Exposure to treated wastewater could occur through many scenarios, but non-dietary ingestion via swimming was chosen as an index exposure scenario with a health endpoint of UTI. Other non-swimming activities such as jet skiing, fishing, boating, kayaking, tubing, canoeing, and playing with water (Sunger et al., 2012) are not typically regulatory drivers, as current benchmarks for recreational water quality are based on swimming (Sunger & Haas, 2015). The full transmission pathway, transfer from gut-associated to urinary tract-associated bacteria, and timing of colonization and infection is not fully understood, but generally begins with contamination of the periurethral area with a uropathogen from the gastrointestinal tract (gut) (Flores-Mireles et al., 2015; Graham et al., 2021; Sarowska et al., 2019). Colonization of the urinary tract may also happen directly from swimming but was not considered in this model due to the absence of quantitative data on this rate of colonization.

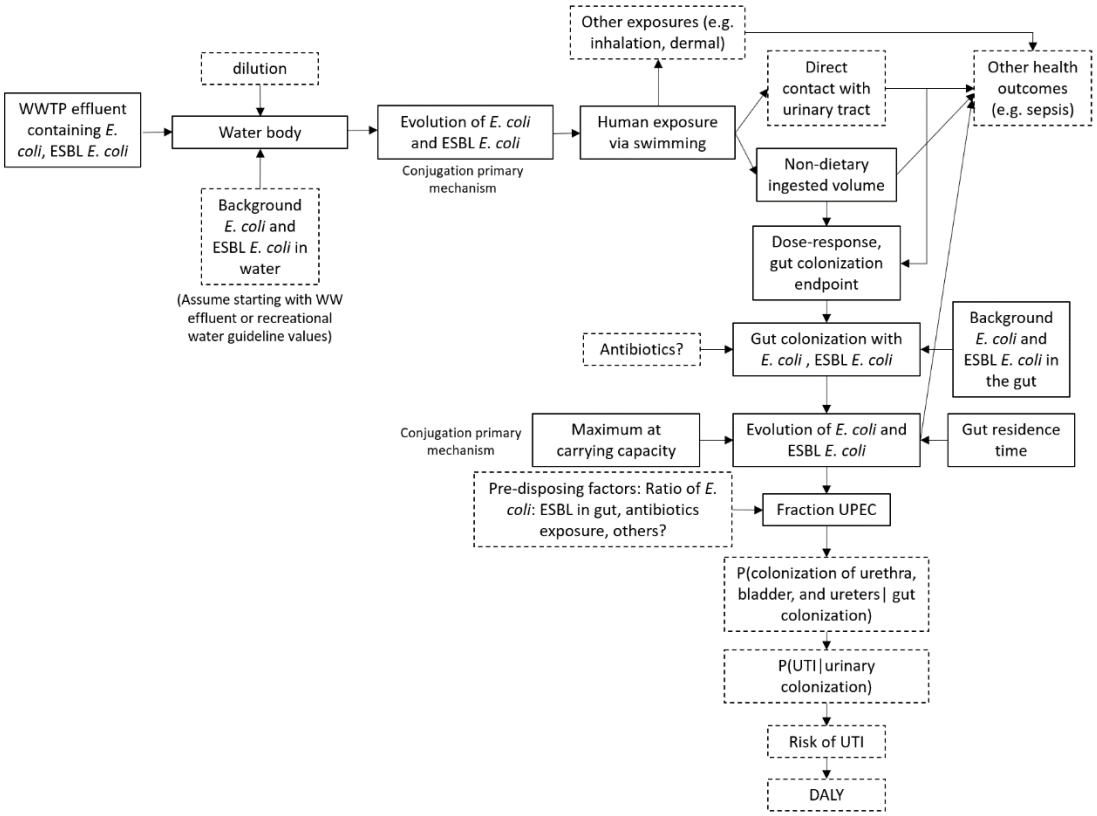

Figure 9: Conceptual model for exposure to antibiotic susceptible *E. coli* and ESBL *E. coli* during recreational swimming. Dotted line boxes are uncertainties not incorporated into the current model or beyond the current model scope.

Previous population ecology models have focused primarily on single species interactions as a starting point, intending to expand to multi-species models (Lopatkin, Sysoeva, et al., 2016). In this model, the focus was limited to a single species (s) of *E. coli* bacteria limited to two populations: (1) antibiotic susceptible *E. coli* (s_0) and (2) ESBL

(resistant) *E. coli* (s_1). The model was limited to a single species to demonstrate a use case of population ecology modeling without introducing unnecessary complexities. The population dynamics between antibiotic susceptible and ESBL *E. coli* have been previously modeled in the lab (Lopatkin, Sysoeva, et al., 2016). Exploratory modeling case scenarios were studied that considered the impact of multiple parameters on final dose of antibiotic susceptible *E. coli* and ESBL *E. coli* (**Figure 10** and **Table 2**). To conduct this analysis, multiple assumptions and simplifications were required (**Table 3** Summary of model simplifying assumptions).

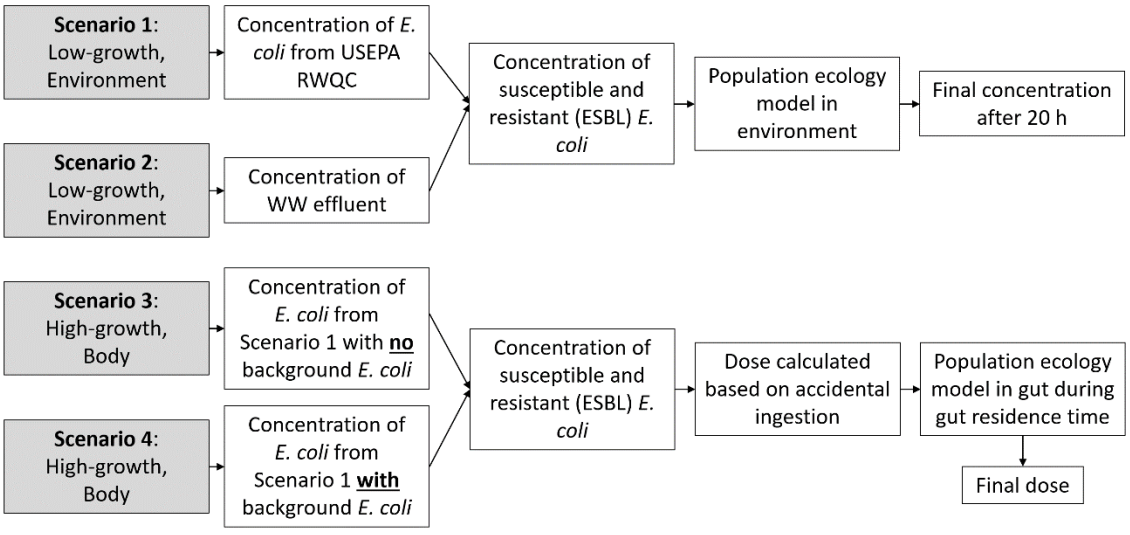

Figure 10: Modeling scenarios for antibiotic susceptible *E. coli* and ESBL *E. coli.* Results from scenario 1 were used as input for scenario 3 and 4 to compare the results with and without background *E. coli*.

3.3.2 Population ecology model

To model conversion between the antibiotic susceptible and ESBL *E. coli* populations, a population ecology model of HGT in bacteria based on bi-molecular logistic growth equations (Lopatkin et al., 2017) was combined with an exposure model for both antibiotic susceptible and ESBL *E. coli*. Acquisition of ESBL primarily occurs via conjugation (HGT) and thus mutation, transformation, and transduction are less relevant in this context (Lopatkin et al., 2017)**.** The model is considered for both "low growth" and "high growth" conditions as a proxy for examining different interactions under conditions that mimic the low growth, low cell density conditions in a surface water environment compared to the higher growth, higher cell density conditions of the human gut. To estimate model conditions for the body, we used the gut as a proxy for the gastrointestinal system, as this location has a high density of bacteria including *E. coli*. Thus, we use 'environment' and 'body' hereafter to refer to these two generic growth scenarios. This is intended to explore whether the human body might represent meaningful dynamics in the context of the larger system and to highlight factors which contribute to overall risks. Populations are described in terms of concentration (colony forming units per liter, CFU/L) in both the environment and body models.

Simulations in the environment and body were conducted to examine antibiotic susceptible and ESBL *E. coli* behavior (1) in the environment starting with an *E. coli* water concentration at the recommended United States Environmental Protection Agency (USEPA) recreational water quality criteria (RWQC) values (USEPA, 2012); (2) in the

environment starting with an *E. coli* water concentration with values from treated wastewater effluent to simulate a worst case scenario; (3) in the human body (gut) assuming no background *E. coli* in the human gut; and (4) in the body assuming some contribution of pre-existing *E. coli* in the gut unrelated to the recreational water event. Population dynamics were modeled depending on the exposure scenarios described in **Figure 10**.

Equations 24-25 were used to model ecological and evolutionary dynamics of bacteria in either the environment or body (denoted by "e" or "b" subscripts in **Table 2**), where fitness cost, α_{fit}, is a unitless value that describes the burden on a cell to retain the antibiotic resistant plasmid; bacterial growth, μ, describes the rate at which bacterial populations increase [h^{-1}]; carrying capacity, N, describes the maximum population in a given niche [CFU/ L]; conjugation rate, η [CFU L^{-1} h^{-1}]; plasmid loss rate, κ, describes the rate at which a plasmid containing a resistance determinant (e.g. antibiotic resistance gene) is lost from a resistant bacteria [h^{-1}]; and bacterial inactivation, I, describes the rate which the viable population is decreasing due to other factors (e.g. anthropogenic toxins or solar inactivation in the environment) [h^{-1}]. In the original model (Lopatkin et al., 2017)**,** fitness cost is applied to the antibiotic susceptible (s_0) term. Here it is applied to the resistant (s_1) term for ease of interpretation. In the current formulation, if α_{fit}>1, the plasmid is considered beneficial and if α_{fit}<1 it is costly.

$$\frac{ds_0}{dt} = \mu s_0 \left(1 - \frac{(s_0+s_1)}{N}\right) - \eta s_0 s_1 + \kappa s_1 - I s_0 \quad (24)$$

$$\frac{ds_1}{dt} = \alpha_{fit}\mu s_1\left(1 - \frac{(s_0+s_1)}{N}\right) + \eta s_0 s_1 - \kappa s_1 - I s_1 \quad (25)$$

This model was developed in Python version 7.3.0 with Monte Carlo sampling using 10,000 iterations (Burmaster & Anderson, 1994) for initial conditions of **equation 24 and 25** at the start of the environmental ("low-growth") and human body ("high-growth") scenarios, respectively (described further in **methods sections 3.3.2.1- 3.3.2.2**). These equations were implemented using PyTorch and solved these equations using the "torchdiffeq" package (Paszke et al., 2019). A model unit analysis is provided in the **Appendix B, Section 1** and model code is provided in **Appendix B, Section 2**.

3.3.2.1 Scenario 1 and 2: Low-growth for environmental model

Scenario 1 used the USEPA RWQC for an environmental concentration with an geometric mean (GM) of 126 and statistical threshold value (STV, 90th percentile of the water quality distribution intended not to be exceeded by more than 10 percent of samples taken) of 410 CFU/ 100 mL for *E. coli* (USEPA, 2012). These levels were used to simulate a lognormal distribution for *E. coli* in ambient waters with lognormal parameters μ= ln(126), σ=0.92 CFU/L (c_0). The initial conditions for susceptible (s_0) and resistant (s_1) populations for the environmental concentration were computed according to **equations 26 and 27**. The subset of total *E. coli* considered to be ESBL (F_v) was taken from a large study of Dutch recreational waters influenced by WWTPs ranging from 0.05-1% (Blaak et al., 2014) (**equations 26-27**). These values are likely to change regionally with varied conditions and are used here due to limited literature data.

$$s_0 = (1 - F_e)c_0 \quad (26)$$

$$s_1 = F_e c_0 \quad (27)$$

Scenario 2 used treated wastewater effluent for an environmental concentration of antibiotic susceptible and ESBL *E. coli* with $bla_{\text{CTX-M}}$ gene. These distributions for treated wastewater effluent were taken from a large study over eleven sites in France (Brechet et al., 2014). This represents a worst-case-scenario where swimmers come into direct contact with treated wastewater effluent. For both scenarios, it was assumed that the water body was homogenously mixed and that there was a one-time inoculation of *E. coli* for the starting concentration as opposed to a constant flow of wastewater effluent entering the water body. This model could also be representative of a combined sewer overflow event. The physical dilution was assumed to be zero as the model does not consider additional *E. coli* entering the environment after the initial concentration is set. Additional *E. coli* from other sources was not considered.

The relative change in the two populations can be described by **equations 24 and 25**. The fitness cost, α_{fit}, is a unitless value that describes the necessary resources for a cell to retain the antibiotic resistant plasmid (Lopatkin et al., 2017). Since negligible growth of fecal-associated bacteria is assumed to occur outside of a mammalian host in a nutrient-limited environment under typical ambient surface water conditions, the fitness cost for the environmental model ($\alpha_{fit,e}$) [unitless] and the bacterial growth rate (μ_e) [hr^{-1}] was assumed to be zero (Petersen & Hubbart, 2020). The growth rates of the bacterial

populations are bounded by a maximum allowable concentration per unit volume, referred to as the carrying capacity (N) [CFU/L]. Due to the null value for the fitness cost (α_{fit}) and bacterial growth rate (μ_e) for the environmental model, the carrying capacity term (N_e) is also null and therefore set to one in the environmental model to prevent a division by zero or null value. The rate at which HGT occurs via conjugation is shown by the conjugation efficiency rate (η) multiplied by both the antibiotic susceptible and ESBL *E. coli* populations in **equations 24 and 25** [(CFU/L) $^{-1}$ hr^{-1}]. The plasmid loss rate in the environment (κ_e) will is zero [hr^{-1}] because no bacterial growth is expected for *E. coli* in the environment. The inactivation rate in the environment for both bacterial populations, I_e, was calculated using the methods described in (Schijven et al., 2015) for a temperature of 20°C and a value of prediction uncertainty of 50%. This is a general model for all water types, as inactivation of *E. coli* is temperature-dependent (Franz & Schijven, 2014) and is assumed to be the same for both antibiotic susceptible and ESBL *E. coli*. Information was not available for assessing relative differences in persistence of antibiotic susceptible and resistant strains under similar environmental conditions.

The literature was reviewed to determine conjugation rates in environmental matrices for *E. coli* species as a ratio of transconjugants / recipients×donors×time, due to the need for converting frequently reported frequencies or ratios into rates for use in **equation 24-25** (Lopatkin et al., 2017). Units are rarely reported in a time-normalized format and absolute concentrations are also typically not reported (e.g., CFU/mL of each species used). The best available information was from Amos et al. (2014) from an

experiment using *E. coli* strains from a wastewater-impacted river (Amos et al., 2014). The authors conduced conjugation experiments with *E. coli* strain DH10B and transfer of $bla_{\text{CTX-M-15}}$, a dominant ESBL gene (Bonnet, 2004; Borgogna et al., 2016; D'Andrea et al., 2013) (see **Table 3** for limitations). Mid-exponential recipients and donors at a 1:1 ratio were spotted onto an agar plate and incubated for 16 h at 30°C for the conjugation mating experiments. The donor *E. coli* strains were isolated from river sediment samples taken from downstream and upstream of a WWTP. Ratios of transconjugants / recipients enumerated after the assay ranged from 1.70×10^{-7} to 1.32×10^{-3}. All values observed were normalized to a 16 h experimental duration and a donor cell concentration of ~0.15×10^{8} cell/mL based on a mid-log phase optical density of 0.2) (Stevenson et al., 2016). This resulted in a range of η values from 7.08×10^{-19} to 5.50×10^{-15} $(\text{CFU/L})^{-1}$ h^{-1}. Only one other study was available providing conjugation frequencies for ESBL determinants from environmental sources (including soil, sewage, and water samples from farms) with ratios of transconjugant *E. coli* J53 containing $bla_{\text{CTX-M-14}}$ to donors cells ranging from 6.40×10^{-2} to 2.0×10^{-7} in detectable samples (Tansawai et al., 2019). Experiments were conducted overnight in broth cultures and absolute concentrations were not reported. If a similar concentration assumption was made with regard to the recipient concentration, this would result in T/DRdt ranging from 4.27×10^{-12} to 1.33×10^{-17} $(\text{CFU/L})^{-1}$ h^{-1}, which overlaps with the range of values observed in Amos et al. (Amos et al., 2014).

3.3.2.2 Scenario 3 and 4: High-growth for body model

High-growth conditions were modeled using concentrations from scenario 1 (t=5 hr) to simulate non-dietary ingestion for adults during a swimming event (45 minutes) in recreational water. The differential equations (**equation 24-25**) were initialized using values for the antibiotic susceptible *E. coli* population (s_0) and the ESBL *E. coli* population (s_1) from the concentration in the environment model. These starting concentrations can be considered the initial dose ($dose_{0,1}$) of both *E. coli* populations (**equation 28**).

$$s_0 = dose_0 = s_0\left(\frac{V_i}{V_i+V_{gut}}\right) + s_{gut}(1-F_{body})\left(\frac{V_{gut}}{V_i+V_{gut}}\right) \quad (28)$$

$$s_1 = dose_1 = s_1\left(\frac{V_i}{V_i+V_{gut}}\right) + s_{gut}F_{body}\left(\frac{V_{gut}}{V_i+V_{gut}}\right) \quad (29)$$

Scenario 3 assuming no background *E. coli* in the body (s_{gut}=0) (Dufour et al., 2017; US Environmental Protection Agency, 2011; USEPA, 2019). The concentration ingested ($s_{0,1}$) was multiplied by the volume ingested (V_i) [L] (US Environmental Protection Agency, 2011) and was normalized by the volume of the gut for male and female adults (V_{gut}) [L] (Rao et al., 2006). Scenario 4 has additional background *E. coli* present in the gut ($s_{gut}\neq0$). The concentration ingested ($s_{0,1}$) was multiplied by the volume ingested and normalized by the volume of the gut. The microbial background population of *E. coli* was also normalized and added to the ingested concentration. The background concentration of *E. coli* in the gut was used in conjunction with the estimated percentage

of ESBL *E. coli* (Bernard et al., 2016) in order to obtain estimates of antibiotic susceptible and ESBL *E. coli* background populations in the gut (F_b).

The ingested bacteria ($s_{0,1}$) then underwent population density changes described by **equations 24 and 25** for the duration of the residence time (t_r) [hr], or the time taken for matter to move through the digestive tract (Cummings et al., 1976). During the residence time, the antibiotic susceptible and ESBL *E. coli* populations will be affected by the low-cost fitness cost ($\alpha_{fit,b}$) of 0.98 [unitless], representing the additional biological cost of maintaining a resistant plasmid. Bacterial growth is considered in the gut, as *E. coli* will grow in the gut which is its primary environment (Berendonk et al., 2015). The bacterial growth rate of susceptible and ESBL *E. coli* in the body (μ_b) was modeled using a positive uniform distribution [hr^{-1}] (Lopatkin et al., 2017). The growth of the bacterial populations were bounded by the carrying capacity in the body (N_b) [CFU/L] (Lopatkin et al., 2017). The plasmid loss rate in the body (κ_b) was modeled as a point value of [hr^{-1}] and is the rate at which resistant plasmids were lost from the ESBL *E. coli* population. The inactivation rate of the bacterial populations in the gut (I_b) was modeled as a point value [hr^{-1}] (Lopatkin et al., 2017). No physical dilution (excretion) of bacterial populations is assumed during the body residence time.

3.3.2.3 Exposure model

After the allotted residence time, the concentration of antibiotic susceptible and resistant *E. coli* was multiplied by the fraction of the *E. coli* in the gut considered to be

UPEC isolates was applied (F_{UPEC}) as shown by **equations 30 and 31**. These equations return the final dose of each population.

$$dose_{s0,final} = s_0 F_{UPEC} \quad (30)$$

$$dose_{s1,final} = s_1 F_{UPEC} \quad (31)$$

In a standard QMRA, , a curve would be fit to quantal data of at least 3 doses with unique probabilities of response that pass the Cochran-Armitage test of trend (Haas et al., 1999). However, due to the nature of dose response parameters already accounting for *in vivo* population ecology, applying the dose response parameter to the final dose values described above is not compatible with the typical dose response approach. Dose response data that can be applied to *in vivo* population ecology models is needed to continue the QMRA beyond exposure assessment for this model.

3.3.2.4 Sensitivity analysis

A Spearman rank correlation coefficient was computed for all Monte Carlo input and output variables using the Spearmanr function from the stats package in Python. Variables were compared to antibiotic susceptible and ESBL *E. coli* doses from scenario 4, which considered a high-growth with background *E. coli* population. The value of the correlation coefficient indicates the strength of the relationship of the variable to the final result.

Table 2. Exposure model parameters. See Table 3 descriptions of assumptions for assumed values.

Parameter	Symbol	Unit	Value	Distribution	Source
Fitness cost					
Environment	$\alpha_{fit,e}$	Unitless	0.00	Point	(Lopatkin et al., 2017)
Body	$\alpha_{fit,b}$	Unitless	0.98	Point	(Lopatkin et al., 2017)
Bacterial growth rate					
Environment	μ_e	hr^{-1}	0.00	Point	Assumed
Body	μ_b	hr^{-1}	Min: 0.00 Max: 0.30	Uniform	(Lopatkin et al., 2017)
Carrying capacity					
Environment	N_e	CFU/L	1.00	Point	Assumed
Body	N_b	CFU/L	Min: 10^4 Max: 10^{15}	Uniform	(Lopatkin et al., 2017; Lunestad et al., 2016)
Conjugation efficiency rate					
Environment	η_e	$(CFU/L)^{-1}\ hr^{-1}$	alpha: 4.76×10^{-1} beta: 6.16×10^4	Beta	(Amos et al., 2014)
Body	η_b	$(CFU/L)^{-1}\ hr^{-1}$	Min: $10^{-6.25}$ Max: $10^{-8.48}$	Uniform	(Saliu et al., 2020)
Plasmid loss rate					
Environment	κ_e	hr^{-1}	0.00	Point	Assumed
Body	κ_b	hr^{-1}	1.0×10^{-3}	Point	(Lopatkin et al., 2017)
Inactivation rate					
Environment	I_e	hr^{-1}	0.53	Point	
Body	I_b	hr^{-1}	0.05	Point	(Lopatkin et al., 2017)
Bacterial concentration in treated wastewater effluent					
Susceptible *E. coli* (wastewater effluent)	c_0	CFU/ L	Mean: 3.7×10^6 Sd: 6.0×10^6	Truncated Normal	(Brechet et al., 2014)

ESBL *E. coli* (wastewater effluent)	c_1	CFU/ L	Mean: 2.2×10^4 Sd: 3.1×10^4	Truncated Normal	(Brechet et al., 2014)
Susceptible *E. coli* (RWQC)	c_0	CFU/ L	Mean: ln(126) Sd: 0.92	Lognormal	(USEPA, 2012)
Dilution rate					
Environment Body	δ_e δ_b	hr^{-1} hr^{-1}	0.00 0.00	Point Point	Assumed Assumed
Background *E. coli*					
Environment	s_{env}	CFU/ L	0.00	Point	Assumed
Body	s_{gut}	CFU/ L	Min: 10^6 Max: 10^7	Uniform	Assumed
Volume					
Volume ingested	V_i	L	Mean: 0.017 Sd: 0.019 Truncated at 0.00	Truncated Normal	(US Environmental Protection Agency, 2011)
Volume in gut	V_{gut}	L	Min: 0.20 Max: 0.75	Uniform	(Amoueyan et al., 2020; Barker et al., 2013; Rao et al., 2006)
Residence time					
Body	t_{res}	hr	Mean: 54.2 Sd: 2.5	Normal	(Cummings et al., 1976)
Probability parameters					
Fraction of total environmental *E. coli* that are ESBL *E. coli*	F_e	Unitless	Min: 5×10^{-4} Max: 0.01	Uniform	(Blaak et al., 2014)
Fraction of total environmental *E. coli* that are ESBL *E. coli*	F_b	Unitless	Min: 5×10^{-5} Max: 0.023	Uniform	(Bernard et al., 2016)
Fraction of *E. coli* that are UPEC	F_{UPEC}	Unitless	Min: 0.050 Max: 0.088	Uniform	(Diallo et al., 2013; Franz et al., 2015; Johnson et al., 2017)

3.4 Results

3.4.1 Scenario 1 and 2: Low-growth for environmental model

The concentrations of antibiotic susceptible and ESBL *E. coli* in recreational waters were modeled over a 20-hour period with impacts of bacterial conjugation efficiency and bacterial inactivation in water. Two cases were investigated using initial concentrations from RWQC (scenario 1) and treated wastewater effluent (scenario 2). **Figure 11** shows the population ecology model progressing in time. When initial concentrations from RWQC were used, the microbial populations were not dense enough for notable conjugation to take place. Both antibiotic susceptible and ESBL *E. coli* experience inactivation until the populations are depleted. When initial concentrations of treated wastewater effluent are used, conjugation is seen to take place during the first hours of the simulation, leading ESBL *E. coli* to be the dominant population. After conjugation has occurred, both the antibiotic susceptible and ESBL *E. coli* experience inactivation until the populations are depleted.

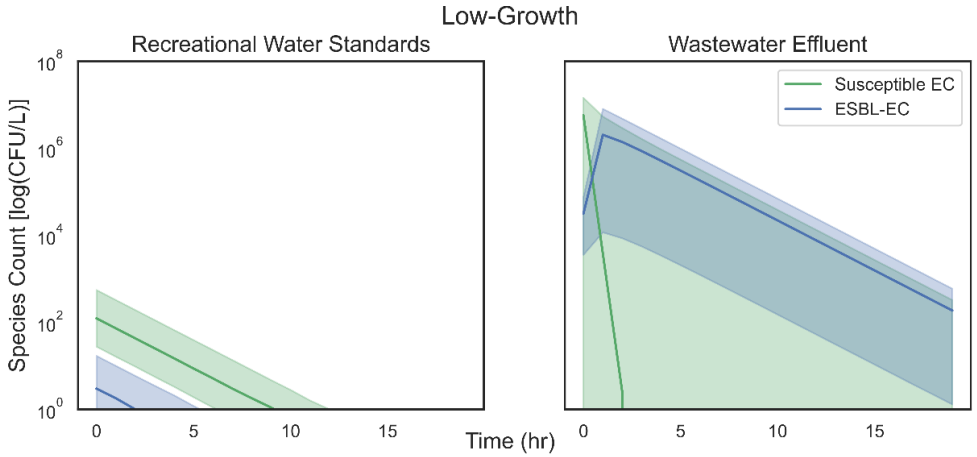

Figure 11. Species concentration in the environment with different initial antibiotic susceptible and ESBL *E. coli* starting concentrations. Concentrations form RWQC (left) and treated wastewater effluent (right) were used as starting concentration. Antibiotic susceptible *E. coli* concentrations are shown in green and ESBL *E. coli* concentrations are in blue. The lines represent the median values of the Monte Carlo simulation and the shaded regions are the 5^{th} and 95^{th} percentiles.

3.4.2 Scenario 3 and 4: High-growth for body model

Population simulations in the body accounted for select ecological and evolutionary changes (growth, conjugation efficiency, carrying capacity, plasmid loss rate, and inactivation) as well as processes that focused on relevant subsets of total commensal *E. coli* (UPEC fractions). Ingested concentrations were taken from the environment scenario where RWQC was used for the initial concentrations (scenario 1). The high-growth gut scenario allows for high cell density and represents favorable growth as well as conjugation conditions. The antibiotic susceptible and ESBL *E. coli* populations were modeled for a residence time of up to 70 hours (**Figure 12**) for scenario 3 (without background *E. coli*) and scenario 4 (with background *E. coli*).

For scenario 3, antibiotic susceptible and ESBL *E. coli* populations increased steadily over the simulated residence time within the human gut. The populations do not reach a concentration where conjugation is prominently observed. Antibiotic susceptible *E. coli* was the dominant population and reached average value of 2.13×10^3 CFU/L

(median: 3.14 × 10^2 CFU/L). ESBL *E. coli* reached an average value of 8.40 ×10^5 CFU/L (median: 2.30 CFU/L).

When background *E. coli* populations exist in the gut, there is a rapid change in the prominent population due to the high conjugation rate. The ESBL *E. coli* population increases rapidly as the antibiotic susceptible *E. coli* undergoes conjugation and becomes ESBL *E. coli*. The ESBL *E. coli* population continues to grow for the duration of the residence time. The antibiotic susceptible *E. coli* decreases until it reached the point where population growth is equal to the population loss due to conjugation and inactivation. By the end of the simulation, ESBL *E. coli* was the dominant population with an average value of 4.71 ×10^{12} CFU/L (median: 3.77 ×10^9 CFU/L) whereas antibiotic susceptible *E. coli* was 3.51x10^4 (median: 3.44 ×10^3 CFU/L).

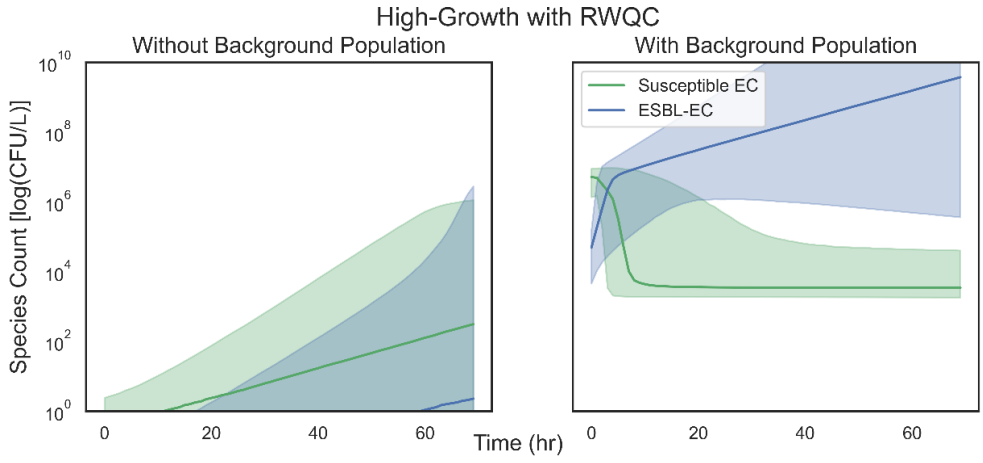

Figure 12. Species concentration in the body without (scenario 3) and with (scenario 4) background populations in the gut.

3.4.3 Scenario 3 and 4: Final dose results

Predicted doses of *E. coli* in the gut were computed for antibiotic susceptible and ESBL *E. coli* after the gut residence time had elapsed (**Figure 13**). Scenario 3 without any background *E. coli* in the gut yielded an average dose of 2419 CFU (median: 4.82) for antibiotic susceptible *E. coli* and 459 CFU (median: 0.04 CFU) for ESBL *E. coli*. For Scenario 4 with background *E. coli* in the gut yielded an average dose of 1366 CFU (median: 113 CFU) for antibiotic susceptible *E. coli* and 7.69 $\times 10^{9}$ CFU (median: 2.74 $\times 10^{7}$ CFU) for ESBL *E. coli*.

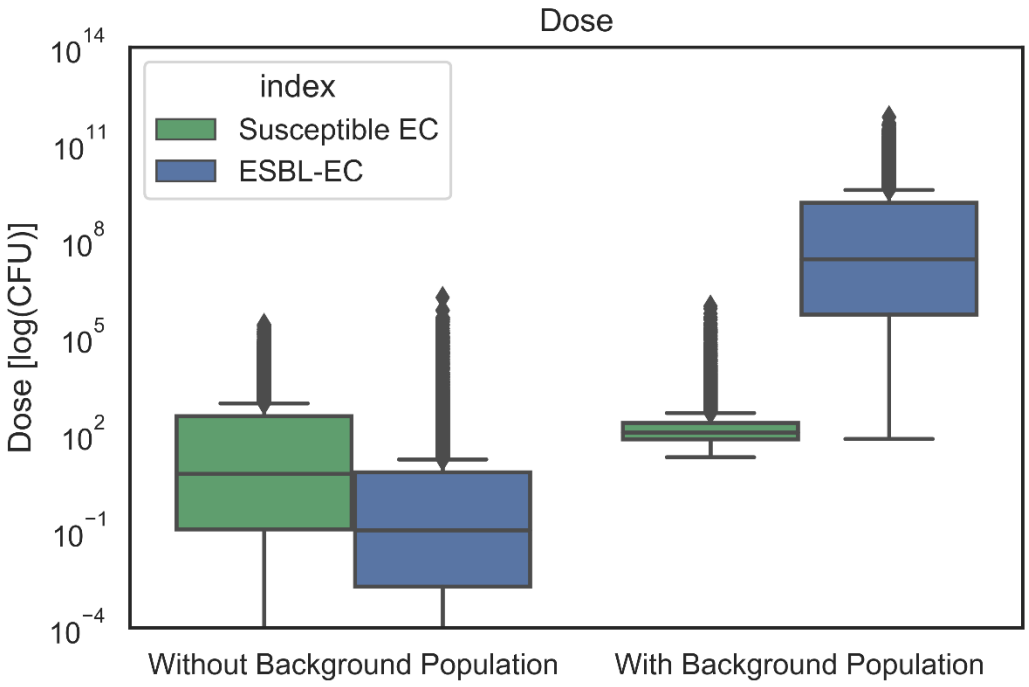

Figure 13. Dose without and with background *E. coli* in the gut.

3.4.4 Sensitivity Analysis

Influential variables in the population ecology-exposure model are shown in **Figure 14**. The final dose from scenario 3 with no background *E. coli* population in the gut (s_b = 0) was most highly impacted by the growth rate in the body with a strong, positive Spearman correlation coefficient of 0.96 for antibiotic susceptible *E. coli* and 0.84 for ESBL *E. coli*. Both antibiotic susceptible and ESBL *E. coli* populations for this case also saw weak positive correlation values for the volume of recreational water ingested and starting concentrations of antibiotic susceptible and ESBL *E. coli* in the environment. The final dose from scenario 4 with background *E. coli* population in the gut ($s_b > 0$) was most highly impacted by the conjugation rate in the body for the antibiotic susceptible population with a strong negative Spearman correlation coefficient of -0.96. There was also a weak positive correlation for percent UPEC *E. coli* (0.24). The ESBL population was highly impacted by the growth rate, with a strong positive Spearman correlation coefficient of 0.99. There was also a weak positive correlation for background *E. coli* in the gut.

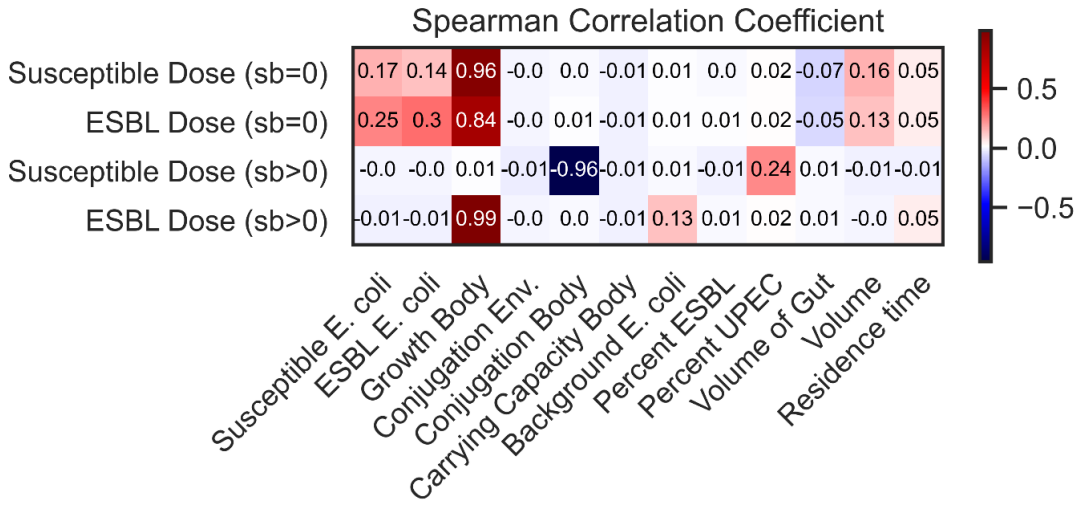

Figure 14. Sensitivity analysis using Spearman's correlation coefficients for antibiotic susceptible and ESBL *E. coli* final dose for scenario 3 (no background *E. coli* in the gut, sb = 0) and for scenario 4 (with background *E. coli* in the gut, sb > 0) against all Monte Carlo variables.

3.5 Discussion

This model for population-ecology and exposure assessment investigated four different scenarios. Scenario 1 and 2 were representative of a low-growth environment for cases that assumed a homogenous concentration of *E. coli* at the RWQC standards and at treated wastewater effluent concentrations, respectively. Antibiotic susceptible and ESBL *E. coli* starting concentrations ranged from 10^0 to 10^3 CFU/L for scenario 1 and from 10^4 to 10^7 CFU/L for scenario 2. The difference in magnitude between these scenarios is large enough to observe different driving effects on each model. For scenario 1, inactivation is

the driving variable here. Both the antibiotic susceptible and ESBL *E. coli* populations decline until they are depleted. However, is scenario 2, conjugation is observed to be the driving variable for the first few hours. The ESBL *E. coli* population grows rapidly as the antibiotic susceptible population acquires the ESBL plasmid until the antibiotic susceptible population is depleted. Both populations still experience inactivation at the same rate as scenario 1, but it is less obvious until after the first two hours of the model.

Scenario 3 and 4 were representative of high-growth model representative of the human gut. These cases that assumed a homogenous starting concentration of *E. coli* throughout the gut taken from time t=5 in scenario 1. Scenario 3 only considered the starting concentrations from scenario 1, while scenario 4 considered the concentrations from scenario 1 in addition to a background *E. coli* population in the gut. Similar to the differences in scenario 1 and 2, scenarios 3 and 4 have a difference in magnitude between starting concentrations to observe different driving effects on each model. Scenario 3 sees a slow linear growth for the duration of the residence time. The populations do not reach a concentration where conjugation is prominently observed. In additional cases (not shown), conjugation started to become a prominent factor after the antibiotic susceptible *E. coli* population reached 10^4 CFU/L and ESBL *E. coli* population reached 10^1 during the residence time. In scenario 4, conjugation is observed to be the driving variable during the first few hours until the growth of the antibiotic susceptible population is equal to the population loss due to conjugation and inactivation. Growth drives the ESBL population to continue to increase for the duration of the residence time.

The final dose for scenarios 3 and 4 were calculated after HGT occurred in the gut. The final dose was measured during the available range of residence time as a Monte Carlo variable. For scenario 3, the final dose of antibiotic susceptible *E. coli* was larger than that of ESBL *E. coli.* Scenario 4 has a larger final dose of ESBL *E. coli* and lower value of antibiotic susceptible *E. coli* that is spread over a much smaller range. This occurs because the antibiotic susceptible population has reached a steady state with the population growth equaling the population loss due to conjugation and inactivation. In additional cases run that were not displayed in this analysis, the steady state of ESBL *E. coli* is also reached when the sum of both populations is equal to the carrying capacity.

To date, few models have attempted to address the exposure or risk from antibiotic resistant pathogens quantitatively, with the exception of some studies focusing mostly on exposure without considering *in vivo* population dynamics (Leonard et al., 2015; Leonard, Yin, et al., 2018; Leonard, Zhang, et al., 2018; Njage & Buys, 2017; O'Flaherty, Cummins, et al., 2019; O'Flaherty, Solimini, et al., 2019; Rousham et al., n.d.; Schijven et al., 2015). UTI infections cost the US over $1.6 billion annually and globally are an important cause of both antibiotic susceptible and antibiotic-resistant infections (Foxman, 2002; Foxman et al., 2000; Stamm & Hooton, 1993). Therefore, the ability to predict these infections is paramount for targeting resources and reducing disease. Reducing disease could be achieved by closing recreational beaches during times of increased pathogen concentration in wastewater effluent or modifying the WWTP processes to achieve a higher log removal of pathogens. Existing risk frameworks have pointed out the need for filling in numerous

gaps to undertake quantitative modeling to address these needs (Ashbolt et al., 2013; Hamilton et al., 2022; Pruden et al., 2018). Modeling can be used to define what concentrations are associated with a particular risk level and allow for evaluation of the appropriateness of that risk level for the purposes of protecting public health.

The current preliminary analysis demonstrates the potential for combining a population ecology model with exposure assessment for identifying drivers of pathogen dose to identify and rank these factors for future data collection efforts. Limitations and assumptions of the model framework are provided in **Table 3** with their respective data collection needs. Additional studies are needed to get to a risk endpoint, including understanding conditional probabilities (e.g., colonization progressions and morbidity ratios) associated with the progression and development of UTI as a function of colonization of different parts of the urinary and gastrointestinal tracts as well as human host characteristics and susceptibilities (e.g. antibiotic dosing, ratio of susceptible *E. coli* to ESBL, or other pre-disposing factors). Understanding, and continuing to develop applicable disability adjusted life year (DALY) values for use in site-specific risk assessments is recommended for further investigation. Additionally, there is an opportunity for behavioral data to be incorporated to account for the time of day when recreational waters are most used. In the population-ecology model, growth parameters were assumed to be zero in the environment (e.g., growth rate, carrying capacity, fitness cost, and plasmid loss rate). However, these are uncertain point estimates that would benefit from additional data collection, especially in relevant matrices (e.g. water and wastewater). Additionally,

growth and inactivation rates are likely to fluctuate with the seasons as temperatures and UV exposure change. Quantification of these kinetics is challenging and will require studies that are able to parse ARG fate (within a live or dead cell, for example).

Table 3. Summary of model simplifying assumptions

Category	Assumption	Data collection and research needs
Pathogenesis	• Assumed that all *E. coli* in gut have ability to colonize the urinary tract in absence of quantitative rates of "transfer" • Probability of UTI given gut colonization is uncertain but likely to be related to ratio of ESBL to total *E. coli* (Ruppé et al., 2013) • Population susceptibilities not considered (e.g., prior UTI, catheter use, bladder dysfunctions, age, sex differences, or other demographics) • Parameters specific to high-income North-American populations	• Conditional probabilities of colonization and UTI given *E. coli* and ESBL exposures • Quantification of population susceptibility impacts on risk of UTI • Expansion of current work to low- and middle-income water, sanitation, and hygiene (WASH) settings
Microbial dynamics	• Antibiotic susceptible *E. coli* assumed present in all fecal samples • Single species, single plasmid/gene dynamics considered. $bla_{\text{CTX-M-15}}$, a dominant ESBL gene (Bonnet, 2004; Borgogna et al., 2016; D'Andrea et al., 2013), but multi-species models are available and could be considered in future work (Lopatkin et al., 2017) • Low growth and high growth conditions are representative of general trends for low growth, low density conditions in the environment and high density, high growth conditions in the human gut • Conjugation rates derived using environmental strains and grown in culture are assumed representative of environmental and human body matrices. More information is needed on conjugation rates measured *in situ* in environmental matrices.	• Ecological parameters measured in relevant matrices and reported with standardized units (e.g. HGT per unit time with absolute concentrations reported, plasmid loss rates, and inactivation rates) • Quantification of impact of antibiotics and other stressors on ecological parameters at environmentally relevant concentrations • Development of multi-species population ecology QMRA models • Consideration of other relevant ARG and cross-species transfers

	• A homogenous ordinary differential equation can be used to explore the fundamental dynamics of plasmid transfer in the environment and human gut assuming well-mixed conditions. This greatly simplifies human gut physiology where density and structural constraints change at the mm scale (Contijoch et al., 2019). • Effect of antibiotics or other stressors on dynamics not considered • Growth rate is minimal in the environment due to presence of low-nutrient, high-stress conditions in surface water. This assumption results in fitness cost also not being considered in the environment as the growth term goes to null • Plasmid loss rate depends on reproducing cells, and therefore if growth is negligible in environmental water, plasmid loss will also be assumed negligible • Mutation was not considered: An accumulation of mutations that could affect resistance do not arise over the course of the timescale studied; assumption that HGT rate is >> mutation rate (Foster-Nyarko & Pallen, 2022) and therefore the mutation rate is not included in the current calculations. Fully formed resistance genes transferred during conjugation will dominate compared to accumulation of resistance by random mutation and selection. We assume that it is rare to have a single mutation that can cause a drastic phenotypic change. In the context of AMR, HGT is the main contributor to resistance between the resistance genes are already optimized through the evolution process and a more	

	significant player in the spread of resistance compared to individual mutations. • Conjugation is assumed to be the dominant HGT mechanism: Plasmids are prevalent in the environment, contain many ARGs, and have broad host ranges. By comparison, phages have narrower host ranges and other restrictions related to the amount of DNA packaged but are less studied (transduction is a lesser consideration). Similarly, uptake of naked DNA is thought to be lesser (transformation is a lesser consideration) • Populations used in conjugation experiments (donors, recipients, and transconjugants) did not report absolute concentrations for donors, therefore an estimate for the donor density was used given that cells were reportedly grown to mid-log phase. If more detailed information is reported, other models are available for extrapolating rates of plasmid transfer over other conditions(Simonsen et al., n.d.) • Assumed the antibiotic susceptible and ESBL *E. coli* were homogeneously distributed in both the low-growth (environment) and high-growth (gut) models.	
Exposure	• Concentrations of *E. coli* in recreational water at existing USEPA recreational water criteria values; no additional input sources to the water body considered and no additional dilution/background *E. coli* considered. • Non-oral exposures not considered (e.g. direct colonization of urogenital tract during immersion in recreational water) • Exposure to antibiotics or other stressors not considered	• Population-specific exposure parameters for water immersion and colonization of gastrointestinal and urogenital tract • Quantification of *E. coli* and relevant pathogenic and resistant subsets (e.g.

	• Environmental inactivation of *E. coli* and ESBL *E. coli* assumed to be same • Environmental inactivation assumed for this calculation at 20°C and to follow first-order kinetics with an empirical constant previously derived (Schijven et al., 2015) • Gut transit time measured for healthy young men on unregulated diet assumed to be representative of general gut transit time	UPEC, ESBL) in water environments and human body • Quantification of growth/inactivation kinetics for susceptible vs. resistant *E. coli* strains • Expansion to other exposure scenarios and niches
Dose response	• Fraction of total *E. coli* (including ESBL) that is UPEC remains constant in the body; UPEC and ESBL are independent outcomes • Dose response relationship does not differ for ESBL *E. coli* compared to susceptible *E. coli* • Shedding of *E. coli* assumed to be representative of "colonization of gastrointestinal tract" endpoint • Exposure to antibiotics or other stressors and impacts on dose response not considered • Dose response-time kinetics and impact of background *E. coli* on risk not considered due to in vivo kinetics implicitly included in current dose response paradigm (e.g. exponential, Beta-Poisson models) • Person-to-person transmission and impact of prior infection and/or immunity not considered • Likelihood of recurrence of UTI after first episode not considered	• Development of additional dose response models for antibiotic resistant strains of bacteria and conditional upon other exposures such as antibiotics (Chandrasekaran & Jiang, 2019) • Consideration of dose response-time kinetics with reference to antibiotic resistant organisms (Haas, 2015; Huang & Haas, 2009) • Additional information on colonization and shedding • Incorporation of person-to-person transmission dynamics (Brouwer et al., 2017) • Consideration of immunity and other dynamics for repeated exposures (Pujol et al., 2009)

HGT is thought to be an important factor for predicting the likelihood of the spread of antimicrobial resistance generally, with attention focused on identifying the hosts of ARGs and their ability confer resistance to new strains, especially for *E. coli* and other pathogens (Rice et al., 2020; Stadler et al., 2018). Specifically, conjugation is likely the dominant mechanism of HGT within some environments (Pruden et al., 2018; Tamanai-Shacoori et al., 1995), warranting its focus in the current work. Dilution of wastewater streams and specific timings can be investigated with the current modeling framework to identify relevant edge-cases under which temporal dynamics of pathogen evolution do present meaningful contributions to risk. In particular, incorporation of multi-species and antibiotic models have been performed for laboratory conditions and could be expanded to address more environmentally-relevant conditions (Lopatkin et al., 2017).

One of the key bottlenecks is for dose response models. Models are needed for assessing differences between antibiotic susceptible and resistant microorganisms, as well as the extent to which an ARG can be incorporated in the dose response modeling process either independently or as a corollary to their associated ARB (Ashbolt et al., 2013). This work models differences in survival as part of the exposure analysis, before applying any existing dose response relationships in future work. The advantage of this approach is the flexibility in modelling various scenarios and utilization of existing knowledge for dose response.

There is currently sparse data available for calibrating, verifying, or validating the current model. QMRA models are typically validated by comparing model estimates to attack rates in well-documented outbreaks where exposure is measured, or where dose reconstruction is feasible. QMRA models are useful for comparing the risks from an exposure event to existing health benchmarks, but health benchmarks can also be informed by QMRAs. Water exposures and disease clusters for *E. coli* have demonstrated elevated risks in some cases (Gordon et al., 2017; Hayward, 2020) but have not provided sufficient information for calibration. The current model is likely more applicable for a female population, as UTI are more common in women than men (Harrington & Hooton, 2000; Medina & Castillo-Pino, 2019); additional exploration of gender differences in risk predictions for UTI is warranted.

As *E. coli* is a currently accepted fecal indicator bacteria for water environments and increasingly advocated as an indicator organism for monitoring AMR (Anjum et al., 2021), there is an opportunity to collect additional data to parameterize models. Current approaches for simultaneous estimation of growth and plasmid-transfer rates (Mishra et al., 2021) represent a possible step forward for modeling efforts. Considering the interrelated nature of AMR dynamic processes present large uncertainties (Bengtsson-Palme et al., 2021) but are an important step forward for characterizing and predicting the environmental dimensions of AMR.

3.6 Additional proposed work

Traditional dose response models (e.g., exponential and Beta-Poisson) are typically an "opaque box" implicitly representing the entirety of in vivo body kinetics (including surviving various barriers and gut conditions) without necessitating an understanding of the mechanistic process. To avoid a mismatch when applying modelled *in vivo* doses of *E. coli* to a dose response model fit to oral ingestion, model scenarios including consideration of background *E. coli* in the gut were computed based on a population load endpoint only for comparison with a true "dose" for a no-background scenario.

Recent mechanistic dose response models have been proposed for ARB that incorporate differences in *in vivo* survival as part of the dose response (Chandrasekaran & Jiang, 2019, 2021). One of these models proposed for antibiotic susceptible (to the antibiotic Gentamicin) and resistant *E. coli* considers the probability of bacterium death using a stochastic death process. In summary, the probability of illness is calculated using the dose, the probability of bacterium death, and the time until symptoms are observed in the dosed population in a clinical feeding study. The authors report using this approach in place of traditional exponential dose response models. This approach will be explored with the current model described above by removing the inactivation term from **equations 24-25** and changing the first terms of **equations 28-29** to include the probability of bacterium

death and the time until symptoms are expected to observed. This will be used in place of the dose response parameter (r) and residence time in the gut (t_{res}).

3.7 Acknowledgements

The authors would like to acknowledge funding support from Water Research Foundation Project 4813 Critical Evaluation and Assessment of Health and Environmental Risks from Antibiotic Resistance in Reuse and Wastewater. Additional support was provided by the School of Sustainable Engineering and the Built Environment startup funds at Arizona State University. The authors are grateful for the support of Mary Simons and Richard Kurtz of Seaford High School, New York for supporting this work. The views expressed in this article are those of the authors and do not necessarily represent the views or the policies of the U.S. Environmental Protection Agency.

CHAPTER 4

QUANTITATIVE MICROBIAL RISK ASSESSMENT (QMRA) TOOL FOR MODELING SARS-COV-2 AND OTHER INFECTION RISKS FOR WASTEWATER TREATMENT PLANT WORKERS

In preparation for an April 2023 submission to Journal of Exposure Science and Environmental Epidemiology.

This chapter will be prepared as a manuscript for journal submission. The list of current authors is as follows: Ashley Heida, Kelly A. Reynolds, Ahamed Ashraf, Olusola O. Ogunseye, Yoonhee Jung, Lester Shulman, Luisa Ikner, Walter Betancourt, Kerry A. Hamilton, Amanda M. Wilson

4.1 Abstract

Wastewater treatment plants (WWTPs) provide vital services to the public by removing contaminants from waste streams before returning discharge to the environment. WWTP workers can be exposed to pathogens from wastewater while performing necessary job tasks. Exposure routes can include inhalation or ingestion of bioaerosols that are produced by the WWTP during treatment processes involving aeration or mechanical movement. Workers who come into contact with bioaerosols from these exposure routes can be at risk of respiratory or gastrointestinal infection. Therefore, WWTP working environments pose

potential hazards and risks to workers. The objectives of this model are to (1) aggregate information related to multi-pathogen and multi-pathway risk assessment for wastewater workers; (2) develop a QMRA model for multi-pathogen and multi-pathway risks; and (3) create a web-based application to perform and communicate risk calculations for wastewater workers. Case studies were performed investigating infection risk across eight different pathogens for seven different job tasks. It was observed that the ingestion risk among job tasks was highest for "walking the WWTP", which involved exposure from splashing, bioaerosols, and hand-to-mouth contact from touching contaminated surfaces. There was also a notable difference in exposure risk during peak (5 am-9 am) and non-peak hours (9 am and after), with risks during the peak flow hours of the early morning being 5 times greater than non-peak hours. Additionally, the use of PPE was investigated by looking at the differences in respiratory risks with mask usage or N95 respirator usage. N95 respirator usage significantly reduced median respiratory risks by 3.75 times, however, the most significant reduction of risk was associated with a difference in shift timing from peak hours to non-peak hours, assuming a 5-fold difference in pathogen concentrations between peak- and non-peak times. Due to the influence of exposure timing, more comparative data are needed for pathogens in wastewater during peak and non-peak hours. Risk management strategies for WWTP workers should be carefully considered, as scheduling change may have a significant impact on occupational risk reduction.

4.2 Introduction

Wastewater treatment plants (WWTPs) provide vital services to the public for removing contaminants from waste streams before returning discharge to the environment, especially as de facto wastewater reuse is common across the US (Rice et al., 2013). However, WWTP working environments pose potential hazards and risks to workers (Malakahmad et al., 2012). Wastewater contains a mixture of chemical and microbial hazards, including pathogenic bacteria, viruses, protozoans, chemical contaminants, and heavy metals (Li et al., 2022; Masclaux et al., 2014; Moubarz et al., 2022; Petersen & Hubbart, 2020; Staszowska, 2022; Vikesland et al., 2017). Both well-known and emerging pathogenic microorganisms are of particular concern due to their potential to cause acute illness.

Aerated wastewater (WW) contains pathogens that can increase human health risks (Lu et al., 2020). WWTP worker exposures and risks have been documented (Khuder et al., 1998; Smit et al., 2005) that include a wide range of symptoms (Smit et al., 2005). Khuder et al. (1998) showed via a questionnaire that WWTP workers have a greater prevalence of self-reported gastroenteritis, gastrointestinal symptoms, and headaches than college maintenance and oil refinery workers who were also surveyed. Smit et al. (2005) also conducted a questionnaire and measured personal endotoxin exposure over a year. They found that numerous symptoms were reported that were clustered as “lower respiratory and

skin," "flu-like and systemic symptoms," and "upper respiratory symptoms". Kallawicha et al. (2016) found that contact dermatitis or other eczema was more prevalent in areas with higher ambient bioaerosol exposure by investigating data from a national health database (Kallawicha et al., 2016). Bioaerosols are aerosols containing biological material, in this case, pathogens (Douwes et al., 2008). Generally, exposure control programs for WWTPs are typically recommended (Lee et al., 2007).

Exposure to untreated wastewater can occur through multiple routes (e.g., bioaerosol inhalation, accidental ingestion via hand-to-mouth transfer or liquid exposure, or other routes beyond the scope of this model) (Amoah et al., 2022; Korzeniewska, 2011; Korzeniewska et al., 2013; Rodríguez-Molina et al., 2021). Aeration of wastewater in WWTPs from wind or the mechanical movement of bioreactors and grit tanks are examples of processes that can aerosolize wastewater (Dada & Gyawali, 2021; Korzeniewska & Harnisz, 2013). Different types of aeration can introduce different quantities and size distributions of aerosols into the air (Han et al., 2020).

Emerging pathogens are of particular concern for wastewater workers, with previous risk assessments addressing Ebola outbreak concerns (Haas et al., 2017), Monkeypox virus (Rosa et al., 2022), and the more recent COVID-19 pandemic, caused by the virus SARS-CoV-2 (Brisolara et al., 2021). Pathogens such as adenovirus, rotavirus, norovirus, *Legionella* spp., and others are also a concern for infection from accidental wastewater

exposure or reuse exposures, warranting consideration of potential risks (Medema et al., 2004; Stobnicka-Kupiec et al., 2022). Aerosol transmission is likely to drive COVID-19 risks (Jones, 2020), as the SARS-CoV-2 virus is likely to be inactivated in the human gut and to date not been cultured from wastewater (Sobsey, 2021). Still, some reports have suggested that the fecal-oral pathway, hand-to-mouth transfer, or oral ingestion more generally could still be possible (Huang et al., 2021; Xie et al., 2020). However, it should be noted that the COVID-19 risks from this pathway (ingestion of wastewater) are likely to be low and are uncertain to date (de Oliveira et al., 2021; Kumar et al., 2021).

While engineering strategies to control aerosol generation at the source are the most effective approach according to the hierarchy of controls (CDC & NIOSH, 2023), other strategies can also reduce exposures and potential risks. Exposure reduction strategies include wearing appropriate personal protective equipment (PPE) such as masks, respirators, goggles, gloves, or other personal coverings to reduce exposure to WW and subsequent pathogens. Relevant exposure pathways include contact or fomite transfer of pathogens to the face (spread of pathogens from one surface to another via contaminated hands and, subsequently, to facial mucosa), splash hazards, whole-body contact hazards, abrasion, cut, or puncture hazards, and respiratory hazards (LeChevallier et al., 2020).

To bolster infectious disease preparedness efforts and increase the safety of WWTPs, it is important to assess occupational risks and understand the impact of various potential

risk management strategies. To prioritize risk management measures, quantitative microbial risk assessment (QMRA) is a frequently used method to evaluate the anticipated health risks from concentrations of pathogens observed in the environment for different exposure scenarios. The approach to QMRA described by Haas et al. (1999) consists of four steps. A microbial hazard is identified in the environment of interest, the degree of exposure to the hazard is assessed, the dose is related to the probability of an adverse outcome, and the risk is characterized in terms of a quantitative estimate of the probability of the outcome, with context provided for risk management and communication purposes (Haas et al., 2014). For this study, our pathogens of interest (reference pathogens) in wastewater include *Cryptosporidium hominis*, *Escherichia coli*, *Giardia duodenalis*, *Legionella pneumophila*, norovirus, rotavirus, and SARS-CoV-2 due to their epidemiologic importance and known occurrence in wastewater, or potential to cause infection in WW settings, acknowledging limitations surrounding limited evidence of SARS-CoV-2 transmission via wastewater matrices (Kumar et al., 2021).

QMRA models of wastewater bioaerosols have been performed for *E. coli* (Chen et al., 2021; Yan et al., 2021), adenovirus (Carducci et al., 2018), *Legionella pneumophila* (Xu et al., 2020), *Staphylococcus aureus* (Chen et al., 2021; Ma et al., 2022), SARS-CoV-2 (Zaneti et al., 2020), and other indicator microorganisms (Han et al., 2019; Wang et al., 2019). Ma et al. (2022) (Ma et al., 2022) performed a QMRA with *Staphylococcus aureus* exposure from a WWTP in China during different seasons and showed that infection risk

was 1.15-6.11 times greater during summer months than winter months. They also investigated PPE usage with a QMRA model and found that workers who did not use PPE were at a risk 23-36 times higher than workers who did. Mbanga et al. (2020) (Mbanga et al., 2020) estimated WWTP workers' exposure risk from *E. coli* and *Enterococcus* spp. in a WWTP in South Africa. They found the monthly probability of infection for WWTP workers who were exposed to 1 mL of untreated wastewater ranged from 91.9-94.5% and for treated effluent ranged from 3.1-32.6% depending on the time of year. Carducci et al. (2018) (Carducci et al., 2018) performed a QMRA with adenovirus exposure from WWTP bioaerosols and predicted a high risk (> 15% chance of illness for less than 3 minutes of exposure) to workers who are exposed. Medema et al. (2004) calculated the annual probability of infection from Legionellosis or gastrointestinal infection to be high for occupational workers of WWTPs, especially during cleaning tasks (reported for cleaning the sludge-dewatering installation). As a result, the authors recommended further aerosol exposure barriers for WWTP workers (Medema et al., 2004). However, there are gaps in the literature for viral QMRAs for WWTP workers, and for multi-pathogen, multi-pathway models that can be used to evaluate wastewater worker risks (Divizia et al., 2008; Douwes et al., 2003; Maal-Bared, 2023).

Web-based risk applications are increasingly used in combination with QMRA models due to their utility for communicating risks with multiple stakeholders and dynamically exploring model assumptions for a variety of applications associated with pathogen

exposures in water and wastewater (see **Appendix C, Section 2**). Gerrity et al. (2019) (Gerrity et al., 2019) developed a web application to customize a QMRA for direct potable reuse including input on the type of pathogen with distribution, level of log removal, treatment train failure scenarios, and more. Rocha-Melogno et al. (2021) (Rocha-Melogno et al., 2021) developed the web application Aerosol-Mediated Infectious Disease Risk Assessments (AMIDRAs), which includes a QMRA for diarrheal disease near open sewers and a QMRA for SARS-CoV-2 aerosolized transmission indoors. In addition to Rocha-Melogno et al. (2021) (Rocha-Melogno et al., 2021), Schijven et al. (2021) (Schijven et al., 2021) and Parhizkar et al. (2021) (Parhizkar et al., 2021) have also developed web applications for QMRA SARS-CoV-2 aerosolized transmission indoors. Additional web applications have been developed for the generalized risk of SARS-CoV-2 for a variety of scenarios depending on numerous variables including activity or event type, physical characteristics such as age and gender, vaccination status, and mask-wearing (Chande et al., 2020; Hu et al., 2020; Olsson et al., 2021; Ranney & Goldberg, 2020).

To date, applications for assessing the risk of occupational exposure are scarce. Additionally, there is a need for site-inclusive exploration of multiple pathogen risks, given the variability in pathogen occurrence by the treatment plant, season, and sewershed characteristics, among other factors (Li et al., 2022; Lu et al., 2020). As a result, this work aims to (1) aggregate information related to multi-pathogen and multi-pathway risk assessment for wastewater workers; (2) develop a QMRA model for multi-pathogen and

multi-pathway risks; and (3) create a web-based application to perform and communicate risk calculations for wastewater workers.

4.3 Methods

4.3.1 Modeling framework

Two different exposure routes were modeled: (1) accidental ingestion (including hand-to-mouth ingestion for certain exposure scenarios and ingestion of non-respirable aerosols (Maal-Bared, 2023), and (2) aerosol inhalation (<5 μm) (Randall et al., 2021). The health endpoint for the accidental ingestion model was a gastrointestinal infection. The volumes of wastewater estimated to be respirable (<5 μm) range was used in the aerosol inhalation model with a health endpoint of respiratory infection.

4.3.2 Index pathogens and exposure routes

C. hominis, *E. coli*, *G. duodenalis*, norovirus, and rotavirus were considered for the ingestion model. *L. pneumophila* was considered in the aerosol inhalation model, as it causes respiratory infections Pontiac Fever or Legionnaires' Disease. Delta and Omicron variants for SARS-CoV-2 were modeled in both ingestion and inhalation pathways, acknowledging uncertainties regarding the fecal-oral route as a means of SARS-CoV-2 infection.

4.3.3 Exposure types

Available exposure settings are based on identified WWTP worker tasks from Maal-Bared (2023) (Maal-Bared, 2023). Settings include:

(1) An office at the WWTP (working in the office or on-site trailers);
(2) Walking the plant (walking through plant areas, exposure from splashing or bioaerosols);
(3) Minor contact (adjusting valves, wiring, or job setup);
(4) Moderate contact (sampling, lab work, maintenance to primary equipment);
(5) High contact (sampling, lab work, maintenance to primary equipment);
(6) Direct splash (accidental splash to the face); and
(7) Lagoon sampling (sampling at a WW lagoon that would be applicable in decentralized and/or low-resource contexts).

The exposure time for tasks 2-5 and ingested volume for tasks 1-6 are informed by Maal-Bared (2023) (Maal-Bared, 2023). Due to a lack of data to better inform a range of expected ingestion volumes, the point values were varied by ±25% to create triangle distributions to be used in the Monte Carlo simulation with 10,000 iterations (Burmaster & Anderson, 1994). Exposure times for tasks 2 and 5 are assumed to occur between a period of 0.4 and 4.0 hours as informed by Maal-Bared, 2023 (Maal-Bared, 2023), and ingestion volumes were reported on a per-shift basis (assuming an 8 hour shift) for tasks 1-6 ranging from

1.00×10^{-3} to 5.0 mL (Maal-Bared, 2023). These values were previously adjusted by Maal-Bared, 2023 to account for the expected percent of an average day that a worker would spend performing the job tab task (percent exposure, F_{exp}). Task 1 is hand-to-mouth exposure, so it is assumed no bioaerosols are inhaled in office areas. Task 6 is a direct splash to the face, which is assumed to be immediate and only considers ingested volume, not aerosol inhalation. The exposure time for task 7, the lagoon sampling scenario, is an estimate based on the assumed lagoon sampling time during a shift. This does not include time processing the samples. The ingested volume for this scenario was estimated from the methods described by Julian et al. (2018) (Julian et al., 2018) for a sampling scenario that involved contact with a sampling container (bucket) and hand-to-mouth contact of two partial finger areas (**Appendix C, Section 1**).

For QMRA, estimates of the distribution of aerosolized pathogens are typically developed for pathogen- and process-specific scenarios. Aerosolization information is sparse for specific wastewater unit processes. Therefore, the literature was reviewed to obtain estimates that are summarized in **Table 4**. A review paper (Kitajima et al., 2020) reported PFU/L and PFU/m^3 for various treatment processes in WWTPs and wastewater lagoons. Matsubara and Katayama (2019) (Matsubara & Katayama, 2019) reported select values for aerosols and wastewater samples across multiple points of a WWTP for norovirus genogroup 2, bacteriophages, poliovirus, and murine norovirus. The authors reported both CFU/mL of wastewater sampled and CFU/m^3 of air sampled for norovirus

genogroup 2 at the activated sludge chamber and the grit chamber (raw sewage entry). These values informed the partitioning coefficient (PC) for the activated sludge chamber ($1.7x10^{-4}$ L/m^3) and for the grit chamber ($1.6x10^{-5}$ L/m^3). Gholipour et al., (2021) (Gholipour et al., 2021) reported a PC for a pumping station and activated sludge chamber at a WWTP based on based on SARS-CoV-2 RNA as a uniform distribution (Min =10^{-5}, Max = 10^{-4} L/m^3). Due to the lack of specificity in PC for different processes at the WWTP, these distributions were combined to inform the PC for tasks 2-5. Tasks 1 and 6 do not consider aerosol exposure and are therefore not assigned a PC. The PC for task 7, the lagoon sampling scenario, was informed by Brenner et al. (1988) (Brenner et al., 1988) who reported the CFU/mL of lagoon water sampled and CFU/m^3 of air sampled for five different sampling events from May to October near a wastewater lagoon. The PC for the lagoon was modeled as a uniform distribution from the minimum ($2.6x10^{-3}$ L/m^3) to the maximum ($1.6x10^{-3}$ L/m^3) from the available data in Brenner et al. (1988) (Brenner et al., 1988).

Values informed by Matsubara and Katayama (2019) and Gholipour et al., (2021) are comparable to partitioning coefficients for *Legionella* aerosolization from showers (10^{-6} to 10^{-5} CFU/m^3 /CFU/L i.e. L/m^3) (Gholipour et al., 2021; Matsubara & Katayama, 2019; Schoen & Ashbolt, 2011a). Stobnicka-Kupiec et al. (2022) (Stobnicka-Kupiec et al., 2022) report gc/m^3 (identified as potentially infectious via viability-PCR coupled with qPCR (v-qPCR), for influent and treated effluent. Ratios between reported concentrations of

airborne rotavirus, norovirus, and SARS-CoV-2 virus to those detected in influent and effluent wastewater included a range (on the order of 10^{-5} up to 10^{-1} L/m^3) that overlapped with these values.

Westrell et al. (2004) reported ingested doses from droplet spray for estimated annual ingestion of wastewater by WWTP workers at the pre-aeration process (1 mL/12-hour shift) and the belt press (5 mL/12-hour shift). The frequency of exposure to the pre-aeration process was 52 times a year and for the belt press was 208 times per year. The annual ingestion volumes were divided by an assumed 260 working days a year, accounting for weekends and holidays, and by 12 hours per shift. A per-exposure risk lasting 1-hr was estimated so it was comparable to the 1-hour aerosol exposure risk estimations. The volumes from Westrell et al. (2004) fall within the range of expected droplet ingestion based on specific tasks from Maal-Bared (2023) which was used in this model (Maal-Bared, 2023). Maal-Bared (2023) found that droplet ingestion could range from 0.001 mL/ day for minor contact with some wastewater (adjusting valves, electrical work, job setup, etc.) to 5.0 mL/ day for walking through plant areas (inspections or other activity that does not require primary contact with wastewater). The ingested volumes for Tasks 1 and 2 are high (median 3.0 and 5.0 mL) due to the high amount of contact workers have with surfaces when working in an office setting or while walking the plant over the course of a working day (Maal-Bared, 2023).

Table 4: Exposure settings and associated partitioning coefficients with exposure times for aerosol inhalation, and accidentally ingested volume from droplet or hand-to-mouth exposures.

Task	*PC (L/m^3)*	*PC Ref*	*Exposure time (hrs/task/ day)*	*Ingested volume (mL/task/ day)**	*Percent exposure (F_{exp})***
1. Office	-	-	-	Triangle (2.25, 3.00, 3.75) (hand-to-mouth)	15%
2. Walking the plant	Uniform (min = 1.00×10^{-5}, max = 1.70×10^{-4})	(Matsubara and Katayama, 2019) (Gholipour et al., 2021)	Triangle (0.30, 0.40, 0.50)	Triangle (3.75, 5.00, 6.25) (hand-to-mouth and droplet)	10%
3. Minor contact	Uniform (min = 1.00×10^{-5}, max = 1.70×10^{-4})	(Matsubara and Katayama, 2019) (Gholipour et al., 2021)	Triangle (0.60, 0.80, 1.00)	Triangle (7.50×10^{-4}, 1.00×10^{-3}, 1.25×10^{-3}) (droplet)	20%
4. Moderate contact	Uniform (min = 1.00×10^{-5}, max = 1.70×10^{-4})	(Matsubara and Katayama, 2019) (Gholipour et al., 2021)	Triangle (0.60, 0.80, 1.00)	Triangle (1.50×10^{-2}, 2.00×10^{-2}, 2.50×10^{-2} (droplet)	7%
5. High contact	Uniform (min = 1.00×10^{-5}, max = 1.70×10^{-4})	(Matsubara and Katayama, 2019) (Gholipour et al., 2021)	Triangle (3.00, 4.00, 5.00)	Triangle (6.80×10^{-2}, 9.00×10^{-2}, 1.10×10^{-1}) (droplet)	1%

6. Direct splash	-	-	-	Triangle (7.50×10^{-3}, 1.00×10^{-2}, 1.25×10^{-2}) (droplet)	1%
7. Lagoon sampling	Uniform (min=1.60×10^{-3}, max=2.60×10^{-3})	(Brenner et al., 1988)	Triangle (0.75, 1.00, 1.25)	Lognormal (-1.05, 1.45) (hand-to-mouth)	-

*All exposure times and ingested volumes for tasks 1-6 were reported as point values in Maal-Bared (2023) (Maal-Bared, 2023). These values were used as the mode for triangular distributions with the minimum and maximum values being set as 25% above or below the mode.

** Percent exposure or full time equivalent of job task. This percentage was applied to Maal-Bared, 2023 values exposure time and ingested volume prior to reporting.

4.3.4 Estimation of infection risk adjusted for time of day

The time of day was incorporated with a peak differential concentration factor by calculating risk during peak flow times (5:00 am- 9:00 am) and non-peak times (9:00 am-5:00 am). It was assumed that pathogen concentration would be larger in morning hours, due to typically higher loads of fecally-shed pathogens in wastewater during this time of day, associated with people generally defecating first thing in the morning (Heaton et al., 1992; Nguyen Quoc et al., 2022). Pathogen concentrations were assumed to be five times higher from 5:00 am to 9:00 am relative to during other times, assuming the WWTP or

wastewater lagoon serve a residential area (Nguyen Quoc et al., 2022). A study which sampled at a neighborhood level reported similar trends but reported low recovery efficiencies for SARS-CoV-2 (Bivins et al., 2021). Depending upon the time of day considered in the modeling scenario, the reported concentration was adjusted (e.g., if a non-peak concentration was inputted, peak concentrations were estimated within the data visualization by multiplying the concentration by a factor of 5).

4.3.5 Inhalation model

Inhaled daily dose from pathogens in bioaerosols for each job task was informed by **equation 32.**

$$Dose = (C_{water})(PC)(F_{res})(e^{-\lambda t})(I)(M)(t) \quad (32)$$

The concentration in the water (C_{water} number of organisms/L) was multiplied by a partitioning coefficient (PC, L/m^3). The fraction of respirable (F_{res}) aerosols are among those that are <5 µm was modeled as a uniform distribution from the aerosol distributions 0.5 m after rotating brushes (66%) to the distribution at the air-water interface (73%) (Han et al., 2020). An inhalation rate for adults assumed light intensity activity (USEPA, 2011) (I, m^3/min), and an exposure time (Maal-Bared, 2023) (t, hr). Inactivation of aerosols was incorporated, where λ is a first order decay rate (hr^{-1}). For scenarios where a face covering was assumed, $Dose$ was multiplied by mask penetration (M).

4.3.6 Ingestion model

Accidentally ingested WW per day from large (>5μm) aerosols (tasks 2-5), WW ingested from a direct splash to the face (task 6), and the equivalent volume ingested from hand-to-mouth transfer (tasks 1 and 7) were calculated by **equation 33** for each job task**.**

$$Dose = (C_{water})(V) \tag{33}$$

The volume (V) accidentally ingested was varied by task. V for tasks 1-6 were informed by (Maal-Bared, 2023). For task 7, V was calculated using method described in (LeChevallier et al., 2020) (**Appendix C, Section 1**).

4.3.7 QMRA

The risk for infection from each pathogen was calculated with a pathogen-specific dose response. Three different dose response model equations were used across the eight pathogens (**Table 5**). An exponential dose response model (**equation 34**) was used for *C. hominis, E. coli, G. duodenalis, L. pneumophila,* rotavirus, SARS-CoV-2 (Delta), and SARS-CoV-2 (Omicron). A Beta-Poisson model (**equation 35**) was used for rotavirus and norovirus and a fractional Poisson model (**equation 36**) was also used for norovirus.

$$Risk_{\text{inf}} = 1 - e^{-r\,dose} \tag{34}$$

$$Risk_{\text{inf}} = 1 - \left(1 + \frac{Dose}{\beta}\right)^{-\alpha} \tag{35}$$

$$Risk_{\text{inf}} = P * \left(1 - e^{-\frac{Dose}{\mu_a}}\right) \quad (36)$$

The total risk of infection (for inhalation or ingestion from all pathogens in those exposure route groups) was calculated with **equation 37** for total inhalation risk and total ingestion risk based on the pathogens selected by the user. The probabilities for infections were considered to happen independently. Co-infections were not considered in the model.

$$Risk_{\text{total}} = 1 - \prod(1 - Risk_{\text{inf}}) \quad (37)$$

Table 5: Exposure route associated with each pathogen and available dose response parameters.

Pathogen	Ingestion	Inhalation	Dose response Parameter		Reference
Cryptosporidium hominis	X		Exponential	Point (5.72×10^{-2})	(Chappell et al., 2006; Messner et al., 2001)
Escherichia coli	X		Exponential	Point (1.95×10^{-6})	(Tacket et al., 2000)
Giardia duodenalis	X		Exponential	Point (1.99×10^{-2})	(Rendtorff, 1954)
Legionella pneumophila		X	Exponential (Sub-clinical)	Lognormal (μ: -2.93, σ: 0.49)	(Armstrong & Haas, 2007a), (Muller et al., 1983a)
			Exponential (Clinical)	Lognormal (μ: -9.69, σ: 0.30)	
Norovirus	X		Beta-Poisson	Point	(McBride, 2014; Van

				(α: 0.104, β: 32.2)	Abel et al., 2017b)
			Fractional Poisson	Point (P: 0.686, μ_a: 579)	
Rotavirus	X		Exponential	Point (1.73×10^{-2})	(Payment & Morin, 1990)
			Beta-Poisson	Point* (α: 7.28×10^{-2}, β: 1.07×10^{-1})	(Ward et al., 1986)
SARS-CoV-2: Delta	X	X	Exponential	Triangular (1.85×10^{-3}, 2.46×10^{-3}, 3.08×10^{-3})	(Pitol & Julian, 2021)
SARS-CoV-2: Omicron	X	X	Exponential	Triangular (5.54×10^{-3}, 7.38×10^{-3}, 9.23×10^{-3})	(Riediker et al., 2022)

*Original N_{50} value converted to β with $\beta=N_{50}/(2^{1/\alpha}-1)$ (From QMRAwiki)

For SARS-CoV-2, we used a previously utilized dose-response curve to represent Delta variant dose response (Pitol & Julian, 2021). We assume Omicron is 3 times more infectious than Delta variant, supported by multiple studies, (Riediker et al., 2022) by increasing *k* (the probability that a single viral particle reaches a site of infection and initiates infection) by 3. Each *k* value was decreased by 25% and increased by 25% to inform minimums and maximums, respectively, for a triangular distribution.

Due to uncertainty regarding the degree of pathogen infectivity and/or viability in wastewater, an assumed ratio of infectious and/or viable pathogen per gc could also be

selected if the user indicated the pathogen concentration is from molecular methods, with drop-down options of 1/100 through 1/1,000,000, decreasing by 1 $\log_{10}$ per option. There are limited data elucidating this ratio in published literature. However, our range includes those that have been reported in other studies, (Sinclair et al., 2008; Tyagi et al., 2021). It should be noted that lower ratios may be more appropriate for wastewater-specific contexts. If the concentration is indicated to be from molecular methods and a ratio is selected, the concentration of infectious virus in the water (C_{water}) per mL is multiplied by the ratio of infectious pathogen in the model. In the case of culture methods, we assume PFU for viruses, CFU for bacteria, or $TCID_{50}$ are representative of number of viable and/or infectious organisms (Tyagi et al., 2021). A viability ratio of 1/10,000 was applied to the concentrations of SARS-CoV-2 Delta and Omicron variants (Sender et al., 2021)

4.3.8 Sensitivity analysis

A Spearman rank correlation coefficient heatmap was calculated for a single respiratory infection case study. The final risks were compared to the Monte Carlo variables used for that case. 10,000 iterations were used for the Monte Carlo analysis (Burmaster & Anderson, 1994). The sensitivity analysis was performed with the ggpubr package in R version 4.2.1.

4.3.9 Risk calculator app

An interactive web application was developed using RShiny. Adjustable input parameters were used for pathogen concentrations, dose response models, personal protective equipment usage, sample timing, and job activity type as implemented in the QMRA models described above (**Table 6**). Risk outputs were coded for visualization as box plots, with a comparison to user-chosen risk comparison levels. To demonstrate the outputs of the web application, a range of hypothetical but representative scenarios were chosen, and the simulations were parameterized with values in **Table 7**.

1) Differences in infection risk predicted across pathogen types given typical wastewater concentrations
2) Differences in infection risk from selected pathogens *C. hominis* and *L. pneumophila* across different tasks
3) Differences in infection risk during peak and non-peak hours
4) Differences in infection risk from *L. pneumophila* with and without PPE

Table 6. Risk calculator tool inputs

Input Parameter	Input Type	Choices
Pathogen of interest	Multiselect	*Cryptosporidium hominis*, *Escherichia coli*, *Giardia duodenalis*, *Legionella pneumophila*, Norovirus, rotavirus, SARS-CoV-2 (Delta variant), SARS-CoV-2 (Omicron variant)

Exposure setting	Drop down menu	Office, Walking the plant, Minor contact, Moderate contact, High contact, Direct splash, Lagoon sampling
Exposure time	Drop down menu	Early morning (5 am-9 am), Late morning and after (9 am-5 am)
PPE Usage	Drop down menu	None, Cotton Mask, Cloth Mask, Surgical Mask, N95 Mask
Risk comparison level	Drop down menu	1/1,000; 1/10,000; 1/100,000; 1/1,000,000
Concentration (log_{10}/mL)	Slider or user entry	min=-3, max=7, increment=1
Sample type	Drop down menu	Molecular, culture
Ratio of infectious particles to genome copies	Drop down menu	1/100; 1/1,000; 1/10,000; 1/100,000; 1/1,000,000
Dose response parameter	Drop down menu	Exponential, Beta-Poisson, Fractional Poisson
Exposure Setting	Drop down menu	Office, Walking the plant, Minor contact, Moderate contact, High contact, Direct splash, Lagoon sampling

Table 7. Parameters, distributions, and their sources

Parameter	Variable	Units*	Distribution/Point Value	Source
Concentration in wastewater: *C. hominis*	C_{water}	#/L	Uniform (min=10^2, max=10^4)	(Inc. Metcalf & Eddy et al., 2013; US EPA, 2019)
Concentration in wastewater: *E. coli*	C_{water}	#/L	Uniform (min=10^5, max=10^{10})	(Chahal et al., 2016; Matthews et al., 2010)

Concentration in wastewater: *G. duodenalis*	C_{water}	#/L	Uniform (min=10^4, max=10^5)	(Inc. Metcalf & Eddy et al., 2013; US EPA, 2019)
Concentration in wastewater: *L. pneumophila*	C_{water}	#/L	Uniform (min=10^3, max=10^5)	(Caicedo et al., 2019)
Concentration in wastewater: Norovirus	C_{water}	#/L	Uniform (min=10^1, max=10^9)	(Eftim et al., 2017)
Concentration in wastewater: Rotavirus	C_{water}	# /L	Uniform (min=10^0, max=10^5)	(Inc. Metcalf & Eddy et al., 2013; US EPA, 2019)
Concentration in wastewater: SARS-CoV-2	C_{water}	# /L	Uniform (min=10^3, max=10^6)	(Weidhaas et al., 2021)
Partitioning coefficient	PC	L/ m^3	**See Table 4**	(Brenner et al., 1988; Gholipour et al., 2021; Matsubara & Katayama, 2019)
Fraction of respirable aerosols (<4.7 um)	F_{res}	Fraction (unitless)	Uniform (min=0.66, max=0.73)	(Han et al., 2020)
Inhalation rate (men and women ages 31 to <41, moderate intensity – similar to ages 21 to <31)	I	m^3/min	Normal (mean=2.7×10^{-2}, SD=5.0×10^{-3}) Range 1.7×10^{-2} – 3.7×10^{-2}	(Bussard, 2011)
Exposure time	t	hr	**See Table 4**	(Maal-Bared, 2023)

Cotton cloth mask penetration (3-ply)	M	Fraction (unitless)	Normal (mean=0.49, SD=0.077)	(Lindsley et al., 2021)
Surgical mask penetration	M	Fraction (unitless)	Normal (mean=0.41, SD=0.069)	(Lindsley et al., 2021)
N95 mask penetration	M	Fraction (unitless)	Beta (α=3, β=8)	(Wilson et al., 2021)
Inactivation rate of *L. pneumophila* in aerosols	λ	hr^{-1}	Point (0.125 for $0<t<30$ seconds, 3.1×10^{-4} for $t>30$ seconds)	(Hamilton et al., 2018)
Inactivation rate of SARS-CoV-2 in aerosols	λ	hr^{-1}	Triangular (min=0.096, mode=0.253, max=0.420)	(Jones, 2020; van Doremalen et al., 2020; Wilson et al., 2021)
Volume ingested	V	mL	**See Table 4**	(Maal-Bared, 2023)
Percent exposure	F_{exp}	%	**See Table 4**	(Maal-Bared, 2023)
Diurnal effect factor	-	Factor (unitless)	Point (Non-peak (9 am and after) concentration in wastewater is 5 times greater than peak (5 am-9 am))	(Nguyen Quoc et al., 2022)
Dose response parameter	$k, \alpha, \beta, P, \mu_a$	Unitless	**See Table 5**	**See Table 5**

*Units of measurement determined based on user inputs from **Table 6** for variables "sample type" and "ratio of infectious particles to genome copies". For example, if a culture-based measurement is chosen, 100% viability is assumed and bacterial units default

to CFU. If a molecular-based measurement is specified, the user is prompted for the ratio of infectious particles to genome copies, and units default to gc/L.

4.4 Results

4.4.1 Description of general model outputs

The risk calculator application includes several inputs to visualize how risk from inhalation of aerosols or ingestion of droplets (or via hand-to-mouth contact) changes according to the job task performed, the time of day, assumed fraction of infectious virus per gene copy (gc), pathogen type, etc. (**Table 6**). As users change inputs in this interface, the plotted risk distributions change, showing whether risks are below, above, or overlapping with a selected risk comparison level. Global variables that affect the risk results for both ingestion and inhalation pathways include selected pathogens, exposure setting, exposure time, and PPE usage. A user-specified risk comparison level for visual comparison could also be selected, with drop-down options of 1/1,000 through 1/1,000,000, decreasing by 1 $\log_{10}$ per option. The user input for the risk comparison level is provided as there is currently no widely adopted human health risk benchmark specific to occupational wastewater exposures. All plots graph this horizontal level for visual comparison to estimated risk distributions at the 1/10,000 level. These variables are shown on the top of the sidebar of the calculator (**Figure 15**).

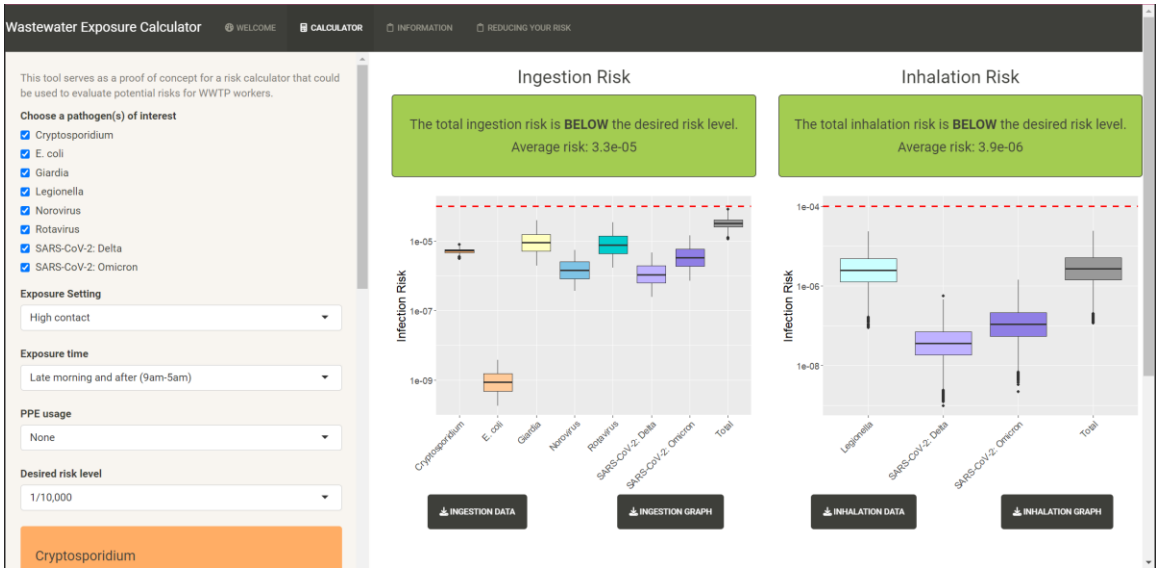

Figure 15: Calculator page with individual pathogen risks and total risks for ingestion and inhalation. The dotted red line displays the risk comparison level that is selected by the user. Global variables including selected pathogens, exposure setting, exposure time, PPE usage, and risk comparison level are shown at the top of the sidebar.

Each pathogen has a submenu to allow for user inputs that include the concentration of pathogens in wastewater as a $\log_{10}$ concentration, point value, lognormal, or uniform distribution. This concentration could be specified as being in molecular units (e.g., gc/mL) or culture-based units (e.g., plaque forming units (PFU), colony forming units (CFU), or $TCID_{50}$/mL). If the concentration is in molecular units, the user has to select the approximate ratio of infectious pathogen in the sample from 1/100 to 1/1,000,000. The

calculator also includes pathogen-specific dose response parameters. For pathogens that have more than one commonly available dose response parameter, a drop-down menu allows the user to choose from a selection of available dose response models (**Figure 16**).

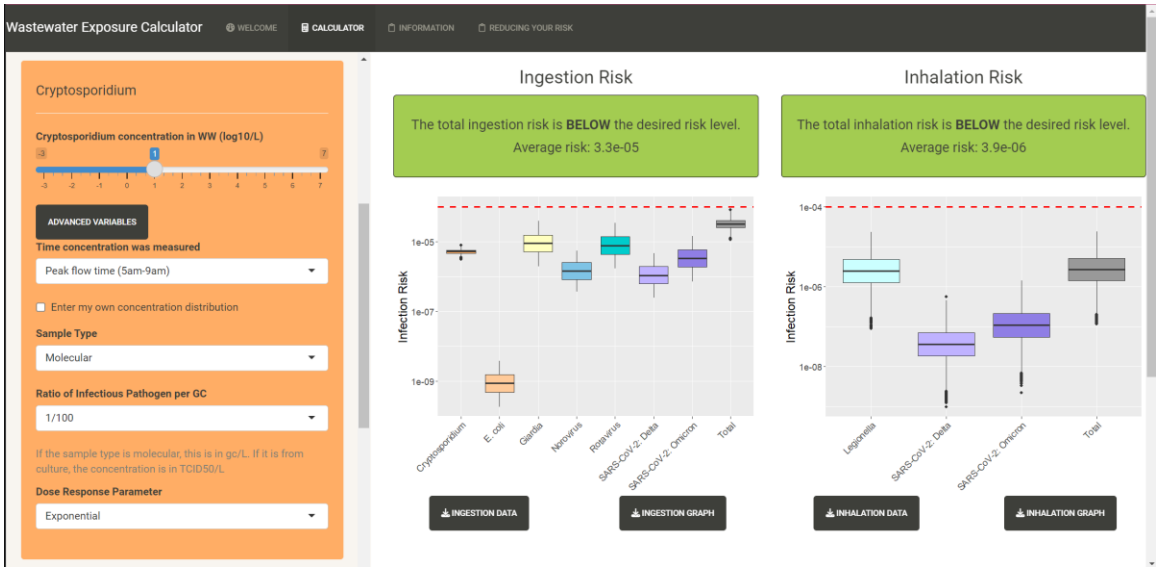

Figure 16: Calculator page with pathogen-specific parameters for *C. hominis*. Users can enter their concentration of *C. hominis* in the wastewater and specify the time of day the sample was collected and the sample type, as well as the dose response parameter.

4.4.2 Web application evaluation using scenario analysis

4.4.2.1 Difference in infection risk predicted across pathogen types given typical wastewater concentrations

The concentrations of pathogens in wastewater were assumed to be measured during peak hours (5 am-9 am) and no diurnal effect factor was applied when the exposure time was also during peak hours. Literature estimates for concentration were assumed to provide ranges with 100% infectivity for all pathogens was assumed except for SARS-CoV-2 Delta and Omicron variants. For these, a viability ratio of 1/10,000 was applied (Sender et al., 2021). The exposure setting was set as "high contact" and was assumed to be performed during peak hours (5 am to 9 am). High contact tasks include tasks that involve primary contact with wastewater such as sampling, lab work, and maintenance of primary equipment (**Section 4.3.3 Exposure Types**). No PPE was assumed to be worn during the duration of the task. Infection risks for all pathogens and total risks for gastrointestinal infection and respiratory infection are shown in gray (**Figure 17**). *G. duodenalis* had the highest median daily risk of gastrointestinal infection and SARS-CoV-2 Delta had the lowest. *L. pneumophila* had the highest respiratory risk. The numeric results for all scenario analyses presented here are reported in **Table 8.**

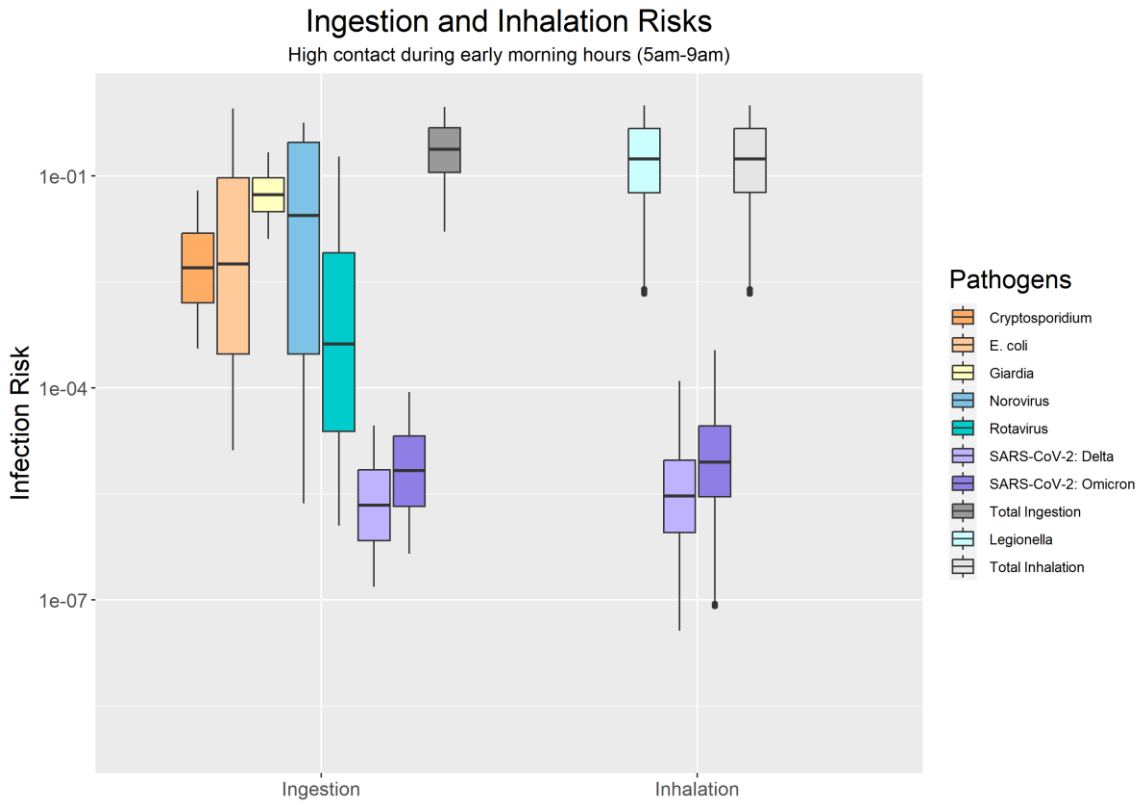

Figure 17: Ingestion and inhalation risk graphs for all pathogens modeled for a "high contact" exposure setting during peak hours (early morning, 5 am-9 am).

Table 8: Summary of risk results for scenario analysis for Monte Carlo simulation with 10,000 iterations. Ingestion and inhalation summary statistics for all pathogens modeled for a "high contact" exposure setting during peak hours (early morning, 5 am-9 am) with no PPE.

Scenario	Min	1st Qu.	Median	Mean	3rd Qu.	Max
Ingestion, Cryptosporidium	3.6e-04	1.6e-03	5.0e-03	1.1e-02	1.5e-02	6.3e-02
Ingestion, E. coli	1.3e-05	3.0e-04	5.7e-03	1.1e-01	9.5e-02	9.0e-01
Ingestion, Giardia	1.3e-02	3.1e-02	5.4e-02	6.6e-02	9.5e-02	2.1e-01
Ingestion, Norovirus	2.3e-06	3.0e-04	2.8e-02	1.5e-01	3.0e-01	5.7e-01
Ingestion, Rotavirus	1.1e-06	2.4e-05	4.2e-04	1.2e-02	8.1e-03	1.9e-01
Ingestion, SARS-CoV-2: Delta	1.5e-07	6.9e-07	2.2e-06	4.7e-06	6.9e-06	3.0e-05
Ingestion, SARS-CoV-2: Omicron	4.5e-07	2.1e-06	6.7e-06	1.4e-05	2.1e-05	8.7e-05
Ingestion, Total Ingestion	1.6e-02	1.1e-01	2.4e-01	3.0e-01	4.8e-01	9.5e-01
Inhalation, Legionella	2.2e-03	5.8e-02	1.7e-01	2.9e-01	4.7e-01	1.0e+00
Inhalation, SARS-CoV-2: Delta	3.7e-08	9.0e-07	2.9e-06	7.9e-06	9.5e-06	1.3e-04
Inhalation, SARS-CoV-2: Omicron	8.2e-08	2.9e-06	8.9e-06	2.4e-05	2.9e-05	3.4e-04
Inhalation, Total Inhalation	2.2e-03	5.8e-02	1.7e-01	2.9e-01	4.7e-01	1.0e+00

4.4.2.2 Differences in infection risk from *C. hominis* and *L. pneumophila* across different job tasks

The gastrointestinal infection risk from *C. hominis* and respiratory risk from *L. pneumophila* was compared among different exposure settings that workers may encounter

while working in WWTPs. It was assumed that the tasks were performed during early morning hours (5 am-9 am) and that no PPE was worn. Walking the WWTP (task 2) and working in the office (task 1) had the highest median daily risks of *C. hominis* infection (**Figure 18**). This is expected due to the high amount of contact workers have with surfaces when working in an office setting. While walking the plant, contact with surfaces is included along with exposure to aerosols. Lagoon sampling (task 7) has the largest range due to the variability in accidental ingestion from hand-to-mouth contact (**Appendix C, Section 1**).

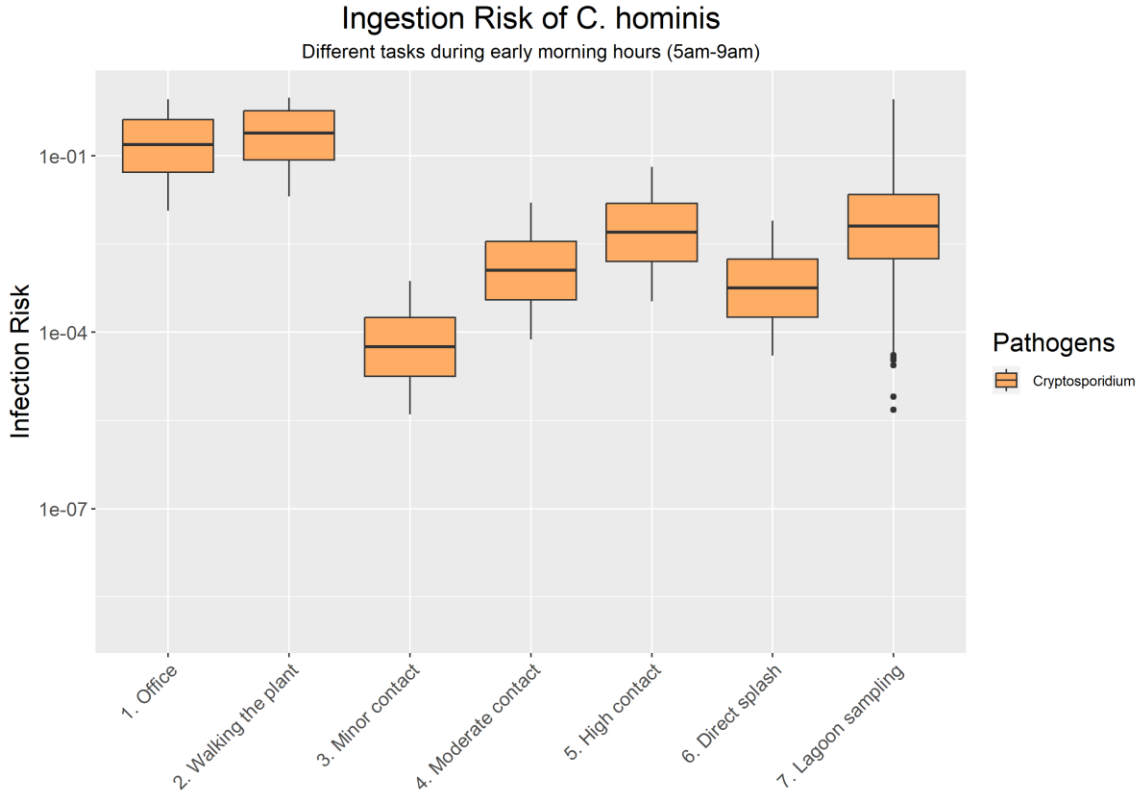

Figure 18: Infection risk from *C. hominis* for different exposure settings with late morning exposure and no PPE.

Infection risks from *L. pneumophila* are shown in **Figure 19** for job tasks that include aerosol exposure. The infection risk from walking the plant (task 2) is much lower than the infection risk from *C. hominis* because volume from contact with surfaces is not included in this model. Lagoon sampling (task 7) has the highest risk of infection.

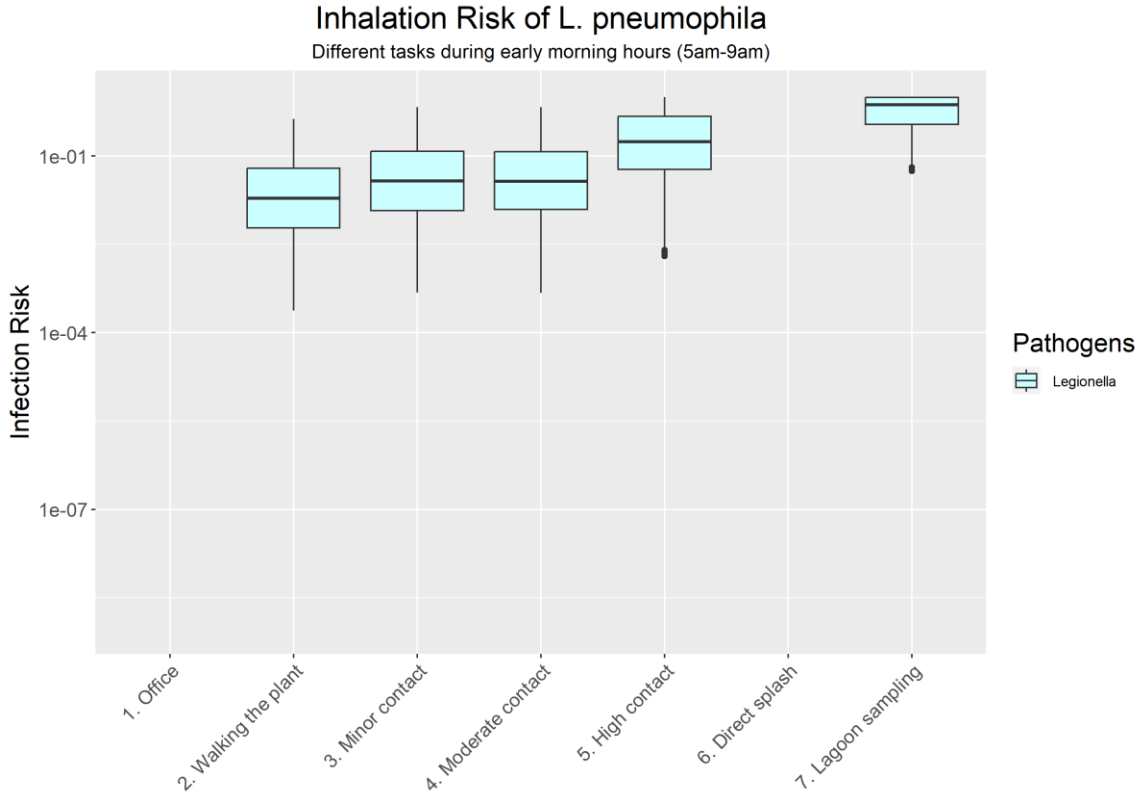

Figure 19: Infection risk from *L. pneumophila* for different exposure settings with late morning exposure and no PPE.

4.4.2.3 Differences in infection risk during peak and non-peak hours

Ingestion and inhalation risks for available pathogens were calculated at peak hours (early morning, 5 am-9 am) and nonpeak hours (late morning, 9 am and after), for "high contact" (task 5), without PPE. During peak and non-peak hours, *G. duodenalis* had the highest median daily risk of gastrointestinal infection and SARS-CoV-2 Delta had the lowest (**Figure 20**). A factor of 5 was assumed for this difference based on the results from Nguyen Quoc, 2022 (Nguyen Quoc et al., 2022). More information is needed to inform the selection of this value, as reported diurnal concentrations of pathogens varies in the literature (Bivins et al., 2021).

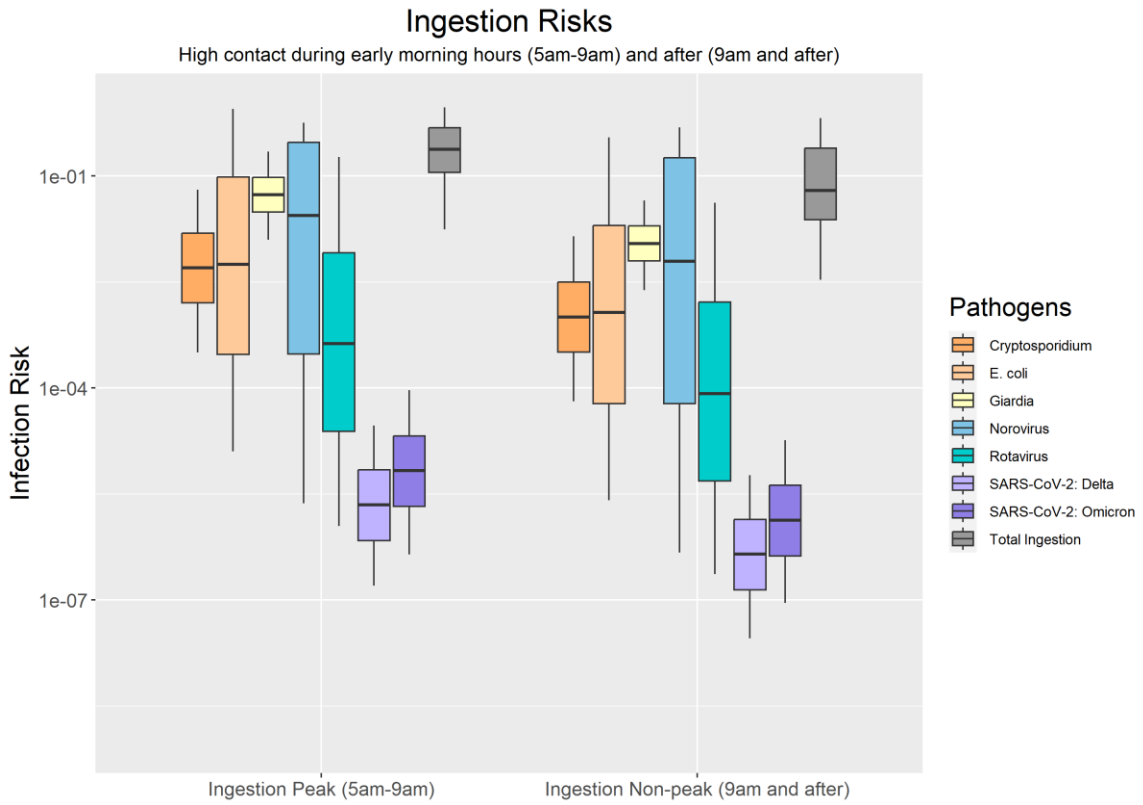

Figure 20: Ingestion risks for available pathogens during peak hours (early morning, 5 am-9 am) and non-peak hours (late morning and after, 9 am-5 am), for "high contact", without PPE.

During peak and non-peak hours, the median daily respiratory infection risk from *L. pneumophila* is the largest, followed by the infection risk of SARS-CoV-2: Omicron and SARS-CoV-2: Delta (**Figure 21**).

Figure 21: Inhalation risks for available pathogens during peak hours (early morning, 5 am-9 am) and nonpeak hours (late morning, 9 am and after), for "high contact", without PPE.

4.4.2.4 Differences in infection risk for *L. pneumophila* with and without PPE

The available PPE options for this model include cloth masks, surgical masks, and N95 respirators. For this model, it was assumed that these face coverings completely prevented

ingestion-associated exposures. The risk of *L. pneumophila* was calculated for a high contact exposure scenario during peak hours (early morning, 5 am to 9 am) (**Figure 22**). The median risk was lowest with the usage of an N95 respirator. Wearing an N95 respirator reduces the median daily risk of infection 3.75 times compared to not wearing a face covering.

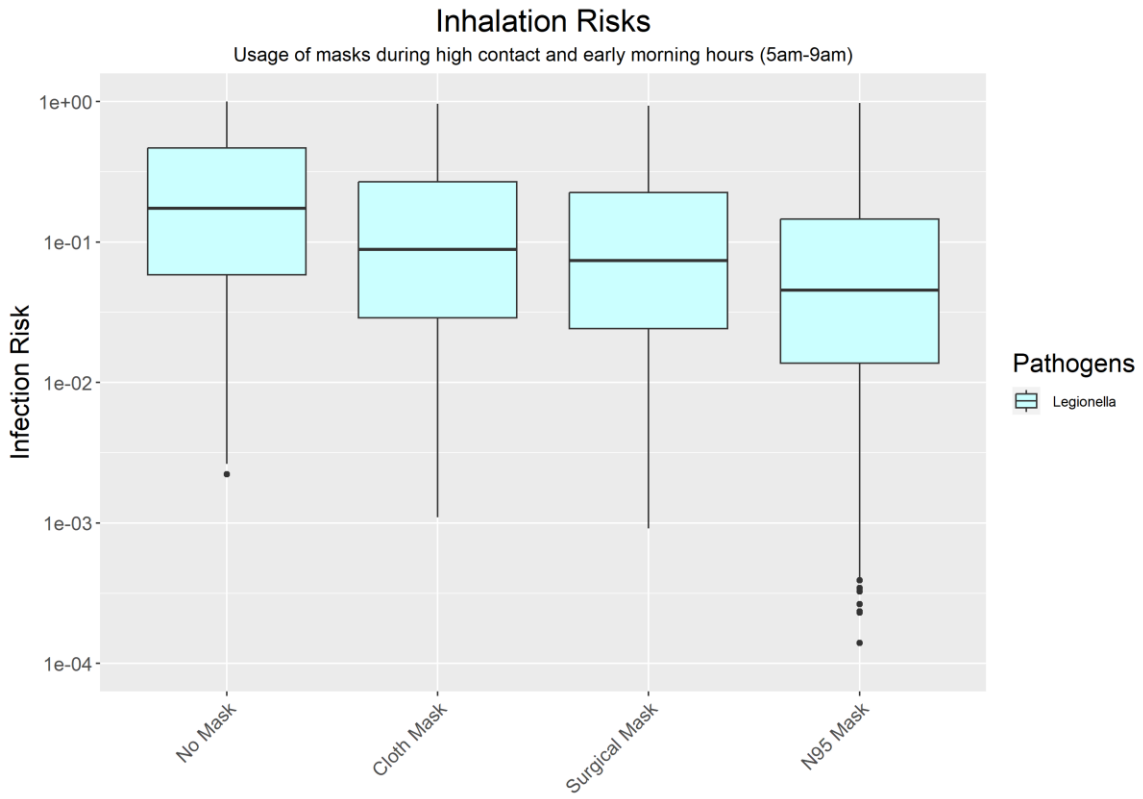

Figure 22: Inhalation risks during peak hours with and without face covering.

4.4.3 Sensitivity analysis for explored conditions

A sensitivity analysis was performed with Spearman correlation coefficients for a single respiratory infection case study. The sensitivity analysis was conducted for the infection risk scenario of a high contact exposure scenario during peak hours (early morning, 5 am-9 am), with an N95 respirator used for the duration of the exposure (**Figure 23**).

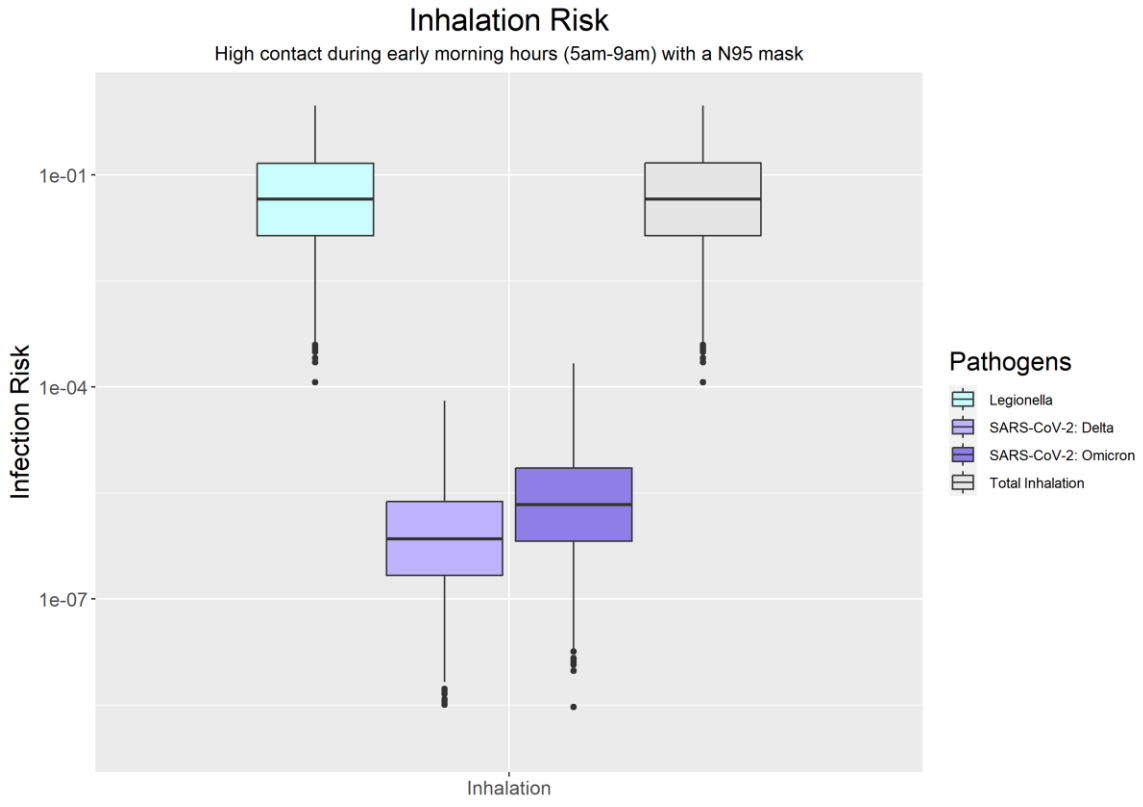

Figure 23: Respiratory infection risks used in the sensitivity analysis for a high contact exposure scenario during peak hours (early morning, 5 am to 9 am) with an N95 respirator.

The final daily risks calculated in **Figure 23** were used to calculate Spearman's correlation coefficients for the output (risk) versus each Monte Carlo variable used for that case (**Figure 24**). Inhalation risks for *L. pneumophila*, SARS-CoV-2: Omicron, SARS-CoV-2: Delta, and total inhalation risk were most highly correlated with the partitioning coefficient (0.37 to 0.38) and N95 mask efficiency (-0.31 to -0.32).

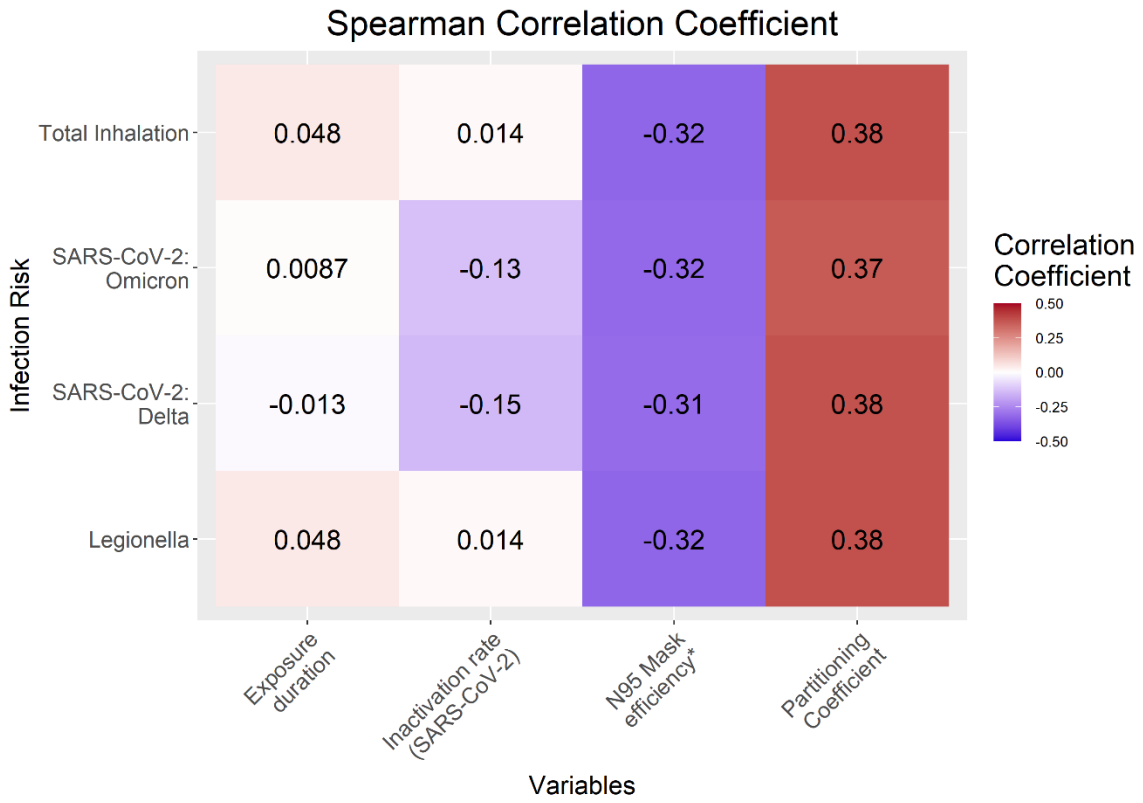

Figure 24: Sensitivity analysis with Spearman's correlation coefficients for Monte Carlo variables. *Denotes that the value used in this sensitivity analysis was one minus N95 mask efficiency ($1 - M$) for ease of interpretation (i.e. a 95% efficiency is modeled as 0.05).

4.5 Discussion

4.5.1 Implications of web application development

We developed a tool for relating pathogen concentrations in sewage to estimated wastewater worker infection risks from accidental ingestion or inhalation of wastewater. The web application, titled the Wastewater Exposure Calculator, offers a customizable tool for WWTP managers to explore the range of possible risks using site-specific information. This calculator can incorporate the pathogens of concern, the type of job tasks, the time of day, and the use of available PPE. The model is intended to provide a framework that can be built upon to evaluate combinations of site-specific recommendations for decisions such as scheduling job tasks, implementing physical barriers between bioaerosols and workers, or recommending different types of PPE. While this model is primarily focused on assessing risks at centralized WWTPs which are common in urban and peri-urban communities, the tool can be expanded to rural or low-resource settings given additional information on exposure volumes and timing. The rural and low-resource settings may not be fully represented by the exposures presented in the web applications (**Table C2**).

4.5.2 Scenario analysis findings and utility for exploration of management interventions

The Wastewater Exposure Calculator can explore many different cases by varying performed tasks, exposure times, concentrations of pathogens, dose response parameters, and PPE. Case studies comparing infection risks for (1) individual pathogens, (2) *C. hominis* and *L. pneumophila* for different tasks, (3) gastrointestinal and respiratory infection risks for exposure during peak and non-peak hours, and (4) respiratory infection risks for masks, N95 respirators, and no PPE. For case (1) individual pathogens, *G. duodenalis* had the highest median gastrointestinal infection risk and SARS-CoV-2 Delta had the lowest. *L. pneumophila* had the highest respiratory infection risk.

Case (2) investigated the risk of gastrointestinal infection from *C. hominis* among different exposure settings that workers may encounter while working in WWTPs. An exposure time during early morning hours was assumed and no PPE was accounted for. Walking the WWTP and working in the office had the highest risk of infection. This was due to the high amount of contact workers had with surfaces or different aerosols during the time. Maal-Bared (2023) (Maal-Bared, 2023) clarifies that the volume transferred to workers' hands from the surfaces they come into contact with is very low, but the number of contacts is high. Throughout a workday, the authors estimate that individuals working in an on-site office will ingest up to 3.0 mL per 8-hour shift. Lagoon sampling has the

largest range due to the variability surrounding these sampling events. For the risk of respiratory infection from *L. pneumophila* was highest for lagoon sampling events and lowest for walking the plant.

Comparing ingestion scenarios, the risk of working in an office on-site at the treatment plant is ~5000 times greater than the risk of a direct splash of wastewater to the face. The ingestion volumes reported in Maal-Bared (2023) (Maal-Bared, 2023) were calculated using information collected from focus groups of professionals who worked at WWTPs. This study was representative of an urban, industrial, and municipal WWTP and included individuals from the utility crew, maintenance crew, operations team, engineers, laboratory staff, and health a safety scientists. Reported office hygiene was problematic for several reasons. According to the focus group results, many WWTPs did not have designated eating or smoking areas, nor did they have appropriate locker rooms for workers to change into and out of coveralls or other work clothes. Workers reported wearing contaminated PPE in the office eating or smoking areas, and therefore contamination of office surfaces was assumed.

Case (3) investigated infection risks during peak and non-peak hours. *G. duodenalis* had the highest risk for both peak and non-peak hours for all pathogens considered in the ingestion risk scenario, and SARS-CoV-2 Delta was the lowest, noting that a 10^{-4} infectivity relationship assumed is highly uncertain and was chosen due to lack of cultured

SARS-CoV-2 from WWTP, and likely barriers to fecal-oral transmission (Sender et al., 2021). *L. pneumophila* had the highest risk for respiratory infection risk, followed by SARS-CoV-2 Omicron and SARS-CoV-2 Delta. The infection risk levels increased by 5-fold for all pathogens from non-peak to peak timing for the modeled scenarios, emphasizing that shift timing plays an important role in risk outcomes.

Case (4) investigated the usage of cloth masks, surgical masks, and N95 respirators and their impact on the risk of respiratory infection from inhalation. The use of any face covering modeled here reduced the risk of infection when compared to a no-mask scenario. It should be noted that respirators would be nearly completely effective for mitigating droplet exposures, especially for large droplets (100µm) (Wang et al., 2021), so ingestion risk was not modeled for this event.

The exposure reduction provided by the addition of PPE (3.75 times reduction) is not as significant as the reduction seen by peak vs non-peak exposure timings (5 times reduction) **(Figures 20 and 22)**. Peak concentrations were assumed to be five times higher than non-peak concentrations (Nguyen Quoc et al., 2022) and these trends were confirmed for SARS-CoV-2 for similar studies at the neighborhood level (Bivins et al., 2021). However when sampling at the influent for a WWTP these trends were not observed (Ahmed et al., 2021). Therefore, further research is needed to determine the pathogen concentration differences for peak and non-peak hours at WWTP. Comparing

concentrations over time for an individual WWTP could help scheduling become safer for workers even in the absence of PPE. Additionally, the usage of PPE while workers are in the office, walking the WWTP, or sampling at WW lagoons has the greatest potential to reduce risks from ingestion exposures.

4.5.3 Limitations of the modeling tool

The proposed modeling framework and web application provides a generalizable tool that can be customized using site-specific data. However, some variables are not coded as user-specified inputs due to the limited availability of information in the literature (e.g., aerosol partitioning information). Factors that individual WWTPs are likely to have data for were prioritized as user-controlled inputs to the web application. The PPE options included (i.e., masks) are an incomplete list of potential PPE or workplace barriers. Additional considerations like other forms of PPE (e.g., gloves, face shields, and coveralls) could be incorporated into the model with additional data availability.

This calculator has options for eight reference pathogens. A much broader swath of microorganisms poses a potential risk to human health. These eight were chosen due to their epidemiologic importance and representativeness of bacterium (*E. coli* and *L. pneumophila*), viruses (norovirus, rotavirus, SARS-CoV-2 Delta and Omicron), and parasites (*C. hominis* and *G. duodenalis*). Fungi are also present in WWTPs in addition to bacteria and viruses (Staszowska, 2022) but were not included in the scope of this model

due to a lack of dose response information, for example (Haas, 2015b). Norovirus was modeled with a Beta-Poisson and fractional Poisson model. Norovirus is used as a viral reference pathogen to set pathogen $\log_{10}$-reduction targets (Jahne et al., 2023). Additional dose response models including the hypergeometric dose response (α: 0.04, β: 0.055) (Teunis et al., 2008) are not considered in this model but can be added to future versions. In addition to the risks posed by these pathogen-containing groups, WWTPs allow the proliferation of antibiotic resistance genes and resistant bacteria, the risk of which could also be considered (Petersen & Hubbart, 2020; Vikesland et al., 2017).

The large uncertainty in ratios of infectious viruses to RNA measurements (i.e., gc/ L) has important implications for the interpretation of results, especially for SARS-CoV-2 estimates. A viability ratio of 1/10,000 was used for SARS-CoV-2 (Sender et al., 2021). A review of the literature indicated that culture-based quantification methods for environmental samples of norovirus are not routinely used and therefore there is a lack of viability data (Eftim et al., 2017).

While there were relatively high viral loads of SARS-CoV-2 (2-3 $\log_{10}$ gc/L) that were determined to be potentially infectious by Stobnicka-Kupiec et al. (2022) (Stobnicka-Kupiec et al., 2022) in both influent and effluent samples, SARS-CoV-2 has not been successfully cultured from sewage to date to the author's knowledge. This raises uncertainties in several important factors: 1) what fraction of "potentially infectious" gc/L

is truly infectious, and 2) the sensitivity of cell culture methods for detecting the infectious virus. Early in the SARS-CoV-2 pandemic, it was known that SARS-CoV-2 was shed in stool, and therefore the virus was also present in WWTPs (Alam & Ali, 2021), however, its infectious state has not been fully ascertained (de Oliveira et al., 2021; Huang et al., 2021; Kumar et al., 2021; Sobsey, 2021; Xie et al., 2020). While it has been shown that it is possible to quantify SARS-CoV-2 from feces (Xiao et al., 2020) or urine (Sun et al., 2020) of individuals infected with COVID-19, it has been very rare to successfully isolate a viable sample (Ahmed et al., 2021). The virus is inactivated by the colonic fluid up to 80% in 24 hours (Zang et al., 2020) and will further decay as it travels through the WW network (Silverman & Boehm, 2020). The inactivated virus has been quantified from WW and used for wastewater-based epidemiology (WBE) to estimate the number of disease cases in a community. This has proven to be a powerful tool in allowing communities to prepare for surges of SARS-CoV-2 cases (Kitajima et al., 2020), rather than a direct risk from wastewater exposures. Therefore, SARS-CoV-2 is likely to be inactivated in WW and may not contribute to a meaningful increase in the risk of infection when aerosolized and inhaled (Brisolara et al., 2021). The focus remains on risk to healthcare professionals and aerosol mediated person-to person transmission (Jones et al., 2020). However, as new information becomes available, uncertainties can be reduced in the ratio specified within the application.

Repeated exposures were not considered in this model, as there is a lack of data available as to how frequently job tasks will be performed among workers. With further job-specific information, annual risks could be calculated and compared to annual risk benchmarks. Disability-adjusted life years (DALYs) can be used to look at benchmarks, but this would require annual risk values. Additionally, site-specific information is needed, as many of the selected values used for this model are informed by the range in the existing literature. Site-specific information can be entered for many variables in the app and the available data file produced in the application with the calculated risk per event can be used to calculate annual risks and DALY values when the frequency of job tasks is available. More specific worker time-activity patterns could be incorporated accounting for the maintenance and operation of specific WWTP unit processes.

4.5.4 Additional exposure settings for consideration

The Wastewater Exposure Calculator is primarily focused on assessing risks at centralized WWTPs which are common in urban and peri-urban communities. The calculator has seven exposure setting tasks, the first six of which are specific to industrial WWTPs. Additional exposure routes in more rural or low-resource settings may not be fully represented by the exposures presented in existing web applications. For example, waste stabilization ponds, or wastewater treatment lagoons, can be used in place of large WWTPs as a low-cost alternative that can still meet treated effluent standards. Wastewater

treatment lagoons are commonly used in the USA (USEPA, 2011), Canada (Statistics Canada, 2016), and Europe (Mara, 2009). The lagoons can be attached to a local sewershed or they can stand alone and be filled with sewage and sludge trucks that regularly fill the lagoon (D'Aoust et al., 2021). Other environmental factors such as humidity and season have been shown to play an important role in the overall infection risk from working with wastewater but have not been included in this model (Stobnicka-Kupiec et al., 2022).

4.6 Conclusion

The Wastewater Exposure Calculator developed in this work offers a customizable tool for WWTP managers to explore the range of possible risks using site-specific information. The tool performs multiple QMRA calculations to estimate WWTP workers' infection risks from accidental ingestion or inhalation of wastewater from multiple pathogens and exposure scenarios. The model is intended to provide a framework that can modified to provide recommendations on a site-specific scale for scheduling tasks, implementing physical barriers between bioaerosols and workers, or recommending different types of PPE. While this model is primarily focused on assessing risks at centralized WWTPs which are common in urban and peri-urban communities, it is also expanded to rural or low-resource settings and the lagoon-sampling related scenario can be used for this purpose. The web application can be found at https://ashleyheida.shinyapps.io/WWapp/.

Factors identified as important risk drivers included exposure timing (peak vs. non-peak), and to a lesser degree, the use of PPE. Therefore, further research is needed to determine the pathogen concentration differences for peak and nonpeak hours at WWTP.

CHAPTER 5

CONCLUSION

Modeling pathogen fate and transport in the built environment can help to better understand pathogens that grow and persist in engineered systems. Computational tools such as QMRA can evaluate the health risks from exposure to pathogens and can help to evaluate the effectiveness of different intervention strategies. Scenario analysis of each model enabled an understanding of how the full range of the variables used in the model affects the model output. Sensitivity analysis can be used to identify variables that have the most influence on the final result (typically a risk output) which can be ranked and identified as driving factors to inform resource allocation and intervention strategies. These methods used in the models described throughout this dissertation have developed customizable model frameworks that can be further built upon and used by decision-makers for their specific settings to better inform the decision-making process.

Chapter 2 presents a computational framework for evaluating an optimal water heater temperature set point for reducing energy costs and health risks for a single showering exposure event. For a single use-case representative of a hot water system leading to a patient room shower in a hospital, it was found that the optimal water heater temperature set point was between the recommended 49°C to prevent scalding (recommended by the CPSC and the DOE), and 60°C to inactivate *L. pneumophila* bacteria (recommended by

NASEM). The optimal set point was dependent on numerous factors that were varied in the sensitivity analysis including the dose response parameter. A sub-clinical dose response parameter is a more conservative health endpoint that includes any infection whether or not it requires medical attention from a health care provider. The optimal set point for sub-clinical cases ranged from 55-59°C, demonstrating that for this particular case, temperatures below the higher recommended value could be protective of public health while reducing costs. The clinical severity dose response model that only includes infections severe enough to necessitate attention from a health care provider had a lower average optimal set point of 48°C. This temperature difference emphasizes the importance of choosing an appropriate dose response parameter for the population that is intended to be represented by this model. For example, if the population of interest in the hospital is immunocompromised then the sub-clinical model may be preferred. The consequences of infection should further be considered and additional economic variables could be accounted for. For example, the impact on quality of life was not evaluated for infection or scalding.

Chapter 3 proposed a population ecology model with an exposure assessment. The model is aimed to progress the field of QMRA toward incorporate mechanistic information on AMR for predicting risk. As a case study demonstrating the approach, the conjugation rate of antibiotic resistant genes was incorporated into the population ecology model to

examine the impacts on the dose of ingested antibiotic susceptible and ESBL *E. coli* during a recreational swimming event.

Two low-growth cases were investigated using initial concentrations from RWQC and treated wastewater effluent. Using initial starting concentrations of treated wastewater effluent led to conjugation being the driving variable in the model over the first hours of the simulation until the antibiotic susceptible *E. coli* populations were depleted. Conjugation was not observed when initial starting concentrations were set to RWQC values, as the concentrations of antibiotic susceptible and ESBL *E. coli* were too low. Similarly, two high-growth scenarios were modeled using concentrations from the low-growth RWQC scenario with and without background *E. coli* in the human gut. Conjugation was the driving variable when background *E. coli* was added to the concentration in the gut until antibiotic susceptible *E. coli* declined until it reached a steady state when the population. After this period, the ESBL population increased due to the growth rate and conjugation. Antibiotic susceptible and ESBL *E. coli* populations increased steadily over the simulated residence time when background *E. coli* was not considered in the gut. The populations did not reach a concentration where conjugation is prominently observed. The final dose from the high-growth scenario with background *E. coli* in the human gut was most highly impacted by the conjugation rate in the body for the antibiotic susceptible population and by the growth rate for the ESBL *E. coli* population. For the high-growth scenario with no background *E. coli* population in the gut, the final dose was

most highly impacted by the growth rate in the body for both antibiotic susceptible and ESBL *E. coli*.

QMRA models calculate to risk of infection or other adverse outcomes using dose response models which represent the entirety of *in vivo* kinetics without necessitating an understanding of the population dynamics. Our high-growth scenarios in this model consider population dynamics for both antibiotic-susceptible and ESBL *E. coli* populations. This approach models differences in survival as part of the exposure analysis, before applying any existing dose response relationships. Therefore, if a dose response model was to be used directly with the final dose from the high-growth scenario, the *in vivo* kinetics would be accounted for twice. Additional research is needed to further understand *in vivo* kinetics for antibiotic susceptible and ESBL *E. coli* so that we can account for microbial gene exchanges in the human gut and further our understanding of population interactions.

Chapter 4 presents a QMRA to estimate WWTP workers' infection risks from accidental ingestion or inhalation of wastewater. This model incorporated pathogens of concern, type of job tasks, time of day, and use of available PPE. The model is intended to provide a framework that can be built upon to eventually provide recommendations for scheduling tasks, implementing physical barriers between bioaerosols and workers, or recommending different types of PPE based on the job task. This model was also presented

as a web application titled the Wastewater Exposure Calculator. This calculator presents a customizable tool intended for eventual use by WWTP managers to explore the range of possible risks for their employees using site-specific information.

C. hominis and *E. coli* posed the highest and lowest risk of gastrointestinal infection, respectively. *L. pneumophila* posed the highest risk of respiratory infection. Out of seven different tasks, the highest risk of infection came from walking the WWTP and working in the on-site office. This was due to the high amount of simulated contact workers had with surfaces and it was suggested in the study from which exposure estimates originated (Maal-Bared et al.) that lapses in hygienic practices could be occurring in shared breakrooms and office spaces. Infection risks were compared during peak and non-peak hours, and resulted in a large difference in infection risk, with risk levels increased by 5-fold for all pathogens from non-peak to peak timing for the modeled scenarios, emphasizing that shift timing plays an important role in risk outcomes. The exposure reduction provided by the use of face coverings was not as significant as the reduction seen by peak vs non-peak exposure timings. Further research is needed to investigate pathogen concentrations at WWTP influent throughout a 24-hour cycle.

Numerous challenges exist for verification or validation of these models. The premise plumbing model presented in chapter 2 could benefit from additional studies that investigate concentrations of *L. pneumophila*, free chlorine, temperature, and other meta-

data on a building-scale. Studies do exist at both the lab (Proctor, 2014; Rhoads et al., 2015, 2017) and building scale (Ley et al., 2020; Salehi et al., 2018), but this information has not been linked to real building to inform intervention strategies. The recreational water quality population ecology model with an exposure assessment presented in chapter 3 could begin to be verified through batch reactors mimicking conditions in recreational water and the gastrointestinal tract. Known concentrations of antibiotic susceptible *E. coli* and ESBL *E. coli* could be added to the reactor and measured after a duration of time. While these reactors would not be looking to quantify a specific rate, they could be used to simulate an environment that is a closer representation of recreational waters and the gastrointestinal tract than in vitro studies, acknowledging challenges in making in situ HGT measurements (Lopatkin et al., 2017; Moralez et al., 2021). Validating the wastewater occupational exposure in chapter 4 could be done with further exposure studies in addition to the collection of diurnal concentration data for each pathogen. Exposure studies could be completed be observing workers completing tasks in all areas, including the on-site offices (Corrao et al., 2013; Nguyen et al., 2018). Additional studies are needed at wastewater lagoons to better understand how sampling activities vary and how available PPE is being used. Measuring concentrations of the pathogens entering the WWTPs and how these concentrations vary throughout the day will be useful in modeling how health risks can shift depending on when tasks are performed. Aerosolization rates specific to different processes within WWTPs would also be beneficial to continue to build on available data

(Brenner et al., 1988; Gholipour et al., 2021; Kitajima et al., 2020; Matsubara & Katayama, 2019).

During the process of developing these models, some of the most prominent challenges included: (1) modeling the biofilm and associated sloughing for the premise plumbing model, (2) investigating available dose response data for antibiotic resistant infections, and (3) modeling occupational exposure during different job tasks at WWTPs as described below.

(1) Modeling the biofilm and associated sloughing for the premise plumbing model. The mass of the biofilm attached to the pipe walls was calculated using density and thickness (Garny et al., 2009). Several bench top experiments were referenced for key variables including the sloughing rate for a low turbulent flow inside a straight hot water pipe (Garny et al., 2009), and the sloughing rate attenuation (Huang et al., 2020). These bench top experiments provide a good starting point to enable modeling of sloughing, but further studies are needed to determine biofilm dynamics in more complex systems that include multiple pipes and junctions as well as varying flow rates.

(2) Investigating available dose response data for antibiotic resistant infections. As antibiotic resistant infections continue to rise in number, dose response parameters specific to these infections will be needed to accurately model the health risks after exposure. Understanding background population of antibiotic susceptible and antibiotic resistant

bacteria in the gastrointestinal tract is needed to model population dynamics and concentration changes. Because dose response parameters already account for *in vivo* population ecology, applying the dose response parameter to the final concentrations of bacterial populations from the gastrointestinal tract model is not compatible with the typical dose response approach. Dose response data that can be applied to *in vivo* population ecology models is needed to continue the QMRA.

(3) Modeling occupational exposure during different job tasks at WWTPs. There exists great variability reported in the literature when quantifying WWTP workers exposure to pathogens. Uncertainties exist in the job tasks performed at municipal WWTPs as well as wastewater lagoons, in the aerosolization rates throughout the WWTP, and in the concentration of pathogens entering the WWTP. Each of these parameters will likely vary based on the specifications of each WWTP, so additional studies adding to the existing values in literature will be helpful for future risk assessments.

All the models presented in this dissertation are presented as companion tools to other direct evidence-based strategies such as modifications to building plumbing management, closing recreational water that contains high levels of contaminants, or using proper PPE when exposure to wastewater is expected. A Monte Carlo analysis was used in each model to converge on median results. 10,000 iterations were used as recommended as a standard practice (Burmaster & Anderson, 1994). An alternative approach to using 10,000 iterations

is to increase the number of iterations until a stable median is reached for each model which could increase the efficiency of the models. Uncertainties in these models can be reduced with site-specific information and validation studies. With further modification to each of these tools, they may also be used in the design process of water and wastewater systems. Ideally, architects could use the water heater model described in Chapter 2 to aid in the design process by evaluating pipe materials, pipe lengths, pipe sizes, stagnant dead ends, or insulation prior to the construction phase. Additionally, building managers could use future iterations of this model to understand the impacts of management strategies such as changing the water heater temperature set point, or adding or removing pipe insulation. Chapter 3 can be used to merge population ecology models with QMRA. This modeling approach could be layered with approaches to source water protection, guidance on treatment log removals, and approaches to beach safety notifications used to inform the public. Risk-based monitoring approaches for AMR determinants is needed, and this type of approach could be used to assess the safety of current RWQC while considering the complexities associated with AMR. Chapter 4 was developed as a web application to calculate risk to WWTP workers. This generalizable framework is intended to be built upon to better understand the site-specific risks at WWTPs because each plant is unique and presents different risk-reduction challenges. As such, these models could constitute a piece in larger consideration of more holistic design and operational of water and wastewater systems, as well as occupational safety and hygiene practices in a WWTP.

REFERENCES

Ahmed, W., Bibby, K., D'Aoust, P. M., Delatolla, R., Gerba, C. P., Haas, C. N., Hamilton, K. A., Hewitt, J., Julian, T. R., Kaya, D., Monis, P., Moulin, L., Naughton, C., Noble, R. T., Shrestha, A., Tiwari, A., Simpson, S. L., Wurtzer, S., & Bivins, A. (2021). Differentiating between the possibility and probability of SARS-CoV-2 transmission associated with wastewater: Empirical evidence is needed to substantiate risk. *FEMS Microbes*, *2*, xtab007. https://doi.org/10.1093/femsmc/xtab007

Ahmed, W., Bivins, A., Bertsch, P. M., Bibby, K., Gyawali, P., Sherchan, S. P., Simpson, S. L., Thomas, K. V., Verhagen, R., Kitajima, M., Mueller, J. F., & Korajkic, A. (2021). Intraday variability of indicator and pathogenic viruses in 1-h and 24-h composite wastewater samples: Implications for wastewater-based epidemiology. *Environmental Research*, *193*, 110531. https://doi.org/10.1016/j.envres.2020.110531

Alam, A., & Ali, L. (2021). Prospects and Risks Related to Potential Transmission of COVID-19 and Other Viruses and Disinfection in Sewage Effluent. *Pakistan Journal of Zoology*, *53*(2). https://doi.org/10.17582/journal.pjz/20200821130834

Allegra, S., Leclerc, L., Massard, P. A., Girardot, F., Riffard, S., & Pourchez, J. (2016). Characterization of aerosols containing Legionella generated upon nebulization. *Scientific Reports*, *6*(1), 33998. https://doi.org/10.1038/srep33998

Amoah, I. D., Kumari, S., & Bux, F. (2022). A probabilistic assessment of microbial infection risks due to occupational exposure to wastewater in a conventional activated sludge wastewater treatment plant. *Science of The Total Environment*, *843*, 156849. https://doi.org/10.1016/j.scitotenv.2022.156849

Amos, G. C. A., Hawkey, P. M., Gaze, W. H., & Wellington, E. M. (2014). Waste water effluent contributes to the dissemination of CTX-M-15 in the natural environment. *Journal of Antimicrobial Chemotherapy*, *69*(7), 1785–1791. https://doi.org/10.1093/jac/dku079

Amoueyan, E., Ahmad, S., Eisenberg, J. N. S., & Gerrity, D. (2020). A dynamic quantitative microbial risk assessment for norovirus in potable reuse systems. *Microbial Risk Analysis*, *14*, 100088. https://doi.org/10.1016/j.mran.2019.100088

Anjum, M. F., Schmitt, H., Börjesson, S., Berendonk, T. U., Donner, E., Stehling, E. G., Boerlin, P., Topp, E., Jardine, C., Li, X., Li, B., Dolejska, M., Madec, J.-Y.,

Dagot, C., Guenther, S., Walsh, F., Villa, L., Veldman, K., Sunde, M., … Pedersen, K. (2021). The potential of using E. coli as an indicator for the surveillance of antimicrobial resistance (AMR) in the environment. *Current Opinion in Microbiology*, *64*, 152–158. https://doi.org/10.1016/j.mib.2021.09.011

Arias, E., Heron, M., & Xu, J. (2017). United States Life Tables, 2013. *NVSS*, *66*(3), 64.

Armstrong, T. W., & Haas, C. N. (2007). A Quantitative Microbial Risk Assessment Model for Legionnaires' Disease: Animal Model Selection and Dose-Response Modeling. *Risk Analysis*, *27*(6), 1581–1596. https://doi.org/10.1111/j.1539-6924.2007.00990.x

Armstrong, T. W., & Haas, C. N. (2008). Legionnaires' disease: Evaluation of a quantitative microbial risk assessment model. *Journal of Water and Health*, *6*(2), 149–166. https://doi.org/10.2166/wh.2008.026

Ashbolt, N. J., Amézquita, A., Backhaus, T., Borriello, P., Brandt, K. K., Collignon, P., Coors, A., Finley, R., Gaze, W. H., Heberer, T., Lawrence, J. R., Larsson, D. G. J., McEwen, S. A., Ryan, J. J., Schönfeld, J., Silley, P., Snape, J. R., Van den Eede, C., & Topp, E. (2013). Human Health Risk Assessment (HHRA) for Environmental Development and Transfer of Antibiotic Resistance. *Environmental Health Perspectives*, *121*(9), 993–1001. https://doi.org/10.1289/ehp.1206316

ASHRAE. (2010). ANSI/ASHRAE Standard 55: Thermal Environmental Conditions for Human Occupancy. *ASHRAE*. http://arco-hvac.ir/wp-content/uploads/2015/11/ASHRAE-55-2010.pdf

ASHRAE. (2018). *ANSI/ASHRAE Standard 188: Legionellosis: Risk Management for Building Water Systems*. https://ashrae.iwrapper.com/ViewOnline/Standard_188-2018

ASHRAE. (2019). *ANSI/ASHRAE/IES Standard 90.1-2019—Energy Standard for Buildings Except Low-Rise Residential Buildings* (D-86270, 86270; p. 424). https://www.ashrae.org/technical-resources/bookstore/standard-90-1

AWWA. (2018). *2017 Water Utility Disinfection Survey Report*. American Water Works Association. https://www.awwa.org/Portals/0/AWWA/ETS/Resources/2017DisinfectionSurveyReport.pdf?ver=2018-12-21-163548-830

AWWARF. (1996). *Characterization and Modeling of Chlorine Decay in Distribution Systems*. AWWA, USA. https://books.google.com/books?id=CG23TIEAuBUC&lpg=PR11&ots=v0ciIF6qnh&dq=AWWARF%20(1996)%20Characterisation%20and%20Modeling%20of%20Chlorine%20Decay%20in%20Distribution%20Systems.%20AWWA%2C%20USA.&lr&pg=PR11#v=onepage&q&f=false

Banerji, A., Jahne, M., Herrmann, M., Brinkman, N., & Keely, S. (2019). Bringing Community Ecology to Bear on the Issue of Antimicrobial Resistance. *Frontiers in Microbiology*, *10*, 2626. https://doi.org/10.3389/fmicb.2019.02626

Barker, S. F., Packer, M., Scales, P. J., Gray, S., Snape, I., & Hamilton, A. J. (2013). Pathogen reduction requirements for direct potable reuse in Antarctica: Evaluating human health risks in small communities. *The Science of the Total Environment*, *461–462*, 723–733. https://doi.org/10.1016/j.scitotenv.2013.05.059

Barnsley, G. P., & Barnsley, S. E. (2007). *Rate of pediatric tap water scald injuries in eastern Ontario*. *15*(1), 5.

Beer, K. D. (2015). Surveillance for Waterborne Disease Outbreaks Associated with Drinking Water—United States, 2011-2012. *MMWR. Morbidity and Mortality Weekly Report*, *64*(31), 842–848. https://doi.org/10.15585/mmwr.mm6431a1

Begier, E. M., Frenette, K., Barrett, N. L., Mshar, P., Petit, S., Boxrud, D. J., Watkins-Colwell, K., Wheeler, S., Cebelinski, E. A., Glennen, A., Nguyen, D., Hadler, J. L., & The Connecticut Bioterrorism Field Epidemiology Response Team. (2004). A High-Morbidity Outbreak of Methicillin-Resistant Staphylococcus aureus among Players on a College Football Team, Facilitated by Cosmetic Body Shaving and Turf Burns. *Clinical Infectious Diseases*, *39*(10), 1446–1453. https://doi.org/10.1086/425313

Bengtsson-Palme, J., Jonsson, V., & Heß, S. (2021). *What is the role of the environment in the emergence of novel antibiotic resistance genes? – A modelling approach* (p. 2021.04.04.438392). https://doi.org/10.1101/2021.04.04.438392

Berendonk, T. U., Manaia, C. M., Merlin, C., Fatta-Kassinos, D., Cytryn, E., Walsh, F., Bürgmann, H., Sørum, H., Norström, M., Pons, M.-N., Kreuzinger, N., Huovinen, P., Stefani, S., Schwartz, T., Kisand, V., Baquero, F., & Martinez, J. L. (2015). Tackling antibiotic resistance: The environmental framework. *Nature Reviews Microbiology*, *13*(5), 310–317. https://doi.org/10.1038/nrmicro3439

Bernard, J., Armand-Lefèvre, L., Luce, E., El Mniai, A., Chau, F., Casalino, E., Andremont, A., & Ruppé, E. (2016). Impact of a short exposure to levofloxacin on faecal densities and relative abundance of total and quinolone-resistant Enterobacteriaceae. *Clinical Microbiology and Infection*, *22*(7), 646.e1-646.e4. https://doi.org/10.1016/j.cmi.2016.04.015

Bertsimas, D., Lukin, G., Mingardi, L., Nohadani, O., Orfanoudaki, A., Stellato, B., Wiberg, H., Gonzalez-Garcia, S., Parra-Calderón, C. L., Robinson, K., Schneider, M., Stein, B., Estirado, A., Beccara, L. a, Canino, R., Bello, M. D., Pezzetti, F., Pan, A., & Group, T. H. C.-19 S. (2020). COVID-19 mortality risk assessment: An international multi-center study. *PLOS ONE*, *15*(12), e0243262. https://doi.org/10.1371/journal.pone.0243262

Bivins, A., North, D., Wu, Z., Shaffer, M., Ahmed, W., & Bibby, K. (2021). Within- and between-Day Variability of SARS-CoV-2 RNA in Municipal Wastewater during Periods of Varying COVID-19 Prevalence and Positivity. *ACS ES&T Water*, *1*(9), 2097–2108. https://doi.org/10.1021/acsestwater.1c00178

Blaak, H., de Kruijf, P., Hamidjaja, R. A., van Hoek, A. H. A. M., Husman, A. M. de R., & Schets, F. M. (2014). Prevalence and characteristics of ESBL-producing E-coli in Dutch recreational waters influenced by wastewater treatment plants. *VETERINARY MICROBIOLOGY*, *171*(3–4, SI), 448–459. https://doi.org/10.1016/j.vetmic.2014.03.007

Blaak, H., Lynch, G., Italiaander, R., Hamidjaja, R. A., Schets, F. M., & Husman, A. M. de R. (2015). Multidrug-Resistant and Extended Spectrum Beta-Lactamase-Producing Escherichia coli in Dutch Surface Water and Wastewater. *PLoS One*, *10*(6), e0127752–e0127752. https://doi.org/10.1371/journal.pone.0127752

Blokker, E. J. M., & Pieterse-Quirijns, E. J. (2013). Modeling temperature in the drinking water distribution system. *Journal - American Water Works Association*, *105*(1), E19–E28. https://doi.org/10.5942/jawwa.2013.105.0011

Blue Cross Blue Shield. (2009). *Typical Costs for Common Medical Services*. Blue Cross and Blue Shield of Massachusetts.

Bonnet, R. (2004). Growing group of extended-spectrum beta-lactamases: The CTX-M enzymes. *Antimicrobial Agents and Chemotherapy*, *48*(1), 1–14. https://doi.org/10.1128/AAC.48.1.1-14.2004

Boolchandani, M., D'Souza, A. W., & Dantas, G. (2019). Sequencing-based methods and resources to study antimicrobial resistance. *Nature Reviews Genetics*. https://doi.org/10.1038/s41576-019-0108-4

Borella, P., Montagna, M. T., Romano-Spica, V., Stampi, S., Stancanelli, G., Triassi, M., Neglia, R., Marchesi, I., Fantuzzi, G., Tatò, D., Napoli, C., Quaranta, G., Laurenti, P., Leoni, E., De Luca, G., Ossi, C., Moro, M., & D'Alcalà, G. R. (2004). *Legionella* Infection Risk from Domestic Hot Water. *Emerging Infectious Diseases*, *10*(3), 457–464. https://doi.org/10.3201/eid1003.020707

Borgogna, T. R., Borgogna, J.-L., Mielke, J. A., Brown, C. J., Top, E. M., Botts, R. T., & Cummings, D. E. (2016). High Diversity of CTX-M Extended-Spectrum beta-Lactamases in Municipal Wastewater and Urban Wetlands. *MICROBIAL DRUG RESISTANCE*, *22*(4), 312–320. https://doi.org/10.1089/mdr.2015.0197

Brazeau, R. H., & Edwards, M. A. (2013). Role of Hot Water System Design on Factors Influential to Pathogen Regrowth: Temperature, Chlorine Residual, Hydrogen Evolution, and Sediment. *Environmental Engineering Science*, *30*(10), 617–627. https://doi.org/10.1089/ees.2012.0514

Brechet, C., Plantin, J., Sauget, M., Thouverez, M., Talon, D., Cholley, P., Guyeux, C., Hocquet, D., & Bertrand, X. (2014). Wastewater Treatment Plants Release Large Amounts of Extended-Spectrum beta-Lactamase-Producing Escherichia coli Into the Environment. *CLINICAL INFECTIOUS DISEASES*, *58*(12), 1658–1665. https://doi.org/10.1093/cid/ciu190

Brenner, E., & Smeets, J. B. J. (2019). How Can You Best Measure Reaction Times? *Journal of Motor Behavior*, *51*(5), 486–495. https://doi.org/10.1080/00222895.2018.1518311

Brenner, K. P., Scarpino, P. V., & Clark, C. S. (1988). Animal viruses, coliphages, and bacteria in aerosols and wastewater at a spray irrigation site. *Applied and Environmental Microbiology*, *54*(2), 409–415.

Brink, H., Slaats, P. G. G., & van Eekeren, M. W. M. (2004). Scaling in domestic heating equipment: Getting to know a complex phenomenon. *Water Science and Technology*, *49*(2), 129–136. https://doi.org/10.2166/wst.2004.0106

Brisolara, K. F., Maal-Bared, R., Sobsey, M. D., Reimers, R. S., Rubin, A., Bastian, R. K., Gerba, C., Smith, J. E., Bibby, K., Kester, G., & Brown, S. (2021). Assessing and managing SARS-CoV-2 occupational health risk to workers handling

residuals and biosolids. *The Science of the Total Environment, 774*, 145732. https://doi.org/10.1016/j.scitotenv.2021.145732

Brouwer, A. F., Weir, M. H., Eisenberg, M. C., Meza, R., & Eisenberg, J. N. S. (2017). Dose-response relationships for environmentally mediated infectious disease transmission models. *PLoS Computational Biology*, *13*(4), 1–28. https://doi.org/10.1371/journal.pcbi.1005481

Brûlet, A., Nicolle, M.-C., Giard, M., Nicolini, F.-E., Michallet, M., Jarraud, S., Etienne, J., & Vanhems, P. (2008). Fatal Nosocomial *Legionella pneumophila* Infection Due to Exposure to Contaminated Water From a Washbasin in a Hematology Unit. *Infection Control & Hospital Epidemiology*, *29*(11), 1091–1093. https://doi.org/10.1086/591739

Burkhardt, J. B., Woo, H., Mason, J., Shang, F., Triantafyllidou, S., Schock, M. R., Lytle, D., & Murray, R. (2020). Framework for Modeling Lead in Premise Plumbing Systems Using EPANET. *Journal of Water Resources Planning and Management*, *146*(12), 04020094. https://doi.org/10.1061/(ASCE)WR.1943-5452.0001304

Burmaster, D. E., & Anderson, P. D. (1994). Principles of good practice for the use of Monte Carlo techniques in human health and ecological risk assessments. *Risk Analysis: An Official Publication of the Society for Risk Analysis*, *14*(4), 477–481. https://doi.org/10.1111/j.1539-6924.1994.tb00265.x

Burmeister, A. R. (2015). Horizontal Gene Transfer. *Evolution, Medicine, and Public Health*, *2015*(1), 193–194. https://doi.org/10.1093/emph/eov018

Bussard, D. (2011). U.S. EPA Exposure Factors Handbook 2011 Edition (Final Report). *U.S. Environmental Protection Agency, Washington, DC.*, *EPA/600/R-09/052F*, 1436.

Caicedo, C., Rosenwinkel, K.-H., Exner, M., Verstraete, W., Suchenwirth, R., Hartemann, P., & Nogueira, R. (2019). Legionella occurrence in municipal and industrial wastewater treatment plants and risks of reclaimed wastewater reuse: Review. *Water Research*, *149*, 21–34. https://doi.org/10.1016/j.watres.2018.10.080

California Department of Public Health. (2011). *Groundwater Replenishment Using Recycled Water*. http://www.cdph.ca.gov/certlic/drinkingwater/Documents/Recharge/DraftRechargeReg-2011-11-21.pdf

Carducci, A., Donzelli, G., Cioni, L., Federigi, I., Lombardi, R., & Verani, M. (2018). Quantitative Microbial Risk Assessment for Workers Exposed to Bioaerosol in Wastewater Treatment Plants Aimed at the Choice and Setup of Safety Measures. *International Journal of Environmental Research and Public Health*, *15*(7), Article 7. https://doi.org/10.3390/ijerph15071490

CDC. (1999). Achievements in Public Health, 1900-1999: Control of Infectious Diseases. *MMWR Weekly*, *48*(29), 621–629.

CDC. (2015). *Legionnaires' Disease Surveillance Summary Report, United States- 2014 and 2015*. Center for Disease Control and Prevention. https://www.cdc.gov/legionella/health-depts/surv-reporting/2014-15-surv-report-508.pdf

CDC. (2017). *Developing a Water Management Program to Reduce Legionella Growth & Spread in Buildings*. https://www.cdc.gov/legionella/downloads/toolkit.pdf

CDC. (2018). *Legionella (Legionnaires' Disease and Pontiac Fever)*. CDC. https://www.cdc.gov/legionella/about/history.html

CDC. (2019). *Antibiotic Resistance Threats in the United States, 2019*. 148.

CDC. (2021). *Legionella: Healthcare Water Management Program FAQs*. https://www.cdc.gov/legionella/wmp/healthcare-facilities/healthcare-wmp-faq.html

CDC, Barskey, A., Binder, A., Edens, C., Lee, S., Smith, J., Schrag, S., Whitney, C., & Cooley, L. (2015). *Legionnaires' Disease Surveillance Summary Report, United States- 2014 and 2015*. Center for Disease Control and Prevention. https://www.cdc.gov/legionella/health-depts/surv-reporting/2014-15-surv-report-508.pdf

CDC, & NIOSH. (2023, January 17). *Hierarchy of Controls*. https://www.cdc.gov/niosh/topics/hierarchy/default.html

Cervero-Aragó, S., Rodríguez-Martínez, S., Puertas-Bennasar, A., & Araujo, R. M. (2015). Effect of Common Drinking Water Disinfectants, Chlorine and Heat, on Free Legionella and Amoebae-Associated Legionella. *PLOS ONE*, *10*(8), e0134726. https://doi.org/10.1371/journal.pone.0134726

Chahal, C., van den Akker, B., Young, F., Franco, C., Blackbeard, J., & Monis, P. (2016). Chapter Two - Pathogen and Particle Associations in Wastewater:

Significance and Implications for Treatment and Disinfection Processes. In S. Sariaslani & G. Michael Gadd (Eds.), *Advances in Applied Microbiology* (Vol. 97, pp. 63–119). Academic Press. https://doi.org/10.1016/bs.aambs.2016.08.001

Chande, A., Lee, S., Harris, M., Nguyen, Q., Beckett, S. J., Hilley, T., Andris, C., & Weitz, J. S. (2020). Real-time, interactive website for US-county-level COVID-19 event risk assessment. *Nature Human Behaviour*, *4*(12), Article 12. https://doi.org/10.1038/s41562-020-01000-9

Chandrasekaran, S., & Jiang, S. C. (2019). A dose response model for quantifying the infection risk of antibiotic-resistant bacteria. *Scientific Reports*, *9*(1), 17093. https://doi.org/10.1038/s41598-019-52947-3

Chandrasekaran, S., & Jiang, S. C. (2021). A dose response model for Staphylococcus aureus. *Scientific Reports*, *11*(1), 12542. https://doi.org/10.1038/s41598-021-91822-y

Chappell, C. L., Okhuysen, P. C., Langer-Curry, R., Widmer, G., Akiyoshi, D. E., Tanriverdi, S., & Tzipori, S. (2006). Cryptosporidium hominis: Experimental challenge of healthy adults. *The American Journal of Tropical Medicine and Hygiene*, *75*(5), 851–857. https://doi.org/10.4269/ajtmh.2006.75.851

Chatterjee, A., Modarai, M., Naylor, N. R., Boyd, S. E., Atun, R., Barlow, J., Holmes, A. H., Johnson, A., & Robotham, J. V. (2018). Review Quantifying drivers of antibiotic resistance in humans: A systematic review. *The Lancet Infectious Diseases*, *18*(12), 1–11. https://doi.org/10.1016/S1473-3099(18)30296-2

Chen, T. Q., Rubanova, Y., Bettencourt, J., & Duvenaud, D. K. (2018). *Neural Ordinary Differential Equations*. 12.

Chen, Y., Yan, C., Yang, Y., & Ma, J. (2021). Quantitative microbial risk assessment and sensitivity analysis for workers exposed to pathogenic bacterial bioaerosols under various aeration modes in two wastewater treatment plants. *Science of The Total Environment*, *755*, 142615. https://doi.org/10.1016/j.scitotenv.2020.142615

Chester, D. L., Jose, R. M., Aldlyami, E., King, H., & Moiemen, N. S. (2005). Non-accidental burns in children—Are we neglecting neglect? *Burns*, *32*(2), 222–228. https://doi.org/10.1016/j.burns.2005.08.018

Chmielewska, A. (2018). Fluctuating temperature of the mains water throughout the year and its influence on the consumption of energy for the purposes of DHW

preparation. *E3S Web of Conferences*, *44*, 00017. https://doi.org/10.1051/e3sconf/20184400017

Clouatre, E., Pinto, R., Banfield, J., & Jeschke, M. G. (2013). Incidence of Hot Tap Water Scalds After the Introduction of Regulations in Ontario: *Journal of Burn Care & Research*, *34*(2), 243–248. https://doi.org/10.1097/BCR.0b013e3182789057

CMS. (2000). *State operations manual Appendix Q. Guidelines for determining immediate jeopardy. Rev. 102*. file:///C:/Users/ashle/Dropbox/Ashley%20Heida/Water%20heater%20project/Water%20Heater%20Papers/CMS_2014.pdf

CMS. (2018). *Centers for Medicare and Medicaid Services. SUBJ: Requirement to Reduce Legionella Risk in Healthcare Facility Water Systems to Prevent Cases and Outbreaks of Legionnaires' Disease (LD). *Revised to Clarify Expectations for Providers, Accrediting Organizations, and Surveyors**. Memorandum. https://www.cms.gov/Medicare/Provider-Enrollment-and-Certification/SurveyCertificationGenInfo/Downloads/QSO17-30-HospitalCAH-NH-REVISED-.pdf

Collier, S. A., Deng, L., Adam, E. A., Benedict, K. M., Beshearse, E. M., Blackstock, A. J., Bruce, B. B., Derado, G., Edens, C., Fullerton, K. E., Gargano, J. W., Geissler, A. L., Hall, A. J., Havelaar, A. H., Hill, V. R., Hoekstra, R. M., Reddy, S. C., Scallan, E., Stokes, E. K., … Beach, M. J. (2021). *Estimate of Burden and Direct Healthcare Cost of Infectious Waterborne Disease in the United States—Volume 27, Number 1—January 2021—Emerging Infectious Diseases journal—CDC*. https://doi.org/10.3201/eid2701.190676

Collier, S. A., Stockman, L. J., Hicks, L. A., Garrison, L. E., Zhou, F. J., & Beach, M. J. (2012). Direct healthcare costs of selected diseases primarily or partially transmitted by water. *Epidemiology and Infection*, *140*(11), 2003–2013. https://doi.org/10.1017/S0950268811002858

Collineau L, A. A., Carson C, Chapman B, Fazil A, Otten A, Parmley J, Reid-Smith RJ, Smith B. (2018). A Farm-to-fork Quantitative Risk Assessment Model for Antimicrobial-resistant Salmonella Heidelberg in Canadian Broiler Chickens. *Society for Risk Analysis Annual Conference*. http://birenheide.com/sra/2018AM/program/singlesession.php3?sessid=T4-H&order=4#4

Collineau, L., Boerlin, P., Carson, C. A., Chapman, B., Fazil, A., Hetman, B., McEwen, S. A., Parmley, E. J., Reid-Smith, R. J., Taboada, E. N., & Smith, B. A. (2019). Integrating Whole-Genome Sequencing Data Into Quantitative Risk Assessment of Foodborne Antimicrobial Resistance: A Review of Opportunities and Challenges. *Frontiers in Microbiology*, *10*(May), 1–18. https://doi.org/10.3389/fmicb.2019.01107

Coniglio, M. A., Ferrante, M., & Yassin, M. H. (2018). Preventing Healthcare-Associated Legionellosis: Results after 3 Years of Continuous Disinfection of Hot Water with Monochloramine and an Effective Water Safety Plan. *International Journal of Environmental Research and Public Health*, *15*(8), Article 8. https://doi.org/10.3390/ijerph15081594

Contijoch, E. J., Britton, G. J., Yang, C., Mogno, I., Li, Z., Ng, R., Llewellyn, S. R., Hira, S., Johnson, C., Rabinowitz, K. M., Barkan, R., Dotan, I., Hirten, R. P., Fu, S.-C., Luo, Y., Yang, N., Luong, T., Labrias, P. R., Lira, S., … Faith, J. J. (2019). Gut microbiota density influences host physiology and is shaped by host and microbial factors. *ELife*, *8*, e40553. https://doi.org/10.7554/eLife.40553

Corrao, C. R. N., Del Cimmuto, A., Marzuillo, C., Paparo, E., & La Torre, G. (2013). Association between Waste Management and HBV among Solid Municipal Waste Workers: A Systematic Review and Meta-Analysis of Observational Studies. *The Scientific World Journal*, *2013*, e692083. https://doi.org/10.1155/2013/692083

Crank, K., Petersen, S., & Bibby, K. (2019). Quantitative Microbial Risk Assessment of Swimming in Sewage Impacted Waters Using CrAssphage and Pepper Mild Mottle Virus in a Customizable Model. *Environmental Science & Technology Letters*. https://doi.org/10.1021/acs.estlett.9b00468

Cummings, J. H., Jenkins, D. J., & Wiggins, H. S. (1976). Measurement of the mean transit time of dietary residue through the human gut. *Gut*, *17*(3), 210–218. https://doi.org/10.1136/gut.17.3.210

Dada, A. C., & Gyawali, P. (2021). Quantitative microbial risk assessment (QMRA) of occupational exposure to SARS-CoV-2 in wastewater treatment plants. *Science of The Total Environment*, *763*, 142989. https://doi.org/10.1016/j.scitotenv.2020.142989

D'Andrea, M. M., Arena, F., Pallecchi, L., & Rossolini, G. M. (2013). CTX-M-type β-lactamases: A successful story of antibiotic resistance. *International Journal of*

Medical Microbiology: IJMM, *303*(6–7), 305–317. https://doi.org/10.1016/j.ijmm.2013.02.008

D'Aoust, P. M., Towhid, S. T., Mercier, É., Hegazy, N., Tian, X., Bhatnagar, K., Zhang, Z., Naughton, C. C., MacKenzie, A. E., Graber, T. E., & Delatolla, R. (2021). COVID-19 wastewater surveillance in rural communities: Comparison of lagoon and pumping station samples. *Science of The Total Environment*, *801*, 149618. https://doi.org/10.1016/j.scitotenv.2021.149618

de Moel, P. J., van der Helm, A. W. C., van Rijn, M., van Dijk, J. C., & van der Meer, W. G. J. (2013). Assessment of calculation methods for calcium carbonate saturation in drinking water for DIN 38404-10 compliance. *Drinking Water Engineering and Science*, *6*(2), 115–124. https://doi.org/10.5194/dwes-6-115-2013

de Oliveira, L. C., Torres-Franco, A. F., Lopes, B. C., Santos, B. S. Á. da S., Costa, E. A., Costa, M. S., Reis, M. T. P., Melo, M. C., Polizzi, R. B., Teixeira, M. M., & Mota, C. R. (2021). Viability of SARS-CoV-2 in river water and wastewater at different temperatures and solids content. *Water Research*, *195*, 117002. https://doi.org/10.1016/j.watres.2021.117002

DeOreo, W. B., Mayer, P. W., Dziegielewski, B., & Kiefer, J. (2016). Residential End Uses of Water, version 2. *Water Research Foundation*, 18.

Diallo, A. A., Brugere, H., Kerouredan, M., Dupouy, V., Toutain, P.-L., Bousquet-Melou, A., Oswald, E., & Bibbal, D. (2013). Persistence and prevalence of pathogenic and extended-spectrum beta-lactamase-producing Escherichia coli in municipal wastewater treatment plant receiving slaughterhouse wastewater. *WATER RESEARCH*, *47*(13), 4719–4729. https://doi.org/10.1016/j.watres.2013.04.047

Dieter, C. A., Maupin, M. A., Caldwell, R. R., Harris, M. A., Ivahnenko, T. I., Lovelace, J. K., Barber, N. L., & Linsey, K. S. (2018). *Estimated Use of Water in the United States in 2015: U.S. Geological Survey Circular 1441*. U.S. Geological Survey.

Divizia, M., Cencioni, B., Palombi, L., & Panà, A. (2008). Sewage workers: Risk of acquiring enteric virus infections including Hepatitis A. *New Microbiologica, 31*(3), 337–341. Scopus.

DOE. (n.d.). *Estimating Costs and Efficiency of Storage, Demand, and Heat Pump Water Heaters*. DOE. Retrieved February 7, 2020, from https://www.energy.gov/energysaver/estimating-costs-and-efficiency-storage-demand-and-heat-pump-water-heaters

DOE. (2016). *Savings Project: Lower Water Heating Temperature*. DOE. https://www.energy.gov/energysaver/services/do-it-yourself-energy-savings-projects/savings-project-lower-water-heating

Dormand, J. R., & Prince, P. J. (1980). A family of embedded Runge-Kutta formulae. *Journal of Computational and Applied Mathematics*, *6*(1), 19–26. https://doi.org/10.1016/0771-050X(80)90013-3

Douwes, J., Eduard, W., & Thorne, P. (2008). Bioaerosols. In *International Encyclopedia of Public Health*. https://doi.org/10.1016/B978-012373960-5.00281-1

Douwes, J., Thorne, P., Pearce, N., & Heederik, D. (2003). Bioaerosol health effects and exposure assessment: Progress and prospects. *The Annals of Occupational Hygiene*, *47*(3), 187–200. https://doi.org/10.1093/annhyg/meg032

Dufour, A. P., Behymer, T. D., Cantú, R., Magnuson, M., & Wymer, L. J. (2017). Ingestion of swimming pool water by recreational swimmers. *Journal of Water and Health*, *15*(3), 429–437. https://doi.org/10.2166/wh.2017.255

Durand, M. A., Green, J., Edwards, P., Milton, S., & Lutchmun, S. (2012). Perceptions of tap water temperatures, scald risk and prevention among parents and older people in social housing: A qualitative study. *Burns*, *38*(4), 585–590. https://doi.org/10.1016/j.burns.2011.10.009

Eftim, S. E., Hong, T., Soller, J., Boehm, A., Warren, I., Ichida, A., & Nappier, S. P. (2017). Occurrence of norovirus in raw sewage – A systematic literature review and meta-analysis. *Water Research*, *111*, 366–374. https://doi.org/10.1016/j.watres.2017.01.017

El Tumi, H., Johnson, M. I., Dantas, P. B. F., Maynard, M. J., & Tashani, O. A. (2017). Age-related changes in pain sensitivity in healthy humans: A systematic review with meta-analysis. *European Journal of Pain*, *21*(6), 955–964. https://doi.org/10.1002/ejp.1011

Emamalipour, M., Seidi, K., Zununi Vahed, S., Jahanban-Esfahlan, A., Jaymand, M., Majdi, H., Amoozgar, Z., Chitkushev, L. T., Javaheri, T., Jahanban-Esfahlan, R., & Zare, P. (2020). Horizontal Gene Transfer: From Evolutionary Flexibility to Disease Progression. *Frontiers in Cell and Developmental Biology*, *8*, 229. https://doi.org/10.3389/fcell.2020.00229

ENERGY STAR. (2008). *ENERGY STAR Residential Water Heaters: Final Criteria Analysis*. ENERGY STAR.

https://www.energystar.gov/ia/partners/prod_development/new_specs/downloads/water_heaters/waterheateranalysis_final.pdf

EPA. (2009). *Indoor Air Quality Tools for Schools Reference Guide*. EPA. https://www.epa.gov/sites/production/files/2014-08/documents/reference_guide.pdf

Erdmann, T. C., Feldman, K. W., & Rivara, P. (1991). *Tap Water Burn Prevention: The Effect of Legislation*. 8.

Flemming, H.-C., Percival, S. L., & Walker, J. T. (2002). Contamination potential of biofilms in water distribution systems. *Water Supply*, *2*(1), 271–280. https://doi.org/10.2166/ws.2002.0032

Flores-Mireles, A. L., Walker, J. N., Caparon, M., & Hultgren, S. J. (2015). Urinary tract infections: Epidemiology, mechanisms of infection and treatment options. *Nature Reviews. Microbiology*, *13*(5), 269–284. https://doi.org/10.1038/nrmicro3432

Food Safety News. (2022). *China records Salmonella outbreak from contaminated water*. Food Safety News. https://www.foodsafetynews.com/2022/05/china-records-salmonella-outbreak-from-contaminated-water/

Foster-Nyarko, E., & Pallen, M. J. (2022). The microbial ecology of Escherichia coli in the vertebrate gut. *FEMS Microbiology Reviews*, *46*(3), fuac008. https://doi.org/10.1093/femsre/fuac008

Foxman, B. (2002). Epidemiology of urinary tract infections: Incidence, morbidity, and economic costs. *The American Journal of Medicine*, *113 Suppl 1A*, 5S-13S. https://doi.org/10.1016/s0002-9343(02)01054-9

Foxman, B. (2014). Urinary tract infection syndromes: Occurrence, recurrence, bacteriology, risk factors, and disease burden. *Infectious Disease Clinics of North America*, *28*(1), 1–13. https://doi.org/10.1016/j.idc.2013.09.003

Foxman, B., Barlow, R., D'Arcy, H., Gillespie, B., & Sobel, J. D. (2000). Urinary tract infection: Self-reported incidence and associated costs. *Annals of Epidemiology*, *10*(8), 509–515. https://doi.org/10.1016/s1047-2797(00)00072-7

Franz, E., & Schijven, J. (2014). Meta-Regression Analysis of Commensal and Pathogenic Escherichia coli Survival in Soil and Water. *Environ. Sci. Technol.*, 9.

Franz, E., Veenman, C., van Hoek, A. H. A. M., Husman, A. de R., & Blaak, H. (2015). Pathogenic Escherichia coli producing Extended-Spectrum β-Lactamases isolated

from surface water and wastewater. *Scientific Reports*, *5*(1), Article 1. https://doi.org/10.1038/srep14372

Garner, E., Chen, C., Xia, K., Bowers, J., Engelthaler, D. M., McLain, J., Edwards, M. A., & Pruden, A. (2018). Metagenomic Characterization of Antibiotic Resistance Genes in Full-Scale Reclaimed Water Distribution Systems and Corresponding Potable Systems. *Environmental Science & Technology*, *52*(11), 6113–6125. https://doi.org/10.1021/acs.est.7b05419

Garner, E., Davis, B. C., Milligan, E., Blair, M. F., Keenum, I., Maile-Moskowitz, A., Pan, J., Gnegy, M., Liguori, K., Gupta, S., Prussin, A. J., Marr, L. C., Heath, L. S., Vikesland, P. J., Zhang, L., & Pruden, A. (2021). Next generation sequencing approaches to evaluate water and wastewater quality. *Water Research*, *194*, 116907. https://doi.org/10.1016/j.watres.2021.116907

Garny, K., Neu, T. R., & Horn, H. (2009). Sloughing and limited substrate conditions trigger filamentous growth in heterotrophic biofilms—Measurements in flow-through tube reactor. *Chemical Engineering Science*, *64*(11), 2723–2732. https://doi.org/10.1016/j.ces.2009.03.009

Gerba, C. P. (2015). Chapter 24—Risk Assessment. In I. L. Pepper, C. P. Gerba, & T. J. Gentry (Eds.), *Environmental Microbiology (Third Edition)* (pp. 565–579). Academic Press. https://doi.org/10.1016/B978-0-12-394626-3.00024-7

Gerrity, D., Kaufman, A., Pecson, B., Seto, E., & Olivieri, A. (2019). *DPRisk*. Water Research Foundation. https://edmundseto.shinyapps.io/QMRAv100/

Ghafourian, S., Sadeghifard, N., Sohelil, S., & Sekawi, Z. (2015). Extended Spectrum Beta-lactamases: Definition, Classification and Epidemiology. *Current Issues in Molecular Biology*. https://doi.org/10.21775/cimb.017.011

Gholipour, S., Mohammadi, F., Nikaeen, M., Shamsizadeh, Z., Khazeni, A., Sahbaei, Z., Mousavi, S. M., Ghobadian, M., & Mirhendi, H. (2021). COVID-19 infection risk from exposure to aerosols of wastewater treatment plants. *Chemosphere*, *273*, 129701. https://doi.org/10.1016/j.chemosphere.2021.129701

Gomez-Valero, L., & Buchrieser, C. (2019). Intracellular parasitism, the driving force of evolution of Legionella pneumophila and the genus Legionella. *Microbes and Infection*, *21*(5–6), 230–236. https://doi.org/10.1016/j.micinf.2019.06.012

Gordon, A., Mathers, A., Cheong, E., Gottlieb, T., Kotay, S., Walker, A., Peto, T., Crook, D., & Stoesser, N. (2017). The Hospital Water Environment as a Reservoir for

Carbapenem-Resistant Organisms Causing HospitalAcquired Infections—A Systematic Review of the Literature. *Clinical Infectious Diseases*, *64*(10), 1435–1444. https://doi.org/10.1093/cid/cix132

Government of Canada. (2011). *Water Temperature and Burns/Scalds*. https://www.canada.ca/en/public-health/services/water-temperature-burns-scalds.html

Graham, J. P., Amato, H. K., Mendizabal-Cabrera, R., Alvarez, D., & Ramay, B. M. (2021). Waterborne Urinary Tract Infections: Have We Overlooked an Important Source of Exposure? *The American Journal of Tropical Medicine and Hygiene*, *105*(1), 12–17. https://doi.org/10.4269/ajtmh.20-1271

Graitcer, P. L., & Sniezek, J. E. (1988). HOSPITALIZATIONS DUE TO TAP WATER SCALDS, 1978-1985. *Public Health Surveillance of 1990 Injury Control Objectives for the Nation*, *37*, 4.

Guyer, J. P. (2016). *An Introduction to Hospital Domestic Water Systems*. 36.

Haas, C. N. (2015). Microbial Dose Response Modeling: Past, Present, and Future. *Environmental Science & Technology*, *49*(3), 1245–1259. https://doi.org/10.1021/es504422q

Haas, C. N., Rose, J. B., & Gerba, C. P. (1999). *Quantitative Microbial Risk Assessment*. John Wiley & Sons, Inc.

Haas, C. N., Rose, J. B., & Gerba, C. P. (2014). *Quantitative Microbial Risk Assessment*. John Wiley & Sons.

Haas, C. N., Rycroft, T., Bibby, K., & Casson, L. (2017). Risks from Ebolavirus Discharge from Hospitals to Sewer Workers. *Water Environment Research*, *89*(4), 357–368. https://doi.org/10.2175/106143017X14839994523181

Hach. (2018). *Chlorine, Free and Total, Low Range: USEPA DPD Method 8021 (Free) 8167 (Total) DOC316.53.01450*. https://www.hach.com/asset-get.download-en.jsa?code=163953

Hamilton, K. A., Hamilton, M. T., Johnson, W., Jjemba, P., Bukhari, Z., LeChevallier, M., & Haas, C. N. (2018). Health risks from exposure to Legionella in reclaimed water aerosols: Toilet flushing, spray irrigation, and cooling towers. *Water Research*, *134*, 261–279. https://doi.org/10.1016/j.watres.2017.12.022

Hamilton, K. A., Prussin, A. J., Ahmed, W., & Haas, C. N. (2018). Outbreaks of Legionnaires' Disease and Pontiac Fever 2006–2017. *Current Environmental Health Reports*, *5*(2), 263–271. https://doi.org/10.1007/s40572-018-0201-4

Hamilton, K., Ashbolt, N., Garner, E., Gupta, S., Haddix, M., Harrison, J., Heida, A., Keenum, I., Lopatkin, A., Medema, G., Schoen, M., Soller, J., Brown, J., Fisher, P., Graham, J., Jahne, M., McLain, J., Keely, S., Mitchell, J., … Pruden, A. (2022). A human health risk modeling framework for environmental sources of AMR: Toward quantitative risk predictions (in revision). *Environmental Science and Techology*.

Hamilton, K., Hamilton, M. T., Johnson, W., Jjemba, P., Bukhari, Z., LeChevallier, M., & Haas, C. N. (2018). Health risks from exposure to Legionella in reclaimed water aerosols: Toilet flushing, spray irrigation, and cooling towers. *Water Research*, *134*, 261–279. https://doi.org/10.1016/j.watres.2017.12.022

Hamilton, K., Hamilton, M. T., Johnson, W., Jjemba, P., Bukhari, Z., LeChevallier, M., Haas, C. N., & Gurian, P. L. (2019). Risk-Based Critical Concentrations of *Legionella pneumophila* for Indoor Residential Water Uses. *Environmental Science & Technology*, *53*(8), 4528–4541. https://doi.org/10.1021/acs.est.8b03000

Han, Y., Yang, K., Yang, T., Zhang, M., & Li, L. (2019). Bioaerosols emission and exposure risk of a wastewater treatment plant with A2O treatment process. *Ecotoxicology and Environmental Safety*, *169*, 161–168. https://doi.org/10.1016/j.ecoenv.2018.11.018

Han, Y., Yang, T., Yan, X., Li, L., & Liu, J. (2020). Effect of aeration mode on aerosol characteristics from the same wastewater treatment plant. *Water Research*, *170*. Scopus. https://doi.org/10.1016/j.watres.2019.115324

Harrington, R. D., & Hooton, T. M. (2000). Urinary tract infection risk factors and gender. *The Journal of Gender-Specific Medicine: JGSM: The Official Journal of the Partnership for Women's Health at Columbia*, *3*(8), 27–34.

Hayward, C. (2020). Water as a Source of Antimicrobial Resistance and Healthcare-Associated Infections. *Pathogens*, *9*(8), 667.

Heaton, K. W., Radvan, J., Cripps, H., Mountford, R. A., Braddon, F. E., & Hughes, A. O. (1992). Defecation frequency and timing, and stool form in the general population: A prospective study. *Gut*, *33*(6), 818–824. https://doi.org/10.1136/gut.33.6.818

Herman, J., Usher, W., Mutel, C., Trindade, B., Hadka, D., Woodruff, M., Rios, F., Hyams, D., & Xantares. (2017). *SALib*. MIT. https://salib.readthedocs.io/en/latest/license.html

Hewitt, A., Macarthur, C., & Raina, P. (2007). The Role of Evidence in Public Health Policy: An Example of Linkage and Exchange in the Prevention of Scald Burns. *Healthcare Policy | Politiques de Santé*, *3*(2), 59–66. https://doi.org/10.12927/hcpol.2007.19392

Heyder, J., Gebhart, J., Rudolf, G., Schiller, C., & Stahlhofen, W. (1986). Deposition of particles in the human respiratory tract in the size range 0.005-15 micrometers. *J. Aerosol Sci.*, *17*(5), 811–825.

Hillebrand, B., & Blokker, E. J. M. (2021). *Modeling the Influence of District Heating Systems on Drinking Water Temperatures in Domestic Drinking Water Systems within Domestic Properties*. 961–968. https://doi.org/10.1061/9780784483466.088

Hockey, R. (2002). Safe hot tap water and the risk of scalds and legionella infection. *Injury Prevention*, *8*(2), 170–170. https://doi.org/10.1136/ip.8.2.170

Hodcroft, E. (2020). *CoVariants*. https://covariants.org/

Hofman, J., Hoek, J. P. V. D., Nederlof, M., & Groenendijk, M. (2007). *Twenty years of experience with centralised softening in the Netherlands: Water quality, environmental benefits, and costs*. https://researchportal.bath.ac.uk/en/publications/twenty-years-of-experience-with-centralised-softening-in-the-neth

Hong, P.-Y., Graham, D., Jiang, S. C., Julian, T. R., Nelson, K. L., Pruden, A., Pype, M.-L., & Manaia, C. M. (2018). Reusing Treated Wastewater: Consideration of the Safety Aspects Associated with Antibiotic-Resistant Bacteria and Antibiotic Resistance Genes. *Water*, *10*(3). AGRICOLA. https://doi.org/10.3390/w10030244

Hu, C., Pendl-Robinson, E., Lipman, E., Starling, J., Luo, M., & Dulieu, M. (2020). *19 and Me: COVID-19 Risk Calculator*. https://19andme.covid19.mathematica.org/

Huang, C., Shen, Y., Smith, R. L., Dong, S., & Nguyen, T. H. (2020). Effect of disinfectant residuals on infection risks from Legionella pneumophila released by biofilms grown under simulated premise plumbing conditions. *Environment International*, *137*, 105561. https://doi.org/10.1016/j.envint.2020.105561

Huang, N., Pérez, P., Kato, T., Mikami, Y., Okuda, K., Gilmore, R. C., Conde, C. D., Gasmi, B., Stein, S., Beach, M., Pelayo, E., Maldonado, J. O., Lafont, B. A., Jang, S.-I., Nasir, N., Padilla, R. J., Murrah, V. A., Maile, R., Lovell, W., … Byrd, K. M. (2021). SARS-CoV-2 infection of the oral cavity and saliva. *Nature Medicine*, *27*(5), Article 5. https://doi.org/10.1038/s41591-021-01296-8

Huang, Y., & Haas, C. (2009). Time-dose-response models for microbial risk assessment. *Risk Analysis*, *29*(5), 648–661. https://doi.org/10.1111/j.1539-6924.2008.01195.x

Hugo Johansson, P. J., Andersson, K., Wiebe, T., Schalén, C., & Bernander, S. (2006). Nosocomial transmission of Legionella pneumophila to a child from a hospital's cold-water supply. *Scandinavian Journal of Infectious Diseases*, *38*(11–12), 1023–1027. https://doi.org/10.1080/00365540600827558

Huyer, D. W., & Corkum, S. H. (1997). Reducing the incidence of tap-water scalds: Strategies for physicians. *CAN MED ASSOC J*, *156*(6), 841–844.

IAPMO. (2016). *2015 Minnesota Plumbing Code Water Pipe Sizing Workshop*. IAPMO.

Inc. Metcalf & Eddy, Tchobanoglous, G., Stensel, H., Tsuchihashi, R., & Burton, F. (2013). *Wastewater Engineering: Treatment and Resource Recover* (5th ed.). McGraw Hill.

Incropera, F. P., Dewitt, D. P., Bergman, T. L., & Lavine, A. S. (Eds.). (2007). *Fundamentals of heat and mass transfer* (6th ed). John Wiley.

International Desalination Association (Ed.). (2006). *Innovation and integration - impact on desalination and water reuse costs: IDA International Water Forum, Dubai, UAE, March 5 - 6, 2006*. IDA. https://www.researchgate.net/profile/Hamza-Elfil/publication/323615931_A_New_Index_for_Scaling_Assessment/links/5aa02af60f7e9badd9a0ba07/A-New-Index-for-Scaling-Assessment.pdf

Jahne, M. A., Schoen, M. E., Kaufmann, A., Pecson, B. M., Olivieri, A., Sharvelle, S., Anderson, A., Ashbolt, N. J., & Garland, J. L. (2023). Enteric pathogen reduction targets for onsite non-potable water systems: A critical evaluation. *Water Research*, *233*, 119742. https://doi.org/10.1016/j.watres.2023.119742

Johnson, J. R., Johnston, B. D., Delavari, P., Thuras, P., Clabots, C., & Sadowsky, M. J. (2017). Phylogenetic Backgrounds and Virulence-Associated Traits of Escherichia coli Isolates from Surface Waters and Diverse Animals in Minnesota and Wisconsin. *Applied and Environmental Microbiology*, *83*(24), e01329-17. https://doi.org/10.1128/AEM.01329-17

Jones, D. L., Baluja, M. Q., Graham, D. W., Corbishley, A., McDonald, J. E., Malham, S. K., Hillary, L. S., Connor, T. R., Gaze, W. H., Moura, I. B., Wilcox, M. H., & Farkas, K. (2020). Shedding of SARS-CoV-2 in feces and urine and its potential role in person-to-person transmission and the environment-based spread of COVID-19. *Science of The Total Environment*, *749*, 141364. https://doi.org/10.1016/j.scitotenv.2020.141364

Jones, R. M. (2020). Relative contributions of transmission routes for COVID-19 among healthcare personnel providing patient care. *Journal of Occupational and Environmental Hygiene*, *17*(9), 408–415. https://doi.org/10.1080/15459624.2020.1784427

Jorgensen, S. B., Soraas, A. V., Arnesen, L. S., Leegaard, T. M., Sundsfjord, A., & Jenum, P. A. (2017). A comparison of extended spectrum beta-lactamase producing Escherichia coli from clinical, recreational water and wastewater samples associated in time and location. *PloS One*, *12*(10), e0186576. https://doi.org/10.1371/journal.pone.0186576

Julian, T. R., Vithanage, H. S. K., Chua, M. L., Kuroda, M., Pitol, A. K., Nguyen, P. H. L., Canales, R. A., Fujii, S., & Harada, H. (2018). High time-resolution simulation of E. coli on hands reveals large variation in microbial exposures amongst Vietnamese farmers using human excreta for agriculture. *Science of The Total Environment*, *635*, 120–131. https://doi.org/10.1016/j.scitotenv.2018.04.100

Kallawicha, K., Chuang, Y.-C., Lung, S.-C. C., Han, B.-C., Ting, Y.-F., & Chao, H. J. (2016). Exposure to ambient bioaerosols is associated with allergic skin diseases in Greater Taipei residents. *Environmental Pollution*, *216*, 845–850. https://doi.org/10.1016/j.envpol.2016.06.057

Katcher, M. L. (1981). *Scald Burns From Hot Tap Water*. *245*(11), 1219–1222.

Katouli, M. (2010). Population structure of gut Escherichia coli and its role in development of extra-intestinal infections. *Iranian Journal of Microbiology*, *2*(2), 59–72.

Khuder, S. A., Arthur, T., Bisesi, M. S., & Schaub, E. A. (1998). Prevalence of infectious diseases and associated symptoms in wastewater treatment workers. *American Journal of Industrial Medicine*, *33*(6), 571–577. https://doi.org/10.1002/(sici)1097-0274(199806)33:6<571::aid-ajim8>3.0.co;2-t

Kitajima, M., Ahmed, W., Bibby, K., Carducci, A., Gerba, C. P., Hamilton, K. A., Haramoto, E., & Rose, J. B. (2020). SARS-CoV-2 in wastewater: State of the

knowledge and research needs. *Science of The Total Environment*, *739*, 139076. https://doi.org/10.1016/j.scitotenv.2020.139076

Kleinbach, E. M., Beckman, W. A., & Klein, S. A. (1993). Performance study of one-dimensional models for stratified thermal storage tanks. *Solar Energy*, *50*(2), 155–166. https://doi.org/10.1016/0038-092X(93)90087-5

Korzeniewska, E. (2011). Emission of bacteria and fungi in the air from wastewater treatment plants—A review. *Frontiers in Bioscience - Scholar*, *3 S*(2), 393–407. Scopus. https://doi.org/10.2741/s159

Korzeniewska, E., & Harnisz, M. (2013). Extended-spectrum beta-lactamase (ESBL)-positive Enterobacteriaceae in municipal sewage and their emission to the environment. *Journal of Environmental Management*, *128*, 904–911. AGRICOLA. https://doi.org/10.1016/j.jenvman.2013.06.051

Korzeniewska, E., Korzeniewska, A., & Harnisz, M. (2013). Antibiotic resistant Escherichia coli in hospital and municipal sewage and their emission to the environment. *Ecotoxicology and Environmental Safety*, *91*, 96–102. https://doi.org/10.1016/j.ecoenv.2013.01.014

Kuchta, J. M., States, S. J., McNamara, A. M., Wadowsky, R. M., & Yee, R. B. (1983). Susceptibility of Legionella pneumophila to chlorine in tap water. *Applied and Environmental Microbiology*, *46*(5), 1134–1139. https://doi.org/10.1128/AEM.46.5.1134-1139.1983

Kumar, M., Alamin, M., Kuroda, K., Dhangar, K., Hata, A., Yamaguchi, H., & Honda, R. (2021). Potential discharge, attenuation and exposure risk of SARS-CoV-2 in natural water bodies receiving treated wastewater. *Npj Clean Water*, *4*(1), Article 1. https://doi.org/10.1038/s41545-021-00098-2

LeChevallier, M. W., Mansfield, T. J., & Gibson, J. M. (2020). Protecting wastewater workers from disease risks: Personal protective equipment guidelines. *Water Environment Research: A Research Publication of the Water Environment Federation*, *92*(4), 524–533. https://doi.org/10.1002/wer.1249

LeChevallier, M. W., Shaw, N. E., Kaplan, L. A., & Bott, T. L. (1993). Development of a Rapid Assimilable Organic Carbon Method for Water. *Applied and Environmental Microbiology*, *59*(5), 1526–1531. https://doi.org/10.1128/AEM.59.5.1526-1531.1993

LeChevallier, M. W., Welch, N. J., & Smith, D. B. (1996). Full-scale studies of factors related to coliform regrowth in drinking water. *Applied and Environmental Microbiology*, *62*(7), 2201–2211. https://doi.org/10.1128/AEM.62.7.2201-2211.1996

Lee, J. A., Thorne, P. S., Reynolds, S. J., & O'Shaughnessy, P. T. (2007). Monitoring Risks in Association With Exposure Levels Among Wastewater Treatment Plant Workers. *Journal of Occupational and Environmental Medicine*, *49*(11), 1235–1248.

Leonard, A. F. C., Yin, X. L., Zhang, T., Hui, M., & Gaze, W. H. (2018). A coliform-targeted metagenomic method facilitating human exposure estimates to Escherichia coli-borne antibiotic resistance genes. *FEMS Microbiology Ecology*, *94*(3). https://doi.org/10.1093/femsec/fiy024

Leonard, A. F. C., Zhang, L., Balfour, A. J., Garside, R., & Gaze, W. H. (2015). Human recreational exposure to antibiotic resistant bacteria in coastal bathing waters. *Environment International*, *82*, 92–100. Scopus. https://doi.org/10.1016/j.envint.2015.02.013

Leonard, A. F. C., Zhang, L., Balfour, A. J., Garside, R., Hawkey, P. M., Murray, A. K., Ukoumunne, O. C., & Gaze, W. H. (2018). Exposure to and colonisation by antibiotic-resistant E. coli in UK coastal water users: Environmental surveillance, exposure assessment, and epidemiological study (Beach Bum Survey). *Environment International*, *114*, 326–333. https://doi.org/10.1016/j.envint.2017.11.003

Lévesque, B., Lavoie, M., & Joly, J. (2004). Residential Water Heater Temperature: 49 or 60 Degrees Celsius? *Canadian Journal of Infectious Diseases*, *15*(1), 11–12. https://doi.org/10.1155/2004/109051

Ley, C. J., Proctor, C. R., Jordan, K., Ra, K., Noh, Y., Odimayomi, T., Julien, R., Kropp, I., Mitchell, J., Nejadhashemi, A. P., Whelton, A. J., & Aw, T. G. (2020). Impacts of Municipal Water–Rainwater Source Transitions on Microbial and Chemical Water Quality Dynamics at the Tap. *Environmental Science & Technology*, *54*(18), 11453–11463. https://doi.org/10.1021/acs.est.0c03641

Li, Y., Yang, L., Song, H., Ba, Y., Li, L., Hong, Q., & Wang, Y. (2022). The changing pattern of bioaerosol characteristics, source and risk under diversity brush aerator speed. *Ecotoxicology and Environmental Safety*, *236*. Scopus. https://doi.org/10.1016/j.ecoenv.2022.113478

Lin, Y. E., Vidic, R. D., Stout, J. E., & Yu, V. L. (1998). Legionella in water distribution systems. *Journal AWWA*, *90*(9), 112–122. https://doi.org/10.1002/j.1551-8833.1998.tb08503.x

Lindsley, W. G., Blachere, F. M., Law, B. F., Beezhold, D. H., & Noti, J. D. (2021). Efficacy of face masks, neck gaiters and face shields for reducing the expulsion of simulated cough-generated aerosols. *Aerosol Science and Technology : The Journal of the American Association for Aerosol Research*, *55*(4), 449–457. https://doi.org/10.1080/02786826.2020.1862409

Liu, Z., Stout, J. E., Boldin, M., Rugh, J., Diven, W. F., & Yu, V. L. (1998). Intermittent Use of Copper-Silver Ionization for Legionella Control in Water Distribution Systems: A Potential Option in Buildings Housing Individuals at Low Risk of Infection. *Clinical Infectious Diseases*, *26*(1), 138–140. https://doi.org/10.1086/516283

Liu, Z., Stout, J., Tedesco, L., Boldin, M., Hwang, C., & Lu, V. (1995). Efficacy of ultraviolet light in preventing Legionella colonization of a hospital water distribution system. *Water Research*, *29*(10), 2275–2280. https://doi.org/10.1016/0043-1354(95)00048-P

Lock, K., Millett, C., Heathcock, R., Joseph, C. A., Harrison, T. G., Lee, J. V., Rao, G., Surman-Lee, S., & on behalf of the Outbreak Control Team. (2008). Public health and economic costs of investigating a suspected outbreak of Legionnaires' disease. *Epidemiology and Infection*, *136*(10), 1306–1314. https://doi.org/10.1017/S0950268807000076

Lopatkin, A. J., Huang, S., Smith, R. P., Srimani, J. K., Sysoeva, T. A., Bewick, S., Karig, D. K., & You, L. (2016). Antibiotics as a selective driver for conjugation dynamics. *Nature Microbiology*, *1*(6), 16044. https://doi.org/10.1038/nmicrobiol.2016.44

Lopatkin, A. J., Meredith, H. R., Srimani, J. K., Pfeiffer, C., Durrett, R., & You, L. (2017). Persistence and reversal of plasmid-mediated antibiotic resistance. *Nature Communications*, *8*(1), 1689. https://doi.org/10.1038/s41467-017-01532-1

Lopatkin, A. J., Sysoeva, T. A., & You, L. (2016). Dissecting the effects of antibiotics on horizontal gene transfer: Analysis suggests a critical role of selection dynamics. *BioEssays*, *38*(12), 1283–1292. https://doi.org/10.1002/bies.201600133

Lowell, G., Quinlan, K., & Gottlieb, L. J. (2008). Preventing Unintentional Scald Burns: Moving Beyond Tap Water. *PEDIATRICS*, *122*(4), 799–804. https://doi.org/10.1542/peds.2007-2979

Lu, R., Frederiksen, M. W., Uhrbrand, K., Li, Y., Østergaard, C., & Madsen, A. M. (2020). Wastewater treatment plant workers' exposure and methods for risk evaluation of their exposure. *Ecotoxicology and Environmental Safety*, *205*. Scopus. https://doi.org/10.1016/j.ecoenv.2020.111365

Lunestad, B. T., Frantzen, S., Svanevik, C. S., Roiha, I. S., & Duinker, A. (2016). Time trends in the prevalence of Escherichia coli and enterococci in bivalves harvested in Norway during 2007–2012. *Food Control*, *60*, 289–295. https://doi.org/10.1016/j.foodcont.2015.08.001

Ma, J., An, D., Cui, B., Liu, M., Zhu, H., Li, M., Ai, X., Ali, W., & Yan, C. (2022). What are the disease burden and its sensitivity analysis of workers exposing to Staphylococcus aureus bioaerosol during warm and cold periods in a wastewater treatment plant? *Environmental Science and Pollution Research*. https://doi.org/10.1007/s11356-022-21447-9

Maal-Bared, R. (2023). Protecting Wastewater Workers by Categorizing Risks of Pathogen Exposures by Splash and Fecal-Oral Transmission during Routine Tasks. *Waste*, *1*(1), Article 1. https://doi.org/10.3390/waste1010007

Malakahmad, A., Downe, A. G., & Fadzil, S. D. M. (2012). Application of occupational health and safety management system at sewage treatment plants. *2012 IEEE Business, Engineering & Industrial Applications Colloquium (BEIAC)*, 347–350. https://doi.org/10.1109/BEIAC.2012.6226080

Mara, D. (2009). Waste stabilization ponds: Past, present and future. *Desalination and Water Treatment*, *4*(1–3), 85–88. https://doi.org/10.5004/dwt.2009.359

Martin, N. A., & Falder, S. (2017). A review of the evidence for threshold of burn injury. *Burns*, *43*(8), 1624–1639. https://doi.org/10.1016/j.burns.2017.04.003

Masclaux, F. G., Hotz, P., Gashi, D., Savova-Bianchi, D., & Oppliger, A. (2014). Assessment of airborne virus contamination in wastewater treatment plants. *Environmental Research*, *133*, 260–265. Scopus. https://doi.org/10.1016/j.envres.2014.06.002

Matsubara, K., & Katayama, H. (2019). Development of a Portable Detection Method for Enteric Viruses from Ambient Air and Its Application to a Wastewater Treatment Plant. *Pathogens*, *8*(3), Article 3. https://doi.org/10.3390/pathogens8030131

Matthews, B., Stratton, H., Schreoder, & Toze, S. (2010). *Pathogen Detection Methodologies for Wastewater and Reservoirs*. Urban Water Security Research Alliance Technical Report No. 32.

Mbanga, J., Abia, A. L. K., Amoako, D. G., & Essack, Sabiha. Y. (2020). Quantitative microbial risk assessment for waterborne pathogens in a wastewater treatment plant and its receiving surface water body. *BMC Microbiology*, *20*, 346. https://doi.org/10.1186/s12866-020-02036-7

McBride, G. (2014). Norovirus dose-response in sewage-related QMRA: The importance of virus aggregation. *International Congress on Environmental Modelling and Software*. https://scholarsarchive.byu.edu/iemssconference/2014/Stream-H/69

Medema, G., Wullings, B., Roeleveld, P., & van der Kooij, D. (2004). Risk assessment of Legionella and enteric pathogens in sewage treatment works. *Water Supply*, *4*(2), 125–132. https://doi.org/10.2166/ws.2004.0037

Medina, M., & Castillo-Pino, E. (2019). An introduction to the epidemiology and burden of urinary tract infections. *Therapeutic Advances in Urology*, *11*, 1756287219832172. https://doi.org/10.1177/1756287219832172

Messner, M. J., Chappell, C. L., & Okhuysen, P. C. (2001). Risk assessment for Cryptosporidium: A hierarchical Bayesian analysis of human dose response data. *Water Research*, *35*(16), 3934–3940. https://doi.org/10.1016/s0043-1354(01)00119-1

Mishra, S., Klümper, U., Voolaid, V., Berendonk, T. U., & Kneis, D. (2021). Simultaneous estimation of parameters governing the vertical and horizontal transfer of antibiotic resistance genes. *Science of The Total Environment*, *798*, 149174. https://doi.org/10.1016/j.scitotenv.2021.149174

Monteiro, L., Figueiredo, D., Dias, S., Freitas, R., Covas, D., Menaia, J., & Coelho, S. T. (2014). Modeling of Chlorine Decay in Drinking Water Supply Systems Using EPANET MSX. *Procedia Engineering*, *70*, 1192–1200. https://doi.org/10.1016/j.proeng.2014.02.132

Moralez, J., Szenkiel, K., Hamilton, K., Pruden, A., & Lopatkin, A. J. (2021). Quantitative analysis of horizontal gene transfer in complex systems. *Current Opinion in Microbiology*, *62*, 103–109. https://doi.org/10.1016/j.mib.2021.05.001

Moritz, A. R., & Henriques, F. C. (1947). Studies of Thermal Injury: II. The Relative Importance of Time and Surface Temperature in the Causation of Cutaneous Burns. *The American Journal of Pathology*, *23*(5), 695–720.

Moubarz, G., Saad-Hussein, A., & Elfiky, A. M. (2022). 16S rRNA gene identification of airborne pathogenic bacteria isolated from bioaerosols of wastewater treatment plant. *Egyptian Pharmaceutical Journal*, *21*(2), 214–222. Scopus. https://doi.org/10.4103/epj.epj_27_22

Muller, D., Edwards, M. L., & Smith, D. W. (1983a). Changes in Iron and Transferrin Levels and Body Temperature in Experimental Airborne Legionellosis. *The Journal of Infectious Diseases*, *147*(2), 302–307.

Muller, D., Edwards, M. L., & Smith, D. W. (1983b). Changes in Iron and Transferrin Levels and Body Temperature in Experimental Airborne Legionellosis. *The Journal of Infectious Diseases*, *147*(2), 302–307. https://doi-org.ezproxy1.lib.asu.edu/10.1093/infdis/147.2.302

Murray, C. J., Ikuta, K. S., Sharara, F., Swetschinski, L., Aguilar, G. R., Gray, A., Han, C., Bisignano, C., Rao, P., Wool, E., Johnson, S. C., Browne, A. J., Chipeta, M. G., Fell, F., Hackett, S., Haines-Woodhouse, G., Hamadani, B. H. K., Kumaran, E. A. P., McManigal, B., … Naghavi, M. (2022). Global burden of bacterial antimicrobial resistance in 2019: A systematic analysis. *The Lancet*, *399*(10325), 629–655. https://doi.org/10.1016/S0140-6736(21)02724-0

Nappier, S. P., Liguori, K., Ichida, A. M., Stewart, J. R., & Jones, K. R. (2020). Antibiotic Resistance in Recreational Waters: State of the Science. *International Journal of Environmental Research and Public Health*, *17*(21), 8034. https://doi.org/10.3390/ijerph17218034

NASEM. (2006). *Drinking Water Distribution Systems: Assessing and Reducing Risks*. National Academies Press. https://doi.org/10.17226/11728

NASEM. (2019). *Management of Legionella in Water Systems*. National Academies Press. https://doi.org/10.17226/25474

Nguyen, C., Elfland, C., & Edwards, M. (2012). Impact of advanced water conservation features and new copper pipe on rapid chloramine decay and microbial regrowth. *Water Research*, *46*(3), 611–621. https://doi.org/10.1016/j.watres.2011.11.006

Nguyen Quoc, B., Saingam, P., RedCorn, R., Carter, J. A., Jain, T., Candry, P., Gattuso, M., Huang, M.-L. W., Greninger, A. L., Meschke, J. S., Bryan, A., & Winkler, M. K. H. (2022). Case Study: Impact of Diurnal Variations and Stormwater Dilution on SARS-CoV-2 RNA Signal Intensity at Neighborhood Scale Wastewater Pumping Stations. *ACS ES&T Water*, acsestwater.2c00016. https://doi.org/10.1021/acsestwater.2c00016

Nguyen, T.-H.-Y., Bertin, M., Bodin, J., Fouquet, N., Bonvallot, N., & Roquelaure, Y. (2018). Multiple Exposures and Coexposures to Occupational Hazards Among Agricultural Workers: A Systematic Review of Observational Studies. *Safety and Health at Work*, *9*(3), 239–248. https://doi.org/10.1016/j.shaw.2018.04.002

Njage, P. M. K., & Buys, E. M. (2015). Pathogenic and commensal *E scherichia coli* from irrigation water show potential in transmission of extended spectrum and AmpC β-lactamases determinants to isolates from lettuce: ESBL and AmpC *E. coli* : irrigation water to lettuce. *Microbial Biotechnology*, *8*(3), 462–473. https://doi.org/10.1111/1751-7915.12234

Njage, P. M. K., & Buys, E. M. (2017). Quantitative assessment of human exposure to extended spectrum and AmpC β-lactamases bearing E. coli in lettuce attributable to irrigation water and subsequent horizontal gene transfer. *International Journal of Food Microbiology*, *240*, 141–151. https://doi.org/10.1016/j.ijfoodmicro.2016.10.011

Ochman, H., Lawrence, J. G., & Groisman, E. A. (2000). *Lateral gene transfer and the nature of bacterial innovation*. *405*, 8.

O'Flaherty, E., Cummins, E., De Giusti, M., Pantanella, F., & Solimini, A. G. (2019). Human exposure to antibiotic resistant-Escherichia coli through irrigated lettuce. *Environment International*, *122*, 270–280. AGRICOLA. https://doi.org/10.1016/j.envint.2018.11.022

O'Flaherty, E., Solimini, A., Pantanella, F., & Cummins, E. (2019). The potential human exposure to antibiotic resistant-Escherichia coli through recreational water. *The Science of the Total Environment*, *650*(Pt 1), 786–795. https://doi.org/10.1016/j.scitotenv.2018.09.018

Olsson, C., Oreman, J., Lindmark, R., Tsykalova, A., Bachar, S., Dobro, S., & Bell, M. (2021). *The microCOVID Project*. https://www.microcovid.org/paper/1-intro#authors

O'Neill, J. (2016). *Tackling drug-resistant infections globally: Final report and recommendations* (pp. 1–81). https://amr-review.org/sites/default/files/160518_Final paper_with cover.pdf

O'Toole, J., Keywood, M., Sinclair, M., & Leder, K. (2009). Risk in the mist? Deriving data to quantify microbial health risks associated with aerosol generation by water-efficient devices during typical domestic water-using activities. *Water Science and Technology*, *60*(11), 2913–2920. https://doi.org/10.2166/wst.2009.722

O'Toole, J., Leder, K., & Sinclair, M. (2008). A Series of Exposure Experiments−recycled Water and Alternative Water Sources. Part A. Aerosolsizing and Endotoxin Experiments. *CRC for Water Quality and Treatment: Adelaide, Australia*.

Papagianeli, S. D., Aspridou, Z., Didos, S., Chochlakis, D., Psaroulaki, A., & Koutsoumanis, K. (2021). Dynamic modelling of Legionella pneumophila thermal inactivation in water. *Water Research*, *190*, 116743. https://doi.org/10.1016/j.watres.2020.116743

Paranjape, K., Bédard, É., Whyte, L. G., Ronholm, J., Prévost, M., & Faucher, S. P. (2020). Presence of Legionella spp. in cooling towers: The role of microbial diversity, Pseudomonas, and continuous chlorine application. *Water Research*, *169*, 115252. https://doi.org/10.1016/j.watres.2019.115252

Parhizkar, H., Van Den Wymelenberg, K. G., Haas, C. N., & Corsi, R. L. (2021). A Quantitative Risk Estimation Platform for Indoor Aerosol Transmission of COVID-19. *Risk Analysis*, *n/a*(n/a). https://doi.org/10.1111/risa.13844

Parr, A., Whitney, E. A., & Berkelman, R. L. (2015). Legionellosis on the Rise: A Review of Guidelines for Prevention in the United States. *Journal of Public Health Management and Practice*, *21*(5), E17–E26. https://doi.org/10.1097/PHH.0000000000000123

Paszke, A., Gross, S., Massa, F., Lerer, A., Bradbury, J., Chanan, G., Killeen, T., Lin, Z., Gimelshein, N., Antiga, L., Desmaison, A., Kopf, A., Yang, E., DeVito, Z., Raison, M., Tejani, A., Chilamkurthy, S., Steiner, B., Fang, L., … Chintala, S.

(2019). *PyTorch: An Imperative Style, High-Performance Deep Learning Library*. 12.

Payment, P., & Morin, E. (1990). Minimal infective dose of the OSU strain of porcine rotavirus. *Archives of Virology*, *112*(3–4), 277–282. https://doi.org/10.1007/bf01323172

Peck, M., Chang Brewer, A., Pressman, M., Blank, E., & Mickalide, A. (2010). Hot Tap Water Legislation in the United States: *Journal of Burn Care & Research*, *31*(6), 918–925. https://doi.org/10.1097/BCR.0b013e3181f93723

Petersen, F., & Hubbart, J. A. (2020). Physical Factors Impacting the Survival and Occurrence of Escherichia coli in Secondary Habitats. *Water*, *12*(6), 1796. https://doi.org/10.3390/w12061796

Picozzi, S. C. M., Casellato, S., Rossini, M., Paola, G., Tejada, M., Costa, E., & Carmignani, L. (2014). Extended-spectrum beta-lactamase-positive Escherichia coli causing complicated upper urinary tract infection: Urologist should act in time. *Urology Annals*, *6*(2), 107–112. https://doi.org/10.4103/0974-7796.130536

Pitol, A. K., & Julian, T. R. (2021). Community Transmission of SARS-CoV-2 by Surfaces: Risks and Risk Reduction Strategies. *Environmental Science & Technology Letters*, *8*(3), 263–269. https://doi.org/10.1021/acs.estlett.0c00966

Pitol, A. K., Kohn, T., & Julian, T. R. (2020). Retention of E. coli and water on the skin after liquid contact. *PLOS ONE*, *15*(9), e0238998. https://doi.org/10.1371/journal.pone.0238998

Potter, M. D. E., Maitz, P. K. M., Kennedy, P. J., & Goltsman, D. (2017). Perineal tap water burns in the elderly: At what cost?: Perineal tapster burns in the elderly. *ANZ Journal of Surgery*, *87*(11), E188–E192. https://doi.org/10.1111/ans.13439

Prasad, B., Hamilton, K. A., & Haas, C. N. (2017). Incorporating Time-Dose-Response into Legionella Outbreak Models. *Risk Analysis*, *37*(2), 291–304. https://doi.org/10.1111/risa.12630

Proctor, C. R. (2014). *Effect of Various Water Chemistry Factors on Legionella Proliferation and the Premise Plumbing Microbiome Composition*. Virginia Tech.

Proctor, C. R., Dai, D., Edwards, M. A., & Pruden, A. (2017). Interactive effects of temperature, organic carbon, and pipe material on microbiota composition and

Legionella pneumophila in hot water plumbing systems. *Microbiome*, *5*(1), 130. https://doi.org/10.1186/s40168-017-0348-5

Pruden, A., Alcalde, R. E., Alvarez, P. J. J., Ashbolt, N., Bischel, H., Capiro, N. L., Crossette, E., Frigon, D., Grimes, K., Haas, C. N., Ikuma, K., Kappell, A., LaPara, T., Kimbell, L., Li, M., Li, X., McNamara, P., Seo, Y., Sobsey, M. D., … Zhou, Z. (2018). An Environmental Science and Engineering Framework for Combating Antimicrobial Resistance. *Environmental Engineering Science*, *35*(10), 1005–1011. https://doi.org/10.1089/ees.2017.0520

Pujol, J. M., Eisenberg, J. E., Haas, C. N., & Koopman, J. S. (2009). The Effect of Ongoing Exposure Dynamics in Dose Response Relationships. *PLoS Computational Biology*, *5*, e1000399. https://doi.org/10.1371/journal.pcbi.1000399

Randall, K., Ewing, E. T., Marr, L. C., Jimenez, J. L., & Bourouiba, L. (2021). How did we get here: What are droplets and aerosols and how far do they go? A historical perspective on the transmission of respiratory infectious diseases. *Interface Focus*, *11*(6), 20210049. https://doi.org/10.1098/rsfs.2021.0049

Ranney, M., & Goldberg, M. (2020). *MyCOVIDRisk*. Center for Digital Health | Medical School | Brown University. https://mycovidrisk.app/

Rao, S. S. C., Summers, R. W., Rao, G. R. S., Ramana, S., Devi, U., Zimmerman, B., & Pratap, B. C. V. (2006). Oral rehydration for viral gastroenteritis in adults: A randomized, controlled trial of 3 solutions. *JPEN. Journal of Parenteral and Enteral Nutrition*, *30*(5), 433–439. https://doi.org/10.1177/0148607106030005433

Rasheduzzaman, M., Singh, R., Haas, C. N., & Gurian, P. L. (2020). Required water temperature in hotel plumbing to control Legionella growth. *Water Research*, *182*, 115943. https://doi.org/10.1016/j.watres.2020.115943

Reiling, J., Hughes, R. G., & Murphy, M. R. (2008). Chapter 28. The Impact of Facility Design on Patient Safety. *Patient Safety*, *2*, 26.

Rendtorff, R. C. (1954). The experimental transmission of human intestinal protozoan parasites. II. Giardia lamblia cysts given in capsules. *American Journal of Hygiene*, *59*(2), 209–220. https://doi.org/10.1093/oxfordjournals.aje.a119634

Rhoads, W. J., & Hammes, F. (2021a). Growth of *Legionella* during COVID-19 lockdown stagnation. *Environmental Science: Water Research & Technology*, *7*(1), 10–15. https://doi.org/10.1039/D0EW00819B

Rhoads, W. J., & Hammes, F. (2021b). Growth of Legionella during COVID-19 lockdown stagnation. *Environmental Science: Water Research & Technology*, *7*(1), 10–15. https://doi.org/10.1039/D0EW00819B

Rhoads, W. J., Ji, P., Pruden, A., & Edwards, M. A. (2015a). Water heater temperature set point and water use patterns influence Legionella pneumophila and associated microorganisms at the tap. *Microbiome*, *3*(1). https://doi.org/10.1186/s40168-015-0134-1

Rhoads, W. J., Ji, P., Pruden, A., & Edwards, M. A. (2015b). Water heater temperature set point and water use patterns influence Legionella pneumophila and associated microorganisms at the tap. *Microbiome*, *3*(1), 67. https://doi.org/10.1186/s40168-015-0134-1

Rhoads, W. J., Pruden, A., & Edwards, M. K. (2017). Interactive Effects of Corrosion, Copper, and Chloramines on Legionella and Mycobacteria in Hot Water Plumbing. *Environmental Science & Technology*, *51*(12), 7065–7075. https://doi.org/10.1021/acs.est.6b05616

Rhoads, W., Pruden, A., & Edwards, M. (2016). Convective Mixing in Distal Pipes Exacerbates Legionella pneumophila Growth in Hot Water Plumbing. *Pathogens*, *5*(1), 29. https://doi.org/10.3390/pathogens5010029

Rice, E. W., Wang, P., Smith, A. L., & Stadler, L. B. (2020). Determining Hosts of Antibiotic Resistance Genes: A Review of Methodological Advances. *Environmental Science & Technology Letters*, *7*(5), 282–291. https://doi.org/10.1021/acs.estlett.0c00202

Rice, J., Wutich, A., & Westerhoff, P. (2013). Assessment of De Facto Wastewater Reuse across the U.S.: Trends between 1980 and 2008. *Environmental Science & Technology*, *47*(19), 11099–11105. https://doi.org/10.1021/es402792s

Richard, R., Hamilton, K. A., Westerhoff, P., & Boyer, T. H. (2020). Tracking copper, chlorine, and occupancy in a new, multi-story, institutional green building. *Environmental Science: Water Research & Technology*, *6*(6), 1672–1680. https://doi.org/10.1039/D0EW00105H

Riediker, M., Briceno-Ayala, L., Ichihara, G., Albani, D., Poffet, D., Tsai, D.-H., Iff, S., & Monn, C. (2022). Higher viral load and infectivity increase risk of aerosol transmission for Delta and Omicron variants of SARS-CoV-2. *Swiss Medical Weekly*, *1*. https://doi.org/10.4414/smw.2022.w30133

Robinson, L. A., & Hammitt, J. K. (2016). Valuing Reductions in Fatal Illness Risks: Implications of Recent Research: Valuing Reductions in Fatal Illness Risks. *Health Economics*, *25*(8), 1039–1052. https://doi.org/10.1002/hec.3214

Robinson, L. A., Hammitt, J. K., Cecchini, M., Chalkidou, K., Claxton, K., Eozenou, P. H.-V., de Ferranti, D., Deolalikar, A. B., Guanais, F., Jamison, D. T., Kwon, S., Lauer, J. A., O'Keeffe, L., Walker, D., Wilkinson, T., Wilson, D., & Wong, B. (2019). *Reference Case Guidelines for Benefit-Cost Analysis in Global Health and Development* (p. 126). Bill & Melinda Gates Foundation.

Rocha-Melogno, L., Crank, K., Bibby, K., Gray, G., & Deshusses, M. (2021). *Aerosol-Mediated Infectious Disease Risk Assessments (AMIDRA)*. https://rapidqmra.shinyapps.io/Rapid_QMRA/

Rodríguez-Molina, D., Berglund, F., Blaak, H., Flach, C.-F., Kemper, M., Marutescu, L., Gradisteanu, G. P., Popa, M., Spießberger, B., Weinmann, T., Wengenroth, L., Chifiriuc, M. C., Larsson, D. G. J., Nowak, D., Radon, K., de Roda Husman, A. M., Wieser, A., & Schmitt, H. (2021). Carriage of ESBL-producing Enterobacterales in wastewater treatment plant workers and surrounding residents—The AWARE Study. *European Journal of Clinical Microbiology & Infectious Diseases*. https://doi.org/10.1007/s10096-021-04387-z

Rosa, G. L., Mancini, P., Veneri, C., Ferraro, G. B., Lucentini, L., Iaconelli, M., & Suffredini, E. (2022). *Detection of Monkeypox virus DNA in the wastewater of an airport in Rome, Italy: Expanding environmental surveillance to emerging threats* (p. 2022.08.18.22278932). medRxiv. https://doi.org/10.1101/2022.08.18.22278932

Rousham Emily K., Asaduzzaman Muhammad, Mozmader T.I.M. Amin Uddin, Amin Mohammed Badrul, Rahman Mahdia, Hossain Muhammed Iqbal, Islam Md. Rayhanul, Mahmud Zahid Hayat, Unicomb Leanne, & Islam Mohammad Aminul. (n.d.). Human Colonization with Extended-Spectrum Beta-Lactamase-Producing E. coli in Relation to Animal and Environmental Exposures in Bangladesh: An Observational One Health Study. *Environmental Health Perspectives*, *129*(3), 037001. https://doi.org/10.1289/EHP7670

Ruppé, E., Lixandru, B., Cojocaru, R., Büke, Ç., Paramythiotou, E., Angebault, C., Visseaux, C., Djuikoue, I., Erdem, E., Burduniuc, O., El Mniai, A., Marcel, C., Perrier, M., Kesteman, T., Clermont, O., Denamur, E., Armand-Lefèvre, L., & Andremont, A. (2013). Relative Fecal Abundance of Extended-Spectrum-β-Lactamase-Producing Escherichia coli Strains and Their Occurrence in Urinary Tract Infections in Women. *Antimicrobial Agents and Chemotherapy*, *57*(9), 4512–4517. https://doi.org/10.1128/AAC.00238-13

Saetta, D., Richard, R., Leyva, C., Westerhoff, P., & Boyer, T. H. (2021). Data-mining methods predict chlorine residuals in premise plumbing using low-cost sensors. *AWWA Water Science*, *3*(1), e1214. https://doi.org/10.1002/aws2.1214

Salehi, M., Abouali, M., Wang, M., Zhou, Z., Nejadhashemi, A. P., Mitchell, J., Caskey, S., & Whelton, A. J. (2018). Case study: Fixture water use and drinking water quality in a new residential green building. *Chemosphere*, *195*, 80–89. https://doi.org/10.1016/j.chemosphere.2017.11.070

Saliu, E.-M., Zentek, J., & Vahjen, W. (2020). In vitro conjugation kinetics of AmpC, broad spectrum and extended-spectrum beta-lactamase-producing Escherichia coli donors and various Enterobacteriaceae recipients. *BMC Microbiology*, *20*(1), 133. https://doi.org/10.1186/s12866-020-01787-7

Sarowska, J., Futoma-Koloch, B., Jama-Kmiecik, A., Frej-Madrzak, M., Ksiazczyk, M., Bugla-Ploskonska, G., & Choroszy-Krol, I. (2019). Virulence factors, prevalence and potential transmission of extraintestinal pathogenic Escherichia coli isolated from different sources: Recent reports. *Gut Pathogens*, *11*, 10. https://doi.org/10.1186/s13099-019-0290-0

Schijven, J. F., Blaak, H., Schets, F. M., & De Roda Husman, A. M. (2015). Fate of Extended-Spectrum β-Lactamase-Producing Escherichia coli from Faecal Sources in Surface Water and Probability of Human Exposure through Swimming. *Environmental Science and Technology*, *49*(19), 11825–11833. https://doi.org/10.1021/acs.est.5b01888

Schijven, J., Vermeulen Lucie C., Swart Arno, Meijer Adam, Duizer Erwin, & de Roda Husman Ana Maria. (2021). Quantitative Microbial Risk Assessment for Airborne Transmission of SARS-CoV-2 via Breathing, Speaking, Singing, Coughing, and Sneezing. *Environmental Health Perspectives*, *129*(4), 047002. https://doi.org/10.1289/EHP7886

Schoen, M. E., & Ashbolt, N. J. (2011a). An in-premise model for Legionella exposure during showering events. *Water Research*, *45*(18), 5826–5836. https://doi.org/10.1016/j.watres.2011.08.031

Schoen, M. E., & Ashbolt, N. J. (2011b). An in-premise model for Legionella exposure during showering events. *Water Research*, *45*(18), 5826–5836. https://doi.org/10.1016/j.watres.2011.08.031

Schoen, M. E., Jahne, M. A., Garland, J., Ramirez, L., Lopatkin, A. J., & Hamilton, K. A. (2021). Quantitative Microbial Risk Assessment of Antimicrobial Resistant and Susceptible Staphylococcus aureus in Reclaimed Wastewaters. *Environmental Science & Technology*. https://doi.org/10.1021/acs.est.1c04038

Scruggs, M. (2020). *How to select a commercial water heater*. Consulting - Specifying Engineer. https://www.csemag.com/articles/how-to-select-a-commercial-water-heater/

Sender, R., Bar-On, Y. M., Gleizer, S., Bernshtein, B., Flamholz, A., Phillips, R., & Milo, R. (2021). The total number and mass of SARS-CoV-2 virions. *Proceedings of the National Academy of Sciences*, *118*(25), e2024815118. https://doi.org/10.1073/pnas.2024815118

Shaheen, M., Scott, C., & Ashbolt, N. J. (2019). Long-term persistence of infectious Legionella with free-living amoebae in drinking water biofilms. *International Journal of Hygiene and Environmental Health*, *222*(4), 678–686. https://doi.org/10.1016/j.ijheh.2019.04.007

Sharaby, Y., Rodríguez-Martínez, S., Oks, O., Pecellin, M., Mizrahi, H., Peretz, A., Brettar, I., Höfle, M. G., & Halpern, M. (2017). Temperature-Dependent Growth Modeling of Environmental and Clinical Legionella pneumophila Multilocus Variable-Number Tandem-Repeat Analysis (MLVA) Genotypes. *Applied and Environmental Microbiology*, *83*(8), e03295-16, /aem/83/8/e03295-16.atom. https://doi.org/10.1128/AEM.03295-16

Shields, W. C., McDonald, E., Frattaroli, S., Perry, E. C., Zhu, J., & Gielen, A. C. (2013). Still Too Hot: Examination of Water Temperature and Water Heater Characteristics 24 Years After Manufacturers Adopt Voluntary Temperature Setting. *Journal of Burn Care & Research*, *34*(2), 281–287. https://doi.org/10.1097/BCR.0b013e31827e645f

Silverman, A. I., & Boehm, A. B. (2020). Systematic Review and Meta-Analysis of the Persistence and Disinfection of Human Coronaviruses and Their Viral Surrogates

in Water and Wastewater. *Environmental Science & Technology Letters*, *7*(8), 544–553. https://doi.org/10.1021/acs.estlett.0c00313

Simonsen, L., Gordon, D. M., Stewart, F. M., & Levin, B. R. Y. 1990. (n.d.). Estimating the rate of plasmid transfer: An end-point method. *Microbiology*, *136*(11), 2319–2325. https://doi.org/10.1099/00221287-136-11-2319

Sinclair, R. G., Choi, C. Y., Riley, M. R., & Gerba, C. P. (2008). Pathogen Surveillance Through Monitoring of Sewer Systems. In *Advances in Applied Microbiology* (Vol. 65, pp. 249–269). Elsevier. https://doi.org/10.1016/S0065-2164(08)00609-6

Singh, R., Hamilton, K. A., Rasheduzzaman, M., Yang, Z., Kar, S., Fasnacht, A., Masters, S. V., & Gurian, P. L. (2020). Managing Water Quality in Premise Plumbing: Subject Matter Experts' Perspectives and a Systematic Review of Guidance Documents. *Water*, *12*(2), 347. https://doi.org/10.3390/w12020347

Smit, L. A. M., Spaan, S., & Heederik, D. (2005). Endotoxin exposure and symptoms in wastewater treatment workers. *American Journal of Industrial Medicine*, *48*(1), 30–39. https://doi.org/10.1002/ajim.20176

Sobsey, M. D. (2021). Absence of virological and epidemiological evidence that SARS-CoV-2 poses COVID-19 risks from environmental fecal waste, wastewater and water exposures. *Journal of Water and Health*, *20*(1), 126–138. https://doi.org/10.2166/wh.2021.182

Søraas, A., Sundsfjord, A., Sandven, I., Brunborg, C., & Jenum, P. A. (2013). Risk Factors for Community-Acquired Urinary Tract Infections Caused by ESBL-Producing Enterobacteriaceae –A Case–Control Study in a Low Prevalence Country. *PLOS ONE*, *8*(7), e69581. https://doi.org/10.1371/journal.pone.0069581

Stadler, T., Meinel, D., Aguilar-Bultet, L., Huisman, J. S., Schindler, R., Egli, A., Seth-Smith, H. M. B., Eichenberger, L., Brodmann, P., Hubner, P., Bagutti, C., & Tschudin-Sutter, S. (2018). Transmission of ESBL-producing Enterobacteriaceae and their mobile genetic elements-identification of sources by whole genome sequencing: Study protocol for an observational study in Switzerland. *BMJ OPEN*, *8*(2). https://doi.org/10.1136/bmjopen-2018-021823

Stalder, T., & Top, E. (2016). Plasmid transfer in biofilms: A perspective on limitations and opportunities. *Npj Biofilms and Microbiomes*, *2*(1), 1–5. https://doi.org/10.1038/npjbiofilms.2016.22

Stamm, W. E., & Hooton, T. M. (1993). Management of urinary tract infections in adults. *The New England Journal of Medicine*, *329*(18), 1328–1334. https://doi.org/10.1056/NEJM199310283291808

Staszowska, A. (2022). Microbiological Quality of Indoor and Outdoor Air in a Municipal Wastewater Treatment Plant – A Case Study. *Journal of Ecological Engineering*, *23*(2), 185–190. Scopus. https://doi.org/10.12911/22998993/145202

Statistics Canada. (2016). *Canada's Core Public Infrastructure Survey: Wastewater and Solid Waste Assets.* https://www.infrastructure.gc.ca/plan/ccpi-ipec-eng.html

Stevenson, K., McVey, A. F., Clark, I. B. N., Swain, P. S., & Pilizota, T. (2016). General calibration of microbial growth in microplate readers. *Scientific Reports*, *6*(1), Article 1. https://doi.org/10.1038/srep38828

Stobnicka-Kupiec, A., Gołofit-Szymczak, M., Cyprowski, M., & Górny, R. L. (2022). Detection and identification of potentially infectious gastrointestinal and respiratory viruses at workplaces of wastewater treatment plants with viability qPCR/RT-qPCR. *Scientific Reports*, *12*(1), 4517. https://doi.org/10.1038/s41598-022-08452-1

Stone, M., Ahmed, J., & Evans, J. (2000). The continuing risk of domestic hot water scalds to the elderly. *Burns*, *26*(4), 347–350. https://doi.org/10.1016/S0305-4179(99)00144-8

Stone, W., Louw, T. M., Gakingo, G. K., Nieuwoudt, M. J., & Booysen, M. J. (2019). A potential source of undiagnosed Legionellosis: Legionella growth in domestic water heating systems in South Africa. *Energy for Sustainable Development*, *48*, 130–138. https://doi.org/10.1016/j.esd.2018.12.001

Sun, D., Jeannot, K., Xiao, Y., & Knapp, C. W. (2019). Editorial: Horizontal Gene Transfer Mediated Bacterial Antibiotic Resistance. *Frontiers in Microbiology*, *10*. https://doi.org/10.3389/fmicb.2019.01933

Sun, J., Zhu, A., Li, H., Zheng, K., Zhuang, Z., Chen, Z., Shi, Y., Zhang, Z., Chen, S., Liu, X., Dai, J., Li, X., Huang, S., Huang, X., Luo, L., Wen, L., Zhuo, J., Li, Y., Wang, Y., … Li, Y. (2020). Isolation of infectious SARS-CoV-2 from urine of a COVID-19 patient. *Emerging Microbes & Infections*, *9*(1), 991–993. https://doi.org/10.1080/22221751.2020.1760144

Sunger, N., & Haas, C. N. (2015). Quantitative Microbial Risk Assessment for Recreational Exposure to Water Bodies in Philadelphia. *Water Environment Research, 87*(3), 211–222. https://doi.org/10.2175/106143015X14212658613073

Sunger, N., Teske, S. S., Nappier, S., & Haas, C. N. (2012). Recreational use assessment of water-based activities, using time-lapse construction cameras. *Journal of Exposure Science & Environmental Epidemiology*, *22*(3), Article 3. https://doi.org/10.1038/jes.2012.4

Tacket, C. O., Sztein, M. B., Losonsky, G., Abe, A., Finlay, B. B., McNamara, B. P., Fantry, G. T., James, S. P., Nataro, J. P., Levine, M. M., & Donnenberg, M. S. (2000). Role of EspB in experimental human enteropathogenic Escherichia coli infection. *Infection and Immunity*, *68*(6), 3689–3695. https://doi.org/10.1128/IAI.68.6.3689-3695.2000

Tamanai-Shacoori, Z., Arturo, M., Pommepuy, M., Mamez, C., & Cormier, M. (1995). Conjugal transfer of natural plasmids between Escherichia coli strains in sterile environmental water. *Current Microbiology*, *30*(3), 155–160. Scopus. https://doi.org/10.1007/BF00296201

Tang, W., Chen, T., Slocum, Z., Lan, Y., Delmelle, E., Chen, D., Mittal, N., Rice-Boayue, J., Shukla, T., Lin, S., Akella, S., Schlueter, J., Munir, M., & Gibas, C. (2022). *A Web-based Spatial Decision Support System of Wastewater Surveillance for COVID-19 Monitoring: A Case Study of a University Campus* (p. 2021.12.29.21268516). https://doi.org/10.1101/2021.12.29.21268516

Tansawai, U., Walsh, T. R., & Niumsup, P. R. (2019). Extended spectrum ß-lactamase-producing Escherichia coli among backyard poultry farms, farmers, and environments in Thailand. *Poultry Science*, *98*(6), 2622–2631. https://doi.org/10.3382/ps/pez009

Teunis, P. F. M., Moe, C. L., Liu, P., E. Miller, S., Lindesmith, L., Baric, R. S., Le Pendu, J., & Calderon, R. L. (2008). Norwalk virus: How infectious is it? *Journal of Medical Virology*, *80*(8), 1468–1476. https://doi.org/10.1002/jmv.21237

Thomas, C. M., & Nielsen, K. M. (2005). Mechanisms of, and Barriers to, Horizontal Gene Transfer between Bacteria. *Nature Reviews Microbiology*, *3*(9), 711–721. https://doi.org/10.1038/nrmicro1234

Thomas, J. M. (2012). *The Risk to Human Health from Free-Living Amoebae Interaction with Legionella in Drinking and Recycled Water Systems*. University of New South Wales.

Tyagi, N., Gurian, P. L., & Kumar, A. (2021). Using QMRA to understand possible exposure risks of SARS-CoV-2 from the water environment. *Environmental Science and Pollution Research*. https://doi.org/10.1007/s11356-021-16188-0

Tyagi, N., & Kumar, A. (2020). Evaluation of recreational risks due to exposure of antibiotic-resistance bacteria from environmental water: A proposed framework. *Journal of Environmental Management*, 111626. https://doi.org/10.1016/j.jenvman.2020.111626

US Census Bureau. (n.d.). *National Population by Characteristics: 2010-2019*. The United States Census Bureau. Retrieved September 24, 2021, from https://www.census.gov/data/tables/time-series/demo/popest/2010s-national-detail.html

US Department of Health and Human Services. (2021). *Guidelines for Regulatory Impact Analysis Appendix D: Updating Value per Statistical Life (VSL) Estimates for Inflation and Changes in Real Income*. ASPE. https://aspe.hhs.gov/reports/updating-vsl-estimates

U.S. Energy Information Administration. (n.d.). *Electric Power Monthly*. U.S. Energy Information Administration. https://www.eia.gov/electricity/monthly/epm_table_grapher.php?t=epmt_5_6_a

US Environmental Protection Agency. (2011). *Exposure Factors Handbook: 2011 Edition* (EPA/600/R-090/052F; pp. 1–1466). c:%5CDocuments and Settings%5Cturner_j%5CDesktop%5CJT_Biblioscape_8_111003%5CJT_Bib8_111003%5Cattachments%5Cefh-complete.pdf

US EPA. (2015, November 30). *National Primary Drinking Water Regulations* [Overviews and Factsheets]. US EPA. https://www.epa.gov/ground-water-and-drinking-water/national-primary-drinking-water-regulations

US EPA, O. (2019, August 13). *Guidelines for Water Reuse* [Other Policies and Guidance]. https://www.epa.gov/waterreuse/guidelines-water-reuse

USEPA. (2011). *USEPA: Principles of design and operations of wastewater treatment pond systems for plant operators, engineers, and managers*. https://scholar.google.com/scholar_lookup?title=Principles%20of%20Design%20and%20Operations%20of%20Wastewater%20Treatment%20Pond%20Systems%20for%20Plant%20Operators%2C%20Engineers%2C%20and%20Managers&author=USEPA&publication_year=2011

USEPA. (2012). Recreational Water Quality Criteria. *Office of Water, U.S. Environmental Protection Agency, Washington, DC*, 69.

USEPA. (2019). *Recommended Human Health Recreational Ambient Water Quality Criteria or Swimming Advisories for Microcystins and Cylindrospermopsin* (EPA 822-R-19-001; p. 249). Office of Water.

USGS. (2021). *Per capita water use: How much water do you use at home?* [USGS Water Science School]. https://water.usgs.gov/edu/activity-percapita.php

Van Abel, N., Schoen, M. E., Kissel, J. C., & Meschke, J. S. (2017a). Comparison of Risk Predicted by Multiple Norovirus Dose-Response Models and Implications for Quantitative Microbial Risk Assessment: Comparison of Risk Predicted by Multiple Norovirus Dose-Response Models. *Risk Analysis*, *37*(2), 245–264. https://doi.org/10.1111/risa.12616

Van Abel, N., Schoen, M. E., Kissel, J. C., & Meschke, J. S. (2017b). Comparison of Risk Predicted by Multiple Norovirus Dose-Response Models and Implications for Quantitative Microbial Risk Assessment: Comparison of Risk Predicted by Multiple Norovirus Dose-Response Models. *Risk Analysis*, *37*(2), 245–264. https://doi.org/10.1111/risa.12616

van den Bunt, G. (2019). Prevalence, risk factors and genetic characterisation of extended-spectrum beta-lactamase and carbapenemaseproducing Enterobacteriaceae (ESBL-E and CPE): A community-based cross-sectional study, the Netherlands, 2014 to 2016. *Eurosurveillance*, *24*(41), 1800594.

Van der Bruggen, B., Goossens, H., Everard, P. A., Stemgée, K., & Rogge, W. (2009). Cost-benefit analysis of central softening for production of drinking water. *Journal of Environmental Management*, *91*(2), 541–549. https://doi.org/10.1016/j.jenvman.2009.09.024

van der Kooij, D. (1990). Assimilable Organic Carbon (AOC) in Drinking Water. In G. A. McFeters (Ed.), *Drinking Water Microbiology* (pp. 57–87). Springer New York. https://doi.org/10.1007/978-1-4612-4464-6_3

van der Kooij, D., Veenendaal, H. R., van der Mark, E. J., & Dignum, M. (2017). Assessment of the microbial growth potential of slow sand filtrate with the biomass production potential test in comparison with the assimilable organic carbon method. *Water Research*, *125*, 270–279. https://doi.org/10.1016/j.watres.2017.06.086

van Doremalen, N., Bushmaker, T., Morris, D. H., Holbrook, M. G., Gamble, A., Williamson, B. N., Tamin, A., Harcourt, J. L., Thornburg, N. J., Gerber, S. I., Lloyd-Smith, J. O., de Wit, E., & Munster, V. J. (2020). Aerosol and Surface Stability of SARS-CoV-2 as Compared with SARS-CoV-1. *New England Journal of Medicine*, *382*(16), 1564–1567. https://doi.org/10.1056/NEJMc2004973

van Heijnsbergen, E., Schalk, J. A. C., Euser, S. M., Brandsema, P. S., den Boer, J. W., & de Roda Husman, A. M. (2015). Confirmed and Potential Sources of *Legionella* Reviewed. *Environmental Science & Technology*, *49*(8), 4797–4815. https://doi.org/10.1021/acs.est.5b00142

van Lier, A., McDonald, S. A., Bouwknegt, M., EPI group, Kretzschmar, M. E., Havelaar, A. H., Mangen, M.-J. J., Wallinga, J., & de Melker, H. E. (2016). Disease Burden of 32 Infectious Diseases in the Netherlands, 2007-2011. *PLOS ONE*, *11*(4), e0153106. https://doi.org/10.1371/journal.pone.0153106

Vikesland, P. J., Pruden, A., Alvarez, P. J. J., Aga, D., Bürgmann, H., Li, X. D., Manaia, C. M., Nambi, I., Wigginton, K., Zhang, T., & Zhu, Y. G. (2017). Toward a Comprehensive Strategy to Mitigate Dissemination of Environmental Sources of Antibiotic Resistance. *Environmental Science and Technology*, *51*(22), 13061–13069. https://doi.org/10.1021/acs.est.7b03623

Viscusi, W. (2005). *The value of life* (Discussion paper No. 517; The Harvard John M. Olin Discussion Paper Series). Harvard Law School.

Viscusi, W. K. (2008). How to value a life. *Journal of Economics and Finance*, *32*(4), 311–323. https://doi.org/10.1007/s12197-008-9030-x

Volk, C., Bell, K., Ibrahim, E., Verges, D., Amy, G., & LeChevallier, M. (2000). Impact of enhanced and optimized coagulation on removal of organic matter and its biodegradable fraction in drinking water. *Water Research*, *34*(12), 3247–3257. https://doi.org/10.1016/S0043-1354(00)00033-6

Wang, J. D., & Levin, P. A. (2009). Metabolism, cell growth and the bacterial cell cycle. *Nature Reviews Microbiology*, *7*(11), 822–827. https://doi.org/10.1038/nrmicro2202

Wang, Y., Deng, Z., & Shi, D. (2021). How effective is a mask in preventing COVID-19 infection? *MEDICAL DEVICES & SENSORS*, *4*(1), e10163. https://doi.org/10.1002/mds3.10163

Wang, Y., Li, L., Xiong, R., Guo, X., & Liu, J. (2019). Effects of aeration on microbes and intestinal bacteria in bioaerosols from the BRT of an indoor wastewater treatment facility. *Science of The Total Environment*, *648*, 1453–1461. https://doi.org/10.1016/j.scitotenv.2018.08.244

Ward, R. L., Bernstein, D. L., Young, E. C., Sherwood, J. R., Knowlton, D. R., & Schiff, G. M. (1986). Human Rotavirus Studies in Volunteers: Determination of Infectious Dose and Serological Response to Infection. *Journal of Infectious Diseases*, *154*, 871–880.

Watts, Aerco, PVI, & Powers. (2018). *Healthcare Solutions F-WWT-Healthcare 1826, MF10448*. http://media.wattswater.com/f-wwt-healthcare.pdf

Weidhaas, J., Aanderud, Z. T., Roper, D. K., VanDerslice, J., Gaddis, E. B., Ostermiller, J., Hoffman, K., Jamal, R., Heck, P., Zhang, Y., Torgersen, K., Laan, J. V., & LaCross, N. (2021). Correlation of SARS-CoV-2 RNA in wastewater with COVID-19 disease burden in sewersheds. *Science of The Total Environment*, *775*, 145790. https://doi.org/10.1016/j.scitotenv.2021.145790

Weir, M. H., Mraz, A. L., & Mitchell, J. (2019). An Advanced Risk Modeling Method to Estimate Legionellosis Risks Within a Diverse Population. *Water*, *12*(1), 43. https://doi.org/10.3390/w12010043

Westinghouse. (2017). *Westinghouse Grid-Enabled Electric Water Heater*. Westinghouse. http://www.westinghousewaterheating.com/literature/WEG-Brochure.pdf

Westinghouse. (2020). *Westinghouse Grid-Enabled Electric Water Heaters*. 2.

WHO. (2007). *Legionella and the prevention of legionellosis* (J. Bartram, Ed.). World Health Organization.

Wilson, A. M., Jones, R. M., Lugo Lerma, V., Abney, S. E., King, M.-F., Weir, M. H., Sexton, J. D., Noakes, C. J., & Reynolds, K. A. (2021). Respirators, face masks, and their risk reductions via multiple transmission routes for first responders within an ambulance. *Journal of Occupational and Environmental Hygiene*, *18*(7), 345–360. https://doi.org/10.1080/15459624.2021.1926468

World Health Organization, Food and Agriculture Organization of the United Nations, & World Organisation for Animal Health. (2016). *Antimicrobial resistance: A manual for developing national action plans* (version 1). World Health Organization. https://apps.who.int/iris/handle/10665/204470

Xiao, F., Sun, J., Xu, Y., Li, F., Huang, X., Li, H., Zhao, J., Huang, J., & Zhao, J. (2020). Infectious SARS-CoV-2 in Feces of Patient with Severe COVID-19. *Emerging Infectious Diseases*, *26*(8), 1920–1922. https://doi.org/10.3201/eid2608.200681

Xie, C., Zhao, H., Li, K., Zhang, Z., Lu, X., Peng, H., Wang, D., Chen, J., Zhang, X., Wu, D., Gu, Y., Yuan, J., Zhang, L., & Lu, J. (2020). The evidence of indirect transmission of SARS-CoV-2 reported in Guangzhou, China. *BMC Public Health*, *20*, 1202. https://doi.org/10.1186/s12889-020-09296-y

Xu, P., Zhang, C., Mou, X., & Wang, X. C. (2020). Bioaerosol in a typical municipal wastewater treatment plant: Concentration, size distribution, and health risk assessment. *Water Science and Technology*, *82*(8), 1547–1559. https://doi.org/10.2166/wst.2020.416

Yan, C., Gui, Z., & Wu, J. (2021). Quantitative microbial risk assessment of bioaerosols in a wastewater treatment plant by using two aeration modes. *Environmental Science and Pollution Research*, *28*(7), 8140–8150. https://doi.org/10.1007/s11356-020-11180-6

Yau, V., Wade, T. J., de Wilde, C. K., & Colford, J. M. (2009). Skin-related symptoms following exposure to recreational water: A systematic review and meta-analysis. *Water Quality, Exposure and Health*, *1*(2), 79–103. https://doi.org/10.1007/s12403-009-0012-9

Yee, R. B., & Wadowsky, R. M. (1982). Multiplication of Legionella pneumophila in Unsterilized Tap Water. *APPL. ENVIRON. MICROBIOL.*, *43*, 5.

Zaneti, R. N., Girardi, V., Spilki, F. R., Mena, K., Westphalen, A. P. C., Colares, E. R. da C., Pozzebon, A. G., & Etchepare, R. G. (2020). *QMRA of SARS-CoV-2 for workers in wastewater treatment plants* [Preprint]. Public and Global Health. https://doi.org/10.1101/2020.05.28.20116277

Zang, R., Gomez Castro, M. F., McCune, B. T., Zeng, Q., Rothlauf, P. W., Sonnek, N. M., Liu, Z., Brulois, K. F., Wang, X., Greenberg, H. B., Diamond, M. S., Ciorba, M. A., Whelan, S. P. J., & Ding, S. (2020). TMPRSS2 and TMPRSS4 promote SARS-CoV-2 infection of human small intestinal enterocytes. *Science Immunology*, *5*(47), eabc3582. https://doi.org/10.1126/sciimmunol.abc3582

Zhang, Y., & Edwards, M. (2009). Accelerated chloramine decay and microbial growth by nitrification in premise plumbing. *Journal - American Water Works Association*, *101*(11), 51–62. https://doi.org/10.1002/j.1551-8833.2009.tb09990.x

APPENDIX A

SUPPLEMENTAL INFORMATION FOR CHAPTER 2

Section 1. Implementation of heat transfer equations in the water heater

The flow of water within the water heater was modeled using a multi-node approach from Kleinbach et al., 1993 that follows **equation 1.1**.

$$\frac{dT_i}{dt} = \alpha_i \frac{v_{main}(T_{main}-T_i)}{V_i} + \beta_i \frac{v_{rec}(T_{rec}-T_i)}{V_i} + \delta_{a,i} \frac{(T_{i-1}-T_i)}{V_i} + \delta_{b,i} \frac{(T_i-T_{i+1})}{V_i} + \varepsilon Q_i - (1-\varepsilon)UA_i \quad (1.1)$$

α_i is equal to one at the location of the mainline and zero elsewhere, β_i is equal to one at the location of the recirculating line and zero elsewhere, $\delta_{a,i}$ is equal to one when a node exists above the node of interest, $\delta_{b,i}$ is equal to one when a node exists below the node of interest, Q_i is the energy input to the system from the heating elements, UA_i is the heat lost through the heating elements when the heating elements are off. ε is a binary term that is one when the heating elements are on and zero when the heating elements are off. v_{main} is the flow rate of water entering the water heater from the main line [L/s], v_{rec} is the flow rate of water entering the uppermost node from the recirculating water line [L/s], and V_i is the volume of node i (i=1-12) [L]. T_{main} is the temperature of the municipal water from the main line [°C], T_{rec} is the temperature of the water entering the water heater from the recirculating line [°C], and T_i is the temperature of each node [°C].

The final term of equation one shown in Kleinbach et al., 1993, that is not shown here is $UA_i(T_i - T_{env})$, which accounts for the heat lost to the environment through the

walls of the water heater. For this model, it is assumed that the walls of the water heater are perfectly insulated and no significant heat is transferred. Therefore, the term $UA_i(T_i - T_{env})$ will go to zero and is not considered in this model. Kleinbach et al. also contains a binary γ_i term, which toggles on and off based on the quantity of water entering from the main line and the recirculating pipe. It is assumed that γ_i remains positive throughout this model so there is no reverse in flow direction.

To use this equation, it needed to be modified into a form that was suitable for PyTorch. The α_i, β_i, $\delta_{a,i}$, and $\delta_{b,i}$ terms are all representative of their associated parameters in the water heater, but a variable ζ_i, needed to be added to account for the water exiting the heater at the hot water line, because that value will not always be equal to the volume of water entering the water heater from the recirculating line. ζ_i is equal to one at the location of the hot water line outlet and is zero everywhere else. $V_{new,i}$ accounts for the volume of water in the node at timestep t that will remain in that node at t=t+1 and is calculated by **equation 1.2**. The difference in the volume of the node V_i and $V_{new,i}$ will be the volume of water that is now in an adjacent node or the hot water line. The volume that is no longer in the node of interest will now be replaced by water from an adjacent node or the hot water line which is accounted for in **equation 1.3**.

$$V_{new,i} = V_i - \alpha_i v_{main} - \beta_i v_{rec} - \delta_{a,i} v_{mix} - \delta_{b,i}(v_{mix} + v_{main}) - \zeta_i v_{out} \tag{1.2}$$

$$T_i(t) = \frac{1}{V_i}\alpha_i v_{main} T_{main} + \beta_i v_{rec} T_{rec}(t-1) + \delta_{a,i} v_{mix} T_{i+1}(t-1) +$$

$$\delta_{b,i}(v_{mix}+v_{main}) T_{i-1}(t-1) + V_{new} T_i(t-1) \qquad (1.3)$$

The heat being added or lost through the heating element is considered in **equations 1.4** and **1.5**. There are two 5500 W heaters in the 316 L water heater with a 295 L storage rating (Westinghouse, 2020). The two heating elements are estimated to be at nodes 3 and 9. The location of these nodes is displayed in **Figure 2** in the main manuscript. The heat entering or exiting the system can be converted from W to ℃/s for each node and is done so in **equations 1.4** and **1.5**.

$$Q_i = (5500\ W)\left(\frac{\frac{1.89\ CHU}{1\ hr}}{1\ W}\right)\left(\frac{1\ hr}{3600\ s}\right)\left(\frac{1\ lb\ 1℃}{1\ CHU}\right)\left(\frac{1}{57.86\ lb}\right) = 0.05℃/s\ in\ node\ i$$

(1.4)

$$UA_i = (550\ W)\left(\frac{\frac{1.89\ CHU}{1\ hr}}{1\ W}\right)\left(\frac{1\ hr}{3600\ s}\right)\left(\frac{1\ lb\ 1℃}{1\ CHU}\right)\left(\frac{1}{57.86\ lb}\right) = 0.005℃/s\ in\ node\ i$$

(1.5)

The results are added to the final temperature for nodes 3 and 9, $T_{i=3,9}(t)$ in **equation 1.6**.

$$T_{i=3,9}(t) = \begin{cases} T_{i=3,9} + Q_{i=3,9}\ t & if\ on \\ T_{i=3,9} - UA_{i=3,9}\ t & if\ off \end{cases} \qquad (1.6)$$

One-dimensional mixing was chosen as to be sufficient for the objective of evaluating an optimal temperature for a heterogeneous system and the multi-node model proposed allows

for system parameters to be easily changed and evaluated without the use of more computationally complex computational fluid dynamics (CFD) approaches.

The chlorine (Chl_i) and planktonic *L. pneumophila* concentration (L_i) throughout the system can be calculated synchronously with the temperature by using analogous methods as shown in **equations 1.7** and **1.8**. Chl_i is the free chlorine concentration in each node i [mg/ L], and Chl_{rec} is the free chlorine concentration of the water in the recirculating line [mg/ L]. Chl_{main} is the free chlorine concentration in the water entering the system from the main line. L_i is the *L. pneumophila* concentration in each node i [CFU/ L], and L_{rec} is the *L. pneumophila* concentration reentering the water heater from the recirculating line [CFU/ L]. L_{main} is the *L. pneumophila* concentration in the water in the main line [CFU/ L].

$$Chl_i(t) = \frac{1}{V_i}\alpha_i v_{main} Chl_{main} + \beta_i v_{rec} Chl_{rec}(t-1) + \delta_{a,i} v_{mix} Chl_{i+1}(t-1) + \delta_{b,i}(v_{mix}+v_{main}) Chl_{i-1}(t-1) + V_{new} Chl_i(t-1) \quad (1.7)$$

$$L_i(t) = \frac{1}{V_i}\alpha_i v_{main} L_{main} + \beta_i v_{rec} L_{rec}(t-1) + \delta_{a,i} v_{mix} L_{i+1}(t-1) + \delta_{b,i}(v_{mix}+v_{main}) L_{i-1}(t-1) + V_{new} L_i(t-1) \quad (1.8)$$

The parameters for these variables are defined in **Table A1.**

Table A1. Model parameters for a multi-node model (Case 0 of the scenario analysis)

Parameter	Symbol	Unit	Value	Distribution	Source
Water heater set point	$Setpt$	°C	48-63	Point	(Westinghouse, 2020)
Pipe lengths (Case 0: see Table 5 for summary of cases)	l_X	m	Initial Pipe: 13 Branching Pipe: 3 Recirculating Pipe: 13	Point	(IAPMO, 2016)
Number of nodes in the water heater	i	-	12	Point	(Kleinbach et al., 1993)
Volume of node in water heater	V_i	L	24.58	Point	(Westinghouse, 2020)
Volume of water entering heater from recirculating line over time	v_{rec}	L/ s	0.17	Calculated	(IAPMO, 2016)
Volume of water mixing between nodes over time	v_{mix}	L/ s	0.3	Point	(Kleinbach et al., 1993)
Temperature of water in municipal water line	T_{main}	°C	Winter: Minimum: 16.5	Concatenated Uniform	(Blokker & Pieterse-Quirijns, 2013;

			Maximum: 21.5 Summer: Minimum: 17 Maximum: 24		Chmielewska, 2018)
Energy input by heating element	Q_i	°C/ s	0.05	Point	(Westinghouse, 2017)
Energy lost by heating element	UA_i	°C/ s	0.005	Point	(Westinghouse, 2017)
Temperature surrounding pipes	T_{env}	°C	Minimum: 20 Maximum: 27	Uniform	(ASHRAE, 2010; EPA, 2009)
Free chlorine concentration in the water entering the system from the mainline	Chl_{main}	mg/ L	Min: 0.01 Max: 4.0	Uniform	(AWWA, 2018)
***L. pneumophila* concentration in the water in the mainline**	L_{main}	CFU/ L	Mean:6.60 Sd: 0.80	Lognormal	(Borella et al., 2004)

Section 2. Water velocity and Reynolds number in pipes

2.1 Water velocity in pipes

The velocity of the water in the main line and the recirculating line is typically set by the installer of the recirculating line pump. The velocity is calculated to be the minimum value to reduce energy consumption based on the user's constraint of what an acceptable heat loss for the system will be. The velocity in the branching pipe is calculated from the flow rate of the fixture at that branch. For this system, a flow rate of 13 L/ min (low efficiency) for a "conventional" showerhead is assumed from Bastow Fjord (K. Hamilton et al., 2019; O'Toole et al., 2008). Using the known flow rate and the size of the branching pipe, the velocity can be calculated with the following equation where D is the pipe diameter and l_x is the length of the pipe. The velocity of the water in the hot water and recirculating lines were calculated (**equation 2.1**) to be 1.5 m/s based on pipe radius, length, and flow rate. This is also the velocity used for the water in the branching pipe when the shower is on, and zero if the shower is off. It is assumed that at least two times that flow would be required as the modeled water heater is large and would likely be serving multiple taps.

$$v = \frac{flow\ rate}{\pi\left(\frac{D}{2}\right)^2 l_x} \tag{2.1}$$

There will be a multitude of factors that will determine the value of velocity flowing through the system. The physical parameters that will influence the velocity include the

pipe diameter, length, bends, fittings, tap opening, and mixing valve(s). The only parameters considered to influence the velocity in this model are the pipe diameter, length, and a single shower fixture. The water pressure should also be taken into consideration, as water pressure can vary greatly, and pressure boosters may be installed depending on the water pressure entering the premise plumbing from the city line. All these factors will also influence the velocity of water in the recirculating line. It should also be acknowledged that with a smaller branching pipe, the velocity will be greater than that in the pipe and the recirculating line. This was not addressed in the current model.

For this model, it is assumed that the velocity will be constant at all points in the pipes when the water is not stagnant in the branching pipe. In a physical system, the velocity will constantly be changing as different taps are opened, and in some systems the recirculating line will be off for a period to save energy. The recirculating line is assumed to be running for the entirety of the model.

The necessary flow rate in m/ s is determined by the tolerable amount of heat lost in the system (3.3°C) using the equation described in **SI Section 3** solved for velocity resulting in **equation 2.2.** U is the overall heat transfer coefficient [W/ m^2K], L is the length of the recirculating pipe [m], c_p is the specific heat of water, ρ is the density of water, D is the diameter of the pipe, T_0 is the temperature of the water entering the pipe

form the water heater, T_F is T_0 minus the tolerable loss of heat in the pipe, and T_{env} is the temperature of the environment.

$$v = \frac{-4UL}{c_p \rho D \, ln\left(\frac{T_F - T_{env}}{T_0 - T_{env}}\right)} \tag{2.2}$$

2.2 Reynolds number

Reynolds number (Re) can be calculated by **equation 2.3** for the pipe ¾" in diameter (D) [m] and the ½" diameter branching pipe that leads to the showerhead. The kinematic viscosity of water, $\frac{\mu}{\rho}$ [m^2/ s], is the viscosity (μ) over the density of water (ρ) (**Table A2**). This resulted in a velocity of 3.04 m/s and a *Re* in the pipe and branch of 52,349 and 41,444, respectively. These values of the Reynold's number are consistent with turbulent flow.

$$Re = \frac{\rho v D}{\mu} \tag{2.3}$$

The parameters for these variables are defined in **Table A2.**

Table A2. Parameters for velocity and Reynolds number

Parameter	**Symbol**	**Unit**	**Value**	**Distribution**	**Source**
Specific heat of water	c_p	J / kgK	4186.8	Point	(Incropera et al., 2007)

Density of water	ρ	kg / m^3	996	Point	(Incropera et al., 2007)
Overall heat transfer coefficients	U	W / m^2K	Uninsulated: 325.9 Insulated: 29.80	Calculated	Supplemental Information, Section 2
Diameter	D	m	Pipe: 0.019 Shower: 0.012	Point	(IAPMO, 2016)
Kinematic viscosity of water (50°C)	$\frac{\mu}{\rho}$	m^2/ s	5.53×10^{-7}	Point	(Incropera et al., 2007)

Section 3. Heat loss in pipes

The water heater in this model is assumed to be perfectly insulated and will experience no transfer of heat to from the water to the environment, however heat loss is considered in the pipes (**equation 3.1**) T [℃] is the temperature of water in the pipe, T_{env} [℃] is the air temperature in the air surrounding the pipe, U [W/ m^{2}K] is the overall heat transfer coefficient specific to that pipe configuration, c_p [J/ kg K] is the specific heat of water, ρ [kg/ m^3] is the density of water, v [m/ s] is water velocity, and D [m] is the diameter of the pipe.

$$\frac{dT}{dt} = (T(t) - T_{env})\left(\frac{-4U}{c_p \rho v D}\right) \tag{3.1}$$

Section 4. Heat transfer coefficients

In order to track the heat lost through the pipes, the overall heat transfer coefficient U [W/ m^{2}K] was calculated for each pipe size and insultation.

4.1 Convective heat transfer coefficient

The convective heat transfer coefficient, h_{conv} [W/ m^{2}K], is the rate at which energy is transferred from the water to the copper pipes. To find h_{conv}, an energy balance equation can be performed starting with **equation 4.1**, where $\dot{E}_{in}$ is the amount of energy entering the shared water to copper surface from the water by convection ($\ddot{q}_{conv}$) and $\dot{E}_{out}$ is the energy leaving the shared water to copper surface and going into the copper pipe by conduction ($\ddot{q}_{cond}$).

$$\dot{E}_{in} - \dot{E}_{out} = 0 \tag{4.1}$$

$$\ddot{q}_{conv} - \ddot{q}_{cond} = 0 \tag{4.2}$$

The equations for convective ($\ddot{q}_{conv}$) and conductive ($\ddot{q}_{cond}$) heat flux [W/ m^2] can be described by **equations 4.3** and **4.4** respectively. T_s is the temperature at the shared surface, T_f is the temperature of the fluid, and T_i is the temperature of the conductive material. k is the thermal conductivity of the conductive material [W/ mK], and L is the radial length of the conductive material [m].

$$\ddot{q}_{conv} = h_{conv}(T_s - T_f) \tag{4.3}$$

$$\ddot{q}_{cond} = k\frac{(T_i - T_s)}{L} \tag{4.4}$$

Substituting $\ddot{q}_{conv}$ and $\ddot{q}_{cond}$ into **equation 4.2** and solving for h_{conv} results in equation 4.5.

$$h_{conv} = \frac{k(T_i - T_s)}{L(T_s - T_f)} \tag{4.5}$$

4.2 Radiative heat transfer coefficient

The radiative heat transfer coefficient from a conductive material (copper or insulation) to air (h_{rad}) [W/ m^{2}K], can be calculated by another energy balance equation with the radiative heat flux ($\ddot{q}_{rad}$) [W/ m^2].

$$\ddot{q}_{cond} - \ddot{q}_{rad} = 0 \tag{4.6}$$

The equation for radiative heat flux ($\ddot{q}_{rad}$) can be described by **equation 4.7**.

$$\ddot{q}_{rad} = h_{rad}(T_s - T_f) \tag{4.7}$$

Equation 4.7 and **equation 4.4** can be substituted into **equation 4.6** and solved for h_{rad} resulting in **equation 4.8**.

$$h_{rad} = \frac{k(T_i - T_s)}{L(T_s - T_f)} \tag{4.8}$$

4.3 System specific variables

To calculate the heat lost to the environment from the water in the pipes, the convective and radiative heat transfer coefficients were calculated. **Figure A1** describes the temperatures and radial lengths used to calculate the convective heat transfer between the water and the copper h_{conv} (**equation 4.5**), the radial heat transfer between copper and air for uninsulated pipes $h_{rad,cu}$ (**equation 4.9**), and the radial heat transfer between insulation and air $h_{rad,ins}$ (**equations 4.10**).

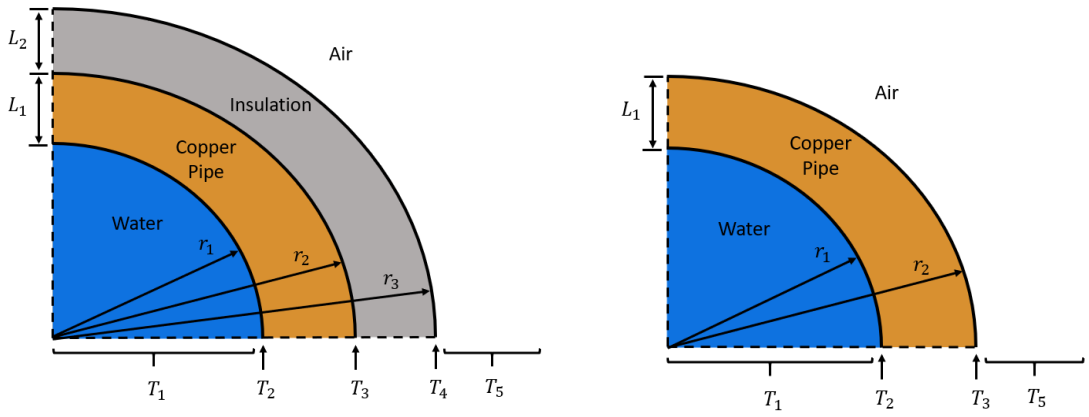

Figure A1: Cross section of insulated pipe (left) and uninsulated pipes (right) with locations of temperatures and radial lengths.

The temperature of the fluid in the pipe was chosen as the mean of the tested temperature range (48-63℃) at $T_1 = 55.50℃$. The temperature of the shared water to copper surface was set to be close to the temperature of the fluid in the pipe at $T_2 =$

55.10℃. The temperature of the shared copper to insulation surface was set to be close to the temperature of the shared water to copper surface at $T_3 = 55.01$℃. The temperature of the outer insulation surface was set to be near the temperature of the surrounding room temperature at $T_4 = 33.5$℃. The temperature of the air surrounding the pipe was set to the average room temperature at $T_5 = 23.5$℃ (ASHRAE, 2010; EPA, 2009). L_1 is the radial length of the copper pipe and L_2 is the radial length of the insulation [m]. k_{cu} is the thermal conductivity of commercial copper and k_{ins} is the thermal conductivity of rubber used for insulation [W/ mK].

$$h_{rad,cu} = \frac{k_{cu}(T_2 - T_3)}{L_1(T_3 - T_5)} \tag{4.9}$$

$$h_{rad,ins} = \frac{k_{ins}(T_3 - T_4)}{L_2(T_4 - T_5)} \tag{4.10}$$

The heat transfer coefficients will vary greatly based on the individual system parameters. For this model, the three heat transfer coefficients, h, were found to be within the expected values (Incropera et al., 2007) for forced convection (25-250 and 100-20,000 $\left[\frac{W}{m^2 K}\right]$) for gases and liquids, respectively. The parameters for these variables are defined in **Table A3.**

Table A3 Parameters for heat transfer coefficient calculation

Parameter	Symbol	Unit	Value	Distribution	Source
Thermal conductivity of commercial copper	k_{cu}	W/ mK	401	Point	(Incropera et al., 2007)
Thermal conductivity of rubber (for insulation)	k_{ins}	W/ mK	0.16	Point	(Incropera et al., 2007)
Radial length of copper pipe	L_1	m	0.005	Point	(IAPMO, 2016)
Radial length of insulation	L_2	m	0.013	Point	(IAPMO, 2016)
Temperature of water	T_1	℃	55.5	Point	(Westinghouse, 2017)
Temperature at shared water/copper interface	T_2	℃	55.1	Point	Assumption based on (Incropera et al., 2007)
Temperature at shared copper/insulation or copper/air interface	T_3	℃	55.01	Point	Estimation
Temperature at shared insulation/air interface	T_4	℃	33.5	Point	Estimation
Temperature of air surrounding pipes	T_5	℃	23.5	Point	(ASHRAE, 2010; EPA, 2009)
Inner radius of copper pipe	r_1	m	0.009	Point	(IAPMO, 2016)

Outer radius of copper pipe/ inner radius of insulation	r_2	m	0.014	Point	(IAPMO, 2016)
Outer radius of insulation	r_3	m	0.027	Point	(IAPMO, 2016)

4.4 Overall heat transfer coefficient

The overall heat transfer coefficient for heat leaving uninsulated ($U_{uninsulated}$) and insulated ($U_{insulated}$) [W/ m^{2}K] pipes is calculated using the convective and radial heat transfer coefficients (see Table A3 for radius definitions). The results are displayed in **Table A4.**

$$U_{uninsulated} = \left(\frac{1}{h_{conv}} + \frac{r_1}{k_{cu}}\ln\left(\frac{r_2}{r_1}\right) + \left(\frac{r_1}{r_2}\right)\frac{1}{h_{rad,cu}}\right)^{-1} \quad (4.11)$$

$$U_{insulated} = \left(\frac{1}{h_{conv}} + \frac{r_1}{k_{cu}}\ln\left(\frac{r_2}{r_1}\right) + \frac{r_1}{k_{ins}}\ln\left(\frac{r_3}{r_2}\right) + \left(\frac{r_1}{r_3}\right)\frac{1}{h_{rad,ins}}\right)^{-1} \quad (4.12)$$

The parameters for these variables are defined in **Table A4.**

Table A4: Calculated values for heat transfer coefficients and overall heat transfer coefficients

Parameter	Symbol	W/ m^{2}K
Convective heat transfer between water and copper	h_{conv}	20,050

Radial heat transfer between copper and air for uninsulated pipes	$h_{rad,cu}$	254
Radial heat transfer between insulation and air	$h_{rad,ins}$	27
Overall heat transfer coefficient (uninsulated)	$U_{uninsulated}$	315
Overall heat transfer coefficient (insulated)	$U_{insulated}$	20

Section 5. Chlorine decay

First-order decay of free chlorine is commonly calculated with a first order decay rate (**equation 5.1**) (AWWARF, 1996; C. Huang et al., 2020), but it lacks any variability due to system parameters, such as temperature, total organic carbon (TOC) or differences between the bulk decay and the wall decay.

$$C = C_0 e^{-kt} \tag{5.1}$$

Instead, an Arrhenius equation was determined to be the best chlorine decay model for this system because it accounts for the influence of temperature throughout the system and parameters had already been estimated (AWWARF, 1996). The Arrhenius equation was used is defined in **equation 5.2**. A is the pre-exponential factor, E_a is the activation energy [J/ mol], R is the universal gas constant [J/ mol K] and T is the absolute temperature [K]. This equation can be used to describe the decay of chlorine in bulk water (Monteiro et al., 2014).

$$k_b = A e^{\frac{-E_a}{RT}} \tag{5.2}$$

Equation 5.2 was modified by AWWARF 1996 (**equation 5.3** and **Table A5**). The pre-exponential factor is dependent on the constant a, the concentration of TOC, and the constant b, which encompasses the activation energy and the universal gas constant. T is

temperature in Kelvin. This equation allows for the free chlorine decay rate to be estimated at varying temperatures and TOC concentrations in the system.

$$k_b = a * TOC * \exp\left(\frac{-b}{T}\right) \quad (5.3)$$

However, the authors caveat this equation is not applicable beyond the range of 5°C to 25°C due to their observed experimental range. In the absence of similar data outside this range, the kinetic equation was applied for the system temperatures in the current model. The parameters for these variables are defined in **Table A1.**

Table A5 Parameters for Chlorine Decay

Parameter	**Symbol**	**Unit**	**Value**	**Distribution**	**Source**
Measured Constant a	a	L/ mg h	1.8×10^6	Point	(AWWARF, 1996)
Total Organic Carbon	TOC	mg/ L	Min: 1 Max: 3	Uniform	(AWWARF, 1996)
Measured Constant b	b	K	6,323	Point	(AWWARF, 1996)
Water Temperature	T	K	Measured	Point	(AWWARF, 1996)

Section 6. *L. pneumophila* growth and inactivation due to temperature

L. pneumophila has been observed multiplying in water temperatures from 25°C to 45°C (Sharaby et al., 2017; Yee & Wadowsky, 1982) and is known to become inactivated from 50°C to 70°C (Cervero-Aragó et al., 2015). No growth or inactivation has been quantified in between 45°C and 50°C or below 25°C in these studies.

6.1 Inactivation rates

The inactivation rates for temperatures from 50°C to 70°C were calculated by assuming a first-order inactivation of *L. pneumophila* by **equation 6.1**.

$$C_f = C_i e^{-k_{temp} t} \tag{6.1}$$

The time for a 4-log reduction of *L. pneumophila* sg. 1 ATCC 33152 was provided in Cervero-Aragó et al., 2015. The time to reduction was found for 50°C (117 minutes), 55°C (10 minutes), 60°C (2 minutes), 65°C (0.8 minutes) and 70°C (0.9 minutes). The first-order decay equation was solved for the inactivation rate (k_{temp}) of *L. pneumophila* at different temperatures using the known 4-log reduction $\log(C_f/C_i)$, and time t (**equation 6.2**).

$$k_{temp} = \frac{-\log\left(\frac{C_f}{C_i}\right)}{t} \tag{6.2}$$

6.2 Growth rates

Sharaby et al., 2017 and Yee and Wadowsky, 1982 recorded values for *L. pneumophila* growth at 25°C, 30°C, 37°C, and 42°C. No significant growth was seen at 45°C. A first order growth of *L. pneumophila* was assumed (**equations 6.1** and **6.2**), with a positive k_{temp} rate. Calculated first-order growth constants are shown in **Table A6**. The current model does not address the lag phase of growth described by Sharaby, 2017.The growth rates from Sharaby, 2017 were chosen to be used with the inactivation rates from Cervero-Aragó et al., 2015 for the purposes of this model because it was more recent than Yee and Wadowsky, 1982. The final values k_{temp} are displayed in equation 6.3 [s^{-1}]. The growth limit of planktonic *L. pneumophila* was set to $10^{4.17}$ CFU/ L (Yee & Wadowsky, 1982). The parameters for these variables are defined in **Table A7.**

$$k_{temp} = \begin{cases} -7.41 \times 10^{-2} & if\ T_{all} \geq 70℃ \\ -8.33 \times 10^{-2} & if\ 65℃ \leq T_{all} < 70℃ \\ -3.33 \times 10^{-2} & if\ 60℃ \leq T_{all} < 65℃ \\ -6.67 \times 10^{-3} & if\ 55℃ \leq T_{all} < 60℃ \\ -5.70 \times 10^{-5} & if\ 50℃ \leq T_{all} < 55℃ \\ 0 & if\ 45℃ \leq T_{all} < 50℃ \\ 3.14 \times 10^{-5} & if\ 42℃ \leq T_{all} < 45℃ \\ 6.97 \times 10^{-5} & if\ 37℃ \leq T_{all} < 42℃ \\ 3.22 \times 10^{-5} & if\ 30℃ \leq T_{all} < 37℃ \\ 2.55 \times 10^{-5} & if\ 20℃ \leq T_{all} < 30℃ \\ 0 & if\ T_{all} < 20℃ \end{cases} \quad (6.3)$$

Table A6: Derived *L. pneumophila* growth rates

Temperature	Growth rate per second	Growth rate per second

	Yee and Wadowsky, 1982	Sharaby, 2017
25°C	2.30×10^{-5}	2.55×10^{-5}
32/30°C	3.08×10^{-5}	3.22×10^{-5}
37°C	4.73×10^{-5}	6.97×10^{-5}
42°C	4.82×10^{-5}	3.14×10^{-5}

Table A7: Growth and inactivation rates of *L. pneumophila*

Parameter	Symbol	Unit	Value	Distribution	Source
Growth/ inactivation Rates of *L. pneumophila* with temperature	k_{temp}	s^{-1}	>70°C: -7.41×10^{-2} 65-70°C: -8.33×10^{-2} 60-65°C: -3.33×10^{-2} 55-60°C: -6.66×10^{-3} 50-55°C: -5.69×10^{-5} 45-50°C: 0.0 42-45°C: 4.82×10^{-5} 37-42°C: 4.73×10^{-5} 30-37°C: 3.08×10^{-5} 20-30°C: 2.30×10^{-5}	Point	(Cervero-Aragó et al., 2015; Sharaby et al., 2017)
Planktonic *L. pneumophila* inactivation rate due to chlorine	$k_{p,chl}$	s^{-1}	Chl<0.01: 0 0.01<Chl<0.15: 1.82×10^{-3} 0.15<Chl<0.35: 1.92×10^{-3} 0.35<Chl_{all}: 2.31×10^{-2}	Point	(Kuchta et al., 1983)
Planktonic *L. pneumophila* growth limit	-	CFU/L	$10^{4.17}$	Point	(Yee & Wadowsky, 1982)

Section 7. Biofilm kinetics in the pipes

The mass of biofilm per unit area (M_b [g/ cm^2]) was calculated with **equation 7.1** using the biofilm density (D_b [g/ cm^3]) (Garny et al., 2009) and the mean volume of biofilm per cm^2 of pipe area based on the biofilm thickness (V_b) [cm^3/ cm^2] (Garny et al., 2009).

$$M_b = D_b V_b \tag{7.1}$$

These values were chosen from the low turbulent flow simulation from Garny et al., 2009. This was selected as the most appropriate for the scenario for the current model. The data was extracted for both the biofilm density and the biofilm thickness using GetData Graph Digitizer® v2.26.0.20 software. A normal curve truncated at zero was fit to the biofilm density, D_b, for calculations and a mean value was found to be 34.5 kg/ m^3. The average thickness of the biofilm was 0.01 cm, which equates to a mean volume of biofilm per cm^2 (V_b) of 0.01 cm^3. Using these averages, the density of biofilm per cm^2 of pipe area was modeled as a normal distribution truncated at zero with an average value of 3.5×10^{-4} g/ cm^2. The biofilm sloughing rate $S_b(t_s)$ was chosen from the low turbulent flow simulation from Garny et al., 2009. The data for the biofilm sloughing rate was extracted using Digitizer software and modeled as a lognormal distribution with an upper truncation limit of 20 gDW/ m^{2}day. The average sloughing rate based on this distribution was 7.39×10^{-9} g/ cm^{2}s.

The quantity of *L. pneumophila* in the biofilm, C_b, was extracted from Figure 6.12 in (J. M. Thomas, 2012). The mean values for the reactor were 13 CFU/ cm^2 for a heated condition and 39 CFU/ cm^2 at ambient temperature. The quantity of *L. pneumophila* for the reactor at ambient temperature was chosen and modeled as a lognormal distribution and decay rates due to temperature were applied appropriately (**SI Section 6**). The quantity of biofilm being sloughed into the water will decline as a first order function as the shower remains on by the values in **equation 7.2** (C. Huang et al., 2020). It is assumed to that there is no sloughing in the branch pipe when the shower is off and the water is stagnant.

$$k_s = \begin{cases} -1.30 & if\ t_s \leq 5\ min \\ -0.06 & if\ t_s > 5\ min \end{cases} \tag{7.2}$$

The quantity of sloughed *L. pneumophila* is C_s. The rate of decay of the biofilm sloughing, k_s, is modeled in **equation 7.2** using two decay rates that are dependent on how long the shower has been on (t_s) (C. Huang et al., 2020). The decay rate of sloughing is applied in **equation 7.4**. Based on data presented in Huang et al. (2020), we assume that *L. pneumophila* that has been sloughed from the biofilm will decay due to both chlorine in the system and due to the water temperature. The inactivation rates for *L. pneumophila* in the biofilm due to chlorine, $k_{b,chl}$, are presented in **equation 7.3** (C. Huang et al., 2020). The final *L. pneumophila* concentration in the system due to biofilm sloughing is calculated using **equation 7.4**. The amount of biofilm that is sloughed will decay in concentration due to k_s, and will experience inactivation due to the chlorine decay rate $k_{b,chl}$ times the

concentration chlorine residual, Chl, as well as experiencing growth or inactivation from temperature k_{temp}. Biofilm calculation parameters are summarized in **Table A8**.

$$k_{b,chl} = \begin{cases} -0.46 & if\ t_s \leq 5\ min \\ -0.10 & if\ t_s > 5\ min \end{cases} \quad (7.3)$$

$$C_s(t) = C_{s,0}\ e^{(k_s + k_{b,chl}Chl + k_{temp})t_s} \quad (7.4)$$

Table A8. Biofilm parameters

Parameter	Symbol	Unit	Value	Distribution	Source
Biofilm density	D_b	kg / m^3	Shape: 3.14 Scale: 38.66	Weibull*	(Garny et al., 2009)
Volume of biofilm per m^2	V_b	m^3 / m^2	1×10^{-4}	Point	(Garny et al., 2009)
Concentration of *L. pneumophila* in biofilm	C_b	CFU / m^2	Min: 3.9×10^5 Max: 7.8×10^9	Uniform	(Schoen & Ashbolt, 2011a; J. M. Thomas, 2012)
Duration of shower	t_s	s	μ: 465 σ: 72	Normal	(DeOreo et al., 2016)

Sloughing rate of biofilm	$S_b(t_s)$	g / cm^2s	Mean log: -18.96 SD log: 0.709	Lognormal	(Garny et al., 2009)
Decay of sloughing rate	k_s	min^{-1}	-1.30: $t_s \leq 5$min -0.06: $t_s >$ 5min	Point	(C. Huang et al., 2020)
Decay of sloughed *L. pneumophila* in biofilm due to chlorine	$k_{b,chl}$	$(mg/L*min)^{-1}$	-0.46: $t_s \leq 5$min -0.10: $t_s >$ 5min	Point	(C. Huang et al., 2020)

*Modeled as a uniform distribution for Sobol Sensitivity Analysis

Section 8. Initialization of the system

To initialize the system:

1. The water heater system was run for 24 hours with no shower and no new water from the main line to mimic stagnation events. The temperature, chlorine, and *L. pneumophila* will act according to the equations described in **Section 2** (Methods) of the manuscript. After 24 hours, the initialized temperature throughout the system is recorded and stored for later.
2. The *L. pneumophila* growth and decay throughout the water heater, hot water line, and recirculating line needed to be estimated beyond the growth and decay rates shown in **Table A7**. While the system runs, it is possible for the water temperature to pass through different temperature zones that either inactivate or promote growth of *L. pneumophila*. This change in water temperature throughout the system will change with pipe length, water velocity, or other physical parameters. The volume of water at different temperatures will also vary depending on the location in the plumbing system. For example, a smaller amount of water will be at a cooler temperature at the end of the recirculating line than the water in node 3 or 9 of the water heater which contain the heating elements and have a larger volume. Therefore, to determine the *average* inactivation or growth rate of *L. pneumophila* due to temperature for the 24-hour initialization period in the water heater, hot water line, and recirculating line, a mass balance equation was performed with the

initialized temperature and volume of each section of the system. The initialized inactivation or growth rates were recorded for each case and stored for later use.

3. For each iteration of the Monte Carlo simulation, the initialized temperature and inactivation or growth rates were loaded. The temperature of the system was set as the previous initialized temperature for each case.
4. To initialize the free chlorine values for the water heater, hot water line and recirculating line, the free chlorine concentration was calculated using the Arrhenius equation for each Monte Carlo iteration (**SI Section 5**). The time that it took the chlorine to decay to be below the limit that it would affect the *L. pneumophila* was calculated. The *L. pneumophila* concentration after the 24-hour initialization period was then calculated using the previously recorded initialized inactivation or growth rates applied over the time that the chlorine was below the limit that would affect the *L. pneumophila* growth. The *L. pneumophila* growth in the branching pipe was calculated as a first order growth equation with the room temperature growth rate applied over a 24-hour period.
5. A growth cap was applied over the entire system so the *L. pneumophila* concentration did not exceed $10^{4.17}$ CFU/ L (Yee & Wadowsky, 1982).
6. The biofilm was calculated for each case as described in **Section 2.7** of the main manuscript. The initialized inactivation or growth rates for *L. pneumophila* was applied to the biofilm in the hot water line and recirculating line for a 24-hour

period. No chlorine decay was applied. The variables used to calculate the biofilm are from sources that conducted experiments at room temperature (Garny et al., 2009; Schoen & Ashbolt, 2011b; J. M. Thomas, 2012), therefore, there was no inactivation or growth rate applied to the biofilm in the branching pipe that remained at room temperature for the 24-hour initialization period.

Section 9. Decay of aerosols and QMRA parameters

The decay of aerosols d_i [s^{-1}] that have been released into the exposure environment was calculated using the aerosol removal rates, d_{1-2} [min^{-1}], from Huang et al., 2020 with the percentage of aerosol sizes, F_{1-10}, from Hamilton et al., 2019. It is a weighted average based on the difference aerosol removal rates for the two aerosol size bins of consideration: 1-2 micrometers and 3-10 micrometers. The decay of the aerosols is calculated in **equation 8.1** and displayed in **Table A9.** The parameters used for the quantitative microbial risk assessment (QMRA) are displayed in **Table A10** and described in **Section 2.8** of the main manuscript.

$$d_i = d_1 F_{1-2} + d_2 F_{3-10} \quad (8.1)$$

Table A9: Calculated aerosol decay values

Parameter	Variable	Value	Unit
Percent aerosols 1-2 micrometer	F_{1-2}	33.89	%
Percent aerosols 3-10 micrometer	F_{3-10}	66.11	%
Aerosol Removal Rate <=2 micrometer	d_1	0.35	1/min
Aerosol Removal Rate >2 micrometer	d_2	1.24	1/min
Decay of aerosols	$\boldsymbol{d_i}$	0.016	1/s

Table A10 QMRA parameters

Parameter	Symbol	Unit	Value	Distribution	Source
Concentration of aerosols	C_{aero}	CFU/ m^3	1-2: μ: 17.5, σ: 0.30 2-3: μ: 17.5, σ: 0.17 3-6: μ: 19.4, σ: 0.35 6-10: μ: 20.0, σ: 0.31	Lognormal	(O'Toole et al., 2008, 2009)
Volume of aerosols	V_{areo}	L/ CFU	1-2: Min: 5.25×10^{-16} Max: 4.19×10^{-15} 2-3: Min: 4.19×10^{-15} Max: 1.41×10^{-14} 3-6: Min: 1.42×10^{-14} Max:1.13×10^{-13} 6-10: Min: 1.13×10^{-13} Max:5.22×10^{-13}	Uniform	(O'Toole et al., 2008, 2009)
Fraction of *L. pneumophila* that partition to each of the aerosol diameters	F	%	1-2: 0.34 2-3: 0.16 3-6: 0.13 6-10: 0.17	Point	(Allegra et al., 2016)
Alveolar deposition efficiency	D	Fraction	1-2: 0.23-0.53 2-3: 0.36-0.62 3-6: 0.10-0.62 6-10: 0.01-0.29	Uniform	(Heyder et al., 1986)
Rate of inhalation	B	m^3/ min	0.013-0.017	Uniform	(Bussard, 2011)
Decay of aerosols	d_i	s^{-1}	-0.016	Point	(K. Hamilton et al., 2019; C.

					Huang et al., 2020)
Dose response parameter for sub-clinical infection	r	s^{-1}	Mean: -2.93 Sd: 0.49	Lognormal	(Armstrong & Haas, 2007b; Muller et al., 1983b)
Dose response parameter for clinical infection	r	s^{-1}	Mean: -9.69 Sd: 0.30	Lognormal	(Armstrong & Haas, 2007b; Muller et al., 1983b)
Disability adjusted life year	$DALY$	years	0.97	Point	(van Lier et al., 2016)
Value of a statistical life	VSL	USD	Min:5,324,706 Max: 17,368,683	Uniform	(US Department of Health and Human Services, 2021)
Remaining Life expectancy	$Life\ Exp$	years	Mean: 31.88 Sd: 18.32 Min: 0	Truncated Normal	(Robinson & Hammitt, 2016)
Morbidity Ratio, elderly	MR_e	Unitless	0.75	Point	(Weir et al., 2019)

Section 10. Scalding and energy costs

The cost of scalding was calculated using data from Moritz and Henriques (1947) (Moritz & Henriques, 1947). Data in the original work were presented in coordinates of temperature and time based on two categories of severity of injury: epidermal injury and epidermal necrosis. A log of the data on both axes was used so linear regressions could be calculated. The points for epidermal injury (mild-moderate injury) were used to find a linear regression shown in red below in **Figure A2**. The points for epidermal necrosis (moderate-severe injury) were used to find a linear regression shown in blue below. The 95% confidence intervals are shaded in grey around each regression.

- **Epidermal Injury:** $y = -0.0342x + 1.783$
- **Epidermal Necrosis**: $y = -0.0359x + 1.793$

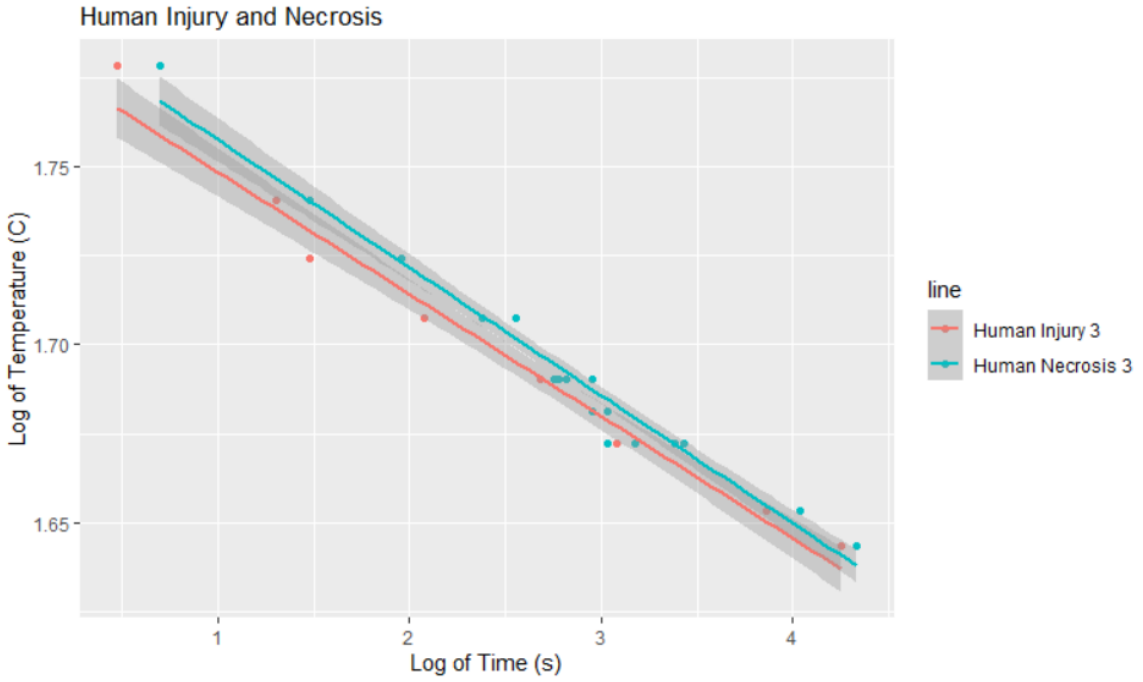

Figure A2. The scalding curve for epidermal injury (red) and epidermal necrosis (blue) based on log of time and log of temperature.

The Monte Carlo model then determined where the severity of the injury lies for each iteration based on the temperature of the water at the showerhead and the time it took for the individual to remove themselves from the water (uniform distribution randomly sampled from 1.0 to 5.0 seconds).

Once it was determined which region each iteration was within, a monetary value was assigned based on approximate costs for each category.

- **No injury** (blue): $0.00

- **Epidermal injury** (yellow): $141.76 to $221.89 (uniform distribution randomly sampled)
- **Epidermal necrosis** (red): $628.69 to $862.90 (uniform distribution randomly sampled)

Differences in datasets could not be evaluated directly with statistical tests due to lack of alignment between temperature and time points (i.e. measurements that occurred at different times and at different temperatures could not be directly compared). The regressions used were not statistically significant from each other ($p>0.05$). Once injury has begun, if the stimulus is not removed there will only be a small amount of time until the injury progresses. We considered expanding the data set be adding the extensive dataset from pig injury and necrosis in Table 2 of Moritz and Henriques (Moritz & Henriques, 1947) which is plotted in **Figure A3**. Adding these data did not change the conclusion that the regressions associated with the two injury categories are not significantly different. Merging the human data in **Figure A2** was also considered shown in **Figure A4**, however the small region between the two regressions indicates that there is a small range of temperatures before onset of burn where there is a physiological difference in burn outcome—a mild burn for a short duration. The merged scenario is a scenario that can be chosen by the user in the code for this model. A sensitivity analysis for the cost of the injury or necrosis was estimated using data from Blue Cross Blue Shield, 2009, and are displayed in **Table A12**.

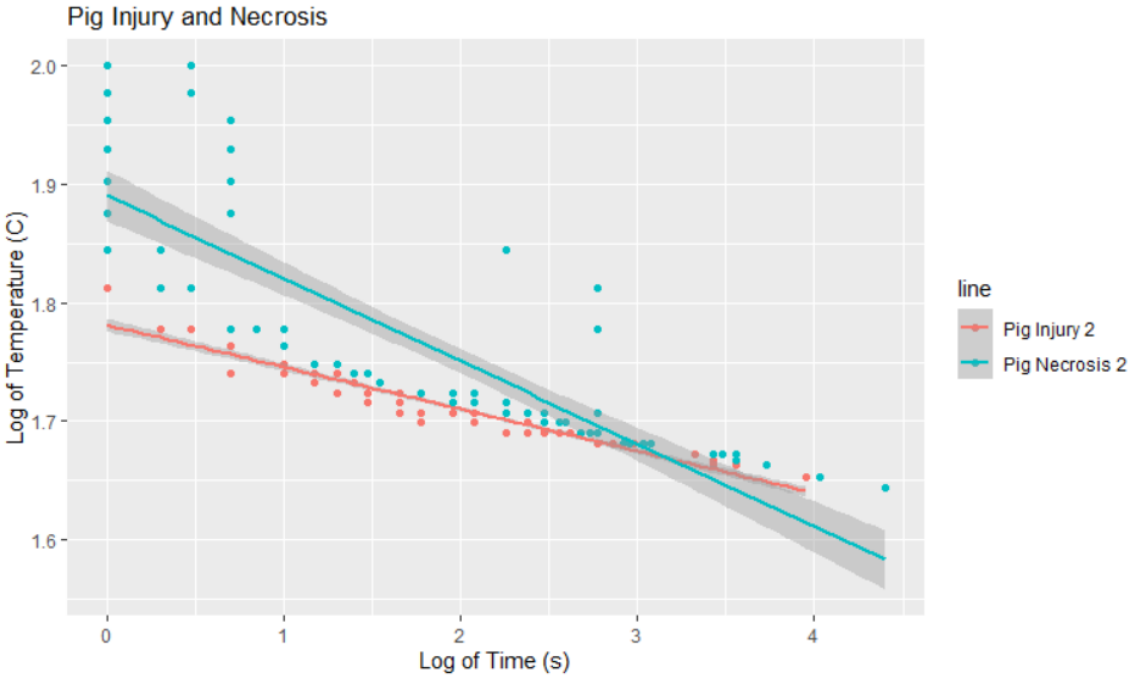

Figure A3. The scalding curve for epidermal injury (red) and epidermal necrosis (blue) based on log of time and log of temperature for pig data.

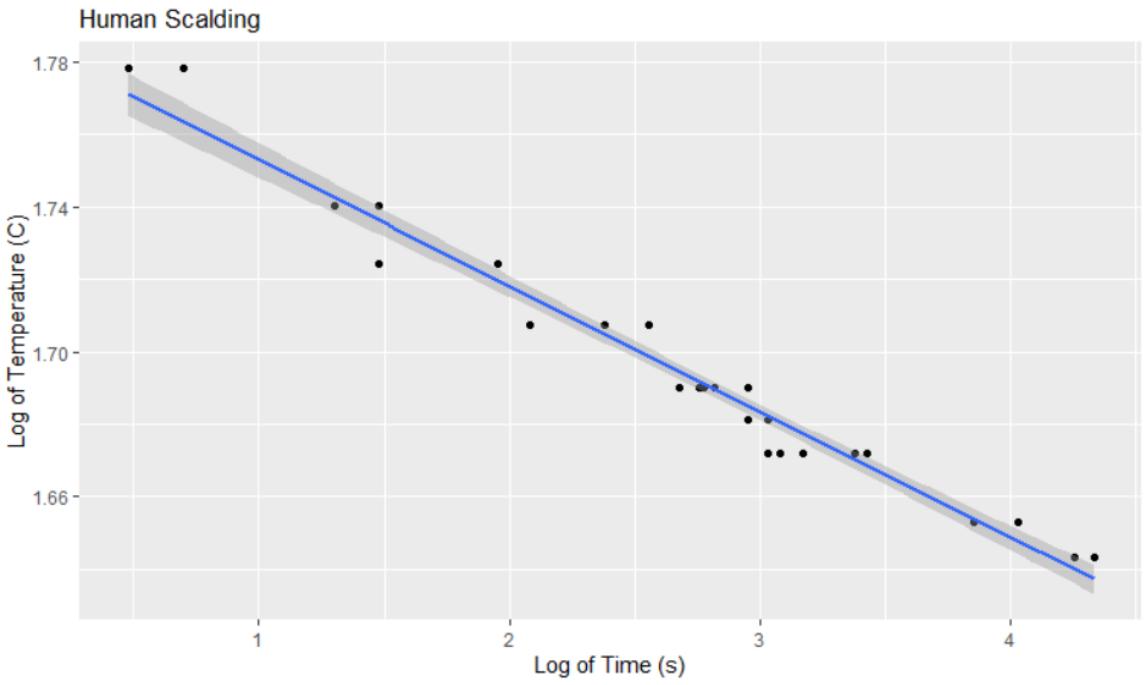

Figure A4. The scalding curve for epidermal injury and epidermal necrosis together based on log of time and log of temperature for human data. Regression equation log(y) = -0.0347*log(x) + 1.788.

Table A11: Sensitivity analysis for three-category scald vs. two-category scald

Case	Three scald categories for human data (no injury, injury, necrosis - Fig S2)	Pooled scalding data with categories for injury with human data (injury or necrosis) vs. no injury (Fig. S5)	Difference in modeled optimum water heater set point
0	55	56	+1
1	54	54	0

2	55	59	+4
3	56	59	+4
4	55	59	+4
5	59	56	-3
6	61	59	-2
7	59	56	-3
8	48	48	0
9	48	48	0
10	48	48	0
11	48	48	0
12	55	52	-3
13	48	48	0
14	55	53	-2
15	48	48	0

Table A12: Scalding model and energy model parameters

Parameter	**Symbol**	**Unit**	**Value**	**Distribution**	**Source**
Burn categories	$injury\ type$	USD	Focal epidermal necrosis: Min: 141.76 Max: 221.89 Complete epidermal necrosis: Min: 628.69 Max: 862.90	Uniform	(Blue Cross Blue Shield, 2009)
Reaction time	$jumptime$	s	Min: 1 Max: 5	Uniform	Estimation

Liters of water used for showering daily	Q_{in}	L / Day	59	Point	U.S. Geological Survey
Price per kWh	P_{kWh}	USD / kWh	Mean: -2.01 Sd: 0.25	Lognormal	(U.S. Energy Information Administration, n.d.)
Energy Factor	EF	-	Min: 0.90 Max: 0.95	Uniform	(ENERGY STAR, 2008)

Section 11. Additional results

A complete set of outputs for the risk of infection, total cost, and heatmaps of water quality parameters throughout the premise plumbing system are shown in Figures A13-A14, respectively.

	Case 0
48°C	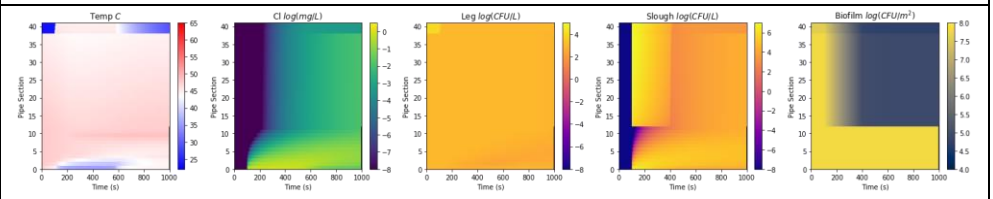
49°C	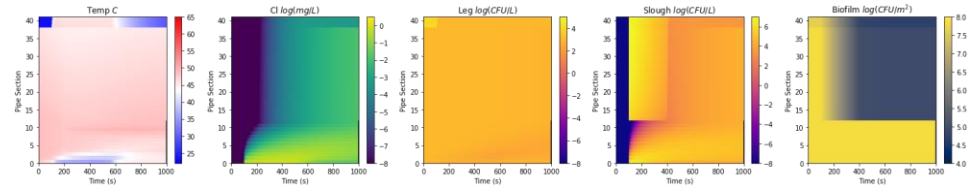
50°C	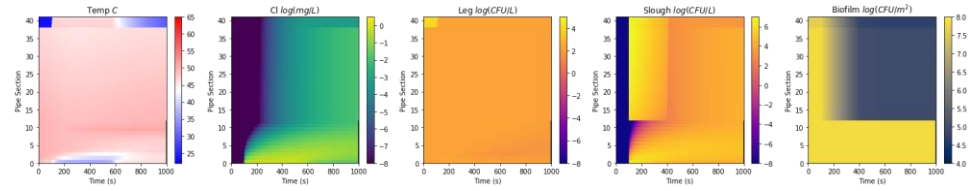
51°C	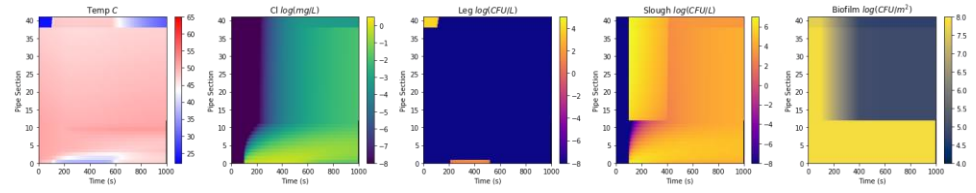

52°C	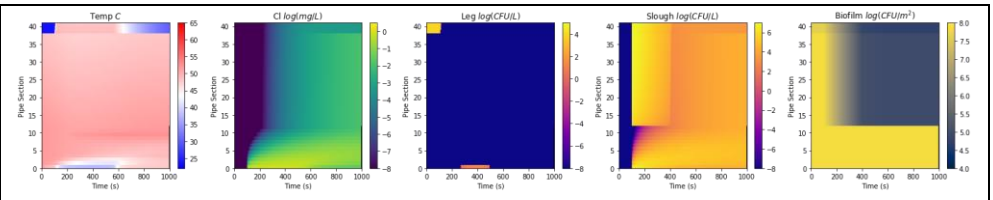
53°C	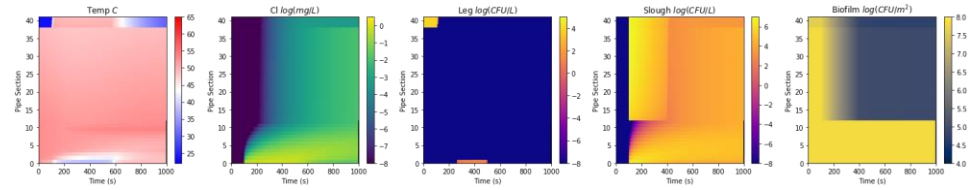
54°C	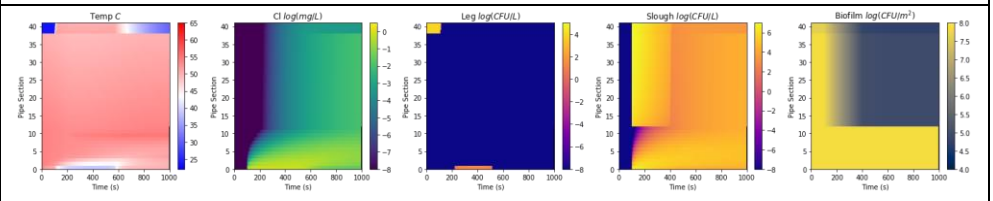
55°C	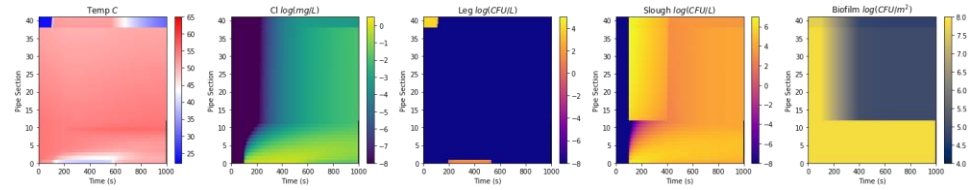
56°C	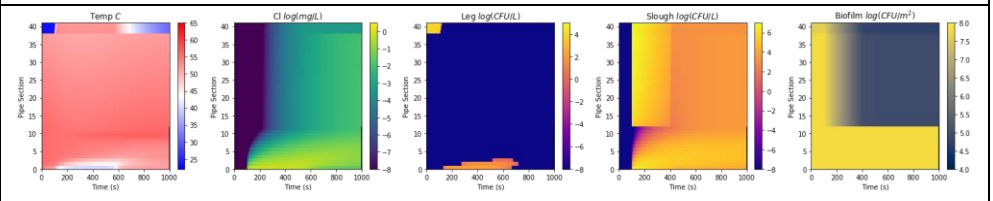

57°C	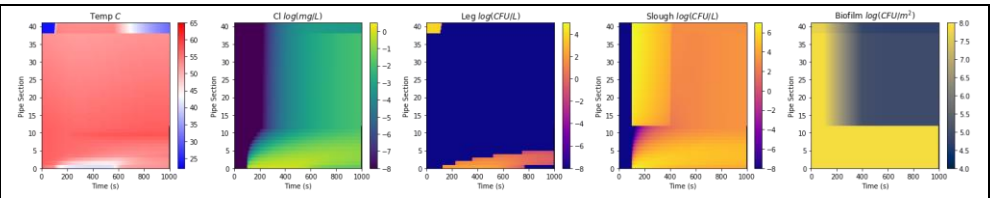
58°C	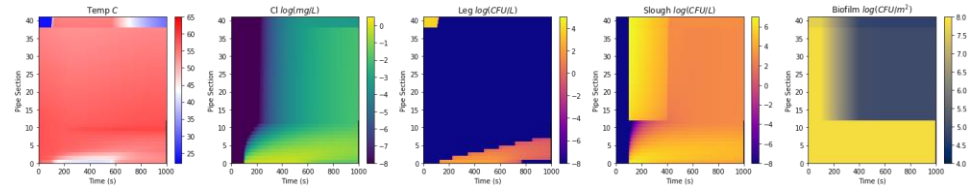
59°C	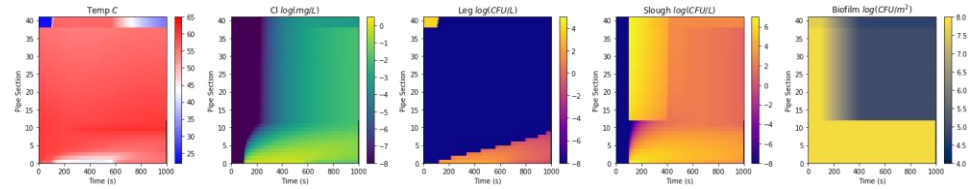
60°C	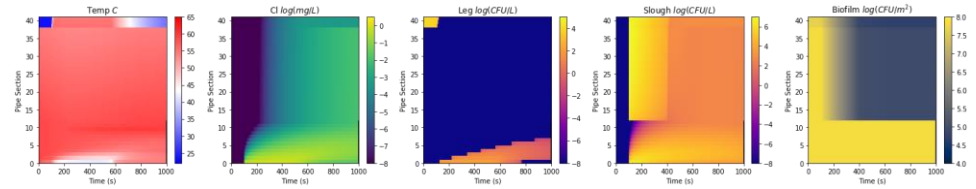
61°C	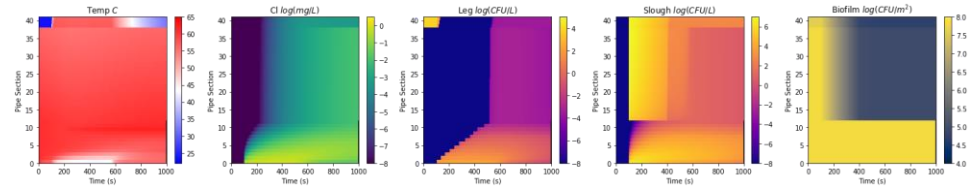

62°C	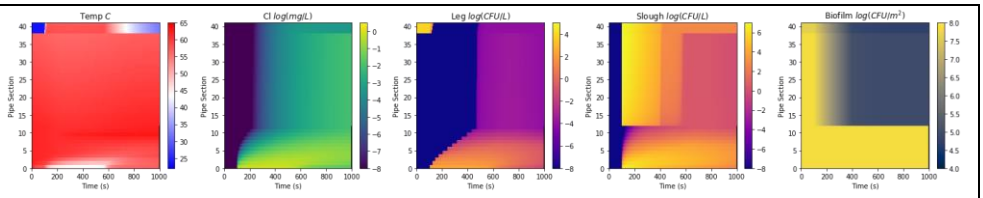
63°C	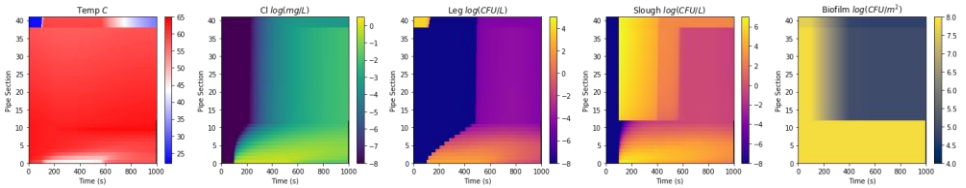

Section 11. Additional results

A complete set of outputs for the risk of infection, total cost, and heatmaps of water quality parameters throughout the premise plumbing system are shown in Figures A13-A14, respectively.

Figure A13: Heatmaps for temperature, chlorine residual, planktonic *L. pneumophila*, sloughed *L. pneumophila*, and *L. pneumophila* remaining in the biofilm.

Case	Risk of Infection or Illness	Total Cost
0	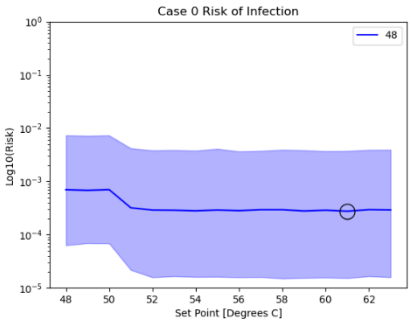	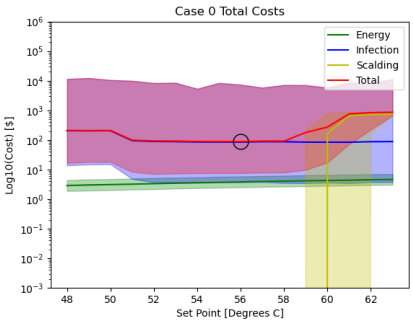
1	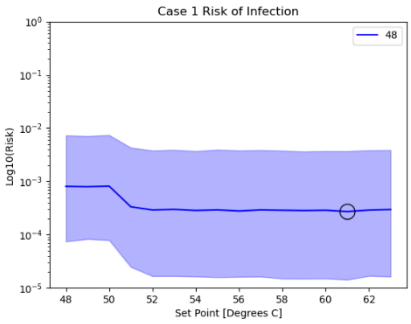	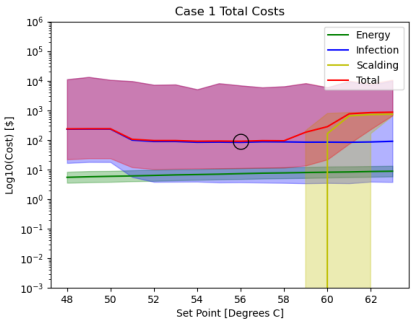

2	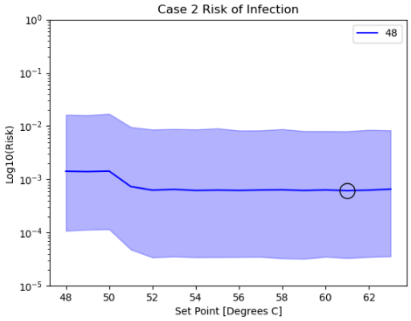 Case 2 Risk of Infection 48 Log10(Risk) Set Point [Degrees C]	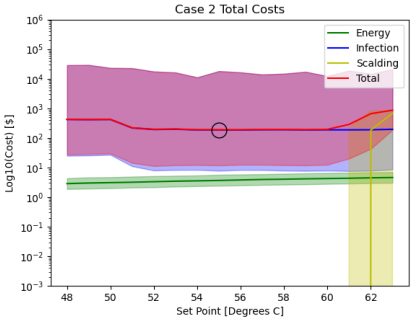 Case 2 Total Costs Energy Infection Scalding Total Log10(Cost) [$] Set Point [Degrees C]
3	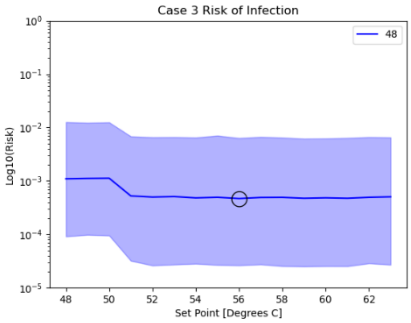 Case 3 Risk of Infection 48 Log10(Risk) Set Point [Degrees C]	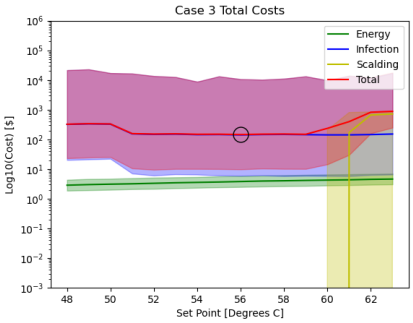 Case 3 Total Costs Energy Infection Scalding Total Log10(Cost) [$] Set Point [Degrees C]
4	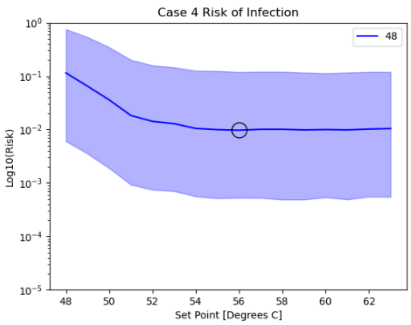 Case 4 Risk of Infection 48 Log10(Risk) Set Point [Degrees C]	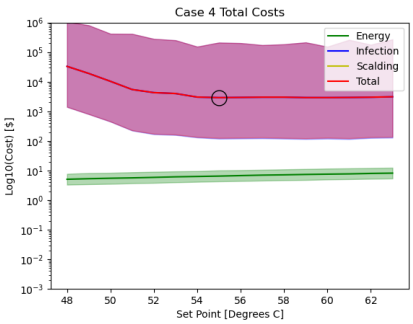 Case 4 Total Costs Energy Infection Scalding Total Log10(Cost) [$] Set Point [Degrees C]

5	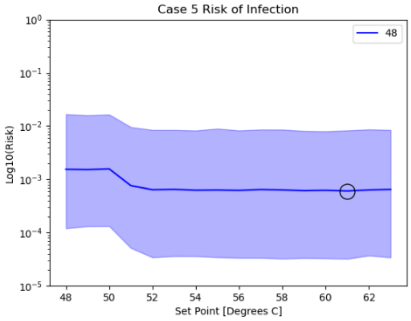 Case 5 Risk of Infection 48 Log10(Risk) Set Point [Degrees C]	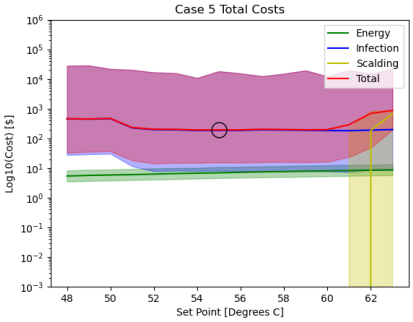 Case 5 Total Costs Energy Infection Scalding Total Log10(Cost) [$] Set Point [Degrees C]
6	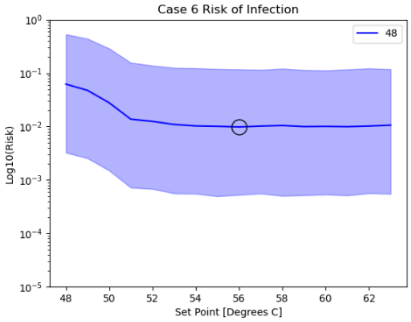 Case 6 Risk of Infection 48 Log10(Risk) Set Point [Degrees C]	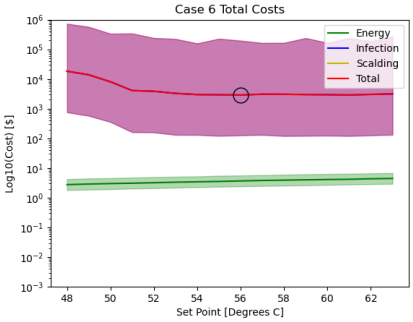 Case 6 Total Costs Energy Infection Scalding Total Log10(Cost) [$] Set Point [Degrees C]
7	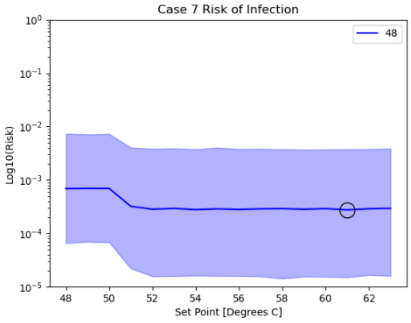 Case 7 Risk of Infection 48 Log10(Risk) Set Point [Degrees C]	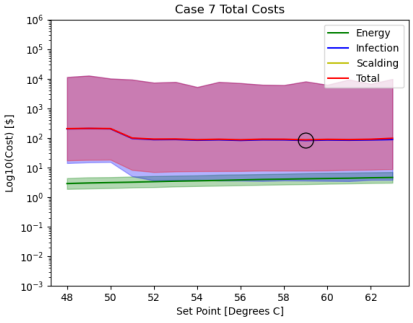 Case 7 Total Costs Energy Infection Scalding Total Log10(Cost) [$] Set Point [Degrees C]

8	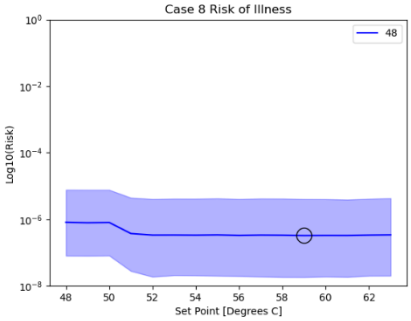 Case 8 Risk of Illness 48 Log10(Risk) Set Point [Degrees C]	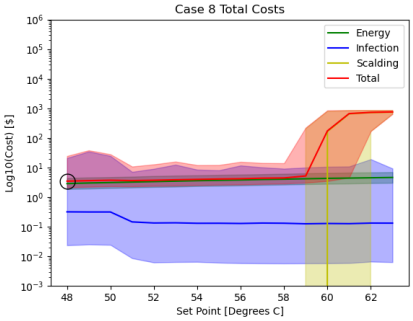 Case 8 Total Costs Energy Infection Scalding Total Log10(Cost) [$] Set Point [Degrees C]
9	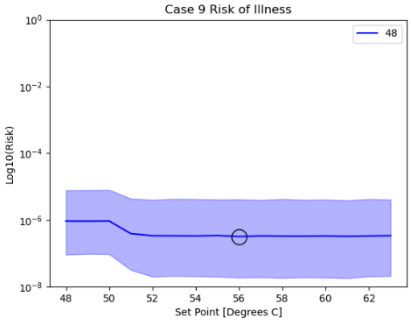 Case 9 Risk of Illness 48 Log10(Risk) Set Point [Degrees C]	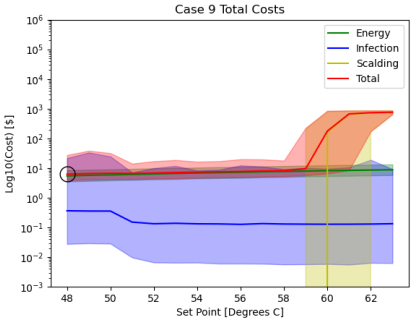 Case 9 Total Costs Energy Infection Scalding Total Log10(Cost) [$] Set Point [Degrees C]
10	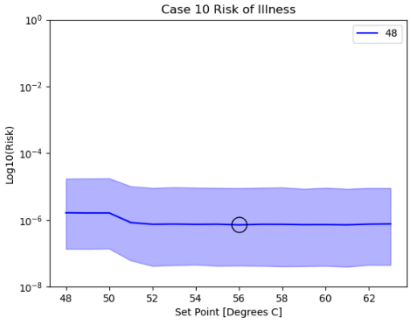 Case 10 Risk of Illness 48 Log10(Risk) Set Point [Degrees C]	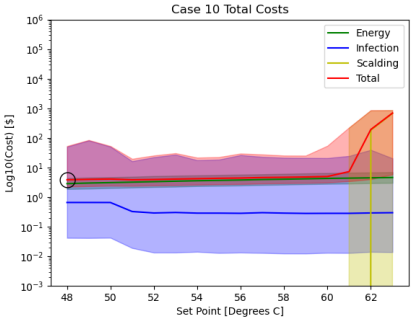 Case 10 Total Costs Energy Infection Scalding Total Log10(Cost) [$] Set Point [Degrees C]

11	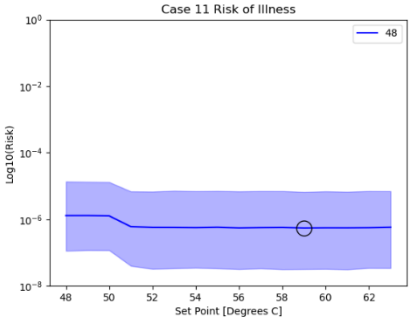 Case 11 Risk of Illness 48 Log10(Risk) Set Point [Degrees C]	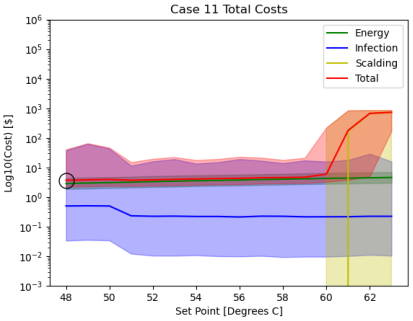 Case 11 Total Costs Energy Infection Scalding Total Log10(Cost) [$] Set Point [Degrees C]
12	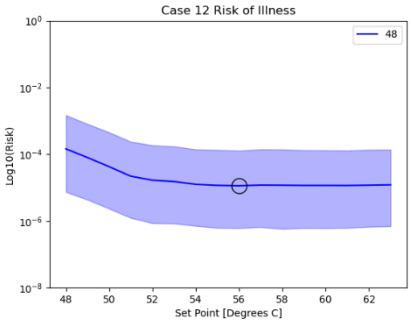 Case 12 Risk of Illness 48 Log10(Risk) Set Point [Degrees C]	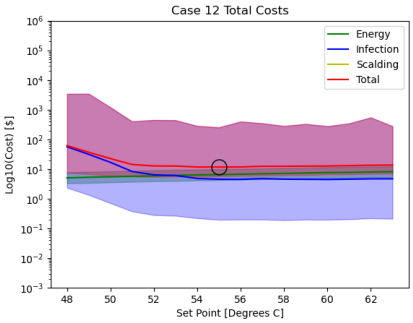 Case 12 Total Costs Energy Infection Scalding Total Log10(Cost) [$] Set Point [Degrees C]
13	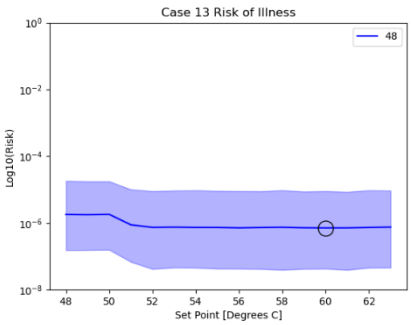 Case 13 Risk of Illness 48 Log10(Risk) Set Point [Degrees C]	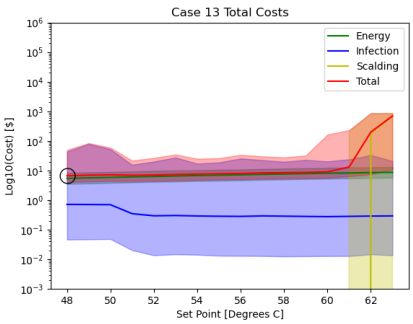 Case 13 Total Costs Energy Infection Scalding Total Log10(Cost) [$] Set Point [Degrees C]

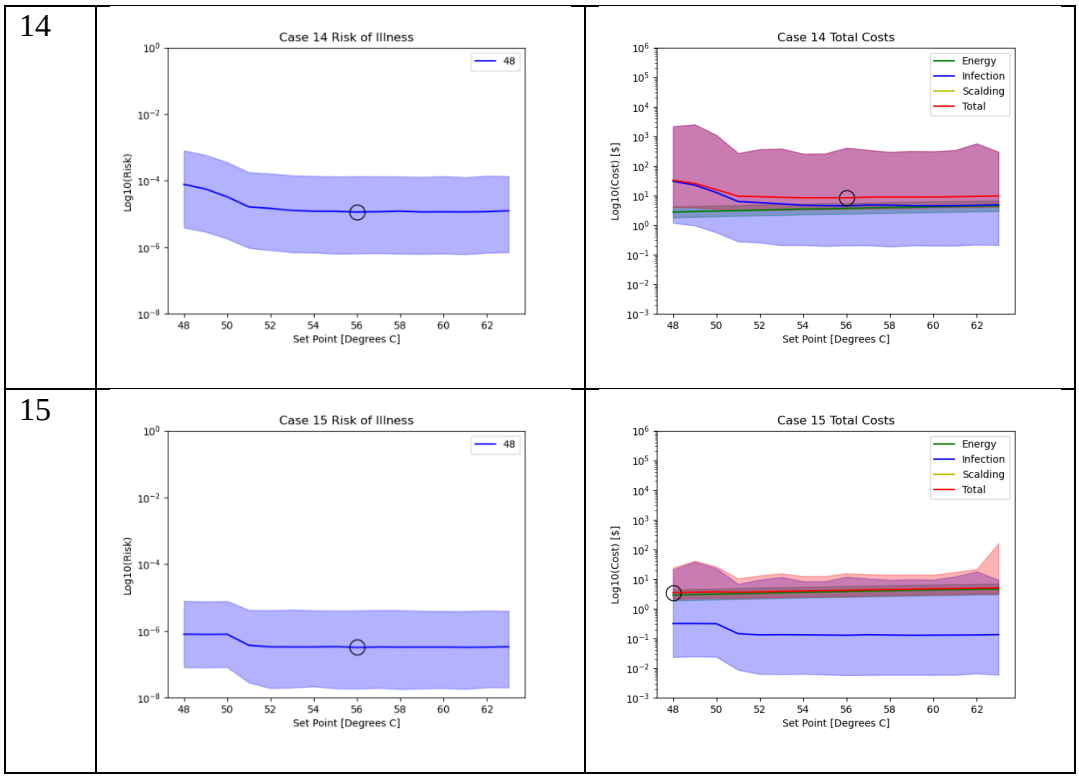

Figure A14: Risk of illness or infection of Legionnaires Disease and total cost graphs for all cases.

APPENDIX B

SUPPLEMENTAL INFORMATION FOR CHAPTER 3

Section 1. Unit analysis for population ecology model

$$\frac{ds_1}{dt} = \mu s_1 \left(1 - \frac{(s_0 + s_1)}{N_m}\right) + \eta s_0 s_1 - \kappa s_1 - \delta_i s_1$$

$$\frac{ds_1}{dt} = \left(\frac{1}{hr}\right)\left(\frac{CFU}{L}\right)\left(\frac{\frac{CFU}{L}}{\frac{CFU}{L}}\right) + \left(\frac{1}{\frac{CFU}{L}\ hr}\right)\left(\frac{CFU}{L}\right)\left(\frac{CFU}{L}\right) - \left(\frac{1}{hr}\right)\left(\frac{CFU}{L}\right) - \left(\frac{1}{hr}\right)\left(\frac{CFU}{L}\right)$$

Section 2. Model code used for Chapter 3.

```
import os
import numpy as np
from scipy.integrate import odeint
from scipy.stats import truncnorm
import matplotlib.pyplot as plt
from matplotlib.patches import Patch
import matplotlib.ticker as mticker
import pandas as pd
import seaborn as sns
from scipy import stats
import time

#############################################################################
# FUNCTIONS
#############################################################################

def transformation(w, t, z):  # Define the function "species_model"
    afit, mu, eta, k, I, c0, c1, d, Nm = z  # Define parameters
    # afit, mu, eta, k, I, c0, c1, d, Nm, background = z  # Define parameters
```

```
    s0, s1 = w  # w hold the initial conditions s0 and s1
    C = (1 - (s1 + s0) / Nm)  # cap growth rates: (1-(s1+s0)/1e8), ie as we approach the
limit growth slows down
    result = [mu * s0 * C - eta * s0 * s1 + k * s1 - I * s0 + c0 * d,  # species 0
              afit * mu * s1 * C + eta * s0 * s1 - k * s1 - I * s1 + c1 * d]  # species 1
    return result  # Return the model results


def run_transformation(afit, mu, eta, k, I, c0, c1, d, Nm, t):
    r0 = pd.DataFrame([])  # s0_result
    r1 = pd.DataFrame([])  # s1_result
    for i in range(n):
        z0 = [afit[i], mu[i], eta[i], k[i], I[i], c0[i], c1[i], d[i], Nm[i]]
        w0 = [c0[i], c1[i]]  # initial species, s0 and s1
        species = pd.DataFrame(odeint(transformation, w0, t, args=(z0,))).round(1)  # Run
odeint function "species_model" with initial conditions (w) and time (t).
        species.columns = ["s0", "s1"]  # Name columns
        r0 = r0.append(species["s0"])
        r1 = r1.append(species["s1"])
    r = pd.DataFrame.append(r0, r1)  # s_results
    return(r)


def truncate_normal(clip_a, clip_b, mean, std,n):
        a, b = (clip_a - mean) / std, (clip_b - mean) / std
        return truncnorm.rvs(a, b, loc=mean, scale=std, size=n)

# For plots
def percentile(n):
    def percentile_(x):
        return np.percentile(x, n)
    percentile_.__name__ = 'percentile_%s' % n
    return percentile_

def plot_shaded(x, mid, lower, upper, color, label):
    plt.plot(x, mid, color + '-', label=label)
    plt.fill_between(x, lower, upper, color=color, alpha=.3)

def draw_plot(data, offset, edge_color, fill_color):
    pos = np.arange(1) + offset
```

```
    bp = ax.boxplot(data, positions=pos, widths=0.8, patch_artist=True,
manage_xticks=False)
    for element in ['boxes', 'whiskers', 'fliers', 'medians', 'caps']:
        plt.setp(bp[element], color=edge_color)
    for patch in bp['boxes']:
        patch.set(facecolor=fill_color)


def lineplot(r, t, title, ylim, savename, date):
    sns.set(style='white')
    s_result = pd.melt(r.reset_index(), id_vars='index')  # ,value_vars=['asset1','asset2'])
    s_result = s_result.rename(columns={"value": "Species", "variable": "Time (hr)"})
    grouped = s_result.groupby(["Time (hr)", "index"])['Species'].agg(
        [percentile(5), percentile(50), percentile(95)]).unstack()
    grouped.astype(float)
    cost_types = sorted(set(s_result["index"]))
    colors = ["g", "b"]
    fig, ax = plt.subplots()
    for cost_type, color in zip(cost_types, colors):
        mid = []
        lower = []
        upper = []
        for time_ in t:
            lower.append(grouped["percentile_5"][cost_type][time_])
            mid.append(grouped["percentile_50"][cost_type][time_])
            upper.append(grouped["percentile_95"][cost_type][time_])
        ax.plot(t, mid, color + '-', label=cost_type)
        ax.fill_between(t, lower, upper, color=color, alpha=.3)
    handles, labels = ax.get_legend_handles_labels()
    idx = np.sort(np.unique(np.array(["Susceptible EC", "ESBL-EC"]),
return_index=True)[1])
    ax.legend(np.array(handles)[idx], np.array(["Susceptible EC", "ESBL-EC"])[idx])

    ax.set_title(title)
    ax.set_xlabel("Time (hr)")
    ax.set_ylabel("Species Count [log(CFU/L)]")
    ax.set_yscale("log")
    ax.set_ylim(ylim)
    fig.savefig(savename.format(date), dpi=600)  # , bbox_inches='tight')
```

```
def double_lineplot(r1, r2, t, title, subtitle1, subtitle2,  ylim, savename, date):
    sns.set(style='white')
    colors = ["g", "b"]
    text_size = 14

    s_result1 = pd.melt(r1.reset_index(), id_vars='index')  # ,value_vars=['asset1','asset2'])
    s_result1 = s_result1.rename(columns={"value": "Species", "variable": "Time (hr)"})
    grouped1 = s_result1.groupby(["Time (hr)", "index"])['Species'].agg(
        [percentile(5), percentile(50), percentile(95)]).unstack()
    grouped1.astype(float)
    cost_types1 = sorted(set(s_result1["index"]))

    s_result2 = pd.melt(r2.reset_index(), id_vars='index')  # ,value_vars=['asset1','asset2'])
    s_result2 = s_result2.rename(columns={"value": "Species", "variable": "Time (hr)"})
    grouped2 = s_result2.groupby(["Time (hr)", "index"])['Species'].agg(
        [percentile(5), percentile(50), percentile(95)]).unstack()
    grouped2.astype(float)
    cost_types2 = sorted(set(s_result2["index"]))

    fig, (ax1, ax2) = plt.subplots(1,2, sharey=True, figsize=(10, 4))
    fig.suptitle(title, size=text_size+2, y = 1.0)
    fig.text(0.5, 0.04, "Time (hr)", ha='center', size=text_size)

    for cost_type, color in zip(cost_types1, colors):
        mid = []
        lower = []
        upper = []
        for time_ in t:
            lower.append(grouped1["percentile_5"][cost_type][time_])
            mid.append(grouped1["percentile_50"][cost_type][time_])
            upper.append(grouped1["percentile_95"][cost_type][time_])
        ax1.plot(t, mid, color + '-', label=cost_type)
        ax1.fill_between(t, lower, upper, color=color, alpha=.3)
    handles, labels = ax1.get_legend_handles_labels()
return_index=True)[1])
    ax1.set_title(subtitle1, size=text_size)
    ax1.set_ylabel("Species Count [log(CFU/L)]", size=text_size)
    ax1.set_yscale("log")
    ax1.set_ylim(ylim)
```

```
    for cost_type, color in zip(cost_types2, colors):
        mid = []
        lower = []
        upper = []
        for time_ in t:
            lower.append(grouped2["percentile_5"][cost_type][time_])
            mid.append(grouped2["percentile_50"][cost_type][time_])
            upper.append(grouped2["percentile_95"][cost_type][time_])
        ax2.plot(t, mid, color + '-', label=cost_type)
        ax2.fill_between(t, lower, upper, color=color, alpha=.3)
    handles, labels = ax2.get_legend_handles_labels()
    idx2 = np.sort(np.unique(np.array(["Susceptible EC", "ESBL-EC"]),
return_index=True)[1])
    ax2.legend(np.array(handles)[idx2], np.array(["Susceptible EC", "ESBL-EC"])[idx2])
    ax2.set_title(subtitle2, size=text_size)
    ax2.set_yscale("log")
    ax2.set_ylim(ylim)

    fig.savefig(savename.format(date), dpi=600)  # , bbox_inches='tight')


os.getcwd()
os.chdir("C:/Users/ashle/OneDrive/Documents/Arizona State
University/Dissertation/Chapter3_Results/")
date = "02_24_2023"  # Name of folder in path for graph storage

# Timer
start_time = time.time()

##############################################################################
# Variables
##############################################################################

# Number on Monte Carlo iterations.
n = 10000

# Fitness cost
afit_env = [0] * n
```

```
afit_body = [0.98] * n  # (alpha_body) the fitness cost, INVERTED FROM 1.02, Lopatkin's SI [Unitless]

# Bacterial growth rate
mu_env = [0] * n
mu_body = np.random.uniform(0, 0.3, n)  # from Lopatkin's SI,[1/hours] growth rate of plasmid population (s1 organism)

# Carrying capacity (max CFU/L)
Nm_env = [1] * n # cant divide by zero
Nm_body = np.random.uniform(10 ** 4, 10**15, n)  #

#Background EC
background_env = [0] * n # background conc are trivial compared to effluent
background_body_none = [0] * n # for no background case
C_percent_ESBL = np.random.uniform(0.017, 0.035, n) #C from ESBL v24
background_body_some = np.random.uniform(10 ** 6, 10**7, n) # From intro of Lunestad et al, 2015. CFU/gram feces, 1 gram ~ 1 mL, from

# Conjugation efficiency rate
eta_env = np.random.beta(4.76e-1, 6.16e4, n)  # [1/hr] from Amos SI, fit in R, conjugate efficiency rate (s0 gains a plasmid)
eta_body = np.random.uniform(10**-6.25, 10**-8.48, n) # From Table 2 in Vahjen et al., 2020. Range for ALL ESBL to ALL E. coli IMT.

# Plasmid loss rate
k_env = [0] * n
k_body = [10 ** -3] * n

# Inactivation rate
I_env = [0.53] * n  # 1/hr, inactivation
I_body = [0.05] * n  # (d_body) from Lopatkin's SI, [1/hours] from table 2, dilution rate (in main paper)

# Bacterial concentration in treated ww effluent
c0_env_ww = truncate_normal(clip_a = 0, clip_b = 3*10**7, mean = 3705000, std = 6007000, n=n) # Brechet et al., 2014
c1_env_ww = truncate_normal(clip_a = 0, clip_b = 1*10**6, mean = 22000, std = 31000, n=n)
```

```
# Bacterial concentration regulation values
c0_env_rwqc = np.random.lognormal(np.log(126), 0.92, n) # CFU/L
c1_env_rwqc = c0_env_rwqc * np.random.uniform(0.005, 0.05, n) # This is 0.05% to 5%
of the susceptible EC

# No "effluent" in body
c0_body = [0] * n
c1_body = [0] * n

# Dilution rates
d_env = [0.50] * n
d_body = [0] * n
d_zero = [0.0] * n

# Volume ingested- normalize using vol and mass_gut to keep concentration in CFU/L
for diff eq.
# Add in Fupec after diff eq, at dose stage.
# Fraction of E.coli in body that are esbl e.coli
Fb = np.random.uniform(5*10**-5, 0.023, n) #unitless, from ESBL v24
Fupec = np.random.uniform(0.05, 0.088, n) #unitless, from ESBL v24
mass_gut = np.random.uniform(0.200, 0.750, n) # L in gut
vol = truncate_normal(clip_a = 0, clip_b = 200, mean = 16/1000, std = ((53 - 21) /
1.645)/1000, n=n)# mL/event -> L/event, mean: 0.017 L/even
s_norm_ing = vol/(vol+mass_gut) #1-10% of the volume in the gut, normalize ingested
volume
s_norm_gut = mass_gut/(vol+mass_gut) # 90-99% of the volume in the gut

# Environmental time and residence time
t_env = range(0, 20)  # (t) hr
t_env_plot = range(0, 20)  # (t) hr
t_body = range(0, 70)  # Time for body model to run: ESBL E. coli can be in the body
BEFORE DOSE (incubation time)
t_body_plot = range(0, 70)  # Time for body model to run: ESBL E. coli can be in the
body BEFORE DOSE (incubation time)
restime = np.random.normal(54.2, 2.5, n)  # Time to pull dose from available t_body:
Residence time from Cummings et al. 1976
t_biggraph = range(0, 100)


# Graphing
```

```
# lower limit/upper limit #10^-1 -10^4 is plotted as 10^0 - 10^5, DALY need 10-7 to
10^-2, risk needs 10^-7 to 10^-3
env_plot = [10 ** 1, 10 ** 6]  # Needs 10^1to10^6
dose_plt = [10 ** -4, 10 ** 14]  # Needs 10^0 to 10^3
risk_plt = [10 ** -10, 10 ** 4]  # Needs 10^-7 to 10^-3
daly_plt = [10 ** -10, 10 ** 4]  # Needs 10-7 to 10^-2


#############################################################################
## Environmental Model
#############################################################################

r_ww = run_transformation(afit = afit_env,
                mu = mu_env,
                eta = eta_env,
                k= k_env,
                I= I_env,
                c0 = c0_env_ww,
                c1 = c1_env_ww,
                d = d_zero,
                Nm = Nm_env,
                t = t_env)

r_rwqc = run_transformation(afit = afit_env,
                mu = mu_env,
                eta = eta_env,
                k= k_env,
                I= I_env,
                c0 = c0_env_rwqc,
                c1 = c1_env_rwqc,
                d = d_zero,
                Nm = Nm_env,
                t = t_env)


double_lineplot(r1 = r_rwqc, r2 = r_ww, t=t_env_plot,
        title="Low-Growth",
        subtitle1="Scenario 1",
        subtitle2="Scenario 2",
        # subtitle1="Recreational Water Standards",
```

```
        # subtitle2="Wastewater Effluent",
        ylim=[10e-1, 10e7],
        savename="{}/lowCase.png", date=date)


##########################################################################
## Body/ GI tract Model
##########################################################################

time_ingested = 5
background = background_body_none

s0_body, s1_body = r_rwqc.loc['s0'][time_ingested], r_rwqc.loc['s1'][time_ingested]
### Add background to the body, normalize using vol ingested and gut_mass
c0 = s0_body * s_norm_ing + background*(1-Fb)*s_norm_gut #~98%
c1 = s1_body * s_norm_ing + background*(Fb)*s_norm_gut #~2%

r_rwqc_none = run_transformation(afit = afit_body,
                mu = mu_body,
                eta = eta_body,
                k= k_body,
                I= I_body,
                c0 = c0,
                c1 = c1,
                d = d_zero,
                Nm = Nm_body,
                t = t_body)


##########################################################################

background = background_body_some
s0_body, s1_body = r_rwqc.loc['s0'][time_ingested], r_rwqc.loc['s1'][time_ingested]
### Add background to the body, normalize using vol ingested and gut_mass
c0 = s0_body * s_norm_ing + background*(1-Fb)*s_norm_gut #~98%
c1 = s1_body * s_norm_ing + background*(Fb)*s_norm_gut #~2%

r_rwqc_some = run_transformation(afit = afit_body,
                mu = mu_body,
                eta = eta_body,
```

```
            k= k_body,
            I= I_body,
            c0 = c0,
            c1 = c1,
            d = d_zero,
            Nm = Nm_body,
            t = t_body)

#############################################################################

double_lineplot(r1 = r_rwqc_none, r2 = r_rwqc_some, t=t_body_plot,
        title="High-Growth with RWQC",
        subtitle1='Scenario 3', #"Without Background Population",
        subtitle2='Scenario 4', #"With Background Population",
        ylim=[10e-1, 10e9],
        savename="{}/highCase_rwqc.png", date=date)

plt.close()

#############################################################################
## Doses
#############################################################################

doses_rwqc_none = pd.DataFrame([])
s0_res_body = r_rwqc_none.loc["s0"]
s1_res_body = r_rwqc_none.loc["s1"]
# Dose response for ESBL E. coli
post_hgt_in_body_s0 = []
post_hgt_in_body_s1 = []
for i in range(n):
   post_hgt_in_body_s0.append(s0_res_body.iloc[i, int(np.round(restime[i]))])
   post_hgt_in_body_s1.append(s1_res_body.iloc[i, int(np.round(restime[i]))])
s0_post_hgt = pd.DataFrame(post_hgt_in_body_s0)
s1_post_hgt = pd.DataFrame(post_hgt_in_body_s1)

print(np.mean(s0_post_hgt))

# Dose for both s0 and s1, include fraction UPEC
ds0 = Fupec * s0_post_hgt.squeeze()  # CFU/event
ds1 = Fupec * s1_post_hgt.squeeze()  # CFU/event
```

```
ds0.index = ["Susceptible EC"] * ds0.shape[0]   #    ds0.index = ["ds0"] * ds0.shape[0]
ds1.index = ["ESBL-EC"] * ds0.shape[0]          #    ds1.index = ["ds1"] * ds0.shape[0]
dose_rwqc_none = pd.concat([pd.DataFrame(ds0), pd.DataFrame(ds1)])
doses_rwqc_none = pd.concat([doses_rwqc_none, dose_rwqc_none], axis=1)

#########################################################################

doses_rwqc_some = pd.DataFrame([])
s0_res_body = r_rwqc_some.loc["s0"]
s1_res_body = r_rwqc_some.loc["s1"]
# Dose response for ESBL E. coli
post_hgt_in_body_s0 = []
post_hgt_in_body_s1 = []
for i in range(n):
    post_hgt_in_body_s0.append(s0_res_body.iloc[i, int(np.round(restime[i]))])
    post_hgt_in_body_s1.append(s1_res_body.iloc[i, int(np.round(restime[i]))])
s0_post_hgt = pd.DataFrame(post_hgt_in_body_s0)
s1_post_hgt = pd.DataFrame(post_hgt_in_body_s1)

print(np.mean(s0_post_hgt))

# Dose for both s0 and s1
ds0 = Fupec * s0_post_hgt.squeeze()  # CFU/event
ds1 = Fupec * s1_post_hgt.squeeze()  # CFU/event
ds0.index = ["Susceptible EC"] * ds0.shape[0]   #    ds0.index = ["ds0"] * ds0.shape[0]
ds1.index = ["ESBL-EC"] * ds0.shape[0]          #    ds1.index = ["ds1"] * ds0.shape[0]
dose_rwqc_some = pd.concat([pd.DataFrame(ds0), pd.DataFrame(ds1)])
doses_rwqc_some = pd.concat([doses_rwqc_some, dose_rwqc_some], axis=1)


#########################################################################

#for all case comparison
def box_and_whisker(data, title, ylab, lower_limit, upper_limit, savename):
    melt = pd.melt(data.reset_index(), id_vars='index')
    plt.yscale("log")
    plt.title(title)
    sns.boxplot(x="variable", y="value", hue="index", data=melt, palette={"b","g"})
    plt.xlabel("")
    plt.ylabel(ylab)
```

```
    plt.ylim([lower_limit, upper_limit])
    plt.savefig(savename.format(date), dpi=600)  # , bbox_inches='tight')
    # plt.close()  # must close because this is not written with fig/ax.



doses = pd.concat([doses_rwqc_none, doses_rwqc_some], axis=1)
# doses.columns = ["Without Background Population","With Background Population"]
doses.columns = ["Scenario 3","Scenario 4"]

### Dose for s0 & s1 after HGT in body
box_and_whisker(data=doses, title="Dose",
            ylab="Dose [log(CFU)]", lower_limit=dose_plt[0], upper_limit=dose_plt[1],
            savename="{}/boxplot_Dose.png")

#############################################################################
##### SPEARMAN RANK CORRELATION AGAINST DOSE OF S1
#############################################################################

name = [c0_env_rwqc,
        c1_env_rwqc,
        mu_body,
        eta_env,
        eta_body,
        Nm_body,
        background_body_some,
        Fb,
        Fupec,
        mass_gut,
        vol,
        restime]

name_ib = ["c0_env_rwqc",
        "c1_env_rwqc",
        "mu_body",
        "eta_env",
        "eta_body",
        "Nm_body",
        "background_body_some",
        "Fb",
```

```
        "Fupec",
        "mass_gut",
        "vol",
        "restime"]

state = {}
for i in range(len(name)):
   state[name_ib[i]]=name[i].squeeze().tolist()

names = ["Susceptible E. coli",
        "ESBL E. coli",
        "Growth Body",
        "Conjugation Env.",
        "Conjugation Body",
        "Carrying Capacity Body",
        "Background E. coli",
        "Percent ESBL",
        "Percent UPEC",
        "Volume of Gut",
        "Volume",
        "Residence time"]



cases_ = ["Susceptible Dose (sb=0)", "ESBL Dose (sb=0)",
          "Susceptible Dose (sb>0)", "ESBL Dose (sb>0)"]
# cases_ = ["Susceptible Dose", "ESBL Dose"]

ds1_list = doses["With Background Population"]["Susceptible EC"].squeeze().tolist()
ds2_list = doses["With Background Population"]["ESBL-EC"].squeeze().tolist()
ds3_list = doses["Without Background Population"]["Susceptible EC"].squeeze().tolist()
ds4_list = doses["Without Background Population"]["ESBL-EC"].squeeze().tolist()
ds_list = [ds3_list, ds4_list, ds1_list, ds2_list]
# ds_list = [ds1_list, ds2_list]

significant = []
colors = []
pv = 0.05

sa = pd.DataFrame([])
```

```
for ds_list in ds_list:
    sastats = pd.DataFrame([])
    spearman = []
    pvalue = []
    for i in name_ib:
        r = stats.spearmanr(ds_list, state[i])[0]
        p = stats.spearmanr(ds_list, state[i])[1]
        spearman.append(r)
        pvalue.append(p)
    sastats = pd.DataFrame(spearman)
    sa = pd.concat([sa,sastats], axis=1)

sa.columns = cases_
sa.index = names
sat = np.array(sa.T)

fig, ax = plt.subplots()
im = ax.imshow(sat,cmap="seismic")

# We want to show all ticks...
ax.set_xticks(np.arange(len(names)))
ax.set_yticks(np.arange(len(cases_)))
# ... and label them with the respective list entries
ax.set_xticklabels(names)
ax.set_yticklabels(cases_)

# Rotate the tick labels and set their alignment.
plt.setp(ax.get_xticklabels(), rotation=45, ha="right",
        rotation_mode="anchor")

# Loop over data dimensions and create text annotations.
for i in range(len(cases_)):
    for j in range(len(names)):
        # if abs(sat[i,j]) > 0.10:
            if abs(sat[i,j]) > 0.40:
                text = ax.text(j, i, round(sat[i, j],2),
                            ha="center", va="center", color="w",size=8)
            if abs(sat[i,j]) < 0.40:
                text = ax.text(j, i, round(sat[i, j],2),
                            ha="center", va="center", color="black",size=8)
```

```
ax.set_title("Spearman Correlation Coefficient")
fig.tight_layout()
plt.grid(False)
fig.colorbar(im,shrink=0.4)

savename="{}/SA.png"
# savename="{}/SA_select.png"
fig.savefig(savename.format(date), dpi=600)  # , bbox_inches='tight')
plt.show()
```

APPENDIX C

SUPPLEMENTAL INFORMATION FOR CHAPTER 4

Section 1. Hand-to-mouth ingestion

Exposure parameters for wastewater workers at lagoons are scarce. This scenario is uncommon at many centralized treatment plants but is more common in scenarios where wastewater lagoons or other decentralized infrastructure may be used to manage wastewater, such as in rural or low-resources areas, or in situations where PPE recommendations are incompletely adhered to (D'Aoust et al., 2021). In addition to the exposure and risk of respiratory infection from bioaerosols, there exists a risk of hand-to-mouth ingestion from transporting wastewater from the lagoon to the location of sample processing. To model the hand-to-mouth ingestion risk, equations from Julian et al. (2018) (Julian et al., 2018) were modified to estimate an ingested volume of wastewater for an hourly rate. Julian et al. (2018) observed Vietnamese farmers who were collecting human excreta for agriculture purposes. The authors performed a literature review summarizing the fraction of the hand in contact with different objects (F_{hand}, F_{mouth}) and the transfer coefficients between contact with the hand and the object ($T_{bucket \rightarrow hand}$) or the mouth ($T_{hand \rightarrow mouth}$). The initial concentration of *E. coli* on the farmers hands (C_{hand}) was estimated to by 0.01 CFU /cm^2. The authors found that hand-to-mouth contact occurred 0-9 times per hand per hours during their study, which is lower than estimates in the U.S. The "bucket" scenario was used as a proxy for the wastewater lagoon sampling equipment.

$$C_{hand,final} = C_{hand} + (F_{hand})[(T_{bucket \rightarrow hand})(C_{water}) - C_{hand}] \quad (1)$$

An assumption was made that the concentration initially on the hands (C_{hand}) was negligible, resulting in equations 1 being rewritten as **equation 2** and **3.**

$$V = (T_{bucket \rightarrow hand})(T_{hand \rightarrow mouth})(F_{hand})(F_{mouth})(A_{hand}) \quad (2)$$

$$Dose = (C_{water})(V) \quad (3)$$

Table C1: Variables used to calculate hand-to-mouth ingestion

Parameter	Variable	Units	Distribution/ Point Value	Source
Transfer efficiency from bucket to hand	$T_{bucket \rightarrow han}$	mL/cm^2	Normal (mean=21, sd=13) Truncated at 0	Greene et al. (2015)
Transfer efficiency from hand to mouth	$T_{hand \rightarrow mout}$	cm^2/cm^2 (unitless)	Normal (mean=34, sd=25) Truncated at 0	Rusin et al (2002) (mean), Julian et al. (2010) (sd)
Fraction of hand in contact with the bucket	F_{hand}	% (unitless)	Uniform (min=0.001, max=0.002)	Auyeung et al. (2008)
Fraction of hand that comes in contact with mouth	F_{mouth}	% (unitless)	Uniform (min=0.10, max=0.18)	Auyeung et al. (2008)
Area of hand	A_{hand}	cm^2	Uniform (min =890, max=1070)	(Bussard, 2011)
Concentration of pathogen in wastewater	C_{water}	CFU/L	**Table 7**	**Table 7**

Section 2. Existing web applications

A literature review was conducted for existing web applications that assess the risk of SARS-CoV-2 infection. Eleven applications were included (**Table C2**).

Table C2. Literature review of existing web applications that look at risk of infection from different pathogens and exposure routes.

Reference	Web application name	Audience	Risk scenarios addressed	Variables
Gerrity et al., 2019(Gerrity et al., 2019) bit.ly/DPRisk	DPRisk	Scientists or public health professionals	QMRA for direct potable reuse	Pathogen with distribution, level of log removal, treatment train failure scenarios, management barriers (blending, dilution, and die-off), exposure distribution, and dose response model.
Rocha-Melogno et al., 2021(Rocha-Melogno	Aerosol-Mediated Infectious Disease Risk Assessments	Scientists or public health professionals	QMRA for SARS-CoV-2 aerosolized transmission indoors AND QMRA for	Can input your own distributions for diarrheal disease QMRA. For COVID-19 QMRA: exposure time, room size, room height,

et al., 2021) https://rapidqmra.shinyapps.io/Rapid_QMRA/	(AMIDRAs)		diarrheal disease near open sewers	number of people in the room, ventilation, mask efficiency, inactivation rate, inhalation rate, viral load shedding, Includes a risk comparison chart at the end.
Tang et al., 2022(Tang et al., 2022)	No title: web-based SDSS framework	Scientists or public health professionals	SARS-CoV-2 wastewater surveillance on University campus	38 wastewater sampling sites collected, geographical data compared to confirmed county cases using ArcGIS.
Crank et al., 2019(Crank et al., 2019) https://germlab.nd.edu/resources/qmraswim/	QMRAswim	Scientists or public health professionals	Risk of crAssphage and PMMoV from recreational swimming	Modeled with untreated domestic sewage. Can model up to 10 pathogens at one time. App options: bacterial/virus concentration, type of distribution, max and min concentration, number of Monte Carlo samples, dose distribution.

Schijven et al., 2021(J. Schijven et al., 2021)	*Air*CoV2	Scientists or public health professionals	QMRA SARS-CoV-2 aerosolized transmission indoors	Virus concentration, exposure time, ventilation, types of aerosolization included breathing, speaking, singing, coughing, and sneezing
Parhizkar et al., 2021(Parhizkar et al., 2021) https://safeairspaces.com/#bcb9fc15-e9d7-4884-876f-384f1c8418a1	Safe Air Spaces	General public	QMRA SARS-CoV-2 aerosolized transmission indoors	Particle emission dynamics, particle deposition to indoor surfaces, ventilation rate, and single-zone filtration. App options: occupant #, floor area, ceiling height, outdoor air supply, filtration card, time in room, mask, high emitter, low emitter.
Olsson et al., 2021(Olsson et al., 2021) https://www.microco	The microCOVID Project	General public	Risk for everyday scenarios	Built in scenarios: indoor hangout, grocery store trip, airplane travel, going to vote, etc. Variables: geographical location, nearby people, distance from people, duration of activity, risk

vid.org/about				profile of person, their vaccine status, your risk tolerance
Ranney and Goldberg, 2020(Ranney & Goldberg, 2020) https://mycovidrisk.app/	MyCOVID Risk	General Public	Returns low/medium/high risk based on user input	Location, setting (indoor vs outdoor), activity (walk, pumping gas, etc.) duration, number of people, percentage of masks.
Hu et al., 2020(Hu et al., 2020) https://19andme.covid19.mathematica.org/	19 and Me	General Public	Risk assessment for SARS-CoV-2	Location, age, gender, symptoms, underlying conditions, level of strenuous activity, number of people you live and interact with, hygiene habits, personal protective equipment, low/medium/high risk activity participation, vaccination status
Chande et al., 2020(Chande et al., 2020)	The COVID-19 Event Risk Assessment Planning Tool	General Public	Risk assessment for SARS-CoV-2 based on	Event size, ascertainment bias, full vaccination percentage

https://covid19risk.biosci.gatech.edu/			geographical location	
Bertsimas et al., 2020(Bertsimas et al., 2020) https://www.covidanalytics.io/mortality_calculator	COVID-19 Mortality Risk (CMR) tool	Scientists or public health professionals	Mortality risk for a single patient based on available app data	Age, gender, vitals, metabolic panel, blood counts, other lab values and comorbidities.
Hodcroft, 2020(Hodcroft, 2020) https://covariants.org/	CoVariants	General public	Information about SARS-CoV-2 variants and mutations	Ability to select variant or mutation of interest and see frequency of variant in time for a geographical location.

289

APPENDIX D

PUBLISHED WORKS AND PRESENTATIONS

Section 1. Published works

Heida, A., Mraz, A., Hamilton, M.T., Weir, M., Hamilton, K.A., 2022. Computational framework for evaluating risk trade-offs in costs associated with legionnaires' disease risk, energy, and scalding risk for hospital hot water systems. Environmental Science: Water Research & Technology 8 (1), 76-97.

Kerry A. Hamilton, Aditya Kuppravalli, Ashley Heida, Sayalee Joshi, Charles N. Haas, Marc Verhougstraete & Daniel Gerrity (2021) Legionnaires' disease in dental offices: Quantifying aerosol risks to dental workers and patients, Journal of Occupational and Environmental Hygiene, 18:8, 378-393, DOI: 10.1080/15459624.2021.1939878

Sayalee Joshi, Rain Richard, Daniella Saetta, Naushita Sharma, Noelle Mushro, Lucas Crane, Lucien Dieter, Grace Violet Morgan, Ashley Heida, Bennett Welco, Treavor Boyer, Paul Westerhoff, Kerry Ann Hamilton, 2022. *Pinpointing drivers of widespread colonization of Legionella pneumophila in a green building: Roles of water softener system and reduced occupancy*. Frontiers in Water.

Under Review:

Jonathan Burkhardt, Walter Grayman, Ahmed Abokifa, Tim Bartrand, Ian Guymer, Feng Shang, Ashley Heida, Kerry A. Hamilton, Alexis Mraz, Mark Hamilton, Mark H. Weir, 2022. *Water Quality in Premise Plumbing Systems*. American Society of Civil Engineers. Under Review.

Brandon Reyneke, Tinta C. Morris, Pilar Fernández-Ibáñez, Kevin G. McGuigan, Ashley Heida, Kerry A. Hamilton, Wesaal Khan, 2022. *Decentralized solar-based water treatment – bridging the last mile to water security in low- and middle-income countries.* Water Security. Under Review.

Section 2. Presentations

HORIZONTAL GENE TRANSFER OF ESBL E. COLI AND QMRA FOR RISK TO SWIMMERS IN RECREATIONAL WATERS

Presented at the Society for Risk Analysis (SRA) virtual conference, December 2021.

QUANTITATIVE MODEL FOR HORIZONTAL GENE TRANSFER OF ESBL E. COLI AND SUBSEQUENT RISK IN RECREATIONAL WATERS CONTAINING WASTEWATER EFFLUENT

Presented at the SSEBE graduate research virtual symposium, February, 2021.

A QUANTITATIVE MODEL FOR EVALUATING THE RISK OF LEGIONNAIRES' DISEASE WHILE FLUSHING PREMISE PLUMBING SYSTEMS AFTER EXTENDED STAGNATION

Presented at the Society for Risk Analysis (SRA) virtual conference, December 2020.

LEGIONELLA PNEUMOPHILA IN PREMISE PLUMBING SYSTEMS

Presented at the Society for Risk Analysis (SRA) conference in Arlington, Virginia, December 2019.

QUANTITATIVE MODEL FOR EVALUATING RISK TRADE-OFFS IN LEGIONNAIRES' DISEASE RISK, ENERGY COST, AND SCALDING RISK FOR HOT WATER SYSTEMS

Presented at the Association of Environmental Engineering and Science Professors (AEESP) conference in Tempe, Arizona, May 2019.

Section 3. Awards

NSF-FUNDED IRECCEE FELLOW | ARIZONA STATE UNIVERSITY | SPRING 2020

Awarded NSF-funded International Research Experience in Civil, Construction, and Environmental Engineering (IRECCEE) fellowship to work with collaborators at Stellenbosch University. Was postponed due to COVID-19.

BIODESIGN TRAVEL GRANT | ARIZONA STATE UNIVERSITY | OCTOBER 2019

Received $500 to attend the Society for Risk Analysis Conference 2019

APPENDIX E

PERMISSION TO USE PUBLISHED WORKS

All co-authors have granted their permission for the previously published work (Chapter 2) and works in preparation (Chapters 3 and 4) to be used in this dissertation.